

**Bio-based thermoset composites  
from epoxidised linseed oil**

Nontipa Supanchaiyamat

PhD

**University of York  
Department of Chemistry**

September 2012



# Abstract

Bio-based thermoset composites were prepared from epoxidised linseed oil (ELO) using bio-derived crosslinkers. The use of Pripol 1009 (a dimerised fatty acid derived from natural oils and fats) as a crosslinker yielded homogenous transparent films. The inclusion of catalysts, in particular, 4-dimethylaminopyridine (DMAP), demonstrated a significant improvement in the mechanical properties of the resins. An infrared spectroscopic study coupled with modulated differential scanning calorimetry revealed the epoxide ring opening, followed by etherification occurred during the curing process. The optimum DMAP catalyst loading was 0.5-1 % with respect to the total resin weight.

The optimised formulation consisting of ELO, Pripol and DMAP were subsequently combined with starch or modified starch in order to improve the resin properties. Normal corn starch, high amylose corn starch and their acid hydrolysed derivatives were included in the formulation. The addition of starch improved the mechanical properties of the films with high amylose starch yielding a film with the most desirable properties.

Expansion of high amylose corn starch (gelatinisation and retrogradation) yielded a high surface area material. The formulation with 20% wt. of gelatinised starch yielded a film with 227% improvement in tensile strength and 166% enhancement in Young's modulus, compared to those with no added starch. Moreover, expanded starch granules uniformly dispersed in the polymer matrix, resulting in a complete disappearance of phase separation. This was attributed to better interfacial adhesion of porous expanded starch and the polymer matrix. Thermal analysis revealed retardation in the cure process in the presence of starch, however the hydroxyl groups of starch were likely to enhance the extent of curing, as indicated by the higher total enthalpy of reaction. Furthermore, these bio-based composites demonstrated excellent thermal stability. Esterification of expanded starch dramatically decreased the water uptake of the resins however, the mechanical properties were compromised, owing to low thermal stability of the esterified starch.



# Table of Contents

<b>Abstract .....</b>	<b>3</b>
<b>List of figures .....</b>	<b>11</b>
<b>List of tables .....</b>	<b>21</b>
<b>Acknowledgments .....</b>	<b>23</b>
<b>Declaration .....</b>	<b>25</b>
<b>Chapter 1 - <i>Introduction</i> .....</b>	<b>27</b>
<b>1.1 Sustainable development and green chemistry .....</b>	<b>29</b>
<b>1.2 Polymers and biopolymers .....</b>	<b>31</b>
<b>1.3 Plant oils.....</b>	<b>32</b>
1.3.1 General .....	32
1.3.2 Epoxidation of plant oils .....	36
1.3.3 Plant oils based epoxy resins.....	39
1.3.4 Linseed oil and epoxidised linseed oil .....	42
<b>1.4 Starch .....</b>	<b>45</b>
1.4.1 General .....	45
1.4.2 Starch composition and organisation of starch granules.....	48
1.4.3 Modification of starch .....	53
1.4.3.1 Physical modification.....	55
1.4.3.2 Chemical modification.....	57
1.4.4 Starch in composites.....	62
1.4.4.1 Starch blends with synthetic non-degradable polymers.....	62
1.4.4.2 Starch blends with synthetic degradable polymers.....	63
1.4.4.3 Starch blends with other biopolymers.....	64
<b>1.5 Scope of the thesis .....</b>	<b>64</b>
<b>Chapter 2 - <i>Epoxidised linseed oil based thermosetting resins</i> .....</b>	<b>67</b>
<b>2.1 Chapter 2 - Summary.....</b>	<b>69</b>
<b>2.2 Introduction .....</b>	<b>69</b>

<b>2.3 Epoxidised linseed oil based thermosetting resins using bio-derived crosslinkers .....</b>	<b>71</b>
2.3.1 Infrared spectroscopy of epoxidised linseed oil and crosslinkers.....	74
2.3.2 Simultaneous thermal analysis of epoxidised linseed oil and crosslinkers....	81
<b>2.4 Thermosetting resins from epoxidised linseed oil and Pripol.....</b>	<b>83</b>
2.4.1 Thermal analysis of epoxidised linseed oil and Pripol mixtures with no added catalyst .....	83
2.4.2 Physical properties of resulting films.....	84
2.4.2.1 Effect of different catalysts on the mechanical properties of the films .....	84
2.4.2.2 Effect of different catalysts on the water uptake of the films.....	86
2.4.2.3 Effect of different catalysts on thermal properties of the films.....	86
<b>2.5 Study of curing reaction .....</b>	<b>87</b>
2.5.1 Mechanistic study of curing reaction by infrared spectroscopy.....	87
2.5.2 Study of curing reaction using thermal analysis .....	95
2.5.3 Study of curing reaction using viscometry.....	98
2.5.4 Proposed mechanism of the system .....	100
<b>2.6 Optimisation of formulation with DMAP.....</b>	<b>102</b>
2.6.1 Effect of amount of catalyst on the mechanical properties of the films .....	102
2.6.2 Effect of curing temperature on the mechanical properties of the films.....	103
2.6.3 Effect of curing time on the mechanical properties of the films.....	104
<b>2.7 Conclusions.....</b>	<b>104</b>
 <b>Chapter 3 - <i>Starch and acid hydrolysed starch in bio-based thermoset composites</i> .....</b>	 <b>107</b>
<b>3.1 Chapter 3 - Summary .....</b>	<b>109</b>
<b>3.2 Introduction.....</b>	<b>110</b>
<b>3.3 Comparison of acid hydrolysis methods for normal corn starch .</b>	<b>112</b>
3.3.1 Solubility and swelling power.....	112
3.3.2 Pasting properties .....	115
3.3.3 Thermal properties .....	119
3.3.4 Morphological properties .....	123
<b>3.4 Films containing normal corn starch and its acid hydrolysed derivatives .....</b>	<b>126</b>
3.4.1 Mechanical properties .....	127
<b>3.5 Acid hydrolysis of high amylose corn starch.....</b>	<b>129</b>

3.5.1 Solubility and swelling power.....	129
3.5.2 Pasting properties .....	131
3.5.3 Thermal properties .....	133
3.5.4 Morphological properties .....	135
3.5.5 <sup>13</sup> C cross polarisation (CP) magic angle spinning (MAS) solid state nuclear magnetic resonance .....	137
<b>3.6 Films containing high amylose corn starch and its acid hydrolysed derivatives.....</b>	<b>140</b>
3.6.1 Mechanical properties .....	140
3.6.2 Morphological study .....	142
<b>3.7 Conclusions.....</b>	<b>144</b>
<b>Chapter 4 - Expanded starch in bio-based thermoset composites ...</b>	<b>147</b>
<b>4.1 Chapter 4 - Summary .....</b>	<b>149</b>
<b>4.2 Introduction .....</b>	<b>149</b>
<b>4.3 Characterisation of expanded starch .....</b>	<b>152</b>
4.3.1 Morphological study .....	152
4.3.2 Porosity of expanded starch .....	153
4.3.3 <sup>13</sup> C cross polarisation (CP) magic angle spinning (MAS) solid state nuclear magnetic resonance .....	155
4.3.4 X-ray diffraction.....	157
4.3.5 Thermal characterisation.....	158
<b>4.4 Films with expanded starch .....</b>	<b>160</b>
4.4.1 Mechanical properties .....	160
4.4.1.1 Effect of different types of starch .....	161
4.4.1.2 Effect of different amounts of starch .....	162
4.4.1.3 Effect of curing temperature .....	163
4.4.2 Morphological study .....	165
4.4.3 Water uptake .....	167
4.4.4 Thermal properties .....	169
4.4.4.1 Effect of different amounts of starch .....	169
4.4.4.2 Effect of starch expansion by gelatinisation or retrogradation .....	172
<b>4.5 Expanded starch in the formulation .....</b>	<b>173</b>
4.5.1 Thermal study.....	173
4.5.2 Rheological properties .....	177

4.5.2.1 Effect of different types of starch (native vs expanded).....	177
4.5.2.2 Effect of different amounts of starch.....	178
4.5.3 Infrared spectroscopic study .....	179
<b>4.6 Role of starch in the formulation.....</b>	<b>182</b>
<b>4.7 Conclusions.....</b>	<b>183</b>
<b>Chapter 5 - Esterified starches and their use in bio-based thermoset composites.....</b>	<b>185</b>
<b>5.1 Chapter 5 - Summary .....</b>	<b>187</b>
<b>5.2 Introduction .....</b>	<b>188</b>
<b>5.3 Characterisation of modified starches .....</b>	<b>190</b>
5.3.1 Physical appearance .....	190
5.3.2 Infrared spectroscopy .....	192
5.3.3 <sup>13</sup> C cross polarisation (CP) magic angle spinning (MAS) solid state nuclear magnetic resonance .....	197
5.3.4 Determination of degree of substitution.....	200
5.3.5 Thermal characterisation.....	203
5.3.6 Thermogravimetric - Fourier transform infrared spectroscopy (TG-FTIR) .....	205
5.3.7 Morphological study .....	217
<b>5.4 Films with esterified starches .....</b>	<b>218</b>
5.4.1 Mechanical properties .....	219
5.4.2 Morphological study .....	220
5.4.3 Water uptake .....	222
5.4.4 Thermal properties .....	223
<b>5.5 Study of curing reaction of the formulations with esterified starches .....</b>	<b>225</b>
5.5.1 Thermal study .....	225
5.5.2 Infrared spectroscopic study .....	227
<b>5.6 Conclusions.....</b>	<b>232</b>
<b>Chapter 6 - Literature comparison and evaluation of the bio-based composites against PVC wearlayer.....</b>	<b>235</b>
<b>6.1 Chapter 6 -Summary .....</b>	<b>237</b>
<b>6.2 Introduction .....</b>	<b>237</b>
<b>6.3 Mechanical properties .....</b>	<b>237</b>



6.4 Water resistance .....	240
6.5 Thermal stability .....	240
6.5 Conclusions .....	242
<b>Chapter 7 - <i>Experimental</i></b> .....	<b>245</b>
7.1 Chemicals .....	247
7.2 Experimental details and instrumentation for chapter 2 .....	247
7.2.1 ELO and bio-derived crosslinkers film preparation.....	247
7.2.2 Simultaneous thermal analysis.....	248
7.3 Experimental details and instrumentation for chapter 3 .....	249
7.3.1 Preparation of acid hydrolysed starch in water .....	249
7.3.2 Preparation of acid hydrolysed starch in ethanol .....	249
7.3.3 Swelling power and solubility tests.....	250
7.3.4 Pasting properties .....	250
7.3.5 Film preparation .....	250
7.4 Experimental details and instrumentation for chapter 4 .....	251
7.4.1 Expansion processes of starch.....	251
7.4.1.1 Gelatinisation .....	251
7.4.1.2 Retrogradation.....	251
7.4.2 BET surface area measurement.....	252
7.4.3 Powder X-ray diffraction .....	252
7.4.4 Film preparation .....	252
7.5 Experimental details and instrumentation for chapter 5 .....	252
7.5.1 Esterification of starch .....	252
7.5.2 Determination of degree of substitution by titration.....	253
7.5.3 Film preparation .....	253
7.5.4 Thermogravimetric-Fourier transform infrared spectroscopy (TG-FTIR) ..	254
7.6 Experimental details and instrumentation for chapters 2, 3 and 4 .....	254
7.6.1 Viscosity measurement .....	254
7.7 Experimental details and instrumentation for chapters 2, 3, 4 and 5 .....	255
7.7.1 Mechanical Test .....	255
7.7.2 Water uptake .....	256
7.7.3 Thermal decomposition temperature of cured films .....	256

7.7.4 Modulated differential scanning calorimetry .....	256
7.7.5 Infrared spectroscopy .....	257
<b>7.8 Experimental details and instrumentation for chapters 3, 4 and 5</b> .....	<b>257</b>
7.8.1 Scanning electron microscopy .....	257
7.8.2 Solid-state <sup>13</sup> C CP MAS NMR analysis.....	257
<b>Chapter 8 - <i>Conclusions and further work</i></b> .....	<b>259</b>
8.1 Conclusions.....	261
8.2 Further work .....	265
<b>Appendix A</b> .....	<b>267</b>
A.2 Chapter 2 .....	269
A.4 Chapter 4 .....	270
A.5 Chapter 5 .....	273
<b>Glossary</b> .....	<b>277</b>
<b>References</b> .....	<b>283</b>

# List of figures

## Chapter 1

**Figure 1.1** – The three spheres of sustainability

**Figure 1.2** – Generic triglyceride structure

**Figure 1.3** – Structure of common fatty acids: A) lauric acid, B) myristic acid, C) palmitic acid, D) stearic acid, E) oleic acid, F) linoleic acid, G) linolenic acid, H)  $\alpha$ -eleostearic acid, I) vernolic acid, J) ricinoleic acid

**Figure 1.4** – Epoxidation using peroxyacid

**Figure 1.5** – Prileshajev epoxidation

**Figure 1.6** – Activated monomer mechanism

**Figure 1.7** – Structure of A) methyl-endomethylenetetra- hydrophthalic anhydride and B) cis-1,2,3,6-tetrahydrophthalic anhydride

**Figure 1.8** – Structures of 3-glycidylpropylheptaisobutyl-T8-polyhedral oligomeric silsesquioxane (G-POSS)

**Figure 1.9** – Auto-oxidation mechanism of drying oils

**Figure 1.10** – Epoxidised linseed oil (ELO)

**Figure 1.11** – Structures of amylose and amylopectin

**Figure 1.12** – Lamellar structure of a starch granule: A) stacks of crystalline lamellae separated by amorphous growth rings, B) expanded view of the crystalline and amorphous region and C) double helices of amylopectin constitute the crystalline lamellae whilst the branch points of the clusters constitute the amorphous lamellae

**Figure 1.13** – Starch granule structure: A) granule (2 - 100  $\mu\text{m}$ ), B) growth rings (120 - 500 nm), C) blocklets (20 - 50 nm) and D) amorphous and crystalline lamellae (9 nm)

**Figure 1.14** – Top view of starch A- and B-polymorphs

**Figure 1.15** – Chemical modification of starch

**Figure 1.16** – Acid hydrolysis mechanism of starch

**Figure 1.17** – Cushion vinyl sheet construction

## **Chapter 2**

**Figure 2.1** – A) Succinic anhydride, B) Itaconic anhydride, and C) Pripol 1009

**Figure 2.2** – Films made from epoxidised linseed oil and bio-derived crosslinkers; A) succinic acid, B) itaconic acid, C) succinic anhydride, D) itaconic anhydride and E) Pripol 1009

**Figure 2.3** – Infrared spectrum of epoxidised linseed oil

**Figure 2.4** – Infrared spectra of ELO and succinic acid cured at 140 °C

**Figure 2.5** – Infrared spectra of ELO and itaconic acid cured at 140 °C

**Figure 2.6** – Infrared spectra of ELO and succinic anhydride cured at 140 °C

**Figure 2.7** – Infrared spectra of ELO and itaconic anhydride cured at 140 °C

**Figure 2.8** – Infrared spectra of ELO and Pripol 1009 cured at 140 °C

**Figure 2.9** – TG and DSC thermograms of the mixtures of ELO with A) succinic acid, B) itaconic acid, C) succinic anhydride, D) itaconic anhydride and E) Pripol 1009

**Figure 2.10** - ELO/Pripol 1009 ratio against heat of reactions

**Figure 2.11** - Mechanical properties of films cured at 140 °C

**Figure 2.12** - Mechanical properties of films cured at 160 °C

**Figure 2.13** – Transparent and flexible ELO based film

**Figure 2.14** – TGA thermograms of ELO-Pripol films with different catalysts

**Figure 2.15** – Infrared spectrum of Pripol 1009

**Figure 2.16** – Imidazolium carboxylate intermediate ( $R_1, R_2 = H$  or  $CH_3$ )

**Figure 2.17** – Infrared spectra of ELO, Pripol and TEA mixture cured at 140 °C

**Figure 2.18** – Infrared spectra of ELO, Pripol and DBU mixture cured at 140 °C

**Figure 2.19** – Infrared spectra of ELO, Pripol and DMAP mixture cured at 140 °C

**Figure 2.20** – Infrared spectra of ELO, Pripol and 1-MeIm mixture cured at 140 °C

**Figure 2.21** – Infrared spectra of ELO, Pripol and 2-MeIm mixture cured at 140 °C

**Figure 2.22** – Imidazole catalyst attached to the epoxy resin ( $R_1, R_2 = H$  or  $CH_3$ )

**Figure 2.23**– Thermograms of reaction mixtures of ELO/Pripol 1009 and different catalysts

**Figure 2.24** – Thermogram of reaction mixture of ELO and DMAP

**Figure 2.25**– Viscosities of the reaction mixtures

**Figure 2.26** – Proposed mechanism of the system

**Figure 2.27**– Mechanical properties of films with different amounts of DMAP

**Figure 2.28** – Mechanical properties of films with different curing temperatures

**Figure 2.29** – Mechanical properties of films cured for different times at 160 °C

### **Chapter 3**

**Figure 3.1** – Effect of temperature and reaction time on solubility of acid hydrolysed normal corn starch in water

**Figure 3.2** – Effect of temperature and reaction time on solubility of acid hydrolysed normal corn starch in ethanol

**Figure 3.3** – Effect of temperature and reaction time on swelling power of acid hydrolysed normal corn starch in water

**Figure 3.4** – Effect of temperature and reaction time on swelling power of acid hydrolysed normal corn starch in ethanol

**Figure 3.5** – Viscosity profiles of native normal corn starch and acid hydrolysed starches in water (1, 4 and 24 hours)

**Figure 3.6** – Viscosity profiles of native normal corn starch and acid hydrolysed starches in water (1, 4 and 24 hours) – enlarged from Figure 3.5

**Figure 3.7** – Viscosity profiles of native normal corn starch and acid hydrolysed corn starches in ethanol (1, 3, 5 and 7 days)

**Figure 3.8** – Viscosity profiles of native normal corn starch and acid hydrolysed corn starches in ethanol(1, 3, 5 and 7 days) – enlarged from Figure 3.7

**Figure 3.9** – TGA thermograms of native normal corn starch and acid hydrolysed starches in water

**Figure 3.10** – TGA thermograms of native normal corn starch and acid hydrolysed starches in ethanol

**Figure 3.11** – TG and DTG traces of native normal corn starch

**Figure 3.12** – Scanning electron micrographs (magnification X500 and X5000) of native normal corn starch (A, B) and acid hydrolysed starches in water with various reaction times: 1 hour (C, D), 4 hours (E, F) and 24 hours (G, H)

**Figure 3.13** – Scanning electron micrographs (magnification X500 and X5000) of native normal corn starch (A, B) and acid hydrolysed corn starches in ethanol with various reaction times: 1 day(C, D), 3 days (E, F), 5 days (G, H) and 7 days (I, J)

**Figure 3.14** – Native normal corn starch film (A) and acid-alcohol treated starch films with various reaction times (B-1 day, C-3 days, D-5days and E-7days)

**Figure 3.15** – Mechanical properties of films based on ELO, Pripol and normal corn starch or acid hydrolysed starch

**Figure 3.16** – Effect of temperature and reaction time on solubility of acid hydrolysed high amylose corn starch

**Figure 3.17** – Effect of temperature and reaction time on swelling power of acid hydrolysed high amylose corn starch

**Figure 3.18** – Viscosity profiles of high amylose corn starch and acid hydrolysed high amylose corn starches (1, 4 and 24 hours)

**Figure 3.19** – Viscosity profiles of high amylose corn starch, acid hydrolysed high amylose corn starches (1, 4 and 24 hours) – enlarged from Figure 3.18

**Figure 3.20** – TGA thermograms of native high amylose corn starch and acid hydrolysed high amylose starches

**Figure 3.21** – Scanning electron micrographs (magnification X500 and X5000) of native high amylose corn starch (A, B) and acid hydrolysed high amylose corn starches with various reaction times: 1 hour (C, D), 4 hours (E, F) and 24 hours (G, H)

**Figure 3.22** –  $^{13}\text{C}$  CP MAS NMR of native normal corn starch (A) and acid hydrolysed normal corn starches with various reaction times: (B) 1 hour, (C) 4 hours and (D) 24 hours

**Figure 3.23** –  $^{13}\text{C}$  CP MAS NMR of native high amylose starch (A) and acid hydrolysed high amylose starches with various reaction times: (B) 1 hour, (C) 4 hours and (D) 24 hour

**Figure 3.24** – Mechanical properties of films based on ELO, Pripol and native high amylose starch or acid hydrolysed high amylose starch

**Figure 3.25** – Mechanical properties of films based on ELO, Pripol and native normal corn (NC) or high amylose corn (HAS) starches or acid hydrolysed starches

**Figure 3.26** – Scanning electron micrographs (magnification X50 and X1000) of the cross-section of film with acid hydrolysed normal corn starch– A) whole film, B) bottom of the film and C) front of the film

**Figure 3.27** – Scanning electron micrographs (magnification X50 and X1000) of the cross-section of film with native high amylose starch– A) whole film, B) bottom of the film and C) front of the film

## **Chapter 4**

**Figure 4.1** – Gelatinisation and retrogradation of starch granules

**Figure 4.2** – Collapse of pore structure in starch gel network due to surface tension forces in water during drying process

**Figure 4.3** – Scanning electron micrographs (magnification X500 and X5000) of native high amylose corn starch (A, B), gelatinised high amylose corn starch (C, D) and retrograded high amylose corn starch (E, F)

**Figure 4.4** –  $^{13}\text{C}$  CP MAS NMR of native high amylose starch (A), gelatinised starch (B) and retrograded starch (C)

**Figure 4.5**–Diffractograms of high amylose starch (HAS), gelatinised starch (GS) and retrograded starch (RS)

**Figure 4.6**– TGA thermograms of unmodified, gelatinised and retrograded starches

**Figure 4.7** – Mechanical properties of films based on ELO, Pripol and unmodified or gelatinised or retrograded starch

**Figure 4.8** – Effect of amount of gelatinised starch on the mechanical properties of films

**Figure 4.9** – Effect of curing temperature on mechanical properties of resulting films

**Figure 4.10** – Films made of ELO, Pripol, gelatinised starch and DMAP cured at various temperatures

**Figure 4.11** – Scanning electron micrographs (magnification X50 and X1000) of the cross-section of film with native high amylose starch– A) whole film, B) bottom of the film and C) front of the film

**Figure 4.12** – Scanning electron micrographs (magnification X50 and X1000) of the cross-section of film with gelatinised starch– A) whole film, B) bottom of the film and C) front of the film

**Figure 4.13** – Effect of different types of starch on water uptake of films - high amylose starch (HAS), gelatinised starch (GS) and retrograded starch (RS)

**Figure 4.14** – Effect of different amounts of starch on water uptake of the films

**Figure 4.15**– TGA thermograms of films with different amounts of added starch

**Figure 4.16** – DTG curves of films with different amounts of added starch

**Figure 4.17** – Thermograms of formulations comprised of ELO, Pripol, DMAP and different types of starch

**Figure 4.18** – Thermograms of various formulations 1) ELO, 2) ELO and DMAP, 3) ELO, GS and DMAP, 4) Pripol, GS and DMAP, 5) ELO, Pripol, GS and DMAP and 6) ELO, Pripol and DMAP

**Figure 4.19** – Viscosity of reaction mixtures of ELO, Pripol and DMAP with 1) no starch, 2) unmodified starch (HAS), 3) gelatinised (GS) and 4) retrograded starch (RS)

**Figure 4.20** – Viscosity of reaction mixture of ELO, Pripol and DMAP with different amounts of starch

**Figure 4.21** – Infrared spectra of ELO and expanded starch mixture (0.5% of total weight DMAP catalyst) cured at 140 °C

**Figure 4.22** – Infrared spectra of Pripol and expanded starch mixture (0.5% of total weight DMAP catalyst) cured at 140 °C

## **Chapter 5**

**Figure 5.1** – Mechanism of acetylation of starch using acetic anhydride and pyridine A) formation of acetyl-pyridine complex, B) formation of acetylated starch

**Figure 5.2** – Mechanism of acetylation of starch using acetic anhydride and DMAP

**Figure 5.3** – Acetylated starch (Ace), maleated starch (Mal), succinic anhydride modified starch (Suc) and itaconic anhydride modified starch (Ita)



**Figure 5.4** – Base-catalysed rearrangement of itaconic anhydride to citraconic anhydride

**Figure 5.5** – Infrared spectrum of unmodified expanded starch

**Figure 5.6** – Infrared spectrum of acetylated starch

**Figure 5.7** – Reaction of maleic anhydride and starch

**Figure 5.8** – Infrared spectrum of maleated starch

**Figure 5.9** – Infrared spectrum of succinic anhydride modified starch

**Figure 5.10** – Infrared spectrum of itaconic anhydride modified starch

**Figure 5.11** –  $^{13}\text{C}$  CP MAS NMR of unmodified expanded starch and acetylated expanded starch

**Figure 5.12** –  $^{13}\text{C}$  CP MAS NMR of maleated starch, succinic anhydride modified starch and itaconic anhydride modified starch

**Figure 5.13** – TGA thermograms of unmodified expanded starch and esterified starches

**Figure 5.14** – A) surface plot of volatiles released during decomposition of unmodified starch, B) 3D plot of IR spectra obtained during TG-FTIR experiment, C) IR spectrum taken at maximum concentration of volatiles

**Figure 5.15** – A) surface plot of volatiles released during decomposition of acetylated starch, B) 3D plot of IR spectra obtained during TG-FTIR experiment, C) IR spectrum taken at maximum concentration of volatiles

**Figure 5.16** – Proposed mechanism of decomposition of cellulose acetate

**Figure 5.17** – IR spectra of evolved gases from TG-FTIR analysis of A) acetic acid and B) acetylated starch

**Figure 5.18** – A) surface plot of volatiles released during decomposition of maleated starch, B) 3D plot of IR spectra obtained during TG-FTIR experiment, C) and D) IR spectra taken at maximum concentration of volatiles

**Figure 5.19** – IR spectra of evolved gases from TG-FTIR analysis of A) maleic anhydride, B) maleic acid and C) maleated starch

**Figure 5.20** – A) surface plot of volatiles released during decomposition of itaconic anhydride modified starch, B) 3D plot of IR spectra obtained during TG-FTIR experiment, C) and D) IR spectra taken at maximum concentration of volatiles

**Figure 5.21** – A) surface plot of volatiles released during decomposition of succinic anhydride modified starch, B) 3D plot of IR spectra obtained during TG-FTIR experiment, C) Gram-Schmidt trace and D) IR spectra taken at maximum concentration of volatiles (333.5 °C)

**Figure 5.22** – IR spectra of evolved gases from TG-FTIR analysis of A) succinic acid and B) succinic anhydride modified starch

**Figure 5.23** – Scanning electron micrographs (magnification X500 and X5000) of unmodified expanded starch (A, B), acetylated starch (C, D), maleated starch (E, F), succinic anhydride modified starch (G, H) and itaconic anhydride modified starch (I, J)

**Figure 5.24** – Films with esterified starches

**Figure 5.25** – Mechanical properties of films with esterified starches

**Figure 5.26** – Scanning electron micrographs (magnification X50 and X1000) of the cross-section of films with esterified starches (A-B – acetylated starch, C-D – maleated starch, E-F – succinic anhydride modified starch, G-H – itaconic anhydride modified starch)

**Figure 5.27** – Water uptake of films with no starch, unmodified starch (Unmod), acetylated starch (Ace), maleated starch (Mal), succinic anhydride modified starch (Suc) and itaconic anhydride modified starch (Ita)

**Figure 5.28**– TGA thermograms of films with unmodified and modified starches

**Figure 5.29**– DTG curves of films with unmodified and modified starches

**Figure 5.27** – Thermograms of formulation comprised of ELO, Pripol, DMAP and esterified starches

**Figure 5.28** – Infrared spectra of the formulation comprised of ELO, Pripol, acetylated starch and DMAP cured at 140 °C

**Figure 5.29** – Infrared spectra of the formulation comprised of ELO, Pripol, maleated starch and DMAP cured at 140 °C

**Figure 5.30** – Infrared spectra of the formulation comprised of ELO, Pripol, succinic anhydride modified starch and DMAP cured at 140 °C

**Figure 5.31** – Infrared spectra of the formulation comprised of ELO, Pripol, itaconic anhydride modified starch and DMAP cured at 140 °C

## **Chapter 6**

**Figure 6.1** – Mechanical properties of bio-based films compared to PVC wearlayer and LDPE (results obtained from the literature a) reference 336, b) reference 335 and c) reference 334)

**Figure 6.2** – Water uptake of bio-based resins with gelatinised and acetylated starches compared to that of PVC wearlayer

**Figure 6.3** – TG and DTG traces of PVC wearlayer

**Figure 6.4** – TGA thermograms of bio-based films with gelatinised and acetylated starches compared to that of PVC wearlayer

## **Chapter 7**

**Figure 7.1** – Dumbbell specimen for tensile test (scales are in millimetre)

**Figure 7.2** – Instron 3367 universal testing machine (A), sample before the test (B) and after the test (C)

## **Appendix A**

**Figure A.2.1** – Infrared spectrum of ELO and DMAP before curing

**Figure A.2.2** – Infrared spectrum of ELO and DMAP after curing

**Figure A.4.1** – TG and DTG curves of epoxidised linseed oil (25-625°C, 10 °C/min)

**Figure A.4.2** – TG and DTG curves of film with native high amylose starch (25-625°C, 10 °C/min)

**Figure A.4.3** – TG and DTG curves of film with gelatinised starch (25-625°C, 10 °C/min)

**Figure A.4.4** – TG and DTG curves of film with retrograded starch (25-625°C, 10 °C/min)

**Figure A.4.5** – Infrared spectrum of expanded starch in toluene

**Figure A.4.6** – Infrared spectrum of homopolymerisation of ELO

**Figure A.5.1** – Infrared spectrum of acetic anhydride

**Figure A.5.2** – Infrared spectrum of acetic acid

**Figure A.5.3** – Infrared spectrum of maleic anhydride

**Figure A.5.4** – Infrared spectrum of succinic anhydride

**Figure A.5.5** – Infrared spectrum of itaconic anhydride

**Figure A.5.6** – IR spectra of evolved gases from TG-FTIR analysis of A) itaconic acid and B) itaconic anhydride modified starch

**Figure A.5.7** – Infrared spectrum of succinic anhydride modified starch taken at the maximum rate of decomposition (286.33 °C)

# List of tables

## Chapter 1

**Table 1.1** – Compositions of industrially important plant oils in % (R (x:y) = composition of the fatty acids; x= chain length in carbon atoms; y= number of double bonds)

**Table 1.2** – Iodine value of important plant oils

**Table 1.3** – Variation of fatty acid composition in linseed oil

**Table 1.4** – Use of starch in industry

**Table 1.5** – Morphology of starch granules from different botanical sources

**Table 1.6** – Amylose content of starches from different botanical sources

**Table 1.7** – Modified starches, their properties and applications

**Table 1.8** – Gelatinisation temperature and enthalpy of starches from different botanical sources

**Table 1.9** – Retrogradation temperature and enthalpy of starches from different botanical sources

## Chapter 2

**Table 2.1** – Tertiary amine and imidazole catalysts

**Table 2.2** – Top 12 biomass-derived platform molecules

**Table 2.3** – IR assignment of characteristic bands of epoxidised linseed oil

**Table 2.4** – Thermal analysis data of epoxidised linseed oil with bi-derived crosslinkers

**Table 2.5** – IR assignment of characteristic bands of Pripol

**Table 2.6** – MDSC analysis of formulations with different catalysts

## Chapter 3

**Table 3.1** – Degradation temperature of acid hydrolysed starches

**Table 3.2** – Degradation temperature of acid hydrolysed high amylose starch in water (method 1)

**Table 3.3** –  $^{13}\text{C}$  CP MAS NMR peak assignment of native starches (NC – Normal corn and HAS – High Amylose Corn) and acid hydrolysed starches (type of starch-hydrolysis time)

#### **Chapter 4**

**Table 4.1** – Surface area of native, gelatinised starch (GS) and retrograded starch (RS)

**Table 4.2** –  $^{13}\text{C}$  CP MAS NMR peak assignment of native high amylose starch, gelatinised starch (GS) and retrograded starch (RS)

**Table 4.3** – Thermal characteristics of native and modified starches

**Table 4.4** – Summary of TGA results of films with various amounts of starch

**Table 4.5** – Summary of TGA results of films with native or gelatinised or retrograded starch

**Table 4.6** – MDSC results of starch formulations

**Table 4.7** – MDSC results of various formulations 1) ELO, 2) ELO and DMAP, 3) ELO, GS and DMAP, 4) Pripol, GS and DMAP

#### **Chapter 5**

**Table 5.1** – Degree of substitution of esterified starches

**Table 5.2** – Thermal characteristics of unmodified expanded starch and esterified starches

**Table 5.3** – Thermal characteristic of the films with unmodified expanded starch and esterified starches

**Table 5.4** – MDSC of esterified starch formulations

#### **Chapter 7**

**Table 7.1** – Amount of crosslinkers in the formulation(molar ratio crosslinker:ELO = 2.5:1)

**Table 7.2** – Curing time required for different formulations

# Acknowledgments

Firstly I would like to thank Professor James Clark and Dr Avtar Matharu for giving me the opportunity to do this PhD. I am grateful for their supervision and encouragement, for providing me the chance of attending and presenting at several international conferences. For financial assistance I would like to thank the Thai Government. I would also like to thank all the members of the Royal Thai Embassies in both London and Paris who have helped during my studies in the UK and France. I would like to thank Armstrong World Industries for collaborating in the project.

I would like to thank several people for their technical support during this project. Paul Elliott for his assistance in the lab. Dr Meg Stark and Karen Hodgkinson for their assistance with SEM. Heather Fish for providing training on the departments NMR service. Dr David Apperley for the solid state NMR service. Dr Vitaly Budarin for his assistance with thermal analysis. Emma Cooper for helping me with the XRD and Cinthia Mena-Durán for her help with the porosimeter.

I would like to particularly thank Dr Peter Shuttleworth for all his help and guidance. A big thanks must also be given to all the people who have helped in proof reading my thesis, including James, Andy, Peter, Peter Hunt and Avtar. Many thanks to James, Avtar, Tom, Rob, Vitaly and Andy for helping prepare for the viva. Huge thanks to all members of the group past and present that have helped with work and have also attended some of the great green chemistry nights out.

I have had a great time in York, thank to all the wonderful people I have met – Camino, Brigid, Blanca, Chema, Olga, Lorenzo and many many more. Thank you all for the amazing memories. Also, thanks to P'Aim and Nat for the great visits from Leeds. I would like to make a very special thank you to Andy (Jao Bun) Hunt for his help, inspiration, understanding and especially for his love. Thanks for taking care of me Jao Bun – You're the best!

Finally to my family, thank you Mum, Dad, P'Pui and Nooch for their love and support throughout my studies in York and also Strasbourg. Thanks for believing in me and always being there for me.





# Declaration

Some of the results of this thesis were obtained by, or in collaboration with other workers, who are fully acknowledged in the text. All other results are the work of the author.

Nontipa Supanchaiyamat

September 2012



# Chapter 1

## *Introduction*



## 1.1 Sustainable development and green chemistry

Mankind has recklessly exploited the Earth's resources for decades by indiscriminately cutting trees in the forests, polluting water supplies and the atmosphere resulting in the extinction of a number of species, ozone depletion and climate change.<sup>1</sup> World governments and organisations have realised these concerns and have put in place policies in the hope of redeeming the situation. One of the key milestones was the formation of the World Commission on Environment and Development (WCED) in 1983 and subsequent publication of their report called "*Our Common Future*" in 1987 (also called "Brundtland report" as the Commission was chaired by then prime minister of Norway, Gro Harlem Brundtland).<sup>2</sup> The definition of sustainable development mentioned in this report is widely accepted and the term was defined as "the development that meets the needs of the present without compromising the ability of future generations to meet their own needs".<sup>3</sup> *Figure 1.1* demonstrates sustainability as a balance between societal, economic and the environmental needs.<sup>4</sup> Sustainable development may be achieved as the economy continuously develops, social equity improves and the environment is protected in unison.<sup>5</sup>



**Figure 1.1 – The three spheres of sustainability (Originally in colour)**

For the main part of the last century, chemistry was associated with new ideas, discovery and innovation, prompting a very positive image. However, in the last few decades, the public image of chemistry has become negative due to increasing hazards, life-threatening accidents and environmental pollution.<sup>6</sup> In the 1990's, Anastas and Warner developed the concept of green chemistry, “the invention, design and application of chemical products and processes to reduce or to eliminate the use and generation of hazardous substances”,<sup>7</sup> with 12 principles of green chemistry (stated below). Today, green chemistry is recognised and widely accepted as a way to pursue sustainable development.

## **The 12 principles of green chemistry:<sup>7</sup>**

### **1. Prevention**

It is better to prevent waste than to treat or clean up waste after it has been created.

### **2. Atom Economy**

Synthetic methods should be designed to maximise the incorporation of all materials used in the process into the final product.

### **3. Less Hazardous Chemical Syntheses**

Wherever practicable, synthetic methods should be designed to use and generate substances that possess little or no toxicity to human health and the environment.

### **4. Designing Safer Chemicals**

Chemical products should be designed to effect their desired function while minimising their toxicity.

### **5. Safer Solvents and Auxiliaries**

The use of auxiliary substances (e.g., solvents, separation agents, etc.) should be made unnecessary wherever possible and innocuous when used.

### **6. Design for Energy Efficiency**

Energy requirements of chemical processes should be recognised for their environmental and economic impacts and should be minimised. If possible, synthetic methods should be conducted at ambient temperature and pressure.

### **7. Use of Renewable Feedstocks**

A raw material or feedstock should be renewable rather than depleting whenever technically and economically practicable.

### **8. Reduce Derivatives**

Unnecessary derivatisation (use of blocking groups, protection/ deprotection, temporary modification of physical/chemical processes) should be minimised or avoided if possible, because such steps require additional reagents and can generate waste.

### **9. Catalysis**

Catalytic reagents (as selective as possible) are superior to stoichiometric reagents.

### **10. Design for Degradation**

Chemical products should be designed so that at the end of their function they break down into innocuous degradation products and do not persist in the environment.

### **11. Real-time Analysis for Pollution Prevention**

Analytical methodologies need to be further developed to allow for real-time, in-process monitoring and control prior to the formation of hazardous substances.

### **12. Inherently Safer Chemistry for Accident Prevention**

Substances and the form of a substance used in a chemical process should be chosen to minimise the potential for chemical accidents, including releases, explosions, and fires.

## **1.2 Polymers and biopolymers**

The word “polymer” is derived from the Greek words “poly” meaning many and “meros” meaning parts or units.<sup>8</sup> According to IUPAC Gold Book, a polymer (also called macromolecule) is “a molecule of high relative molecular mass, the structure of which essentially comprises the multiple repetitions of units derived, actually or conceptually, from molecules of low relative molecular mass”.<sup>9</sup> Polymers can generally be divided into two categories in accordance with their thermal response.<sup>10</sup> Thermoplastics are repeatedly softened upon heating, whilst thermosets are polymers that once cured, cannot be melted again even at high temperature.<sup>11</sup> The most commonly utilised thermoplastics are polyethylene terephthalate (PET), high-density polyethylene (HDPE), low-density polyethylene (LDPE), polyvinyl chloride (PVC), polypropylene and polystyrene with applications in packaging, plastic bottles, trays and bags. The most common groups of thermosets are unsaturated polyesters, which are mainly applied to glass fibre reinforced materials, and epoxy resins which are extensively used in composites, coating and adhesives.<sup>12</sup> These polymers are typically

derived from petroleum, which makes them non-renewable. Moreover, they tend to have low rate of degradability, especially in landfills where oxygen and water penetration are limited.<sup>13</sup>

There are a number of naturally occurring polymers (or biopolymers), for example cellulose, starch, rubber and proteins. Biopolymers can be roughly classified into three different categories: i) polysaccharides, ii) proteins and iii) polynucleotides. Due to their unique natural properties, biopolymers are found in a number of various applications, including the food industry, coatings, adhesives, fuel and packaging materials. Moreover, these naturally occurring polymers are widely available, renewable, mostly low in cost and importantly more environmentally friendly than petroleum based polymers.<sup>14</sup>

By examining the 12 principles of green chemistry, the use of biopolymers agrees with the 7<sup>th</sup> principle, which encourages the use of renewable feedstocks. The utilisation of renewable resources has an added benefit as they are considered carbon neutral.

## **1.3 Plant oils**

### **1.3.1 General**

Plant oils are triglyceride esters of fatty acids with various chain lengths and functionalities depending on the plant, the crop, the season and the growing conditions (*Figure 1.2 and Table 1.1*).<sup>15</sup> Plant oils are globally available and offer the potential for high performance biomass derived materials.<sup>16</sup> In 2010/2011, the world production of major oils (coconut, cottonseed, olive, palm, palm kernel, peanut, rapeseed, soybean and sunflower seed) rose to 147.33 million metric tonnes (MMT) from 84.6 MMT in 1999/2000, representing a growth of approximately 74%.<sup>17</sup> The majority of plant oils produced are utilised within the food industry except for castor and linseed oils, which are mainly used in non-food applications such as lubricants, surface coatings and plastics.<sup>18-20</sup>



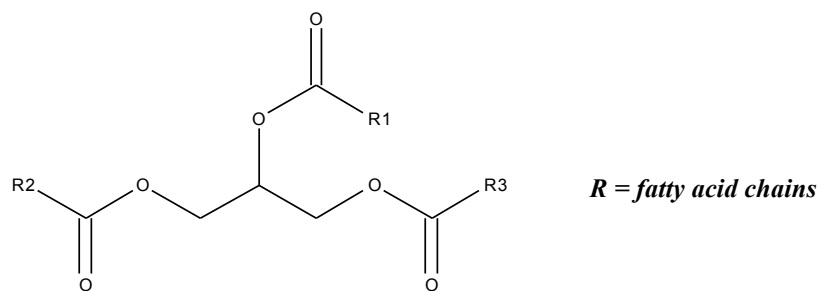


**Figure 1.2 – Generic triglyceride structure**

**Table 1.1 – Compositions of industrially important plant oils in % (R (x:y) = composition of the fatty acids; x= chain length in carbon atoms; y= number of double bonds)<sup>15</sup>**

Fatty acid content (%)									
	Capric	Lauric	Myristic	Palmitic	Stearic	Oleic	Linoleic	Linolenic	Arachidic
<b>R (x,y) =</b>	10:0	12:0	14:0	16:0	18:0	18:1	18:2	18:3	20:0
<b>Sunflower</b>	-	-	-	6	4	28	61	-	-
<b>Palm kernel</b>	5	50	15	7	2	15	1	-	-
<b>Linseed</b>	-	-	-	5	4	22	15	52	-
<b>Soybean</b>	-	-	-	10	5	21	53	8	0.5
<b>Rapeseed</b>	-	-	0.5	4	1	60	20	9	2
<b>Cotton seed</b>	-	-	0.7	21.6	2.6	18.6	54.4	0.7	0.3
<b>Corn</b>	-	-	0.1	4.1	2	25.4	59.6	1.2	0.7

The chemical and physical properties of the oils typically depend on their degree of unsaturation, the length of the fatty acid chain, and the double bond stereochemistry.<sup>15</sup> Higher melting temperature of vegetable oils are typically obtained with long chain fatty acids, a low number of carbon-carbon double bonds and an *E* (*trans*) configuration.<sup>21</sup> The most common fatty acids in plant oils are presented in *Figure 1.3*. Most of the fatty acids in plant oils possess long straight chains with an even number of carbons and their unsaturation is in *Z* (*cis*) configuration. Some fatty acids contain interesting functionalities such as an epoxide in vernolic acid (*Figure 1.3 I*) and a hydroxyl in ricinoleic acid (*Figure 1.3 J*).

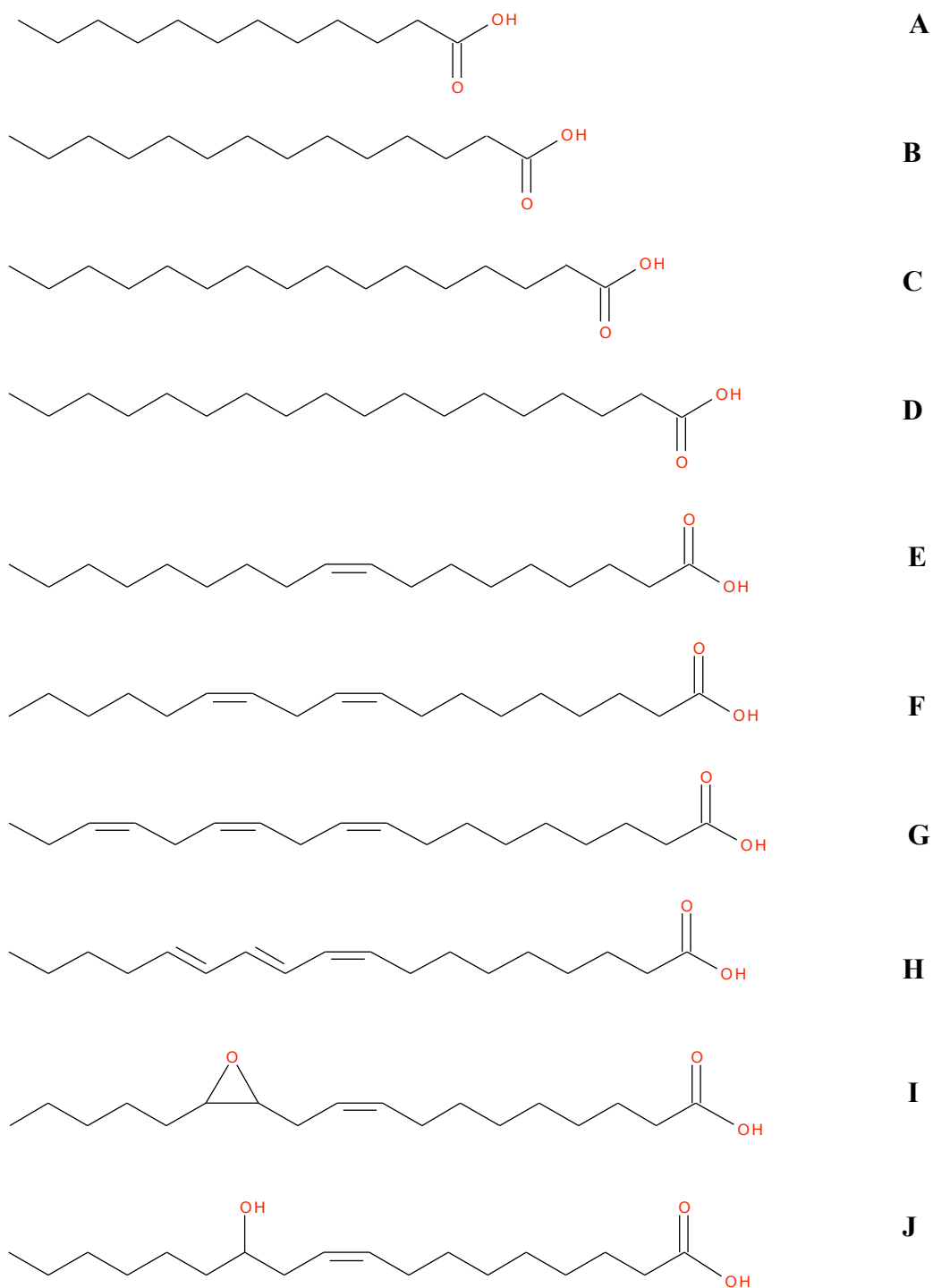


**Figure 1.3 – Structure of common fatty acids: A) lauric acid, B) myristic acid, C) palmitic acid, D) stearic acid, E) oleic acid, F) linoleic acid, G) linolenic acid, H)  $\alpha$ -eleostearic acid, I) vernolic acid, J) ricinoleic acid**

The degree of unsaturation of plant oils is typically determined by measuring the iodine value, which represents the amount of iodine (in g) needed to react with carbon-carbon double bonds in 100 g of vegetable oil. Iodine values of some important vegetable oils in industry are demonstrated in *Table 1.2*. Oils with iodine values greater than 170 are classified as drying oils, owing to the hardening of these oils when exposed to air.<sup>22</sup> Semi-drying oils are those with an iodine value between 100 and 170. Those with an iodine value less than 100 are considered as non-drying oils.<sup>15, 21</sup>

**Table 1.2 – Iodine value of important plant oils<sup>23</sup>**

Plant oils	Iodine value (g (I <sub>2</sub> )/ 100 g oil)
Palm	35-61
Castor	82-88
Rapeseed	94-120
Cottonseed	90-140
Sunflower	110-143
Soybean	117-143
Linseed	168-204

The presence of alkenic functionalities in these oils allows various kinds of polymerisation to occur and also enables a variety of transformations.<sup>24</sup> The most reported modifications to plant oils are for example, radical addition, epoxidation<sup>25</sup> and metathesis.<sup>26, 27</sup>

### 1.3.2 Epoxidation of plant oils

In the epoxidation process, alkene moieties are oxidised to their epoxides, usually in the presence of peroxyacids. Transfer of the oxygen atom from peroxyacid to the alkene occurs via *syn* stereochemistry. Both C-O bonds form on the same face of the double

bond in a one-step concerted mechanism (*Figure 1.4*).<sup>28</sup> Hence, a *cis* alkene leads to a *cis* epoxide and a *trans* alkene to a *trans* epoxide.<sup>20</sup>

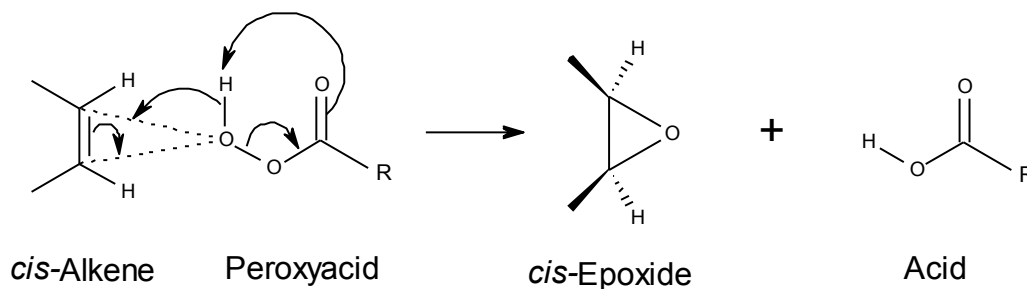


**Figure 1.4 – Epoxidation using peroxyacid**

Epoxidation of unsaturated vegetable oils is industrially carried out by the Prileshajev-epoxidation. A short chain peroxyacid is either pre-formed or *in situ*-generated in the process. In large-scale production the *in situ*-generated acid is preferred considering the danger of handling peroxyacids (*Figure 1.5*). The formation of the peroxyacid in the reaction mixture is a reversible reaction, catalysed by a strong acid catalyst, such as sulfuric acid or an acid ion exchanger.<sup>29, 30</sup> The use of a strong mineral acid leads to many side reactions via epoxide ring-opening and to the formation of diols, hydroxyesters, estolides (fatty acid esters) and other dimers.<sup>31</sup> As a result, the oxirane conversion scarcely exceeds 80%. The use of a strong mineral acid and the formation of the hazardous peroxyacid during the epoxidation make this reaction less attractive. Thus, numerous research has looked at other methods i.e. catalysis in order to improve the selectivity and the “greenness” of this reaction.

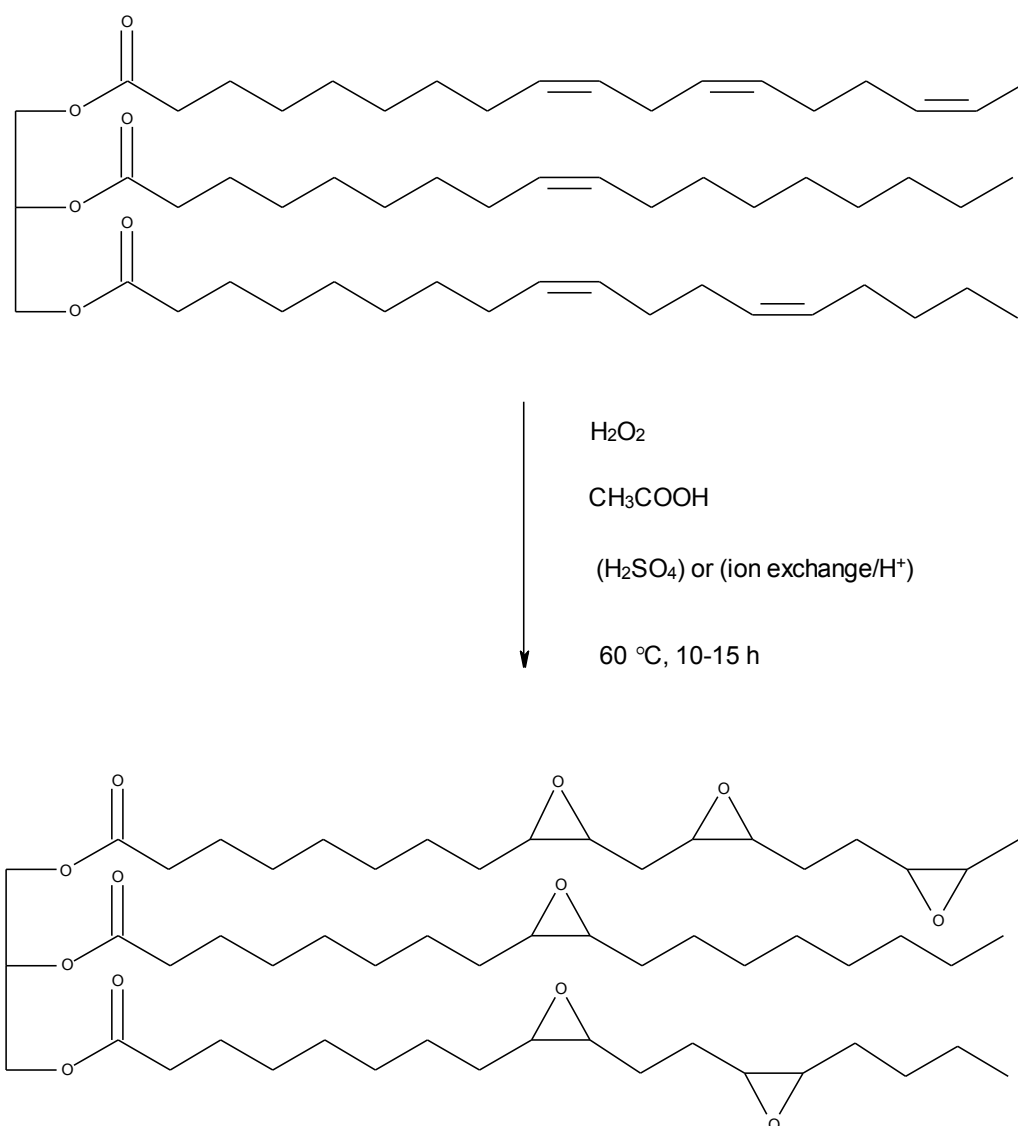


**Figure 1.5 – Prileshajev epoxidation**

Acidic ion exchange resin (AIER) is safer to handle and as such is utilised to minimise the use of strong mineral acid. The porous structure of the solid catalyst and the size of the triglyceride molecules of the vegetable oils induce less side reactions and therefore better selectivity can be obtained.<sup>32</sup> Furthermore, the fact that the AIER is in solid state facilitates the separation between the catalyst and the reaction product. The recovered catalyst was found to be reusable with minimal loss of activity.<sup>33</sup> The selectivity of the reaction was found to depend on several parameters including temperature, formic/acetic acid to ethylenic unsaturation molar ratio, the presence of an inert solvent (stabilises the reaction and minimises side reactions), hydrogen peroxide to ethylenic unsaturation molar ratio and AIER loading. At optimum conditions the conversion of alkene to oxirane can reach 90%.<sup>33, 34</sup>

Chemo-enzymatic epoxidation has attracted a great deal of interest due to its environmentally friendly attributes. Not only can it function in the absence of a strong acid as a catalyst it also showed good epoxide selectivity and conversion under mild conditions.<sup>35</sup> Schneider *et al.* reported that lipase from *Candida antarctica* was very efficient for epoxidation of methyl esters of sunflower oil, showing an oxirane conversion greater than 99%.<sup>36</sup> Moreover, Warwel *et al.* reported that lipase catalysts were still active after fifteen uses.<sup>37</sup>

Other systems include the use of metal catalysts such as titanium,<sup>38</sup> molybdenum,<sup>39</sup> tungsten<sup>40</sup> or rhenium.<sup>41</sup> Epoxidation with molecular oxygen using silver catalyst, which is claimed to be an environmentally friendly method, is also known, however it is mostly restricted to small molecules, such as ethylene and butadiene.<sup>42</sup>

### 1.3.3 Plant oils based epoxy resins

Epoxidised plant oils (EPO) are a great potential feedstock for the production of bio-based polymers especially thermosetting polymers. Thermosetting resins are highly-crosslinked polymers that are cured by heat, pressure, light radiation or a combination of these energy sources.<sup>43</sup> Chakrapani *et al.* investigated the polymerization of epoxidised castor oil (ECO) in the presence of diaryliodonium salt as photoinitiator. ECO was found to have superior reactivity in photoinitiated cationic polymerisation compared to other epoxidised oils. This is believed to be caused by the presence of the hydroxyl groups in the ECO molecules.<sup>44</sup> A similar observation was noted by Ortiz *et al.*, the addition of different methoxy-substituted benzyl alcohols accelerated the curing rate of cationic photopolymerisation of various epoxidised vegetable oils.<sup>45</sup> This is explained on the basis of “activated monomer mechanism” (*Figure 1.6*).<sup>44, 45</sup> Crivello *et al.* also studied the polymerisation of epoxidised plant oils using different onium salts as initiators. The rate of photopolymerisation rate was found to be dependent on the structure of the anionic and cationic photoinitiators and the structure and the epoxy content of the triglyceride monomers.<sup>46</sup> Park *et al.* investigated the polymerisation of ECO and epoxidised soybean oil (ESO) using *N*-benzylpyraziniumhexafluoroantimonate or *N*-benzylquinoxaliniumhexafluoroantimonate as catalysts. The crosslinking density was found to be catalyst dependent, hence glass transition temperature ( $T_g$ ), coefficient of thermal expansion and the mechanical properties of the

product can be differentiated.<sup>47</sup> Furthermore, ECO showed a higher  $T_g$  value and lower coefficient of thermal expansion than those of ESO, which can be attributed to greater number of intermolecular interactions, such as hydrogen bonding in the ECO system.<sup>48</sup>

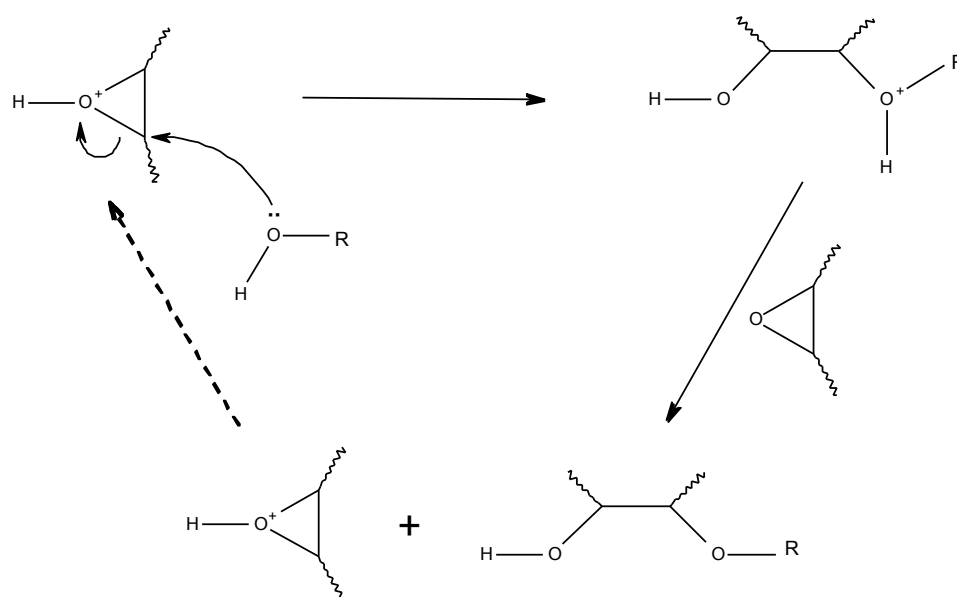


**Figure 1.6 – Activated monomer mechanism**

EPO are on numerous occasions combined with acid anhydrides crosslinkers, in particular, maleic anhydride and unsubstituted- and substituted-phthalic anhydrides.<sup>49-51</sup> Boquillon *et al.* suggested that the structure and the concentration of the crosslinkers played an important role in indicating the properties of the polymerised products. They found that methyl-endomethylenetetrahydrophthalic anhydride and phthalic anhydride showed lower crosslinking density than that of *cis*-1,2,3,6-tetrahydrophthalic anhydride due to steric hindrance and rigid diester segment formed during the cure respectively (*Figure 1.7*).<sup>49</sup> According to Gerbase *et al.* ESO cured with cyclic anhydrides showed thermoset properties.<sup>50</sup> This study showed that anhydrides with rigid structure such as maleic anhydride, phthalic anhydride and hexahydrophthalic anhydride exhibited higher  $T_g$ . Moreover, the augmentation of the epoxide groups in ESO also increased the  $T_g$  of the products.<sup>50</sup>



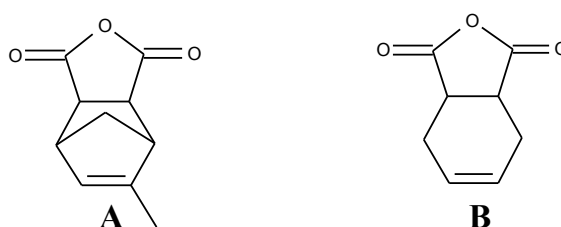


**Figure 1.7 – Structures of A) methyl-endomethylenetetrahydrophthalic anhydride and B) cis-1,2,3,6-tetrahydrophthalic anhydride**

Another method to improve the properties of epoxy plant oils based resin is to blend the epoxidised oils with other compounds. Blends of EPO with diglycidyl ether of bisphenol-A (DGEBA) have intensively investigated by Jin and Park.<sup>52-54</sup> The impact strength of the DGEBA based resin significantly improved with the addition of ESO, which was due to the intermolecular interaction in DGEBA/ESO blends. Moreover, the adhesive lap shear strength increased with the amount of ESO in the resin with the maximum value when 40% of ESO present in the resin.<sup>52</sup> The addition of ECO in the DGEBA based resin could also considerably improve the mechanical properties of the system. This could be due to the inclusion of the soft large segments of ECO in the resin, which enhances the flexibility of the product.<sup>53</sup>

EPO have also been blended with inorganic compounds in order to obtain composite materials. Copolymerisation of epoxidised linseed oil (ELO) and 3-glycidylpropylheptaisobutyl-T8-polyhedral oligomeric silsesquioxane (G-POSS, *Figure 1.8*) resulted in a bio-based nanocomposite. The storage modulus and the  $T_g$  of the composite were higher than those of ELO resin without G-POSS. This was attributed to the reinforcement effect of the G-POSS cage.<sup>55</sup> Moreover, EPO/clay composites were also developed using ESO or ELO and octadecyl-modified montmorillonite.<sup>56</sup> The homogenous materials of organic and inorganic components with good flexibility were obtained with the silicate layers of the clay intercalated and distributed randomly in the polymer matrix.

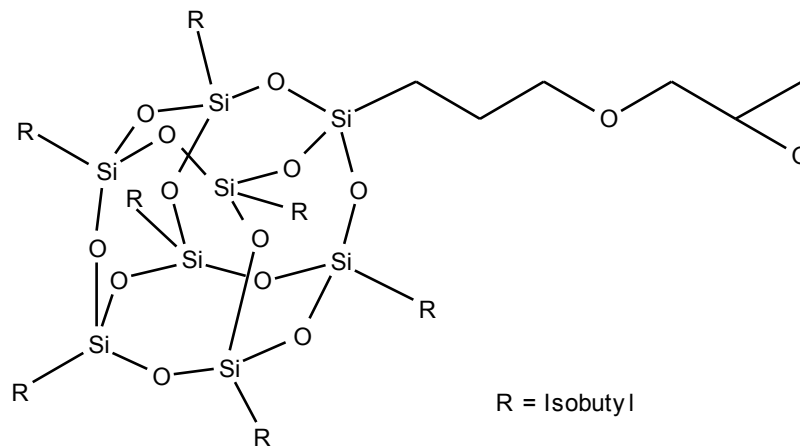


**Figure 1.8 – Structure of 3-glycidylpropylheptaisobutyl-T8-polyhedral oligomeric silsesquioxane (G-POSS)**

### 1.3.4 Linseed oil and epoxidised linseed oil

Linseed oil (LO) is obtained from flax seeds which are traditionally ground into to a fine powder and pressed to extract the oil.<sup>57</sup> It has been used intensively as a medium for paints for hundreds of years due to its capacity of forming a thin film with good optical and mechanical properties after being spread.<sup>58</sup> LO is considered as a drying oil (*cf.* section 1.3.1) as it dries quickly in exposure to air via auto-oxidation as shown in *Figure 1.9*.<sup>59-61</sup>

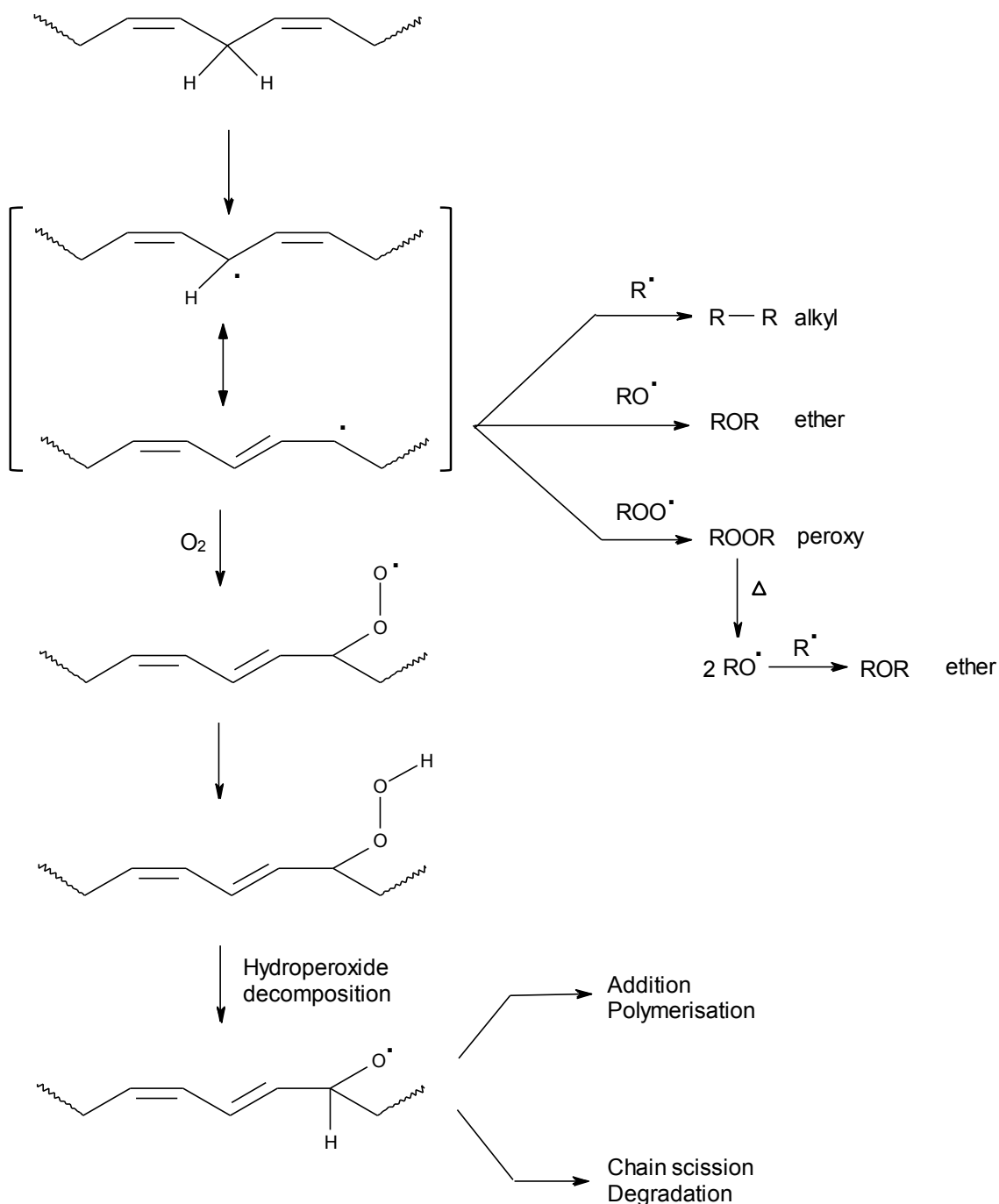
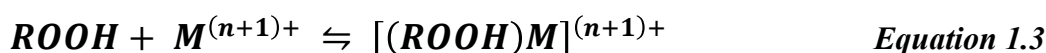
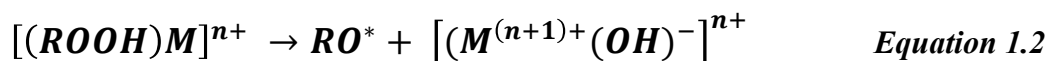
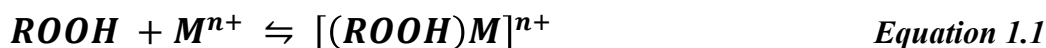


**Figure 1.9 – Auto-oxidation mechanism of drying oils<sup>59-61</sup>**

Although the curing of drying oils automatically occurs on exposure to air, the curing time is considered as being practically too long for commercial applications (several days or weeks). Thus, these drying oils often undergo thermal treatment ( $>270^\circ\text{C}$ ) in the absence of oxygen resulting in polymerisation of the double bonds in the triglyceride molecules. The oils hence become more viscous and they are commonly known as “stand oils”.<sup>62</sup> Another common method to accelerate the drying process is

the addition of metallic compound driers.<sup>59</sup> This can promote the formation of peroxide radicals, initiators of auto-oxidative reaction.<sup>63</sup> Peroxide radical formation via metal hydroperoxide decomposition is demonstrated in *equations 1.1-1.4*.<sup>64, 65</sup>



As stated previously plant oils are mixtures of different triglycerides. LO is mainly comprised of highly unsaturated triglycerides, rich in linoleic acid (C18:2) and linolenic acid (C18:3). Moreover, LO also contains phytosterols, phospholipids and vitamins.<sup>66</sup> The relative amount of fatty acids composition in LO depends largely on the climate and the variety of *Linum usitatissimum* of the seeds as shown in *Table 1.3*.<sup>57</sup>

**Table 1.3 – Variation of fatty acid composition in linseed oil**

Fatty acid	Percentage of total fatty acid (%)			
	Europe	Canada	Argentina	India
Palmitic acid (16:0)	4-6	5-6	4-5	9-10
Linolenic acid (18:3)	56-71	54-61	45-53	50-61
Linoleic acid (18:2)	12-18	14-16	15-24	13-15
Oleic acid (18:1)	10-22	19-20	19-21	10-21
Stearic acid (18:0)	2-3	3-4	5-6	7-8

Epoxidised linseed oil (ELO) (*Figure 1.10*) is commercially available and commonly used as plasticiser and stabiliser in polyvinyl chloride (PVC) and its copolymers. The

high molecular weight of ELO makes it comparable with other plasticisers in the polymer mixture.<sup>67</sup> Moreover, epoxidised seed oils, in particular, ELO and ESO, are known as HCl scavengers in PVC materials.<sup>68</sup> It is well known that HCl is produced during the degradation of PVC. Epoxidised compounds decrease the degradation rate of the polymer especially when being used with metal co-stabilisers.<sup>69</sup>

Other applications of ELO include coatings and adhesives.<sup>70</sup> In flooring applications, linseed oil (or oxidised linseed oil) is utilised in linoleum sheets invented by Frederik Walton in 1860 and is still in current use.<sup>71</sup>

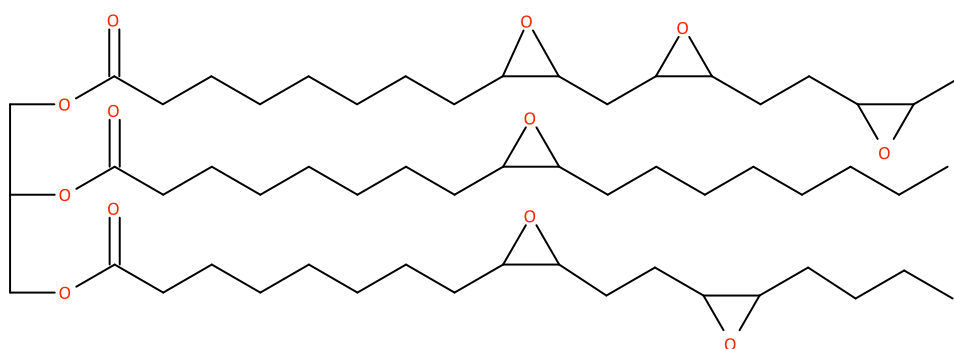


**Figure 1.10 – Epoxidised linseed oil (ELO)**

## 1.4 Starch

### 1.4.1 General

Starch is one of the most abundant biopolymers on the planet alongside cellulose and chitin.<sup>72</sup> Starch is used as an energy storage in plants and is typically found in the form of granules in the plastids of plants.<sup>73</sup> Owing to its versatility, low cost and abundance, starch has numerous applications in both food and non-food industries (*Table 1.4*).<sup>74</sup> The International Starch Institute estimated the world utilisation of starch in 2008 at approximately 66 MMT and expected it to reach 75 MMT in 2012.<sup>75</sup> Different botanical sources of starch greatly influence the properties of the granules including granule size and shape (*Table 1.5*) and the starch composition, which will be discussed in the following section.

**Table 1.4 – Use of starch in industry<sup>76</sup>**

Industry	Use of starch/modified starch
Adhesive	Adhesive production
Agrochemical	Mulches, pesticide delivery, seed coating
Cosmetics	Face and talcum powder
Detergent	Surfactants, builders, co-builders, bleaching agents and bleaching activators
Food	Viscosity modifiers, glazing agents
Medical	Plasma extenders/replacers, transplant organ preservation, absorbent sanitary products
Oil drilling	Viscosity modifier
Paper and board	Binding, sizing, coating
Pharmaceutical	Diluent, binder, drug delivery
Plastics	Biodegradable filler
Purification	Flocculants
Textile	Sizing, finishing and printing, fire resistance

**Table 1.5 – Morphology of starch granules from different botanical sources** <sup>77</sup>

Starch source	Shape	Average Size ( $\mu\text{m}$ )
Elephant yam	Polygonal	17.6 $\pm$ 6.8
New cocoyam	Spherical, polygonal	20.7 $\pm$ 8.1
Sweet potato	Round, polygonal	22.7 $\pm$ 11.4
Kudzu	Round, polygonal	19.9 $\pm$ 7.8
Arrowroot	Oval, spherical	35.1 $\pm$ 16.0
Sago	Oval, spherical	34.3 $\pm$ 22.5
Taro	Polygonal	5.3 $\pm$ 1.5
Yam bean	Spherical, polygonal	7.7 $\pm$ 4.1
Cassava	Round	23.2 $\pm$ 21.4
Corn	Round, polygonal	21.42 $\pm$ 6.2
Rice	Polygonal	4.7 $\pm$ 1.4
Edible canna	Oval, elliptical	38.7 $\pm$ 30.2
Water yam	Rod-like, round	33.8 $\pm$ 14.8
Potato	Oval, Spherical	42.3 $\pm$ 38.1
Lesser Yam	Polygonal	4.9 $\pm$ 1.3

## 1.4.2 Starch composition and organisation of starch granules

Starch is composed of two basic molecular components: amylose and amylopectin, which are both polymers of D-glucose with  $\alpha$ -linkages (*Figure 1.11*).<sup>78</sup> The structure of amylose and amylopectin are identical in terms of their constituent basic units but, differ in their structural organisation. Amylose is a relatively linear molecule, consisting of glucose units linked by  $\alpha$ -1, 4 glycosidic linkages with the molecular weight in the region of  $1 \times 10^5$  -  $1 \times 10^6$  Da. Whilst amylopectin is a highly branched molecule, comprising of an  $\alpha$ -1, 4 backbone structure with approximately 5%  $\alpha$ -1, 6 glycosidic links (molecular weight in the region of  $1 \times 10^7$  -  $1 \times 10^9$  Da).<sup>79, 80</sup> The ratio of amylose to amylopectin in starch varies depending on its botanical origin and also environmental conditions (*Table 1.6*).<sup>81, 82</sup> Naturally occurring starches typically have the amylose content in the range of 17 - 28%. However, genetic mutation allows the production of starch with an amylose content as high as 70% (amylomaize) through to practically 0% (waxy maize).<sup>83</sup> The ratio of amylose to amylopectin in starch determines some of its key physical and mechanical properties and can be one of the key factors in determining its non-food applications.<sup>84</sup> Amylose shows better film formation than amylopectin which gives weak and brittle films.<sup>85</sup>



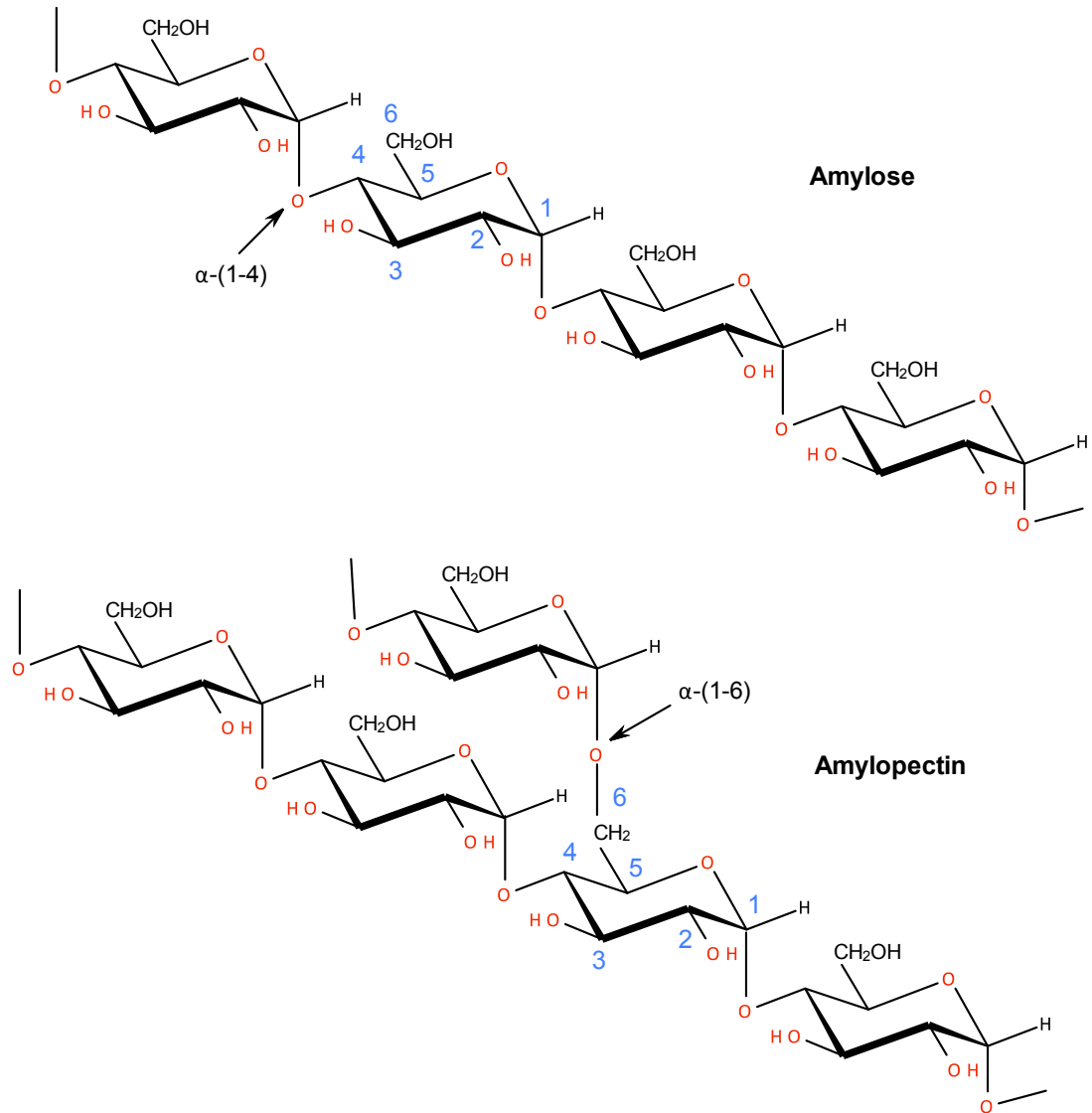


**Figure 1.11 – Structures of amylose and amylopectin (Originally in colour)**

**Table 1.6 – Amylose content of starches from different botanical sources<sup>86, 87</sup>**

Starch sources	Amylose content (%)
Corn	22.4-32.5
High amylose corn	41.6-69.8
Waxy corn	1.4-2.7
Rice	5-28.4
Wheat	18-31.6
Potato	20.1-31

It is well known that starch possesses a semi-crystalline structure.<sup>88, 89</sup> The starch granule crystallinity is associated with its amylopectin content. Studies using X-ray diffraction (XRD) and molecular modelling suggested that amylopectin chains form double helices with 6 glucoses units per turn.<sup>73</sup> These helices associate in clusters to form organised regions also called “crystalline lamellae”.<sup>89</sup> Stacks of crystalline lamellae which are approximately 5-7 nm thick, form the backbone of the starch granules.<sup>90, 91</sup> The concentric crystalline lamellae are interrupted by amorphous lamellae (thickness in the region of 1-4 nm) which contain the branch points of the clusters (*Figure 1.12*).<sup>92</sup> Under polarised light starch granules show a characteristic birefringence pattern (often referred to as a Maltese cross) which reflects the radial arrangement of macromolecules in the granules.<sup>93</sup> Moreover, several reports revealed the existence of “blocklets” inside the crystalline and amorphous growth rings, a concept initially developed by Hanson and Katz in 1934 (*Figure 1.13*).<sup>90</sup> This concept was supported by recent research using atomic force microscopy (AFM) and scanning electron microscopy (SEM).<sup>94</sup> The double helices can assemble into two different types of hexagonal network creating two main polymorphic structures. The A-type polymorph has a more compact structure with a lower water content, whilst the B-type possesses a less dense structure with water channels creating a more open structure (*Figure 1.14*).<sup>89</sup>

The presence of moisture in the B-type polymorph was suggested to contribute to the lower melting point of this polymorphic form.<sup>95</sup> The A-type polymorph is often observed in cereal starches and the B-type polymorph is found in tuber and root starches. However, a third type polymorph (C-type) can occasionally be observed in some legumes such as smooth pea and has been proposed to be an intermediate type between A-type and B-type polymorphs.<sup>96</sup> Another distinct polymorphic structure is the V-type, which is believed to be composed of single helices of amylose forming complexes with various ligands.<sup>97</sup>

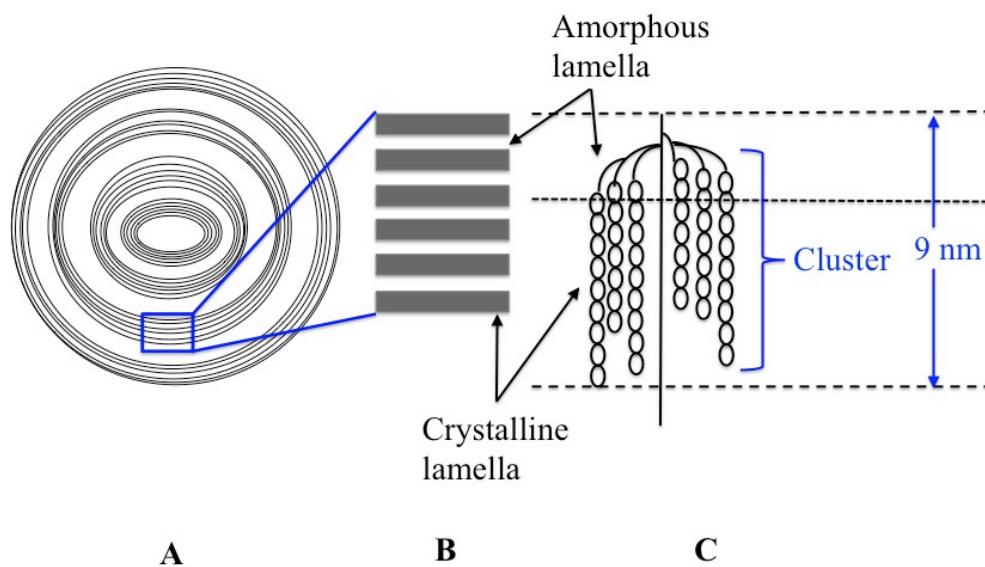


**Figure 1.12 – Lamellar structure of a starch granule: A) stacks of crystalline lamellae separated by amorphous growth rings, B) expanded view of the crystalline and amorphous region and C) double helices of amylopectin constitute the crystalline lamellae whilst the branch points of the clusters constitute the amorphous lamellae (adapted from reference 89)**

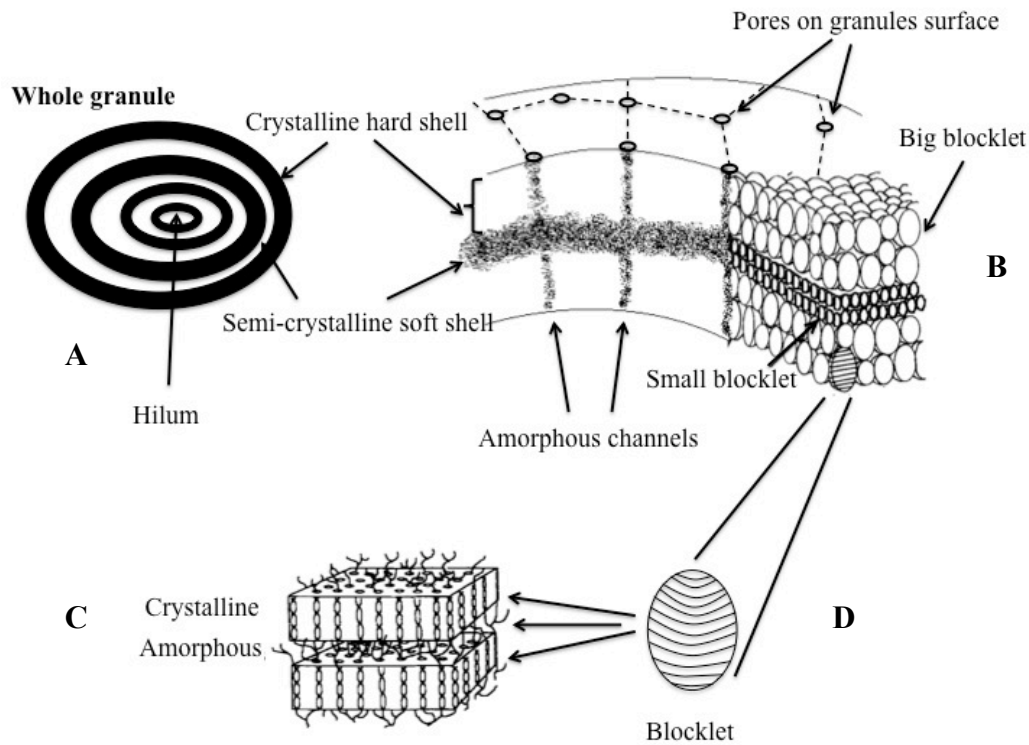


**Figure 1.13 – Starch granule structure: A) granule (2 - 100  $\mu\text{m}$ ), B) growth rings (120 - 500 nm), C) blocklets (20 - 50 nm) and D) amorphous and crystalline lamellae (9 nm) (adapted from references 90 and 98)**

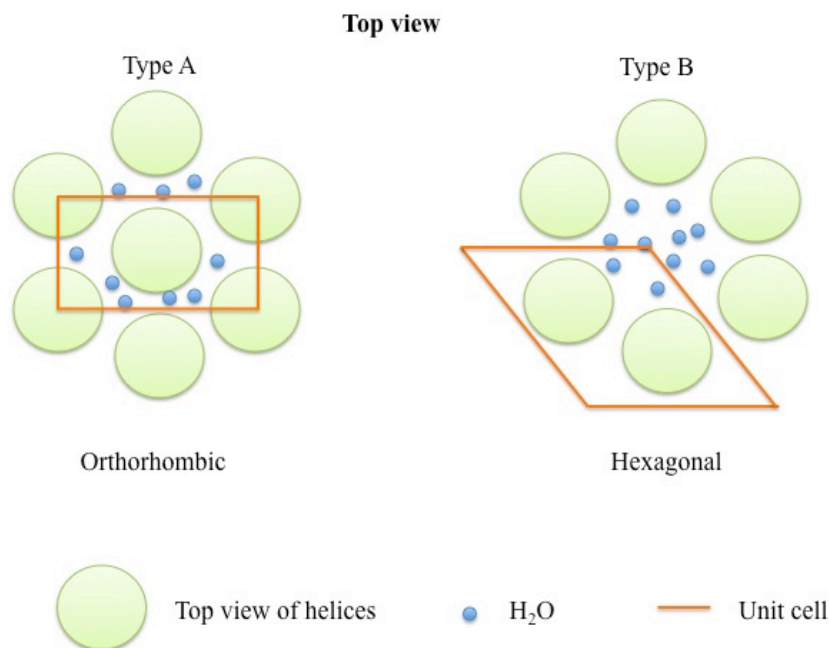


**Figure 1.14 – Top view of starch A- and B-polymorphs (Originally in colour)**

Apart from amylose and amylopectin, which represent approximately 98-99% of the dry weight, starch granules also contain small quantities of other components such as protein, lipids, and minerals (e.g. phosphorus). A fair amount of protein associated to starch granules can be found in cereal starches (0.25-0.5%) but less is present in tuber starches such as potato and tapioca (0.06 and 0.1% respectively).<sup>99</sup> Lipids are found mainly in the form of lysophospholipids (LPL) in wheat, rye and barley and free fatty acids (FFA) in maize.<sup>100</sup> These lipids form a complex with amylose and can represent up to approximately 2% by weight in high amylose starches.<sup>89, 99</sup> The properties of starch granules are affected by the presence of these proteins and lipids in or on the surface of the granules. For example, a high amount of lipids in cereals starches decreases the capacity of starch granules to bind with water, thus reducing the swelling and solubilisation of starch granules.<sup>99</sup> Three forms of phosphorus are found in starch granules: phosphate monoesters, phospholipids and inorganic phosphorus.<sup>89, 101</sup> Phosphate monoesters are largely present in root and tuber starches and covalently bound to amylopectin (up to 0.09% in potato starch). These phosphate groups in the granules prevent the formation of intra- or intermolecular bonds, which assists the molecular dispersion in solution resulting in starch paste clarity and viscosity increase.<sup>102, 103</sup>

### 1.4.3 Modification of starch

Modifications are often required to overcome the limitations of native starches. In particular in terms of their susceptibility to water, high viscosity (after cooking) and incompatibility with some hydrophobic polymers.<sup>104</sup> Modification can be processed physically or chemically, depending on the required properties.<sup>105</sup> *Table 1.7* summarises common methods of starch modification.

**Table 1.7 – Modified starches, their properties and applications**<sup>76, 106</sup>

Modification	Treatment (example)	Advantages over native starch	Applications
Pre-gelatinisation	Heat/ moisture	Cold water soluble	Instant convenience foods, oil drilling
Esterification	Acetic anhydride	Reduced set-back, increased clarity, forms film/fibres	Frozen foods, Instant foods
Partial acid or enzyme hydrolysis	Glycosidic bond cleavage	Increased retrogradation and set back, low hot paste viscosity, high gel viscosity	Confectionery, Textiles
Cationic substitution	Tertiary or quaternary ammonium compounds	Lowered gelatinisation temperature, Increased solubility and dispersability in cold water, and increased binding to negatively charged materials	Pigment retention aid in paper, sizing-coating, textile wrapping
Oxidation	Hypochlorite	Increased clarity, reduced set back	Thickeners, jellies, paper, textiles
Hydroxyalkylation	Propylene oxide	Increased clarity, increased stability	Salad dressing, paper and textile sizes
Cross-linking	Phosphate ester/ Epichlorohydrin	Granule stability, resistance to retrogradation, gelling	Soups, puddings, bakery products

### 1.4.3.1 Physical modification

#### 1.4.3.1.1 Gelatinisation

Starch granules are insoluble in cold water. However, their exposure to high humidity or suspension in water at specific temperatures can lead to absorption of water into the starch granules, which undergo limited irreversible swelling.<sup>107</sup> When heated in water above a critical temperature, the intermolecular hydrogen bonds of starch are weakened, allowing starch to imbibe more water. Penetration of water causes disruption of molecular order within the granules leading to decreased crystallinity in the starch structure. The process is known as gelatinisation of starch. This order-disorder transition involves dissociation of double helices, expansion of granules, loss of crystallinity and amylose leaching.<sup>108</sup> A wide range of techniques have been applied to investigate this phenomenon and different events can be observed during the gelatinisation, including the loss of crystallinity noted by XRD pattern, uptake of heat monitored by differential scanning calorimetry (DSC) and the increase of viscosity detected by rheological measurement.<sup>109, 110</sup> Gelatinisation process can be observed under a polarised light microscope equipped with a hot stage. The loss of the Maltese cross indicates the gelatinisation has occurred and the temperature at which this happens is the gelatinisation temperature.<sup>111</sup> Jenkins and Donald used combined techniques of small- and wide-angle X-ray scattering, DSC and small-angle neutron scattering to follow stages of the gelatinisation of starch in the excess of water. Their results suggested that the swelling initiates in the amorphous regions and once completely swollen the semi-crystalline stacks start to absorb water. The loss of crystallinity and the ultimate breakdown happen relatively late in the process.<sup>112</sup> The most intensively used technique to determine the gelatinisation temperature and the enthalpy change of this process is DSC.<sup>113, 114</sup> The thermogram of starch with excess of water shows an endothermic transition. The enthalpy of the process is the sum of the energy involved in the disruption of starch-starch bonds (endothermic), formation of starch-water bonds (exothermic) and the unwinding of double helices (endothermic).<sup>115</sup> The gelatinisation temperature and enthalpy change depend significantly on the composition and structure of the starch granule. Thus these gelatinisation properties vary with different botanical origins of starch (*Table 1.8*).<sup>116</sup>

**Table 1.8 – Gelatinisation temperature and enthalpy of starches from different botanical sources<sup>86</sup>**

Botanical source	T <sub>o</sub> (°C)	T <sub>p</sub> (°C)	T <sub>f</sub> (°C)	ΔH <sub>gel</sub> (J/g)
Corn <sup>a</sup>	62.3	67.7	84.3	14.0
High amylose corn <sup>b</sup>	66.8	73.7	-	13.7
Waxy corn <sup>b</sup>	66.6	73.6	-	14.2
Rice <sup>a</sup>	62.0	67.4	97.5	11.0
Wheat <sup>a</sup>	51.2	56.0	76.0	9.0
Potato <sup>a</sup>	57.2	61.4	80.3	17.4

*Dry starch/water = 1/1.5 (w/w)<sup>a</sup> or 1/9 (w/w)<sup>b</sup>*

*T<sub>o</sub> = Onset temperature, T<sub>p</sub> = Peak temperature, T<sub>f</sub> = Final temperature and ΔH<sub>gel</sub> = Enthalpy of gelatinisation*

#### **1.4.3.1.2 Retrogradation**

Dispersed starch paste, gel or solution is a thermodynamically unstable system and with time, the gelatinised starch system gradually changes in its texture and crystallinity.<sup>117</sup> The term “retrogradation” is used to describe this event at which the recrystallisation of amylose and amylopectin occurs during the cooling or storage of gelatinised starch. During retrogradation the double helix crystalline structure reforms, and consequently decreases the water-binding capacity of the molecules.<sup>116</sup> The changes during the retrogradation process can be detected using different methods including rheological techniques, XRD and thermal analysis.<sup>118</sup> The short-term development of modulus in starch gel has been linked to the gelation of amylose, whilst the long-term increase in modulus involves the crystallisation of amylopectin.<sup>119</sup> This result is in correlation with the XRD studies, which show that the development of crystallinity of amylose and starch gel progress at a relatively similar rate but the amylose gel crystallinity reaches its maximum in 2 days, whilst the crystallinity of starch gel continues to rise.<sup>120</sup> Amylopectin crystallinity increases with time and reaches its limit in 30-40 days.<sup>121</sup>



DSC studies on retrogradation focus on the melting endotherm of amylopectin which gradually increases with time. The endothermic transition during the retrogradation occurs at slightly lower temperature than one during the gelatinisation and the enthalpies of retrogradation are substantially lower compared to those of gelatinisation (*Table 1.9*).<sup>86</sup> The water content and storage temperature greatly affect the retrogradation behaviour. The greatest crystallinity occurs in gels with 50-60% starch at low temperature but higher than glass transition temperature ( $T_g \approx -5 \text{ }^\circ\text{C}$ ).<sup>122, 123</sup>

**Table 1.9 – Retrogradation temperature and enthalpy of starches from different botanical sources<sup>124</sup>**

Botanical source	$T_o$ ( $^\circ\text{C}$ )	$T_p$ ( $^\circ\text{C}$ )	$T_f$ ( $^\circ\text{C}$ )	$\Delta H_{ret}$ (J/g)
Corn	39.0	50.1	59.4	5.8
High amylose corn	44.1	-	115.4	9.9
Waxy corn	40.2	51.3	60.2	7.3
Rice	40.3	51.0	60.4	5.3
Wheat	38.6	47.6	55.7	0.8
Potato	42.5	55.7	66.9	7.5

*Storage at 4  $^\circ\text{C}$  for 7 days*

$T_o$  = Onset temperature,  $T_p$  = Peak temperature,  $T_f$  = Final temperature and  $\Delta H_{ret}$  = Enthalpy of retrogradation

### 1.4.3.2 Chemical modification

Chemical modification of starches aims to overcome the disadvantages of native starches and introduce desirable properties to the starch structure. Thus the chemically modified starches represent a significant value added and versatile product.<sup>106</sup> Modification typically occurs at the reactive C2, C3 and mainly C6 hydroxyl group positions in starch molecule. Amylose possesses three reactive hydroxyl groups per anhydroglucose unit whilst amylopectin has one fewer due to the  $\alpha$ -1, 6 glucosidic

bonds at the branched points (*Figure 1.11*).<sup>125</sup> Hence the degree of substitution (DS) of modified starches can range from 0-3, though it is theoretically possible that the degree of substitution is slightly higher than 3 if the end group modification is included.<sup>126</sup> Common chemical modifications of starch are summarised in *Figure 1.15*.

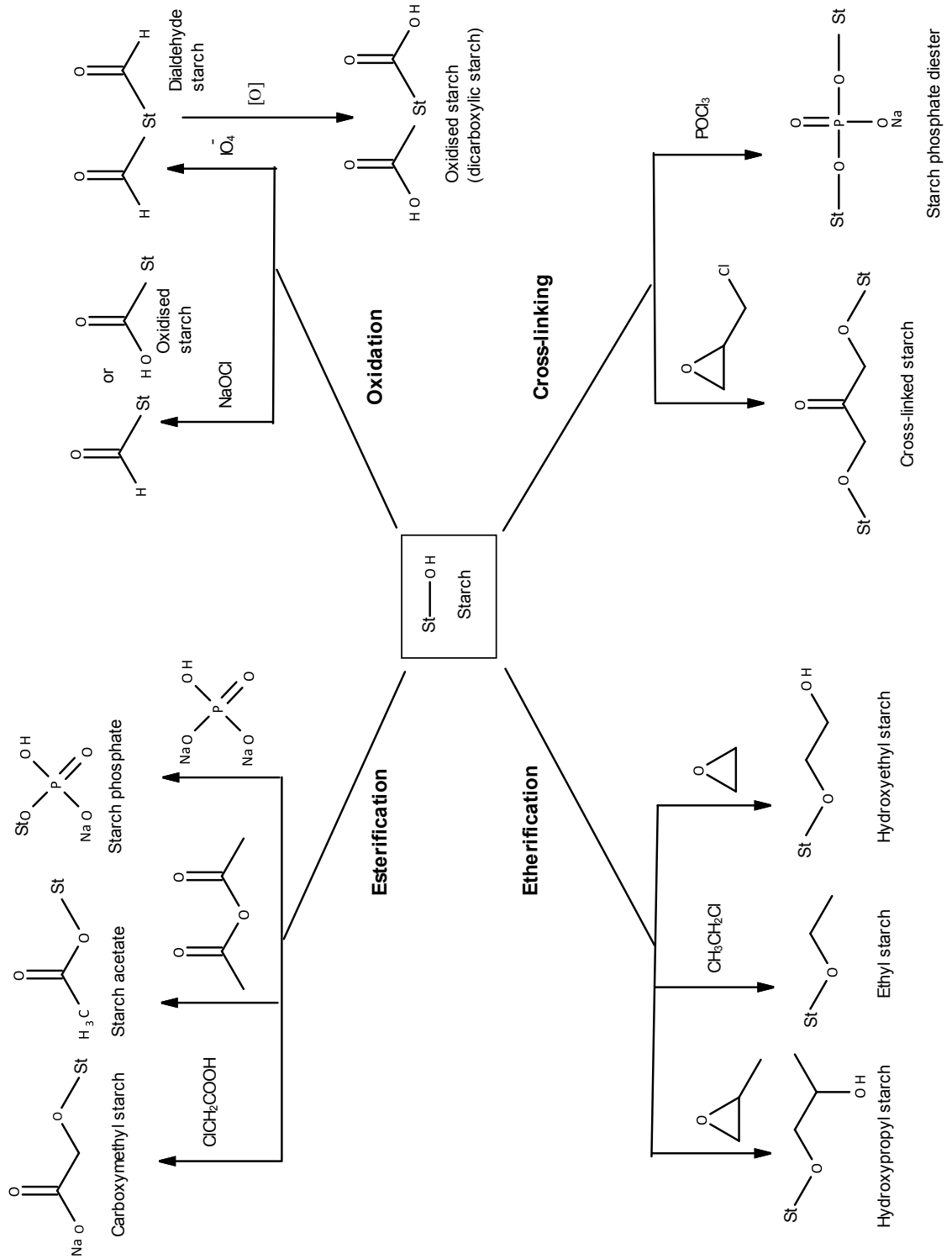


Figure 1.15 – Chemical modification of starch<sup>106</sup>

#### 1.4.3.2.1 Esterification

Esterified starches have been intensively used in various applications in both food and non-food industries for decades.<sup>127</sup> Starch is highly hydrophilic owing to the presence of hydroxyl groups in its molecules. Substituting these hydroxyl groups with less hydrophilic groups can increase the hydrophobicity of the polymer. Moreover, other properties, including processing temperature and solubility in organic solvents in starch esters differ from native starch, depend on the degree of substitution of the modified starches.<sup>128</sup> Starch esters are prepared from aqueous or solvent-based reaction leading to low DS or high DS modified starches respectively.<sup>129</sup> Acetylation of potato starch with different degrees of substitution (DS = 0.3-3) reported by Fang *et al.* showed that the thermal stability and solubility in organic solvents improved with the degree of substitution of starch.<sup>130</sup> Moreover, acetylation changes other properties of starch including decrease of gelatinisation temperature, increase in translucency, viscosity and freeze-thaw stability.<sup>131, 132</sup>

#### 1.4.3.2.2 Acid hydrolysis

Acid modified starch is normally prepared from the treatment of starch with hydrochloric acid or sulfuric acid in order to obtain thin boiling starch (lower molecular weight starch resulting from acid hydrolysis), which is intensively used in food, paper and textiles industries.<sup>133</sup> Acid modified starch was first prepared in 1874 by Nageli using sulfuric acid and then in 1886, Lintner introduced the method using hydrochloric acid. The treated starch was known as Lintner starch.<sup>134</sup> Acid modification decreases the amylose content and swelling power but increases the solubility of treated starch.<sup>135</sup> The intrinsic viscosity of acid modified starch paste is reduced compared to native starch paste.<sup>136</sup> The acid treatment leads to morphological changes of starch granules including the appearance of pores and cracks on the granular surface.<sup>134</sup> The mechanism of acid hydrolysis involves the cleavage of  $\alpha$ -1, 4 glycosidic bonds via electrophilic attack of hydroxonium ion (*Figure 1.16*).<sup>137</sup>

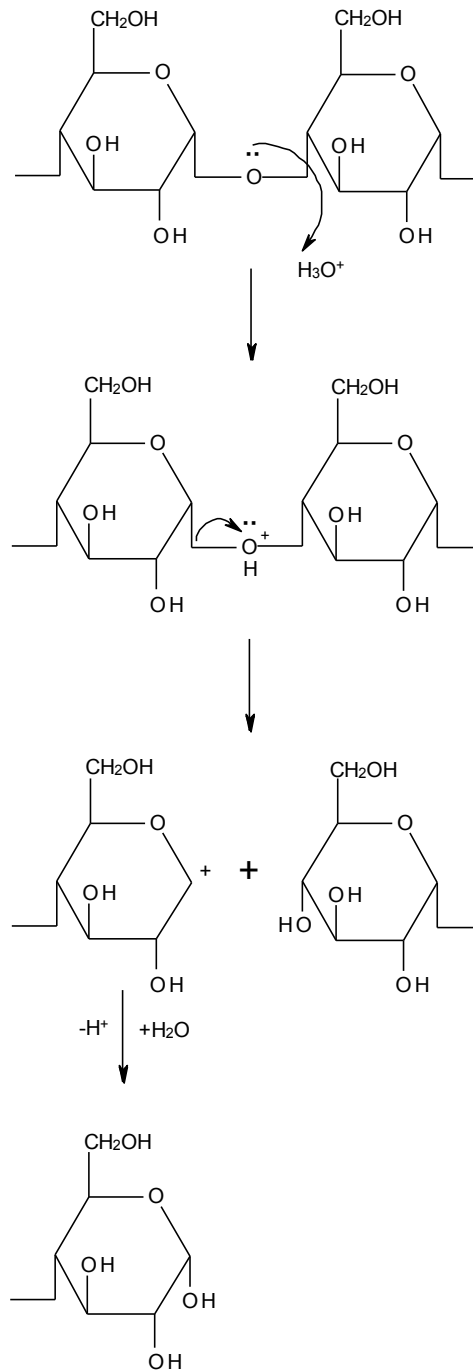


**Figure 1.16 – Acid hydrolysis mechanism of starch**

#### 1.4.3.2.3 Other methods

Other common modified starches include cationic starch, oxidised starch and crosslinked starch. Cationic starches are produced by reacting starch with tertiary or quaternary ammonium compounds.<sup>138</sup> The modification improves the solubility and

dispersability in cold water. The affinity with fibres which is important for paper making is also enhanced.<sup>76</sup>

Oxidation of starch involves the conversion of hydroxyl groups in starch molecules to carbonyl and then carboxyl groups.<sup>125</sup> Commercial oxidised starches are prepared by reaction of starch with an oxidant at specific temperature and pH. The most commonly used oxidising agent is hypochlorite.<sup>139</sup> However, other typical oxidising agents such as hydrogen peroxide and persulfate have also been used.<sup>140, 141</sup> Oxidised starches are intensively used in paper and textiles industries.<sup>142</sup>

Crosslinked starches are widely used as thickening agents in food applications as the crosslinking minimises the loss of viscosity and the rupture of starch granules.<sup>143</sup> The most widely used crosslinkers are epichlorohydrin, phosphoryl chloride and sodium trimetaphosphate.<sup>144</sup>

Another commonly used modified starch is hydroxypropylated starch, which is particularly used in the food industry. This modified starch is commonly prepared by reacting starch with propylene oxide. The paste of hydroxypropylated starch has better clarity and freeze-thaw stability compared to those of native starch.<sup>145</sup> The hydroxypropyl groups attached to starch backbone are believed to introduce mobility to starch chains, resulting in lowering glass transition and crystalline melting temperatures.<sup>146, 147</sup>

#### **1.4.4 Starch in composites**

The use of starch in the production of novel composites has been intensively investigated in the last few decades, due to its unique properties and its biodegradability.

##### **1.4.4.1 Starch blends with synthetic non-degradable polymers**

Blending starch with synthetic polymers has various advantages including the increase of biodegradability and cost reduction. Starch has been used as filler in polyethylene (PE) to yield a partially biodegradable material.<sup>148, 149</sup> Fillers can enhance different properties of the polymer including strength, stiffness, permeability and cost. However,

poor adhesion between fillers and polymer matrix can lead to undesirable consequences, such as decrease of tensile strength and elongation.<sup>150</sup> As starch and polyethylene are incompatible, starch or polyethylene has to be modified to improve the adhesion between the two components.<sup>151</sup> Compatibilisers such as maleic anhydride or acrylic acid are grafted to PE to enhance its compatibility with starch.<sup>152</sup> Moreover, Evangelista *et al.* showed that modifying starch with n-octenyl succinic anhydride could also improve the tensile strength of the PE/starch film.<sup>153</sup>

#### 1.4.4.2 Starch blends with synthetic degradable polymers

Blending starch with non-degradable polymers only yields partially biodegradable products. In order to prepare completely biodegradable starch-based composites starch is typically blended with aliphatic polyesters, polyvinyl alcohol (PVA) or other biopolymers. Common degradable polyesters used in the blends with starch are poly (hydroxyl alkanooates) (PHAs), poly (lactic acid) (PLA) and polycaprolactone (PCL). PHAs are naturally occurring polyesters produced by bacteria.<sup>154</sup> One of the most studied PHAs is poly (3-hydroxybutyrate) (PHB).<sup>155</sup> The combination of starch into PHB resins aims to improve the properties of the polymer and lower the production cost. Godbole *et al.* studied the PHB and starch composites and found that the tensile strength of the films was optimum at PHB/starch ratio 70/30 (wt./wt.).<sup>156</sup> Poly (lactic acid) is a biodegradable thermoplastic polymer of lactic acid which can be obtained through carbohydrate fermentation.<sup>157</sup> Starch and PLA are immiscible due to the poor interfacial attraction between starch granules and PLA matrix. Hence compatibilisers such as maleic anhydride or methylenediphenyldiisocyanate (MDI) are needed in the composite to maintain the mechanical properties of the product.<sup>158, 159</sup> Starch has also been blended with petroleum-derived biodegradable polymers such as PCL and PVA. Averous *et al.* studied the association of PCL with thermoplastic starch and found that, despite the phase separation of the blend, the dimensional stability and hydrophobicity of the blends improved significantly compared to those of native thermoplastic starch (TPS).<sup>160</sup> Interestingly, PCL/high amylose starch gives better mechanical properties than other starches owing to its small granular size allowing good dispersion in PCL matrix.<sup>161</sup> Hydrophilic PVA is compatible with starch and the addition of PVA to starch matrix demonstrated improved tensile strength and elongation.<sup>162</sup> Nonetheless, similar to starch, the fact that PVA is also sensitive to moisture has limited the starch/PVA

blends for many applications. Different methods have been attempted to enhance the water resistance of films including modification of starch and addition of crosslinkers.<sup>163, 164</sup>

#### 1.4.4.3 Starch blends with other biopolymers

Blends of starch with other biopolymers including chitosan, cellulose and pectin have been investigated, as these biopolymers are abundant, cheap, non-toxic and biodegradable. Chitosan has a good film forming property and is also compatible with starch.<sup>165</sup> The addition of starch to chitosan films improves tensile strength and elongation with regular starch showing better performance than waxy starch.<sup>166</sup> Microcrystalline cellulose and methylcellulose were extruded with corn starch to produce edible films. The high ratio of cellulose increases tensile strength and elongation of the films and decreases water vapour transmission rate and gas permeability.<sup>167</sup> Blends of starch and pectin result in edible biodegradable and water sensitive films. As such these films find use in applications such as water-soluble pouches for detergents and insecticides, edible bags for soup or noodles ingredients and drug delivery systems.<sup>168, 169</sup>

The number of reports on composites based on starch and epoxidised plant oils is limited. An emulsion of ESO with water and corn starch was blended with glycols and isocyanate to produce polyurethane (PU) foams. NMR analysis showed possible crosslinking between the oil droplets in the emulsion with isocyanate.<sup>170</sup> Lu *et al.* used epoxidised rapeseed oil to synthesise chlorinated rapeseed oil then in combination with isophoronediiisocyanate, dimethylol propionic acid produced a waterborne PU or poly (urethane-urea). The waterborne PU was then added to plasticised starch to yield a biodegradable film. The addition of PU was claimed to improve the mechanical properties of plasticised starch films.<sup>171</sup>

## 1.5 Scope of the thesis

The aim of the project is to develop novel greener thermosetting resins to be utilised as alternatives to petroleum-derived materials. The resins are envisaged to be based on natural, renewable resources and in particular epoxidised linseed oil with the abundant



polysaccharide, starch. Owing to the high degree of unsaturation in linseed oil, a high epoxy content can be obtained in epoxidised linseed oil. This can result in a significant degree of crosslinking in the resins. Starch is highly available, low in cost and versatile and therefore represents an attractive biopolymer resource. Modifications of the starch are investigated in order to improve the resin performance compatibility to those of petroleum-based materials. The project focuses on bio-based film production which is very important in one of the most widespread industrial applications such as coatings. The required properties of the films, including thermal stability, mechanical strength and water resistance are examined within this work. The project also concentrates on the production process of the bio-based resin to enable it to be compatible to those currently used in industry. In order to compare the properties of the bio-based products and production process against currently available petroleum-based films, a polyvinyl chloride wear layer of widely utilised vinyl floorings was chosen as the benchmark for the project. This transparent or translucent wear layer is situated over the decorative printed layer (*Figure 1.17*) and gives the floor its resistance to abrasion, scratches, cigarette burns, chemicals and stains.<sup>172</sup> As such, the casting of the bio-films should be a solvent-free process and the viscosity of the reaction mixture should be in suitable range of the manufacture process.

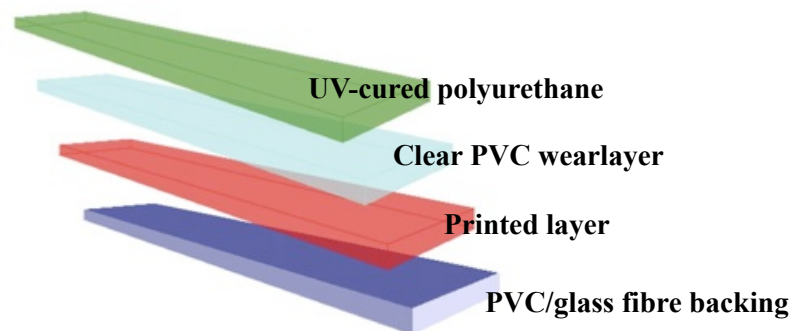


**Figure 1.17 – Cushion vinyl sheet construction (Originally in colour)**



# Chapter 2

## *Epoxidised linseed oil based thermosetting resins*

Aspect of work described in this chapter has been published in:

**N. Supanchaiyamat**, P. S. Shuttleworth, A. J. Hunt, J. H. Clark and A. S. Matharu,  
*Green Chem.*, 2012, **14**, 1759-1765.

*“Thermosetting resin based on epoxidised linseed oil and bio-derived crosslinker”*

**DOI:** 10.1039/C2GC35154D



## 2.1 Chapter 2 - Summary

Thermosetting resins were synthesised from epoxidised linseed oil (ELO) in combination with bio-derived crosslinkers including succinic acid, itaconic acid, succinic anhydride, itaconic anhydride and Pripol 1009. The inclusion of catalysts such as triethylamine (TEA), 1-methylimidazole (1-MeIm), 2-methylimidazole (2-MeIm), 1,8-diazabicyclo [5.4.0] undec-7-ene (DBU) and 4-dimethylaminopyridine (DMAP), were subsequently studied in the formulation with Pripol 1009. The reactive mixture yielded a 99.5% (by weight) bio-derived highly flexible transparent film with significant water resistance. It was demonstrated that the mechanical and thermal properties of the resulting films were significantly influenced by the amine catalysts selected. The use of catalysts significantly enhanced the mechanical properties of the films; tensile strength improved by up to 545% (DMAP), Young's modulus improved by up to 422% (2-MeIm) and elongation at break improved by 14-84%. An infrared spectroscopic study coupled with modulated differential scanning calorimetry (MDSC) was undertaken in an attempt to study the curing mechanism. Epoxide ring opening was clearly evidenced by infrared spectroscopy and the studies suggested that DMAP probably aided crosslinking between ELO and Pripol 1009 via epoxide ring opening, followed by etherification. The optimum DMAP catalyst loading giving the highest value of Young's Modulus was determined at 1%, whilst the tensile strength reached its maximum at 0.5% with respect to the total resin weight. Higher concentrations of DMAP (5% wt.) decreased the Young's Modulus, tensile strength and elongation at break.

## 2.2 Introduction

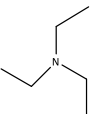
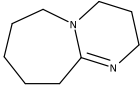
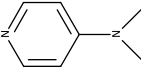
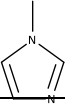
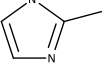
The curing process of plant oil based thermosets has been investigated in numerous studies. The mechanical and thermal properties of the cured products depend on the curing agents chemical nature and concentration, cure condition, and type and concentration of the cure catalysts.<sup>173</sup> Conventional curing agents include acids, anhydrides and amines, which are typically small molecules containing 4-10 carbons. These crosslinked products have a high glass transition temperature ( $T_g$ ), typically between 30-120 °C.<sup>49, 50, 173</sup> Moreover, the primary source of these crosslinkers is largely from petroleum-based feedstocks. In this work, bio-derived crosslinkers

including succinic acid, itaconic acid and Pripol1009 are used in combination with ELO to obtain a polymeric product with high bio-based content.

Catalysts used for epoxy/acid systems can be broadly categorised in four classes: i) bases; ii) onium compounds (phosphonium or aluminium halides); iii) metals and iv) cationic catalysts (Lewis acids). Merfeld *et al.* reported that metal catalysts were worse than bases and onium catalysts in accelerating epoxy/acid reaction. Lewis acids, such as boron trifluoride, show good homopolymerisation of epoxides but, frequently cause side reactions to occur, and additional precautions are needed when handled.<sup>174</sup>

Amine bases have been intensively used in the curing reaction of epoxide and anhydride or acid hardeners and exhibit good catalytic properties in these reactions.<sup>175-177</sup> Selected amines catalysts used in the reaction include triethylamine (TEA), 1-methylimidazole (1-MeIm) and 2-methylimidazole (2-MeIm). These catalysts are widely utilised in the curing of epoxy systems. Furthermore, 1,8-diazabicyclo [5.4.0] undec-7-ene (DBU) and 4-dimethylaminopyridine (DMAP) were also investigated as these bases are known to be more active initiators for crosslinking reactions (*Table 2.1*).<sup>178</sup>

**Table 2.1 –Tertiary amine and imidazole catalysts**

Catalyst	pKa of protonated species	Melting point (°C)	Boiling point (°C)
TEA 	10.75	-115	89
DBU 	12	-70	261
DMAP 	9.2	108-110	194
1-MeIm 	7.06	-60	198
2-MeIm 	7.88	142-143	267-268

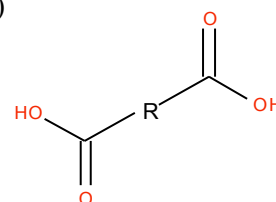
## 2.3 Epoxidised linseed oil based thermosetting resins using bio-derived crosslinkers

Petrochemical molecules such as ethene and benzene are obtained from fractionation of hydrocarbons mixtures, which are collected after the cracking process of crude oil.<sup>179</sup> These platform molecules are subsequently used as building blocks in industry via application of well-established organic chemistry methodologies. Bio-derived platform molecules from biomass superficially adopt a similar idea but differ in the complexities of the products.<sup>180</sup> Table 2.2 shows the top 12 most useful bio-derived building blocks in chemical synthesis according to the US Department of energy.<sup>181</sup>

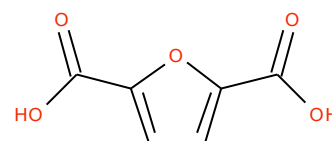
**Table 2.2 – Top 12 biomass-derived platform molecules (US Department of Energy)**

Four carbons 1,4-Diacids (succinic, fumaric and malic acids)

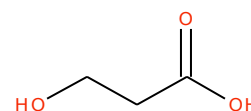
R = -CH<sub>2</sub>CH<sub>2</sub>-, -CH=CH-, -CH<sub>2</sub>CH(OH)-



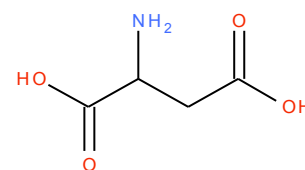
2,5-Furan dicarboxylic acid



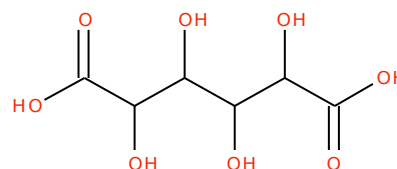
3-Hydroxypropionic acid



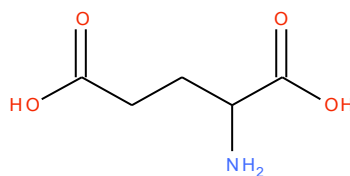
Aspartic acid



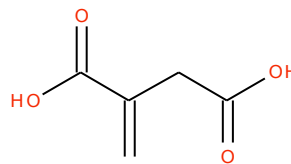
Glucaric acid



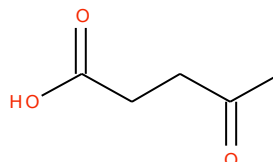
Glutamic acid



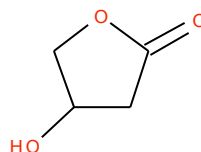
Itaconic acid



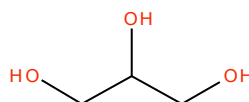
Levulinic acid



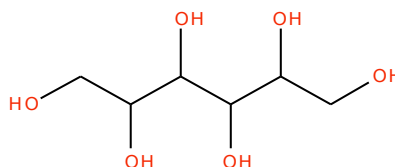
3-Hydroxybutyrolactone



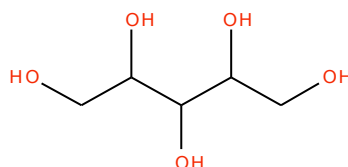
Glycerol



Sorbitol (alcohol sugar of glucose)



Xylitol/arabinitol (sugar alcohols)



In this work, two of these platform molecules, succinic and itaconic acids and their respective anhydrides were used as crosslinkers in ELO based thermosetting resins as well as Pripol 1009 (which is also referred to as Pripol), a commercially available dimerised fatty acid (C36) derived from natural oils and fats (*Figure 2.1*).



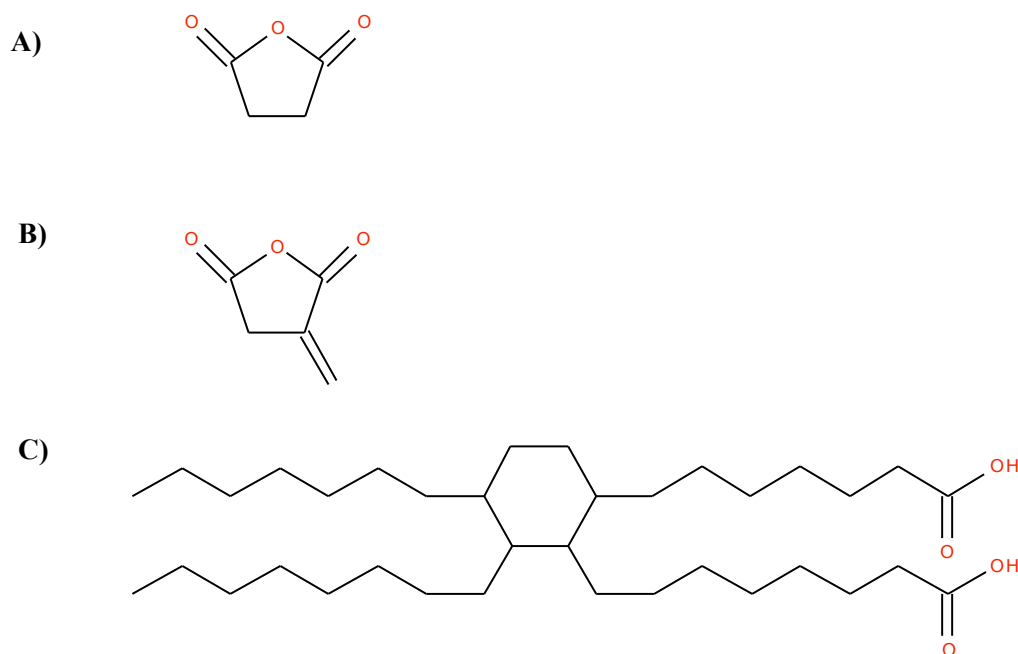


**Figure 2.1 – A) Succinic anhydride, B) Itaconic anhydride, and C) Pripol 1009**

There are approximately 5 epoxide functionalities in an ELO molecule and the crosslinkers have two active functionalities, therefore the molar ratio used was bio-derived crosslinker:ELO = 2.5:1. As all the crosslinkers except for Pripol are solid at room temperature, the mixture appears heterogeneous. However, after curing at 140 °C for 1 hour, the mixtures with succinic anhydride and itaconic anhydride become homogeneous and transparent, whilst ones containing succinic acid and itaconic acid remain heterogeneous (*Figure 2.2*). This is likely due to the lower melting temperatures of the anhydrides (66-68 °C for itaconic anhydride and 119-120 °C for succinic anhydride) compared to those of the corresponding acids (165-167 °C for itaconic acid and 185-187 °C for succinic acid), which are higher than the curing temperature. Mixtures with Pripol start to set after 3 hours of curing and the resultant film is homogeneous and transparent. Whilst Pripol gives good quality transparent films, a film from shorter chain crosslinkers such as itaconic anhydride yields brittle films, which partly cracks before being fully cured. Curing of the reaction mixtures was further evaluated by FT-IR (ATR) and simultaneous thermal analysis.

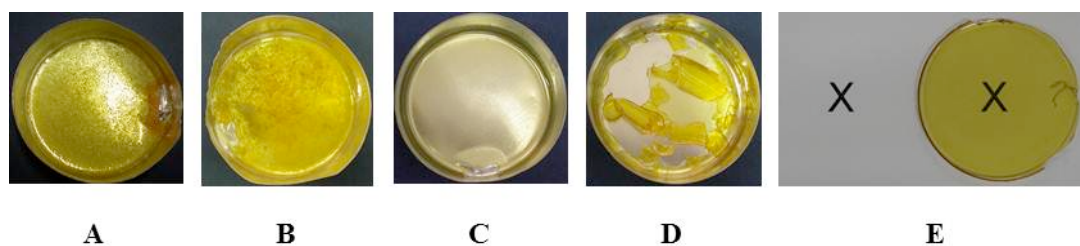


**Figure 2.2 – Films made from epoxidised linseed oil and bio-derived crosslinkers; A) succinic acid, B) itaconic acid, C) succinic anhydride, D) itaconic anhydride and E) Pripol 1009 (Originally in colour)**

### **2.3.1 Infrared spectroscopy of epoxidised linseed oil and crosslinkers**

The IR spectrum of ELO is shown in *Figure 2.3*. The characteristic band of the oxirane ring is detected at  $822\text{ cm}^{-1}$  and the carbonyl group stretching from the ester functionality in the triglycerides is observed at  $1740\text{ cm}^{-1}$ .<sup>182, 183</sup> The characteristic bands of ELO are summarised in *Table 2.3*.

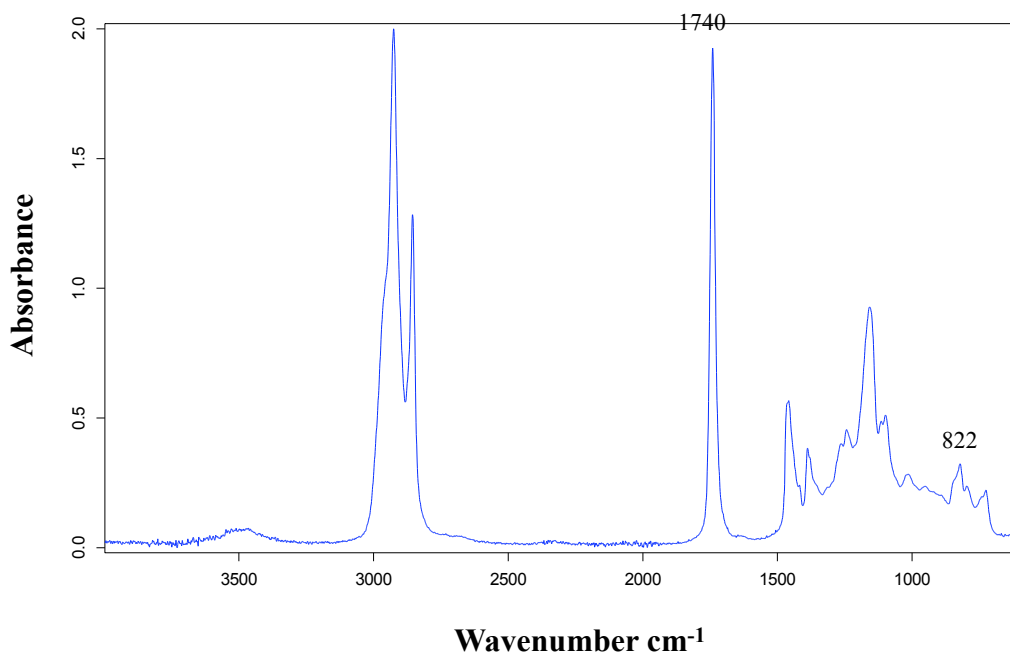


**Figure 2.3 – Infrared spectrum of epoxidised linseed oil**

**Table 2.3 – IR assignment of characteristic bands of epoxidised linseed oil**

Frequencies (Wavenumber $\text{cm}^{-1}$ )	Assignment
2926	Asymmetric C–H stretching of $\text{CH}_2$ , $\text{CH}_3$
2855	Symmetric C–H stretching of $\text{CH}_2$ , $\text{CH}_3$
1740	C=O stretching
1459	Scissoring of $\text{CH}_2$ , asymmetric bending of $\text{CH}_3$
1389	Symmetric bending of $\text{CH}_3$
1158	C–O stretching of O = C–O
1099	C–O stretching of O– $\text{CH}_2$
822	C–O of epoxides
725	In-phase rocking of $(\text{CH}_2)_n$ , $n > 3$

After mixing at room temperature, all the ELO-crosslinker mixtures were heated at 140 °C and samples were taken every hour to investigate the curing reaction of the resins. Reactive mixtures of ELO with bio-derived crosslinkers show common changes in their spectra during the curing process. The band at 822  $\text{cm}^{-1}$  decreases in intensity with curing time, and, in some cases, completely disappears by the end of the reaction (*Figures 2.4-2.8*). This is characteristic of the epoxide ring-opening.<sup>184</sup> The appearance of the characteristic O–H stretching band is also noted at around 3500  $\text{cm}^{-1}$ , indicating the protonation of the alkoxide ions formed during the curing process.<sup>185</sup>

In the mixture of ELO with succinic or itaconic acid, the carbonyl stretch of the ester shifts from 1740  $\text{cm}^{-1}$  to 1735  $\text{cm}^{-1}$ , suggesting that the acid groups in bio-derived diacid reacts and new ester functionalities are formed at the end of the reaction (*Figures 2.4-2.5*).<sup>186</sup>

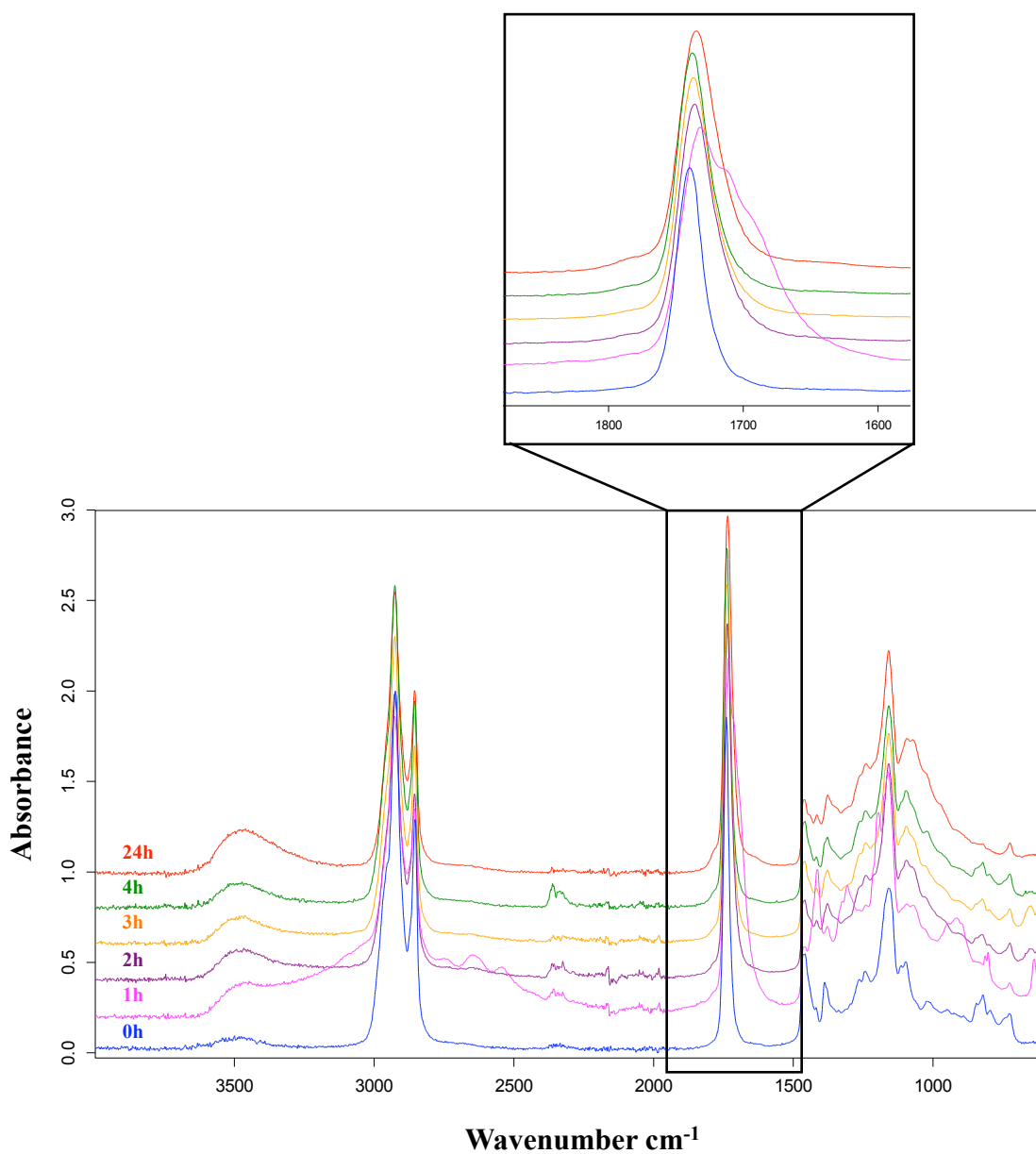


**Figure 2.4 – Infrared spectra of ELO and succinic acid cured at  $140\text{ }^{\circ}\text{C}$  (Originally in colour)**

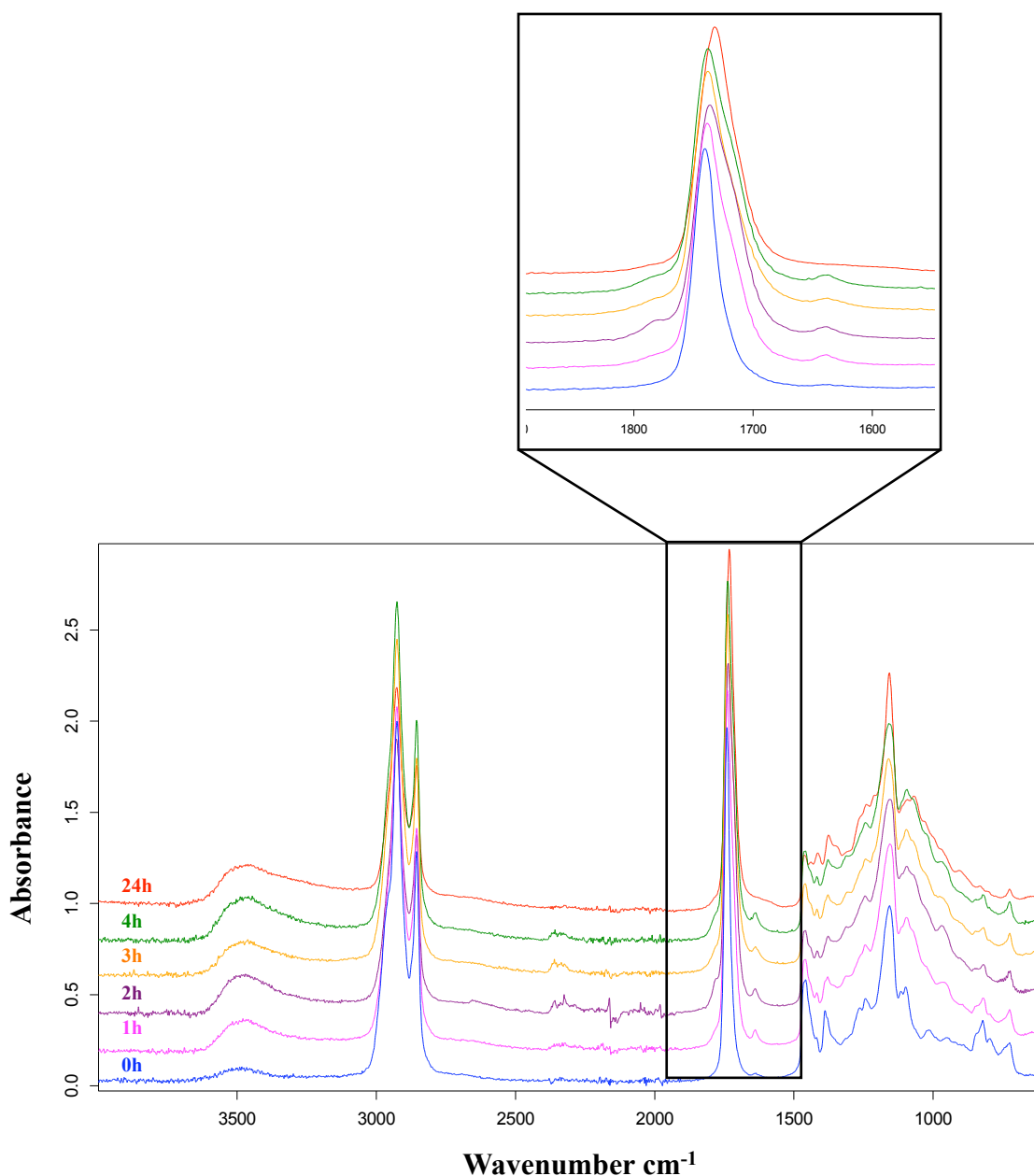


**Figure 2.5 – Infrared spectra of ELO and itaconic acid cured at 140 °C (Originally in colour)**

In the case of mixtures with anhydride crosslinkers, the characteristic bands of the anhydrides are noted at 1787 and 1865  $\text{cm}^{-1}$  or 1774 and 1848  $\text{cm}^{-1}$  at the onset of the observation in succinic anhydride and itaconic anhydride mixtures, respectively (*Figure 2.6-2.7*). Additionally, the stretching vibration of the C-O-C and C-C-O functional groups in the anhydrides can be observed in the region of 900-1300  $\text{cm}^{-1}$ .<sup>51, 187</sup> The intensity of these bands decreases after 1 hour and the bands disappear after 2 hours of curing. The epoxy band at 822  $\text{cm}^{-1}$  slightly reduces its intensity over time, nonetheless

the band can still be seen after 24 hours of curing. This suggests that the ring-opening in anhydride formulations occurs more slowly than that in formulations with acid crosslinkers.

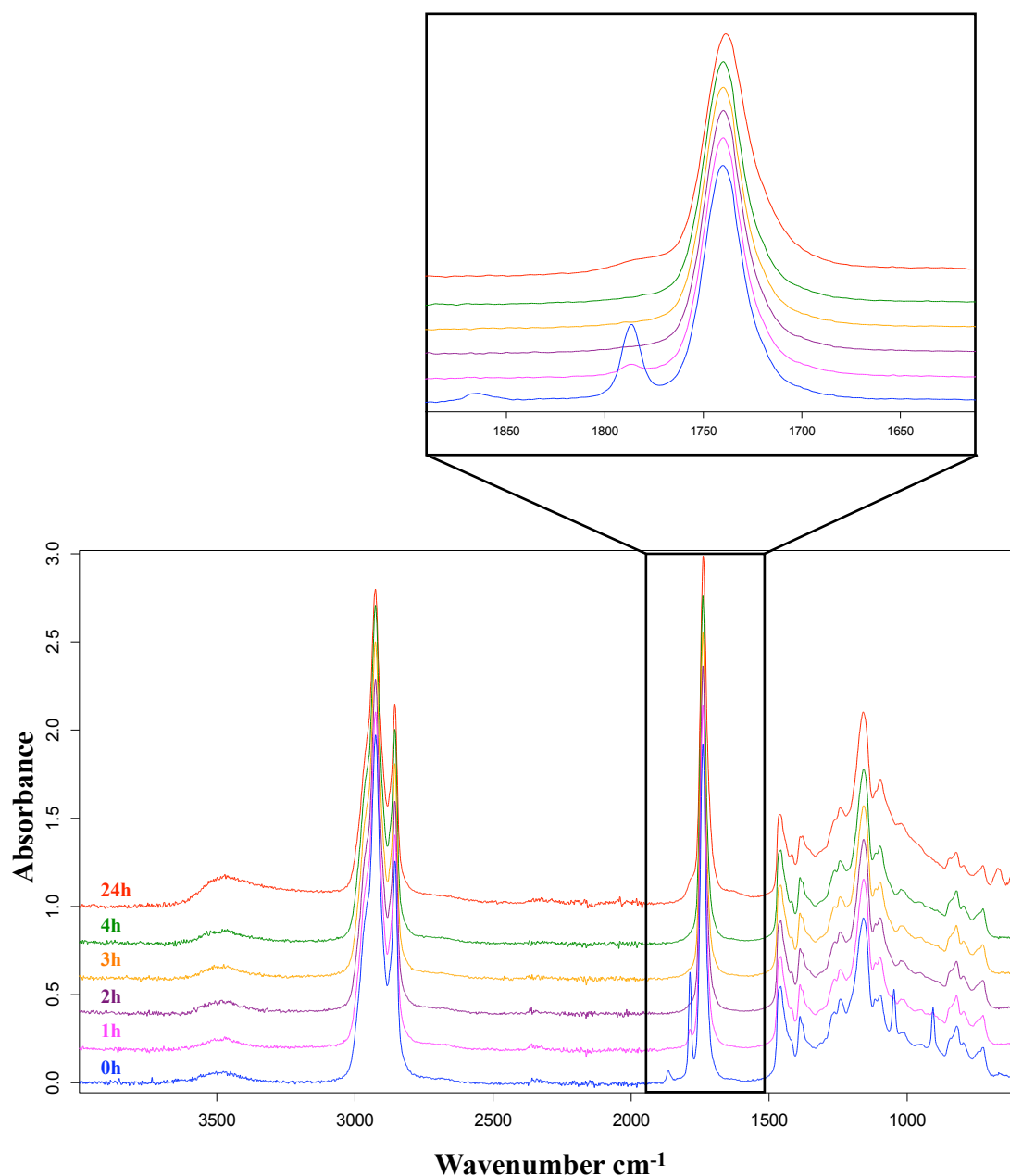


**Figure 2.6 – Infrared spectra of ELO and succinic anhydride cured at 140 °C (Originally in colour)**

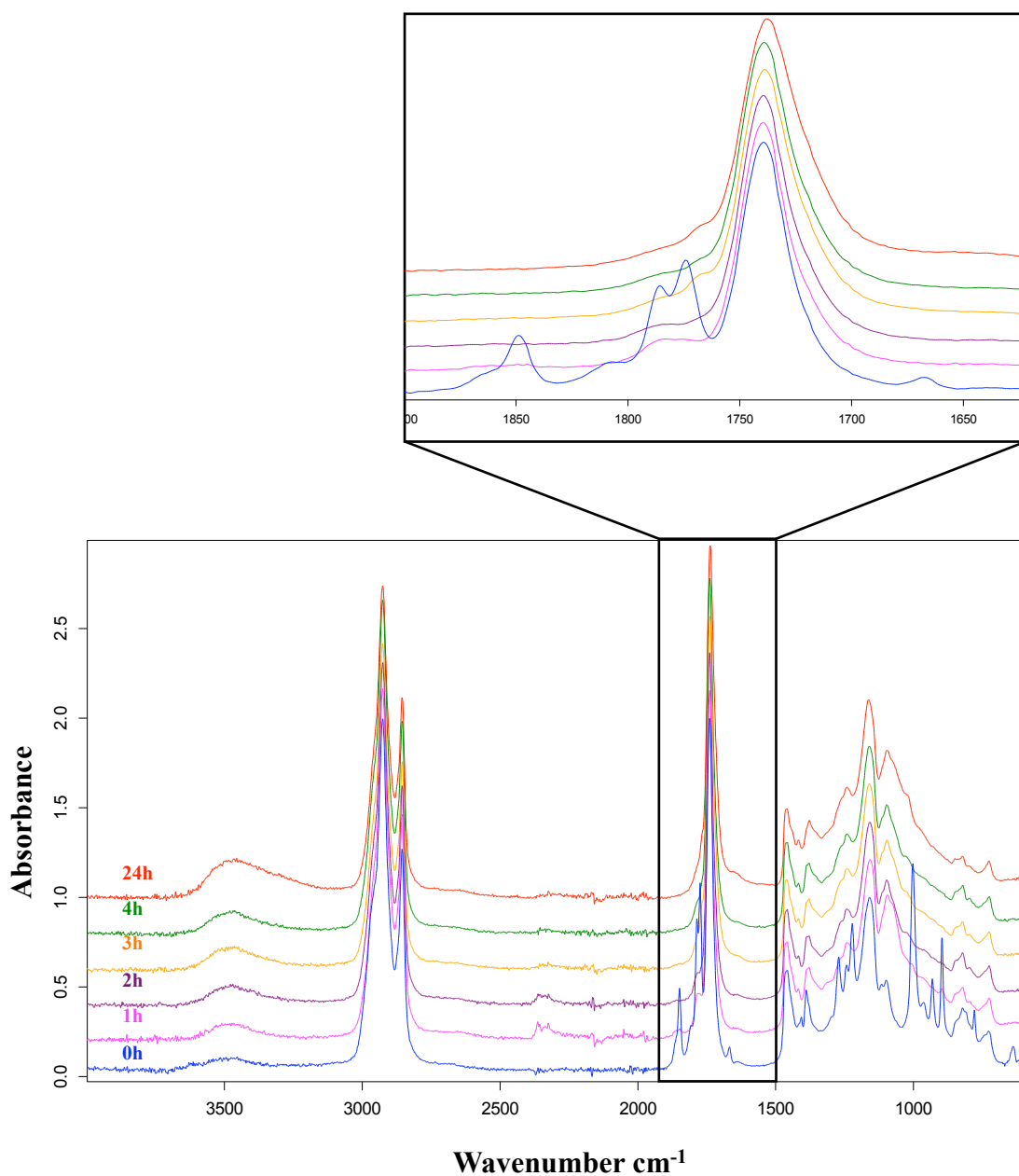


**Figure 2.7 – Infrared spectra of ELO and itaconic anhydride cured at 140 °C (Originally in colour)**

In the case of the long-chain crosslinker Pripol, the characteristic band of the oxirane rings at 822  $\text{cm}^{-1}$  completely disappears after 1 hour of heating (*Figure 2.8*). This indicates a rapid ring-opening reaction in the presence of these crosslinkers owing to the better miscibility of the two components. The stretching vibration of carbonyl in the acid functionality of Pripol shows an intense band at 1709  $\text{cm}^{-1}$  and the band at 1740  $\text{cm}^{-1}$  is associated with the ester carbonyl in ELO. Whilst the acid C=O band reduces its intensity with curing time, the ester C=O band increases its intensity and shifts to 1736

$\text{cm}^{-1}$  after 24 hours. All these observations are evidence of the polyesterification of this system which is in accordance with previous reports.<sup>51, 188</sup>

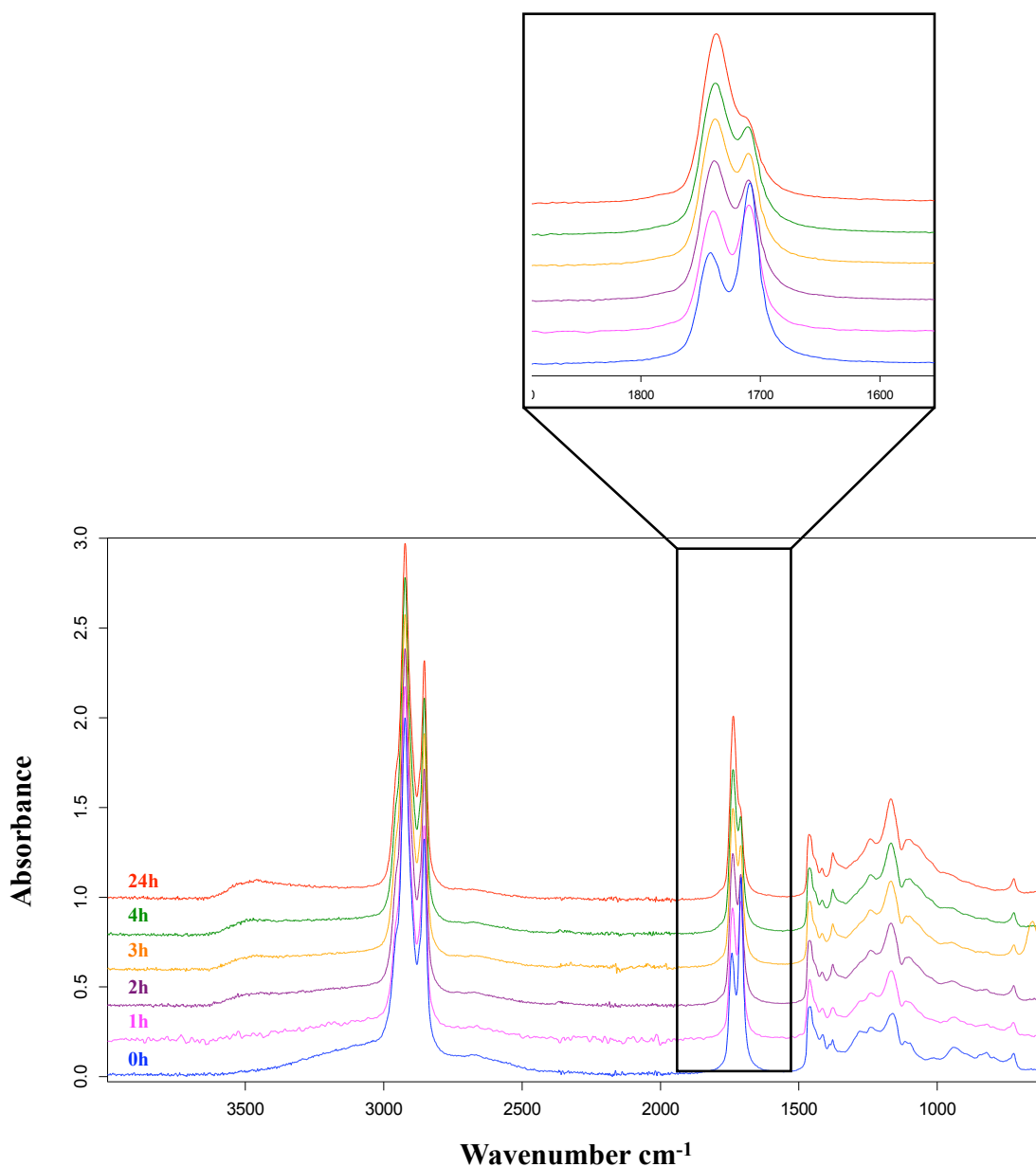


**Figure 2.8 – Infrared spectra of ELO and Pripol 1009 cured at 140 °C (Originally in colour)**



### 2.3.2 Simultaneous thermal analysis of epoxidised linseed oil and crosslinkers

Simultaneous thermal analysis of the reactive mixtures of ELO and bio-derived crosslinkers are performed using STA 625 (DSC/TG). The DSC thermogram of formulation with succinic acid shows two distinct exothermic transitions in the region of 150-280 °C with the peak temperatures of 176 and 194 °C (*Figure 2.9 A*). Similar transitions can also be observed in the itaconic acid formulation but at lower temperature range with the peak temperatures at 156 and 175 °C (*Figure 2.9 B*). This suggests that there are either two different reactions that are occurring during the curing process or alternatively, that there is a two-stage curing process. The mixtures with succinic and itaconic anhydrides demonstrate a sharp endothermic peak at 120 °C and 66 °C respectively (*Figures 2.9 C-D*). These transitions correspond to the melting of the anhydrides (*cf. page 73*). This result is in accordance with the visual observation during film production as the heterogeneous mixture become homogeneous and transparent after 1 hour of curing. An exothermic curing transition is noted with the onset temperature of 183 °C in succinic anhydride system and 150 °C in itaconic anhydride system. Pripol formulation shows one exothermic transition, corresponding to the curing reaction of the system in the region of 125-300 °C (*Figure 2.9 E*). The thermal analysis results are summarised in *Table 2.4*.

**Table 2.4 – Thermal analysis data of ELO with bio-derived crosslinkers**

Crosslinkers	Heat of reaction (mcal/mg)	Onset temperature (°C)	Peak temperature (°C)
Succinic acid	35.6	157	176, 194
Itaconic acid	39.6	134	156, 175
Succinic anhydride	12.9	183	234
Itaconic anhydride	9.7	150	180, 220
Pripol 1009	33.5	158	213

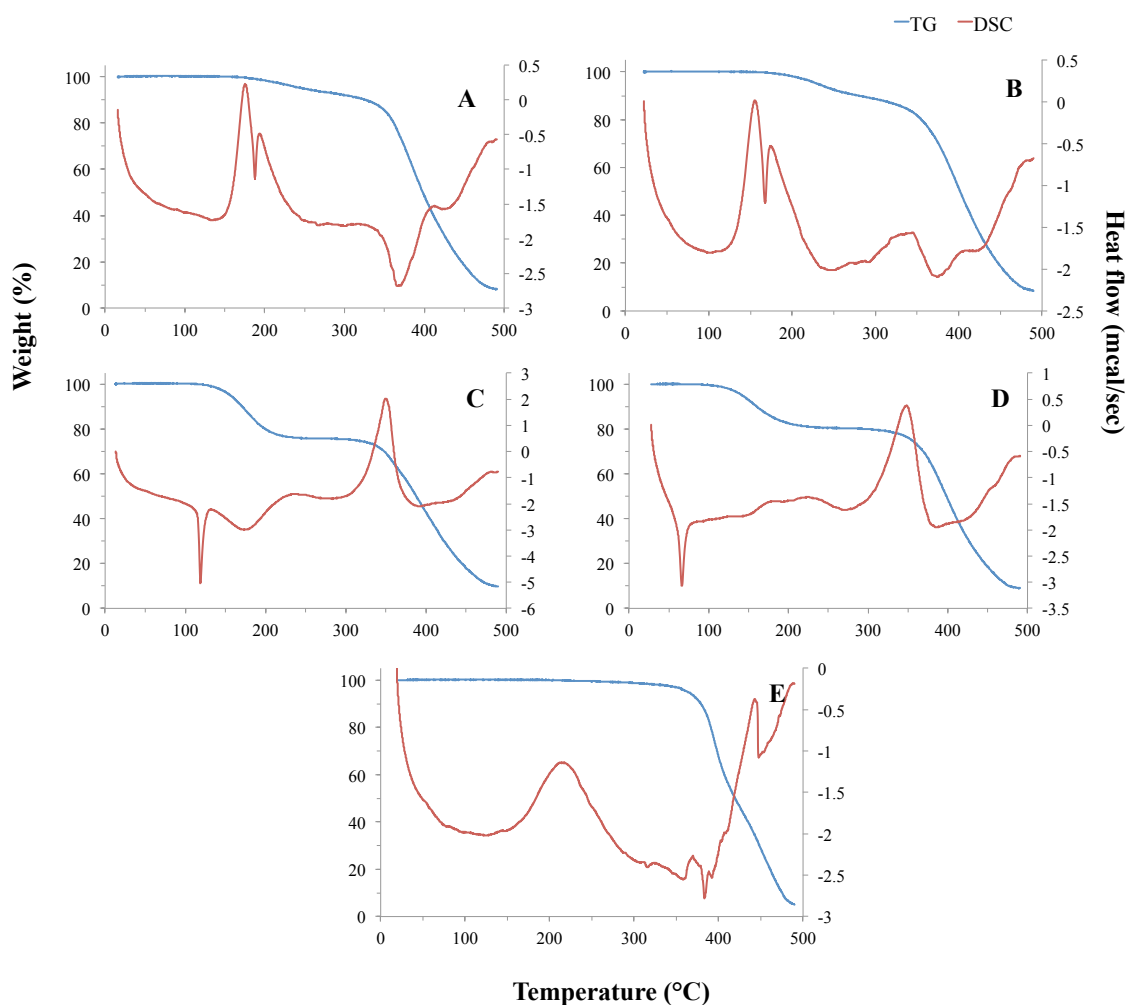


**Figure 2.9 – TG and DSC thermograms of the mixtures of ELO with A) succinic acid, B) itaconic acid, C) succinic anhydride, D) itaconic anhydride and E) Pripol 1009 (Originally in colour)**

The use of Pripol yielded homogeneous transparent films with enhanced flexibility due to the longer chain length of the crosslinker as compared to succinic and itaconic acids. The fact Pripol is a liquid at room temperature was also viewed as a significant advantage for homogenisation over the other crosslinkers investigated, which were solid at room temperature and had a tendency to phase separate on storage of the uncured formulation. This is an important factor to consider if scaling up or if the process was to be commercialised as additional mixing or process steps would be required. The formulation with Pripol exhibited the best overall combination of flexibility,

appearance, homogeneity and strength. As such, Pripol was selected for further studies in this chapter.

## **2.4 Thermosetting resins from epoxidised linseed oil and Pripol**

### **2.4.1 Thermal analysis of epoxidised linseed oil and Pripol mixtures with no added catalyst**

Thermal analysis of the ELO and Pripol mixtures were performed to ascertain the optimum ratio of the two components. Tan *et al.* suggested that larger enthalpies of polymerisation indicated a higher degree of copolymerisation from the epoxidised oil monomers to a cross-linked thermoset resin.<sup>51</sup> The largest enthalpy and thus greatest degree of polymerisation was obtained at a 50:50% wt. ratio of Pripol:ELO (molar ratio of 1.7:1) (*Figure 2.10*).

The stoichiometric ratio  $R$ , which is defined as

$$R = \text{acid equivalents/epoxide equivalents}$$

is 0.7, which is lower than that reported by Boquillon *et al.* for ELO and *cis*-1,2,3,6-tetrahydrophthalic anhydride (THPA) was ( $R=0.8$ ).<sup>49</sup> The lower stoichiometric ratio exhibited with bio-derived diacid is likely due to the long chains in the diacid structure, which can hinder the movement of the crosslinker in the network. Therefore fewer acid groups are able to react with the epoxides within the ELO, resulting in fewer acid equivalents needed for complete curing. A 50:50% wt. ratio of bio-derived diacid:ELO was utilised to produce thermosetting films using tertiary amines or imidazoles as catalysts (1% of resin weight) in further experiments.

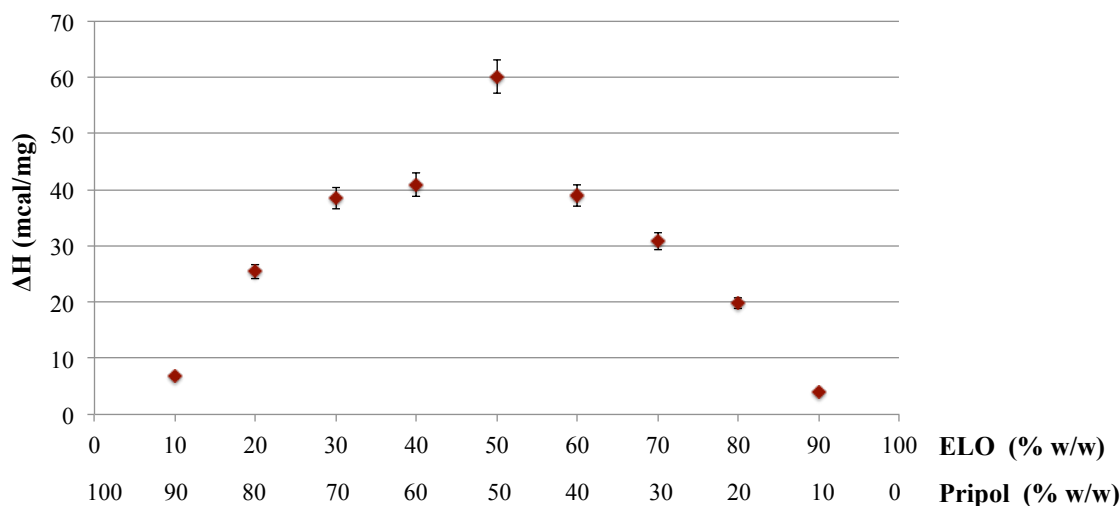


**Figure 2.10 - ELO/Pripol 1009 ratio against heat of reactions**

## 2.4.2 Physical properties of resulting films

### 2.4.2.1 Effect of different catalysts on the mechanical properties of the films

Inclusion of amines significantly improves the mechanical properties of the films; the tensile strength, Young's modulus and elongation at break all significantly improve by 545% (DMAP), 422% (2-MeIm) and 84% (1-MeIm), respectively (*Figure 2.11*). Films cured at 140 °C using 2-MeIm and DMAP as catalysts demonstrate the greatest tensile strength and Young's modulus. Despite the relatively low Young's modulus for the film with 1-MeIm, it gives the best elongation at break of all the samples. The higher elongation at break of this system suggests better mobility of the network, hence less crosslinking.

Curing the samples at 160 °C results in improved film mechanical properties. The tensile strength of the DMAP formulation increases from 1.17 MPa to 1.65 MPa, an improvement of 41%, and compared to the standard without catalyst a 242% increase in Young's modulus is observed. This film demonstrates the best tensile strength, Young's modulus and elongation at break. Interestingly, DMAP, which is not a common catalyst for epoxy systems, appears to be the best catalyst for the formulation (*Figure 2.12*). The 1-MeIm formulation increases its Young's modulus by 85% compared with respect to the same formulation cured at 140 °C, indicating enhanced curing at the higher temperature (160 °C).

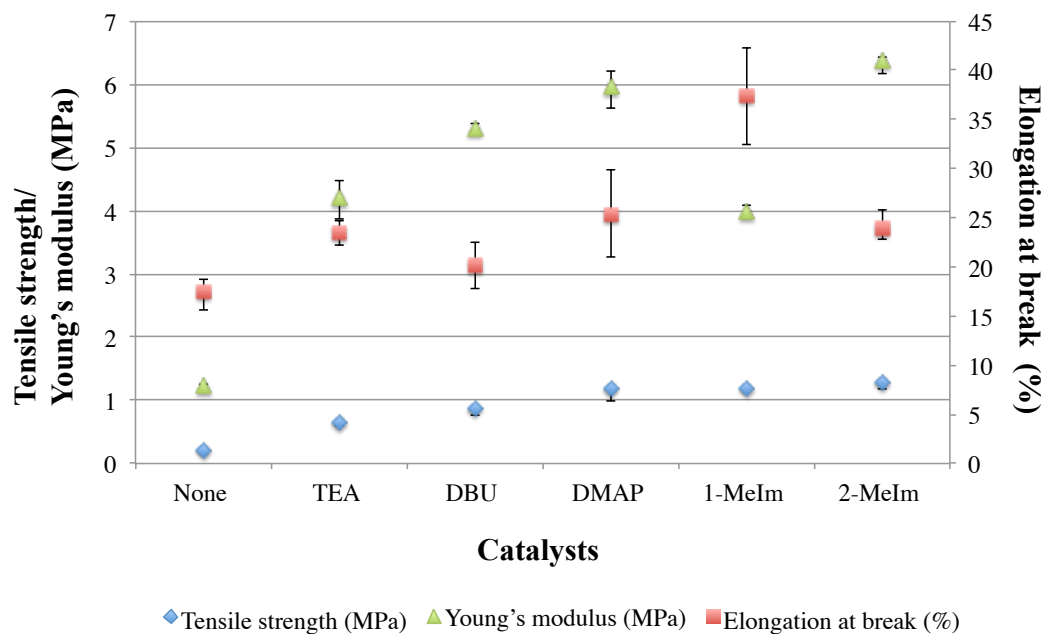


**Figure 2.11 - Mechanical properties of films cured at 140 °C (Originally in colour)**

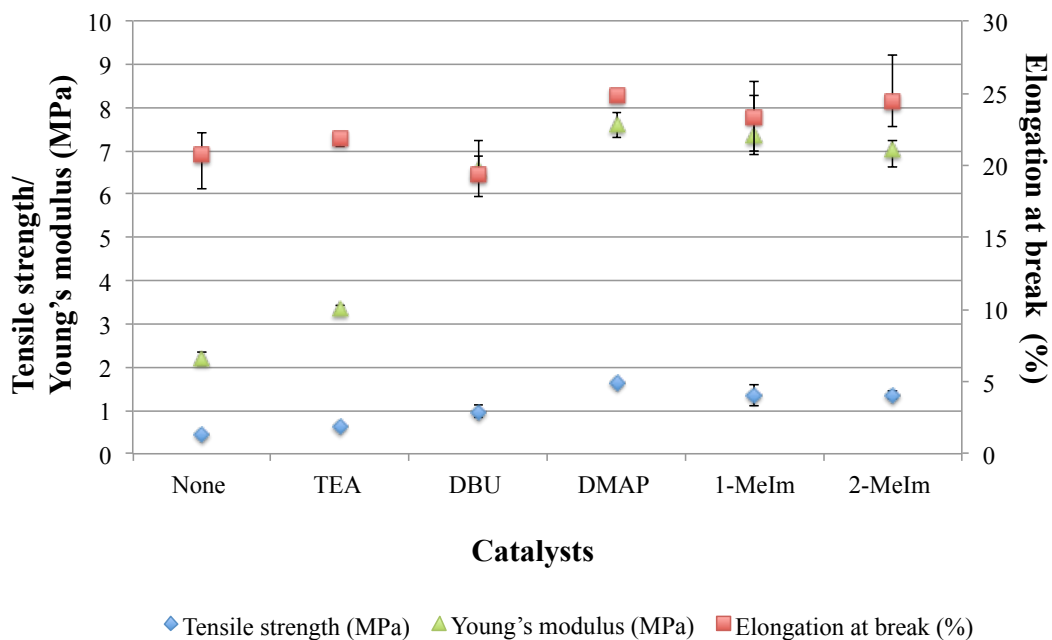


**Figure 2.12 - Mechanical properties of films cured at 160 °C (Originally in colour)**

### 2.4.2.2 Effect of different catalysts on the water uptake of the films

Suitably cured mixtures yielded highly flexible transparent films (*Figure 2.13*) with good mechanical properties and excellent water resistance. The average water uptake was taken from at least three experiments, and calculated using the formulation:

$$\text{Water uptake} = \frac{W_f - W_i}{W_i} \times 100\%$$

, where  $W_i$  = Initial weight of the film and  $W_f$  = Final weight of the film after drying

Water uptake of the films were in the range of 0.4-2% by weight after immersion in distilled water for 24 hours.

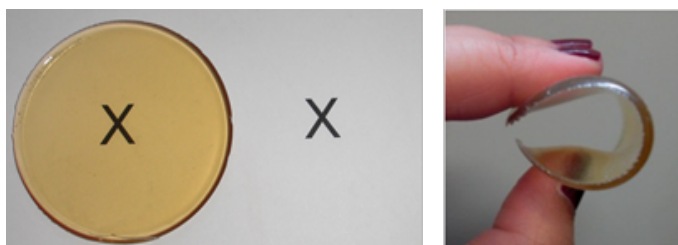


**Figure 2.13 – Transparent and flexible ELO based film (Originally in colour)**

### 2.4.2.3 Effect of different catalysts on thermal properties of the films

All films demonstrated good thermal stability with no weight loss observed between 25-300 °C (*Figure 2.14*). The films start to decompose in the range of 310 to 330 °C. The use of catalysts slightly lowers the decomposition temperature of the products by 5-10 °C.

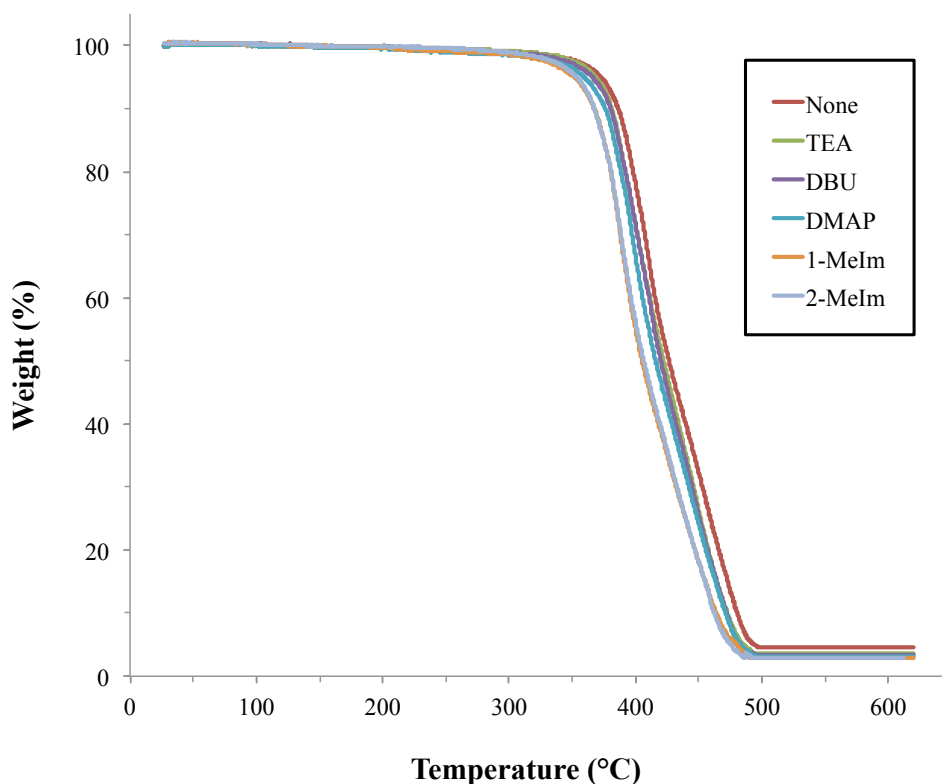


**Figure 2.14 – TGA thermograms of ELO-Prisol films with different catalysts (Originally in colour)**

## **2.5 Study of curing reaction**

### **2.5.1 Mechanistic study of curing reaction by infrared spectroscopy**

The curing mechanism of epoxy resins using amine catalysts have been intensively studied.<sup>189-192</sup> Nevertheless, the mechanism of this system with a long chain diacid and ELO is less known, especially with DBU and DMAP. Infrared spectroscopic measurements were taken every 15 minutes to investigate the curing mechanism of resin mixtures containing 5% catalyst in order to better understand the effect of catalyst addition. *Figure 2.15* shows the spectrum of Prisol and *Table 2.5* summarises the assignment of IR characteristic bands of the diacid.

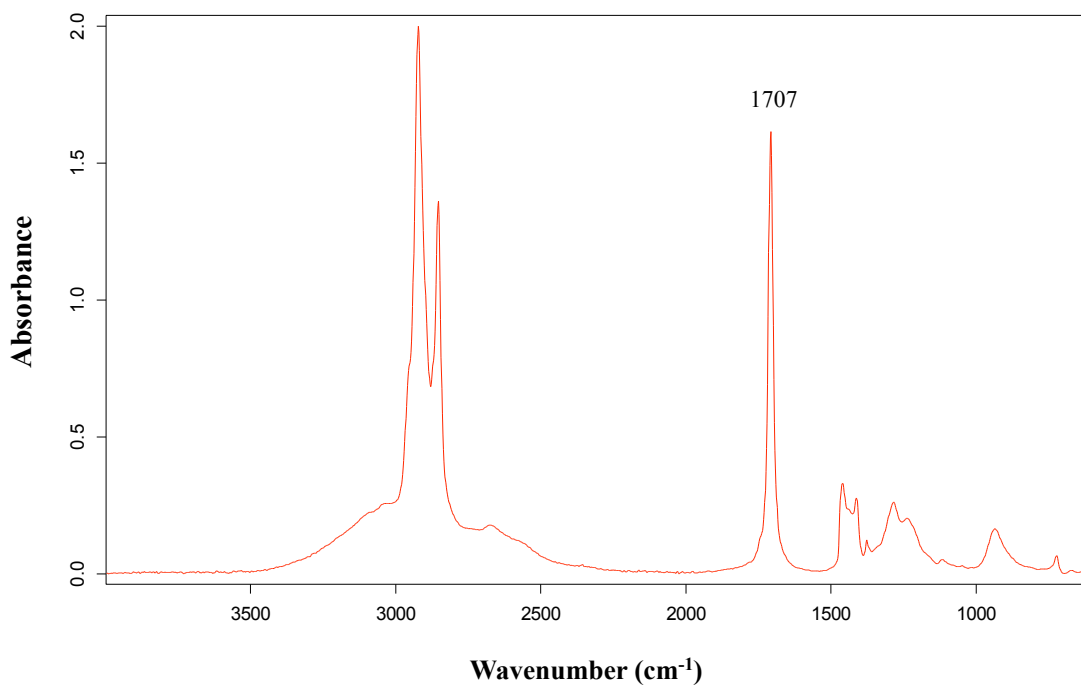


**Figure 2.15 – Infrared spectrum of Pripol**

**Table 2.5 – IR assignment of characteristic bands of Pripol**

Frequencies (Wavenumber cm <sup>-1</sup> )	Assignment
2921	Asymmetric C–H stretching of CH <sub>2</sub> , CH <sub>3</sub>
2853	Symmetric C–H stretching of CH <sub>2</sub> , CH <sub>3</sub>
1707	C=O stretching of carboxylic acid
1460	Scissoring of CH <sub>2</sub> , asymmetric bending of CH <sub>3</sub>
1376	Symmetric bending of CH <sub>3</sub>
1284	C–O stretching of carboxylic acid
935	Out-of-plane O–H of carboxylic acid
725	In-phase rocking of (CH <sub>2</sub> ) <sub>n</sub> , n > 3



Infrared spectra of the samples demonstrate some common changes (*Figures 2.17-2.21*) including the disappearance (end of the observation) of the peak at  $1709\text{ cm}^{-1}$ . The carbonyl stretch of the ester shifts from  $1740\text{ cm}^{-1}$  to  $1735\text{ cm}^{-1}$ , suggesting that the acid groups in bio-derived diacid react and new ester functionalities are formed at the end of the reaction.<sup>186</sup> Moreover, the band at  $821\text{ cm}^{-1}$ , which corresponds to that of epoxide group,<sup>193</sup> decreases in intensity with duration of curing and disappears by the end of the reaction. This is attributed to the epoxide ring-opening.<sup>184</sup> At 0 min, a band at  $1560\text{ cm}^{-1}$  attributed to the carboxylate ion resulting from the deprotonation of carboxyl group in bio-derived diacid, is observed.<sup>194</sup> This band is noted at slightly lower wavenumbers in the formulations with imidazoles. This may be explained by the formation of an imidazolium carboxylate intermediate with a strong  ${}^+\text{NH-O}^-$  bond proposed by Pire *et al.* (*Figure 2.16*).<sup>195</sup>

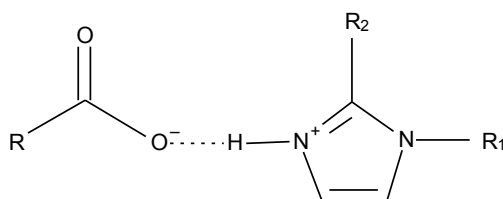


**Figure 2.16 – Imidazolium carboxylate intermediate ( $R_1, R_2 = \text{H or CH}_3$ )**

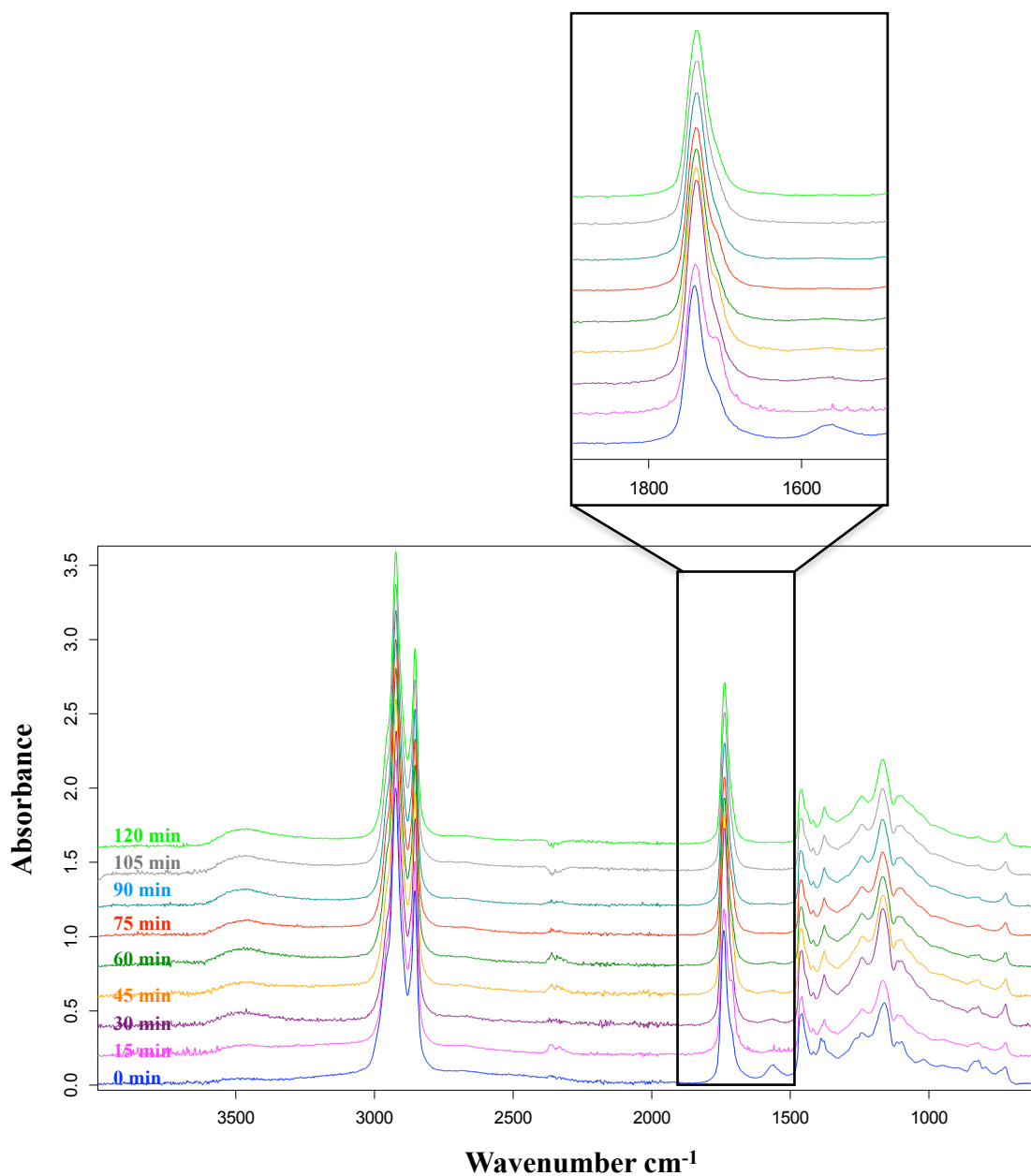


**Figure 2.17 – Infrared spectra of ELO, Pripol and TEA mixture cured at 140 °C (Originally in colour)**

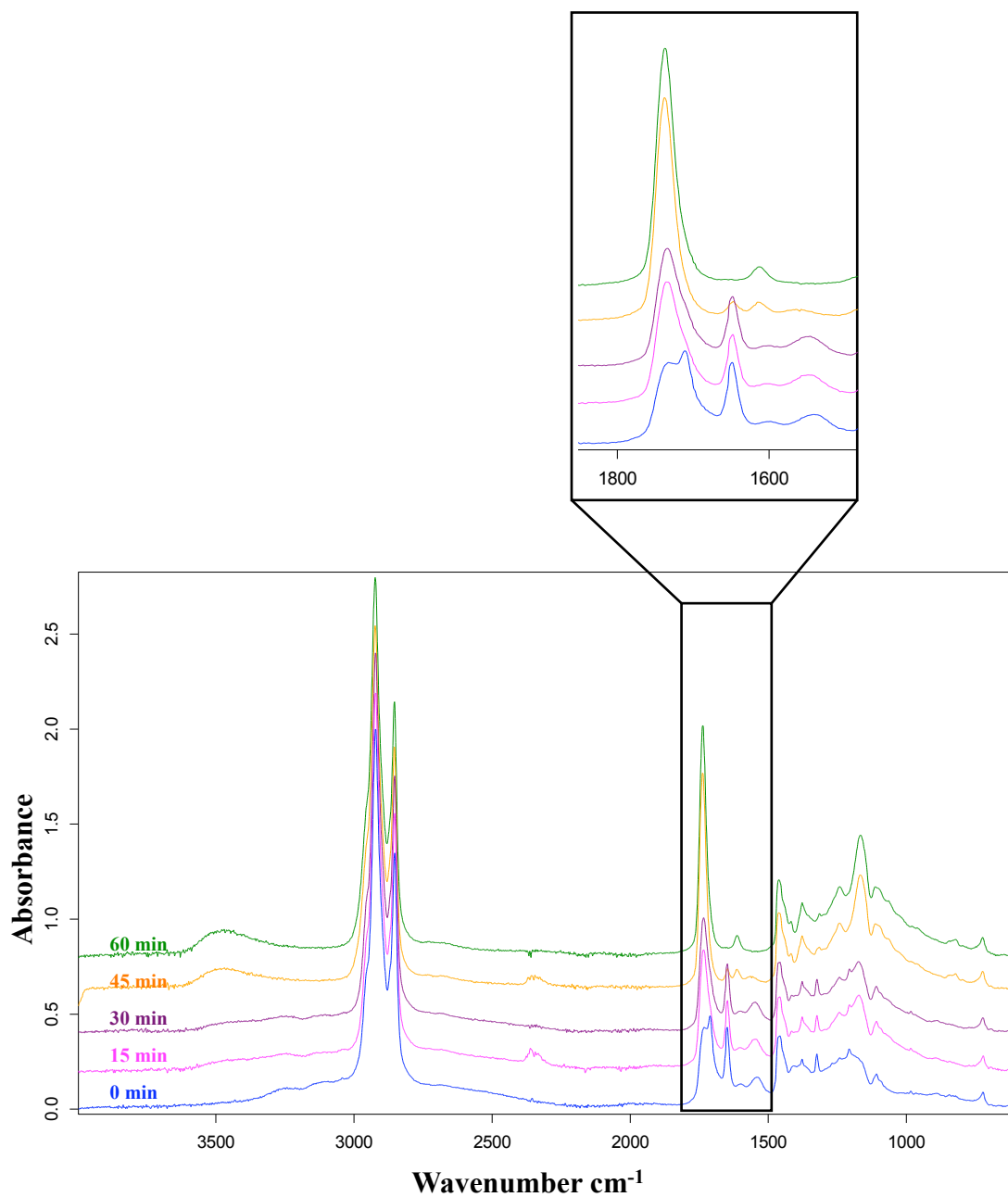


**Figure 2.18 – Infrared spectra of ELO, Pripol and DBU mixture cured at 140 °C (Originally in colour)**

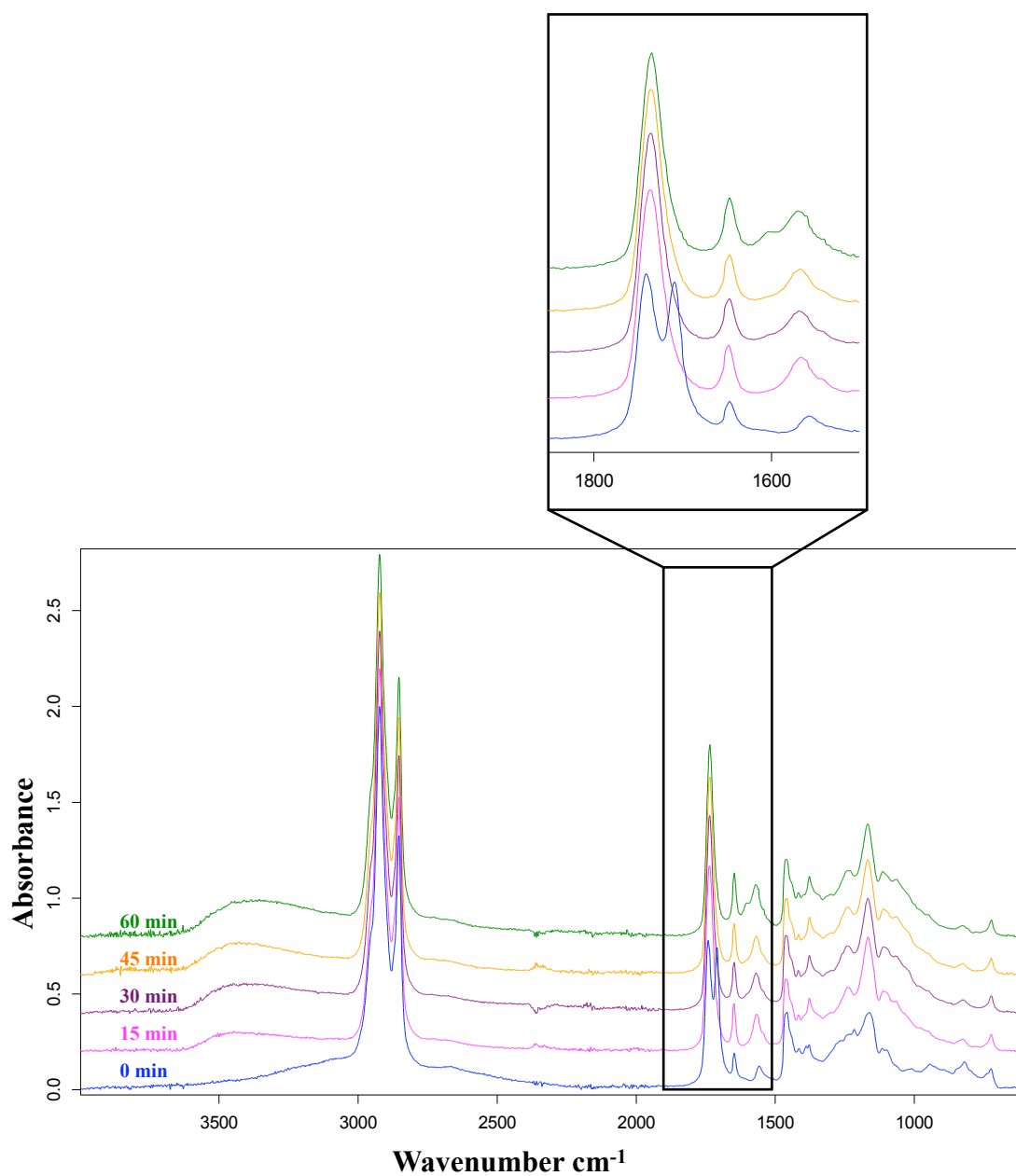


**Figure 2.19 – Infrared spectra of ELO, Pripol and DMAP mixture cured at 140 °C (Originally in colour)**

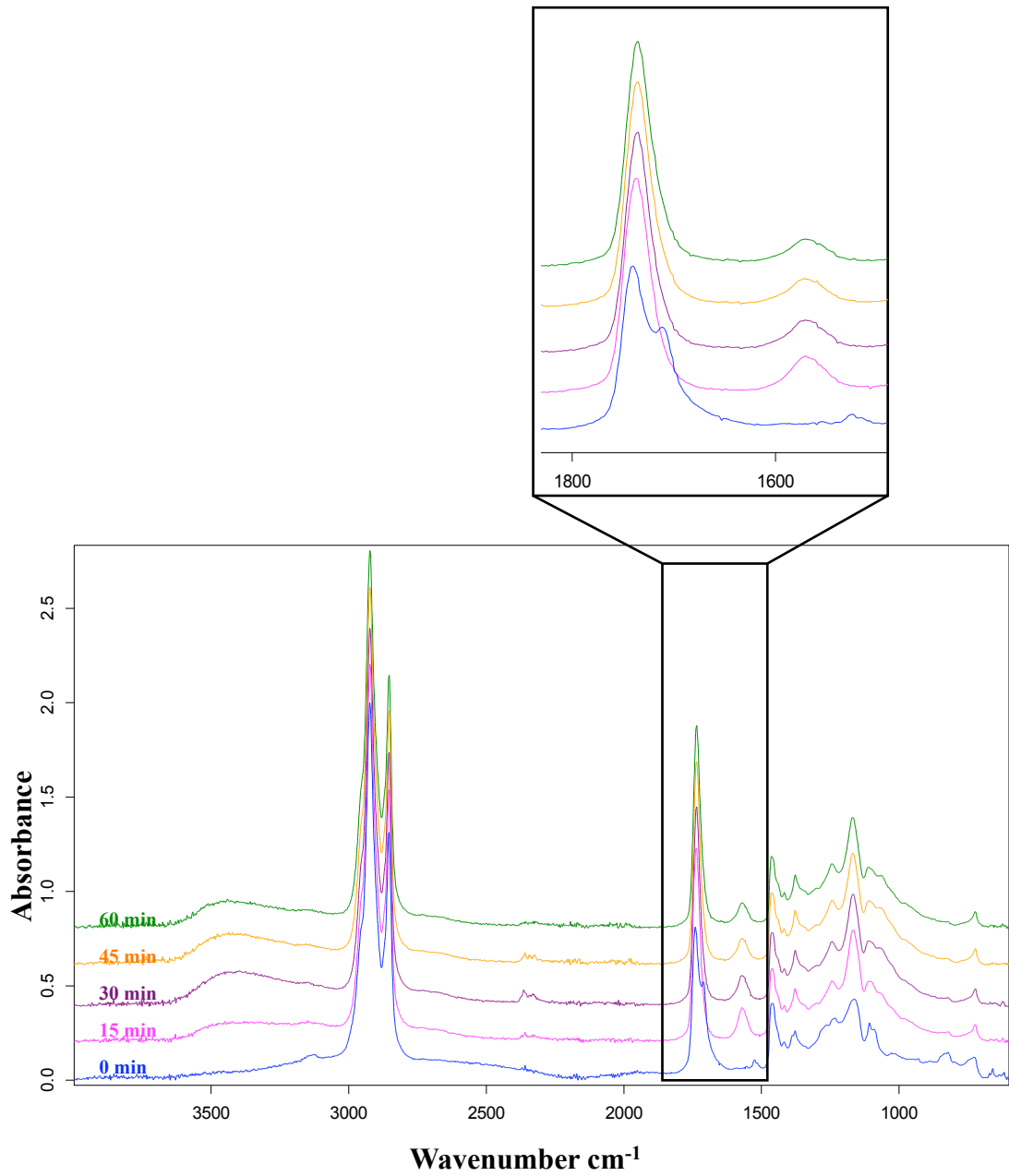


**Figure 2.20 – Infrared spectra of ELO, Pripol and 1-MeIm mixture cured at 140 °C (Originally in colour)**

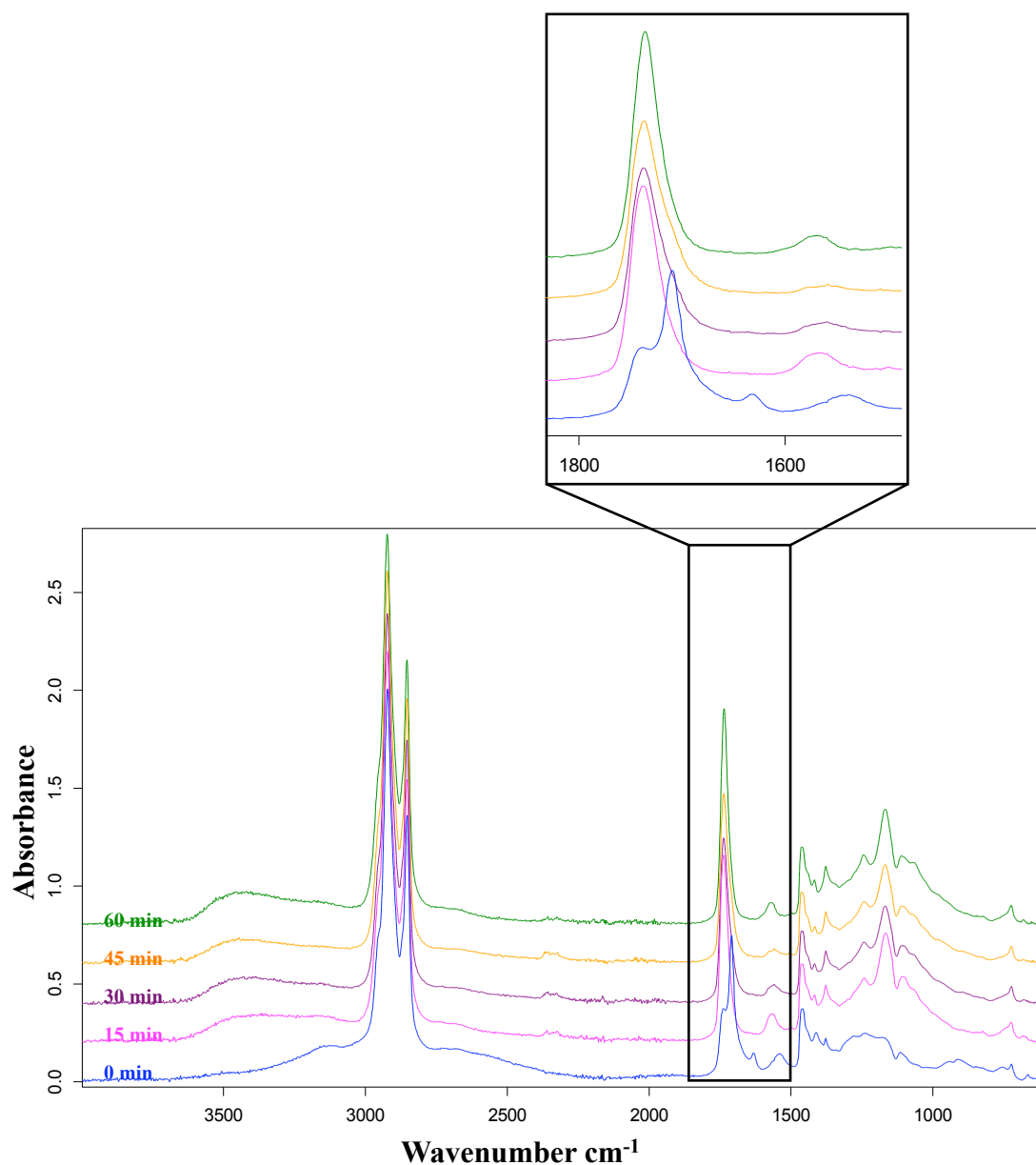
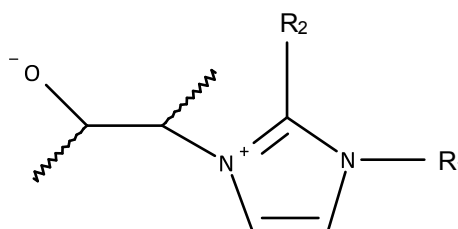


**Figure 2.21 – Infrared spectra of ELO, Pripol and 2-MeIm mixture cured at 140 °C (Originally in colour)**

This study highlighted some significant differences between the spectra of resins cured with different catalysts. At the beginning of the curing, a band at 1648 cm<sup>-1</sup> is observed in the DBU system, corresponding to the protonated amine (*Figure 2.18*).<sup>196-198</sup> This band completely disappears after 60 minutes of curing, whilst a band at 1613 cm<sup>-1</sup> from C=N bond of DBU molecule reappears. Regarding the formulation with DMAP, two intense bands at 1647 and 1570 cm<sup>-1</sup> are observed at the beginning of the curing process and remain until the end of the observation, suggesting the presence of DMAP in the cured resin (*Figure 2.19*). This may be explained by the fact that DMAP is not only

basic but also nucleophilic. It can facilitate the epoxide ring opening via nucleophilic attack of the ring and promote the etherification reaction between oxirane rings.<sup>199</sup> After this reaction, DMAP may remain attached to the resin. A mixture of ELO and DMAP was similarly studied by IR in order to confirm this postulation (*Appendix A – Figures A.2.1-2*). The bands at 1647 and 1570  $\text{cm}^{-1}$  are also noted at the end of the observation. Furthermore, the band around 3500  $\text{cm}^{-1}$  observed at the end of all mixtures, which corresponds to that of hydroxyl group, is also observed in this case but it shifts toward 3300  $\text{cm}^{-1}$ . This might be due to the presence of the attached DMAP in the product, which could influence the O-H bonds formed during the crosslinking and causes the shift of the peak.

Regarding the imidazole catalysts, a band at 1568  $\text{cm}^{-1}$  is noted at the end of the reaction (*Figures 2.20-2.21*). The band is assigned to the stretching of the imidazolium ring.<sup>200</sup> This observation is in agreement with previous report by Matějka *et al.*, which states that the amine catalyst is chemically bound to the resin after the curing process (*Figure 2.22*).<sup>201</sup>



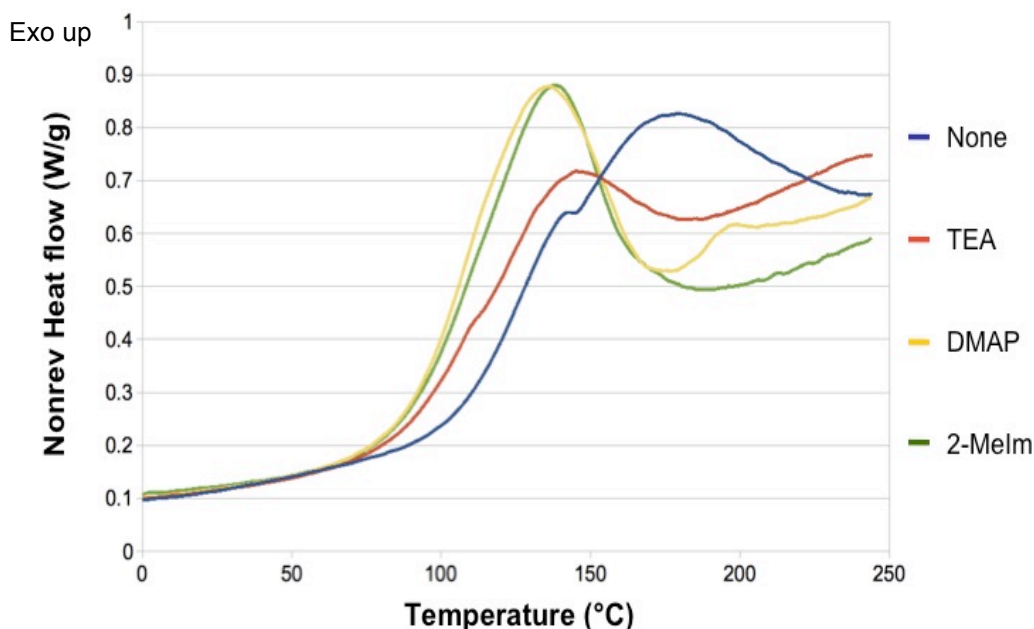


**Figure 2.23 – Thermograms of reaction mixtures of ELO/Pripol 1009 and different catalysts (Originally in colour)**

The addition of amine catalysts was observed to lower the onset temperature of curing and peak temperature as compared to the uncatalysed formulation. Thermograms of the uncatalysed and TEA catalysed formulations reveal a slight shoulder that occurs before the main thermal event, occurring at approximately 145 °C in the formulation containing no catalyst and at approximately 120 °C in the presence of TEA. From these results it can be deduced that a possible two stage curing process occurs. Based on our infrared spectroscopy study of the curing mechanism, the first exothermic peak is due to the ring opening of the epoxide and second thermal event probably corresponds to subsequent etherification-epoxide ring opening and cross-linking reactions. In contrast, DMAP and 2-MeIm containing films show one thermal event only. However, the two thermal events may still be present but could not be resolved by the instrument. As shown in *Figure 2.24*, MDSC was performed on ELO with DMAP, in order to probe the DMAP-ELO interaction. The resultant thermogram also revealed two thermal events occurring over the temperature range 136 – 200 °C. The first thermal event peaked at 150 °C with the second peaking at approximately 170 °C correlating well with our proposal of initial nucleophilic ring opening by DMAP followed by etherification reactions. The infrared spectrum also reveals loss of bands associated with the epoxide ring (821  $\text{cm}^{-1}$ ) and appearance of the O-H stretch at 3500  $\text{cm}^{-1}$  in the cured ELO-DMAP film.



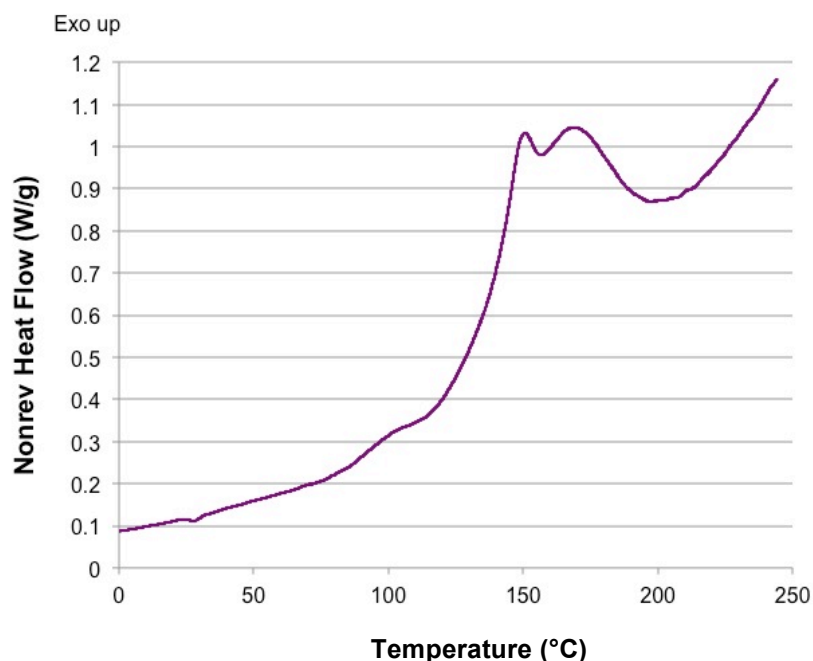


**Figure 2.24 – Thermogram of reaction mixture of ELO and DMAP**

The peak temperature of curing decreases in the order: uncatalysed ( $179.3\text{ }^{\circ}\text{C}$ ) > TEA ( $140.0\text{ }^{\circ}\text{C}$ ) > 2-MeIm ( $137.6\text{ }^{\circ}\text{C}$ ) > DMAP ( $133.4\text{ }^{\circ}\text{C}$ ). Interestingly, the heat of reaction for the curing process decreases in the order: uncatalysed ( $161.9\text{ J/g}$ ) > 2-MeIm ( $160.7\text{ J/g}$ ) > DMAP ( $131.9\text{ J/g}$ ) > TEA ( $79.1\text{ J/g}$ ). The variations in the heat of reaction could potentially be due to the extent of polymerisation between ELO and Pripol 1009.<sup>19</sup> Assuming that full cure is represented by the uncatalysed film ( $161.9\text{ J/g}$ ), then 2-MeIm derived film is comparable ( $160.7\text{ J/g}$ ) and as such is assumed to be the best cured. The heat of reaction of DMAP catalysed films is  $30\text{ J/g}$  lower than uncatalysed formulation however, an additional thermal event peaking at approximately  $200\text{ }^{\circ}\text{C}$  accounted for this deficit. The heat of reaction for the curing process of the formulation containing TEA is significantly lower ( $79.1\text{ J/g}$ ) than the uncatalysed formulation and as such remains relatively uncured. This value represents the enthalpy associated with the main thermal event and the slow second thermal event that appears between  $200\text{--}250\text{ }^{\circ}\text{C}$  may account for any enthalpic shortfall. In addition, the lone pair on the central nitrogen atom of TEA may be less available due to induce steric hindrance resulting from the three flexible ethyl chains, thus reducing its potential to either act as a base or nucleophile.

In an attempt to relate the mechanical properties, in particular the Young's Modulus, outlined in the previous section (*Figure 2.12*) with respect to the thermal data shown in *Figure 2.23* then we must consider the thermal situation at 160 °C (assume drawing a notional vertical line at 160 °C in *Figure 2.23*). Qualitatively, the extent of cure for the uncatalysed and TEA-containing films appears to be significantly smaller than for DMAP and 2-MeIm. The main thermal event for the uncatalysed film has not reached peak (179.3 °C) and thus gives a film with the lowest Young's Modulus. The TEA film reaches peak at 140.0 °C but, thermal events are occurring slowly albeit faster than the uncatalysed film, so a slight improvement in Young's Modulus is observed. This situation changes drastically with DMAP (peak temperature, 133.4 °C) and 2-MeIm (peak temperature, 133.4 °C) as considerable enhancement of the Young's Modulus occurs. The thermograms for DMAP and 2-MeIm are near identical up to 160 °C with both showing a greater extent of curing based on a larger heat of reaction and a more complete thermal event than compared to TEA and the uncatalysed film.

**Table 2.6– MDSC analysis of formulations with different catalysts**

Catalyst	None	TEA	DMAP	2-MeIm
Heat of reaction (J/g)	161.9	79.1	131.9	160.7
Onset temperature (°C)	103.94	82.29	92.61	82.74
Peak temperature (°C)	179.31	140.0	133.36	137.61
Tg (°C)	-17.59	-18.03	-13.33	-10.36

### 2.5.3 Study of curing reaction using viscometry

Viscosity measurement provides important information regarding chain mobility and progress of curing.<sup>200</sup> Initially, sample viscosities of the mixtures decreased due to temperature increase aiding molecular mobility. The viscosities of the samples were in the region of 400-500 centipoise (cP), with the exception of the uncatalysed mixture,

which had a starting viscosity in the region of 1000-2000 cP. This suggests that the addition of catalysts initially decreases the viscosity of the mixture, which allows better movement of the polymer chains in the system.

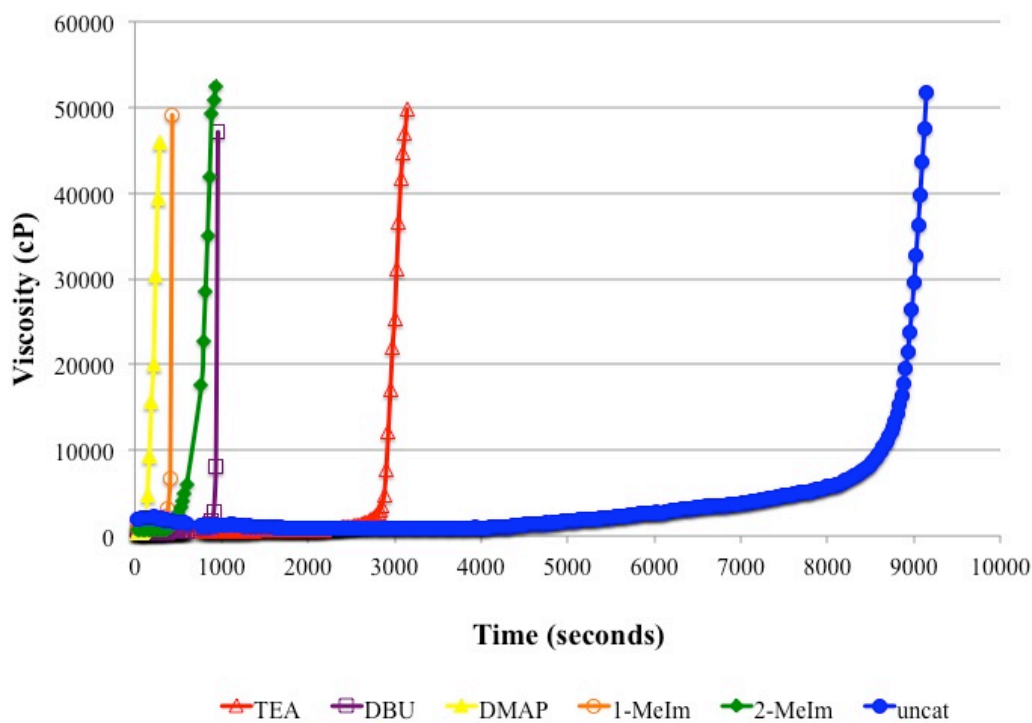


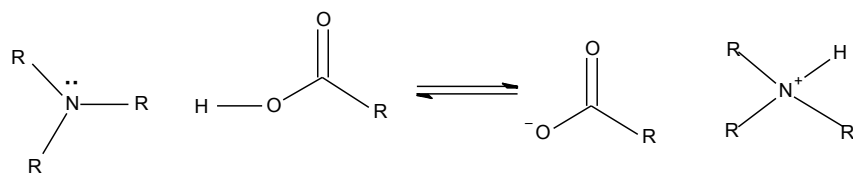
**Figure 2.25– Viscosities of the reaction mixtures (Originally in colour)**

During the curing reaction processes, the viscosity increases as the molecular weight of the polymer increases.<sup>202</sup> The gel point is defined as the point at which the formation of the first macromolecule of infinite dimension occurs and it indicates the transition of a liquid to a solid.<sup>203, 204</sup> At the gel point, the mixture becomes very viscous, and hence difficult to process. The study of the gel point is therefore crucial for the production process of thermosetting polymers. The gel point was defined as the point at which the diverging steady state viscosity becomes infinite.<sup>203, 205</sup> The gel point of the uncatalysed system is significantly greater than other mixtures. This shows the slow polymerisation of this system without catalysts. Other reaction mixtures gel points vary from 9 to 48 minutes (*Figure 2.25*), with TEA mixture taking considerably longer than other catalysed mixtures to gel. This might be due to the steric hindrance in the catalyst molecule, inhibiting the base from catalysing the polymerisation in this “congested”

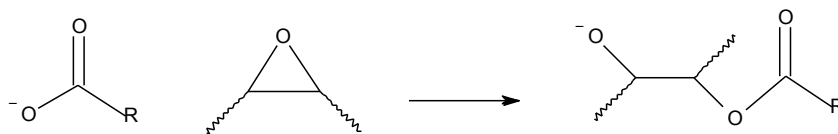
system. The other mixtures' gel points occur within 9-15 minutes, with the reaction with DMAP and 1-MeIm showing the quickest gelation process indicating rapid polymerisation and formation of the cross-linked network.

#### **2.5.4 Proposed mechanism of the reaction system**

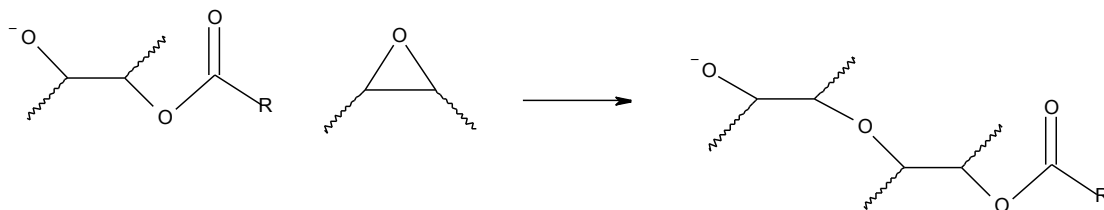
According to spectroscopic and thermal studies, the mechanism of the system is proposed in *Figure 2.26*. The early stage of cure involves deprotonation of the carboxylic acid by tertiary amine or imidazole catalysts, which results in a carboxylate anion (reaction A). The free carboxyl group in the carboxylate anion then reacts with epoxide to yield an alkoxide (reaction B). The alkoxide reacts further with the epoxide leading to a formation of another alkoxide (reaction C). The propagation of the polymerisation occurs through the etherification, which cross-links the system. The protonation of alkoxide occurs during the curing to form the alcohol is shown in reaction D. In the system using catalysts with good nucleophilicity such as DMAP, the catalysts can perform a nucleophilic substitution onto the epoxide to promote the ring-opening reaction (reaction E).



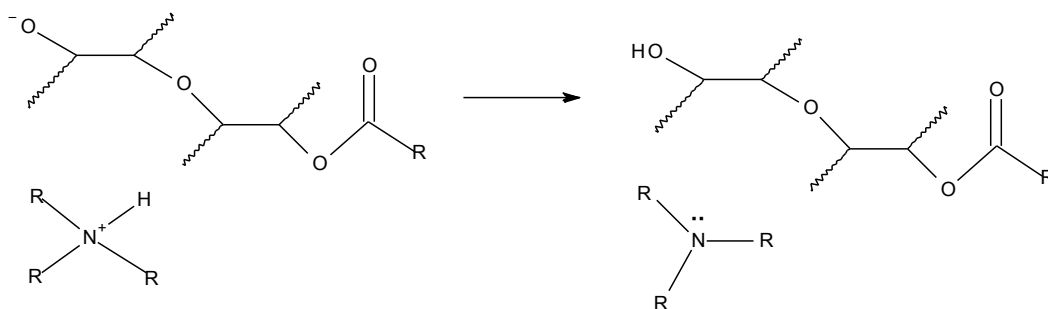
A) Deprotonation of carboxylic acid by amine or imidazole catalyst



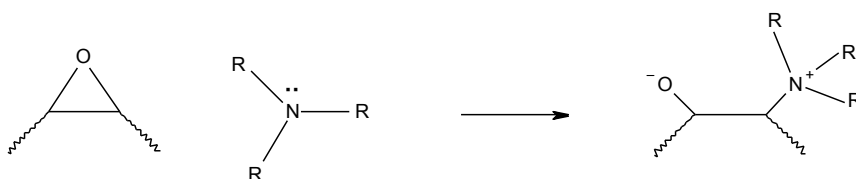
B) Epoxide ring-opening by carboxylate anion



C) Epoxide ring-opening by alkoxide



D) Protonation of alkoxide



E) Epoxide ring-opening by nucleophilic catalyst

**Figure 2.26 – Proposed mechanism of the reaction system**

## 2.6 Optimisation of formulation with DMAP

### 2.6.1 Effect of amount of catalyst on the mechanical properties of the films

The concentration (% of total resin weight) of DMAP was varied from 0.1% to 5% in order to ascertain the influence of catalyst concentration on mechanical properties (Young's Modulus, tensile strength and elongation at break) (*Figure 2.27*). The films were cured at 140 °C for 1 hour except for the uncatalysed film, which was cured for 6 hours.

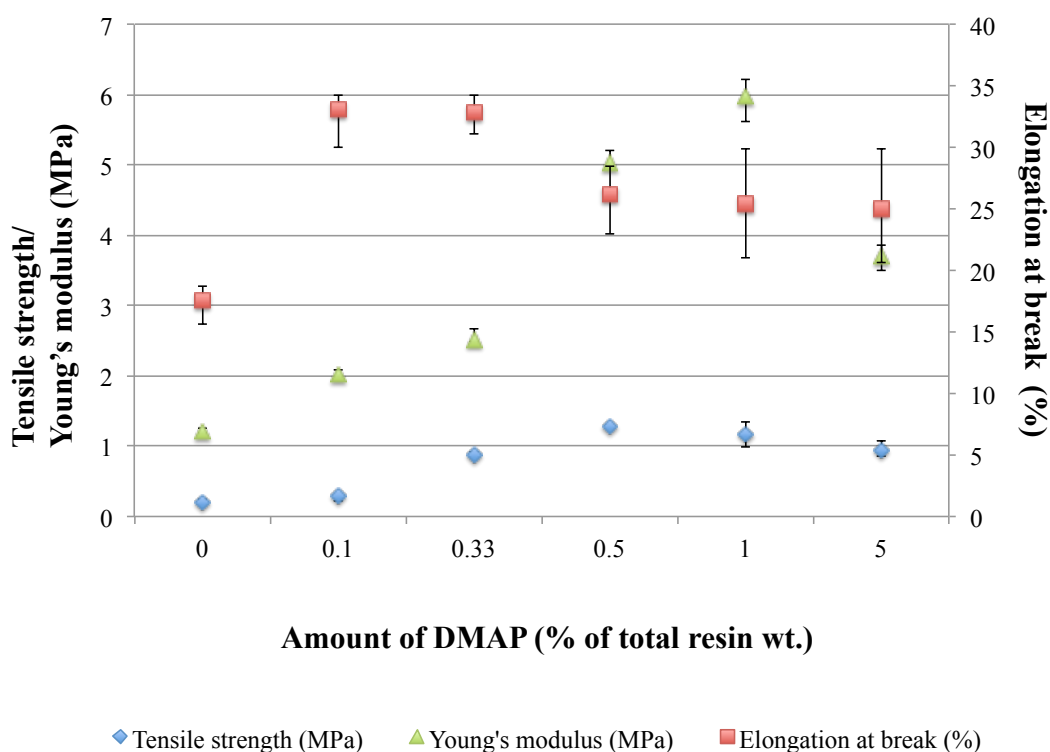


**Figure 2.27 – Mechanical properties of films with different amounts of DMAP (Originally in colour)**

The tensile strength increases with increasing catalyst concentration peaking at 0.5% wt. and then tends to plateau for the remaining concentrations. Interestingly, the Young's Modulus is highest for the formulation comprising 1% DMAP by weight. Thereafter, at a higher concentration (5% wt.) it decreases significantly. Thus, only a small amount of

DMAP is needed in the formulation in order to obtain resins with optimum mechanical properties. Elongation at break is best at low concentrations of catalyst as the curing is still incomplete, hence allowing more mobility of polymer chains. In summary, this bio-based resin is a step forward in the use of greener feedstocks to produce thermosetting resins. The reduction of the amount of catalyst to as low as 0.5-1% of the total resin weight is of great benefit to this system.

### 2.6.2 Effect of curing temperature on the mechanical properties of the films

Different curing temperatures from 140-180 °C were applied to the formulation composed of ELO, Pripol and DMAP (1% of total weight) (*Figure 2.28*). Although, the thermal analysis showed the peak temperature of the system close to 140 °C, the film produced at 160 °C demonstrates higher tensile strength and Young's modulus than those of the film produced at 140 °C. The elongation of both films is comparable. When higher curing temperature (180 °C) was applied, the tensile strength and the elongation at break of the resulting film dramatically decrease by 145% and 81%, respectively. The Young's modulus also slightly decreases to approximately 9%.

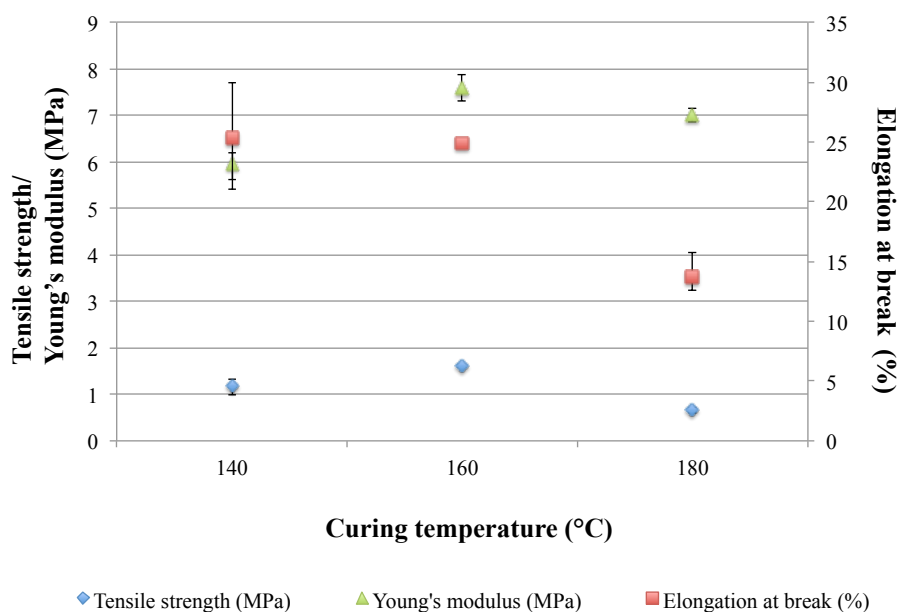


**Figure 2.28 – Mechanical properties of films with different curing temperatures (Originally in colour)**

### 2.6.3 Effect of curing time on the mechanical properties of the films

The effect of the curing time on the mechanical properties of the films is demonstrated in *Figure 2.29*. The standard formulation of ELO, Pripol and DMAP (1% of total weight) was used to produce films using different curing times (15, 30, 45, 60, 90 and 120 minutes) at 160 °C. The tensile strength and elongation at break of the films reaches the maximum after 60 minutes of cure and slightly decreases when the films are heated for longer. The Young's modulus increases with the curing time and plateaus after 60 minutes.

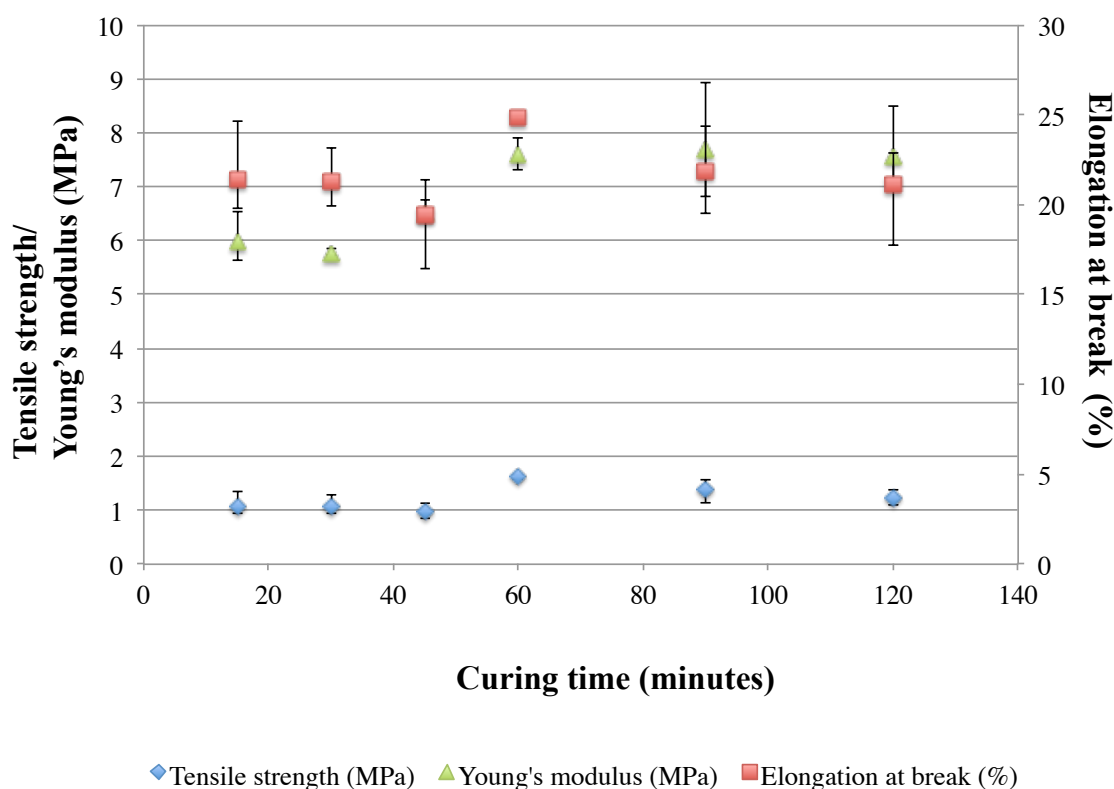


**Figure 2.29 – Mechanical properties of films cured for different times at 160 °C (Originally in colour)**

## 2.7 Conclusions

Novel thermosetting resins based on epoxidised linseed oil (ELO) and bio-derived crosslinkers were investigated. Curing the long-chain diacid Pripol 1009 yielded a transparent film with good flexibility, and thus was chosen for further studies. Different



amine catalysts were discovered to have influence on the product properties. The thermal analysis demonstrated that the optimum ratio of ELO and Pripol 1009 was 50:50% wt. This formulation showed the highest enthalpy of the curing reaction and therefore indicated the greatest degree of conversion of the system. Furthermore, infrared spectroscopy was utilised to study the reaction mechanism of the system. The IR data suggested the formation of carboxylate anion, resulting from the deprotonation of the acid group(s) in Pripol 1009 occurred at the beginning of the reaction. The carboxylate ion then acted as a nucleophile in the ring-opening of the epoxide resulting in an alkoxide, which could be protonated to form an alcohol. The base catalysts assist the proton transfer in the system. The alcohol formed could continue to react with more epoxide and consequently create the polymerised network. This was in agreement with the thermal analysis using modulated differential scanning calorimetry. The thermograms showed that the curing process occurred in two steps, assigned to the formation of alkoxide from the epoxide ring opening and the etherification of alcohol formed in the first reaction and oxirane ring. Interestingly, the use of a relatively small amount of DMAP as catalyst in the formulation gave the best mechanical properties. The production of the film was optimised and the mixture cured at 160 °C for 1 hour yielded a film with the best mechanical properties. The resulting films showed excellent water resistance and good thermal stability.



# Chapter 3

## *Starch and acid hydrolysed starch in bio-based thermoset composites*



### 3.1 Chapter 3 - Summary

Bio-based thermoset composites with exceptionally high content of bio-based feedstocks were prepared from epoxidised linseed oil and native or acid hydrolysed starch. Normal corn starch and high amylose corn starch were modified via acid hydrolysis. Two methods were applied to the normal corn starch and in order to substantiate the modification, different tests and analysis were conducted on the acid hydrolysed starch, and the altered properties were determined accordingly. The solubility of acid hydrolysed starch granules increased with the hydrolysis time, whilst the swelling power decreased due to the rise of crystallinity after acid hydrolysis. Pasting results showed a reduction in peak viscosity after acid treatment, which was associated to shorter starch chains. Hydrolysis moderately affected the thermal stability of the starch by lowering the decomposition temperature of the acid hydrolysed starches compared to that of native starch. Morphological studies of starch granules were performed using scanning electron microscopy, which revealed changes on the granules surface and in some cases significant breakdown of the granules (24-hour hydrolysis). High amylose corn starch was found to be more resistant to acid hydrolysis than normal corn starch, probably due to the greater presence of complex amylose-lipids within the granules, and that variety of starch having a thicker granule membrane. The native and acid hydrolysed starches were included in the optimised formulation obtained from study reported in chapter 2, which consists of ELO, Pripol and 0.5 % of DMAP with respect to the total resin weight. The tensile testing of the resulting films demonstrated that the addition of starch improved the mechanical properties of the resins. The film containing 24-hour acid treated normal corn starch yielded the highest Young's modulus, with an 84.4% improvement compared to that of the film without starch. The film with native high amylose starch had the greatest tensile strength, which was 42.3% higher than that of the film with no added starch. The elongations at break of all films were in the same region at approximately 20%. The SEM micrograms showed that high amylose starch granules had better miscibility with the polymer matrix than the 24-hour acid hydrolysed normal corn starch.

## 3.2 Introduction

Starch is regarded as an attractive raw material in the polymer and composite industry, owing to its abundance, low cost and biodegradability.<sup>150</sup> Corn starch is extracted from corn, which is the largest produced crop in the world. According to the United States Department of Agriculture (USDA), the world production of corn in 2011 was 873.73 MMT, followed by wheat at 649.69 MMT and rice at 463.94 MMT.<sup>206</sup>

Starch has been used as filler in synthetic plastics, such as polyvinyl chloride and polyethylene, in order to improve the degradability of the materials.<sup>153, 207</sup> It has also been blended with degradable polymers such as poly (hydroxybutyrate-co-valerate) (PHBV) and polylactic acid to reduce the production cost.<sup>208, 209</sup> However, the addition of starch filler sometimes compromises the mechanical properties of the products, due to poor interfacial adhesion of starch and the polymer matrix.<sup>153, 208</sup>

Acid hydrolysis has been used to modify the structure of starch granules for more than a century.<sup>137</sup> The cleavage of glycosidic linkages during hydrolysis, results in the decrease of degree of polymerisation of starch.<sup>210</sup> Numerous properties of acid treated starches differ from ones of native starch, including increased solubility, decreased paste viscosity and changes in gelatinisation properties.<sup>135, 139, 211</sup> Two typical methods to prepare acid treated starch include treatment of starch in water with 15% of sulfuric acid for 30 days at room temperature, producing Nägeli amyloextrins, and treatment using 2.2 N hydrochloric acid at 30-40 °C to yield linternised starch.<sup>137, 212</sup> However, several novel techniques have been developed including the use of alcohol instead of water in the hydrolysis process. The different effects on the modification of starch using different alcohols or mixtures of alcohols is suggested to be due to different concentrations of acid inside the granules.<sup>213</sup> Robyt *et al.* reported that alcohols or combination of alcohols influenced the glycosidic linkages to become more susceptible to acid hydrolysis.<sup>214</sup> Moreover, Polaczek *et al.* heated potato starch in alcohols (methanol, 1-propanol and 1-pentanol) at reflux and suggested that alcohols penetrated inside starch granules and expelled the amorphous content of the granules through the hilum. In the consequence, the structure of the starch granules are irreversibly changed.<sup>215</sup>

To the best of the author's knowledge, no research has been conducted on the use of acid hydrolysed starch (or soluble starch) with epoxidised oils to form composites; however, this type of starch has been used in combination with other polymers.<sup>216-218</sup> Poly (styrene-co-butyl-acrylate) has been filled with linternised waxy maize starch in order to reinforce the thermoplastic matrix. The mechanical properties of the composite materials are considerably improved with the amount of starch filler.<sup>216</sup> Starch nanocrystals are prepared via acid hydrolysis of waxy maize starch then subsequently added to sorbitol-plasticised pullulan (polysaccharide produced by strains of fungus *Aureobasidium pullulas*) to produce biopolymer films.<sup>217</sup> The addition of the nanocrystals lowers the water-uptake of the films. The Young's modulus and tensile strength are also dramatically enhanced but the strain at break decreases substantially.<sup>218</sup>

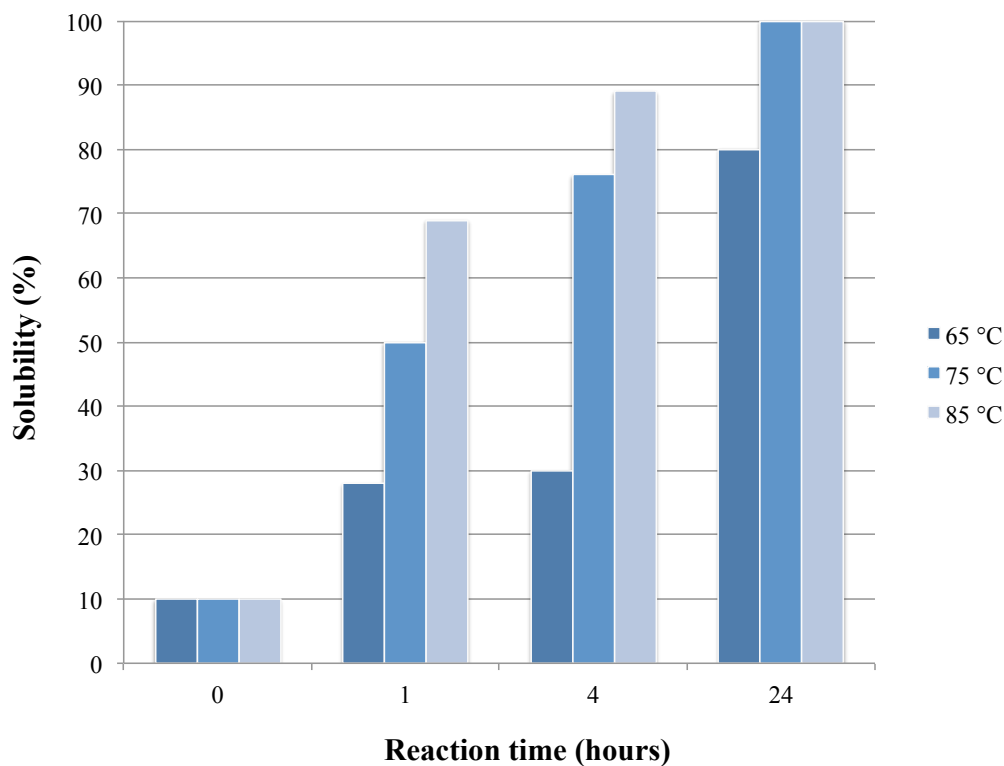
In this chapter, native starch (normal corn and high amylose corn) and their acid hydrolysed counterparts were included in the standard formulation of ELO and Pripol in the presence of DMAP. The acid treatment of starch was carried out in either water or ethanol and the acid hydrolysed products were characterised and subsequently used in the formulation. The resulting films were tested for their mechanical properties and scanning electron microscopy was used for the morphological study of the cross-section of the films.

Herein, two methods of hydrolysis were performed in order to investigate the effect of these different conditions on the properties of the starch product. The first method comprised of treating starch with 1 mol/L of hydrochloric acid (in water) at 50 °C for 1, 4 or 24 hours (method 1),<sup>219</sup> whilst the second method used acidic ethanol at room temperature for 1, 3, 5 or 7 days (method 2).<sup>220</sup> The complete experimental procedures are described in sections 7.3.1 and 7.3.2. Different hydrolysis methods were employed to determine the effect they had on the properties of the starch in composite film formation. The treated starches were analysed to determine their solubility, swelling, pasting and thermal analysis properties, to confirm hydrolysis and assess the suitability of the method for use in these types of film applications.

### 3.3 Comparison of acid hydrolysis methods for normal corn starch

#### 3.3.1 Solubility and swelling power

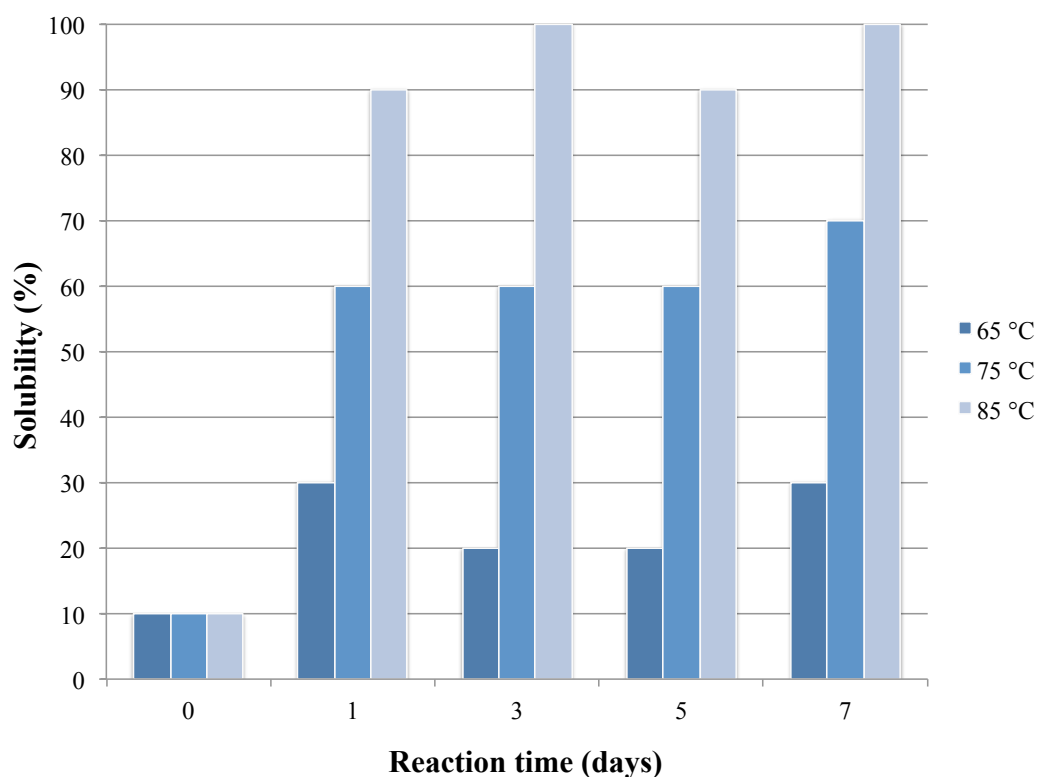
Acid hydrolysis has a significant effect on the solubility of starch granules. The increase in solubility of starch can be observed after acid treatment and tends to increase with the hydrolysis time.<sup>135</sup> All acid hydrolysed starches show higher solubility than that of native starch, confirming its modification. *Figure 3.1* shows the effect of the temperature and hydrolysis time on solubility of acid hydrolysed starch in water (method 1).



**Figure 3.1 – Effect of temperature and reaction time on solubility of acid hydrolysed normal corn starch in water (Originally in colour)**

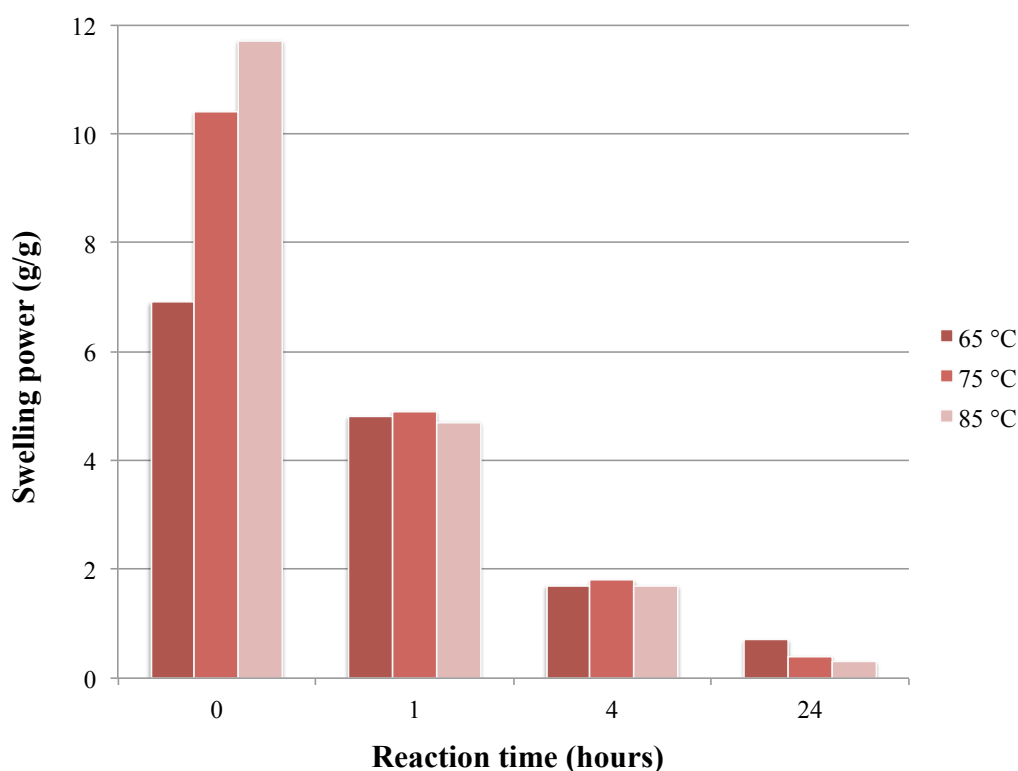


Native corn starch has low solubility at approximately 10% and this scarcely varies with the temperature. Acid treated starches demonstrate significant solubility improvement. The percentage of soluble starch granules increases from 10% to almost 70% at 85 °C after only 1 hour of treatment. The solubility of starch granules increases with temperature and the hydrolysis time. After 24 hours of the treatment, resulting starch exhibits 100% solubility at 75 and 85 °C. The solubility of hydrolysed starch in ethanol (method 2) is shown in *Figure 3.2*. At 75 °C, all acid hydrolysed starches show more than 60% solubility, and between 90-100% at 85 °C. In general, the long duration of acid treatment seems to increase the solubility of the granules, however, there is only a slight difference between the percentages of solubility of the granules from different treatments at each temperature performed ( $\approx 10\%$ ), indicating the hydrolysis time scarcely affect the solubility in this case. It is noted that method 1 yields products with better solubility after 24 hours than method 2, suggesting higher degree of hydrolysis of the modified starch in water.



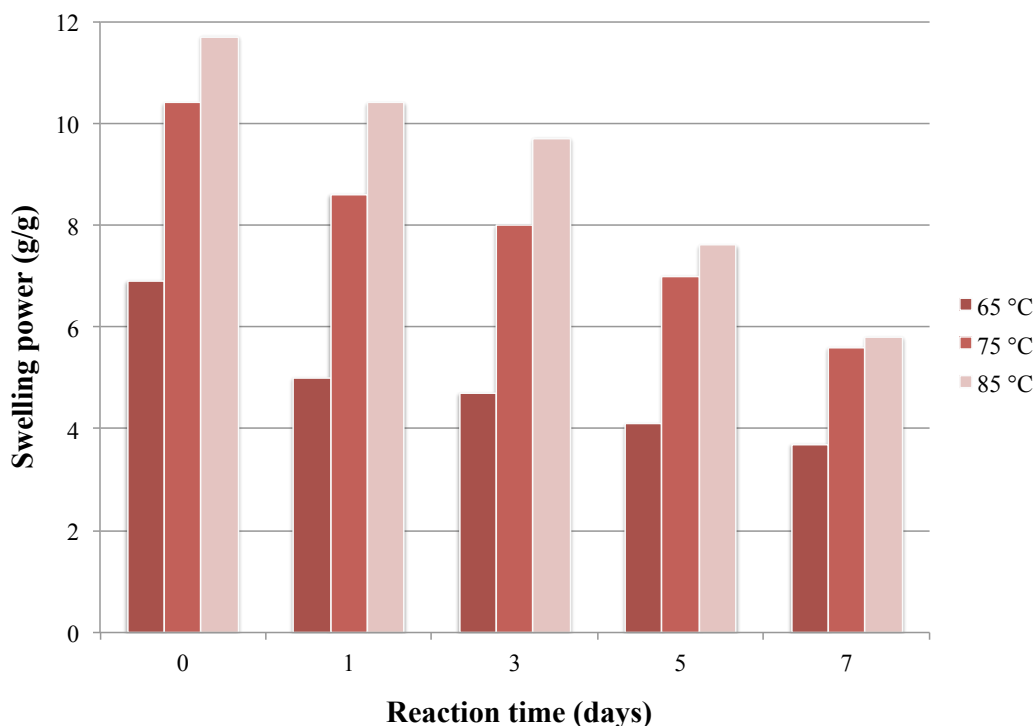
**Figure 3.2 – Effect of temperature and reaction time on solubility of acid hydrolysed normal corn starch in ethanol (Originally in colour)**

Figure 3.3 presents the effect of temperature and hydrolysis time on swelling power of acid treated starch. The swelling capacity of native corn starch increases as the temperature increases. Starch mobility improves as the temperature rises, which facilitate percolation of water, resulting in increase of swelling power.<sup>221</sup> However, the swelling power of acid modified starches is independent to the temperature as the values of swelling power at 65, 75 and 85 °C are relatively similar. It is noteworthy that the swelling capacity decreases as the hydrolysis time increases. The reduction of swelling power after the acid hydrolysis is associated with the increase of crystallinity in starch granules.<sup>221</sup> Acid treatment increases the ratio of relative crystallinity of starch as hydrolysis preferentially occurs in the amorphous regions.<sup>222</sup>



**Figure 3.3 – Effect of temperature and reaction time on swelling power of acid hydrolysed normal corn starch in water (Originally in colour)**

The same observation was made with acid hydrolysed starch in ethanol as the swelling power of starch granules decreases when they are treated with acid for longer time (Figure 3.4). The swelling power of native starch shows positive correlation with the temperature, which is in agreement with previous work reported by Luo *et al.*<sup>223</sup>



**Figure 3.4 – Effect of temperature and reaction time on swelling power of acid hydrolysed normal corn starch in ethanol (Originally in colour)**

### 3.3.2 Pasting properties

It has been described in several reports that pasting viscosity of acid hydrolysed starch decreases compared to that of native starch.<sup>135, 139, 210</sup> The viscosity decrease of acid treated starch paste is associated with shorter chains in starch granules.<sup>211</sup> *Figure 3.5* demonstrates the viscosity profiles of native corn starch and the water acid hydrolysed starches. The unmodified starch paste has the highest peak and final viscosity, whilst the three acid treated starches clearly show a significant reduction in their viscosities. The peak viscosity of the native normal corn starch paste is approximately 15,000 cP. This drops to less than 1,400 cP after only 1 hour of treatment.

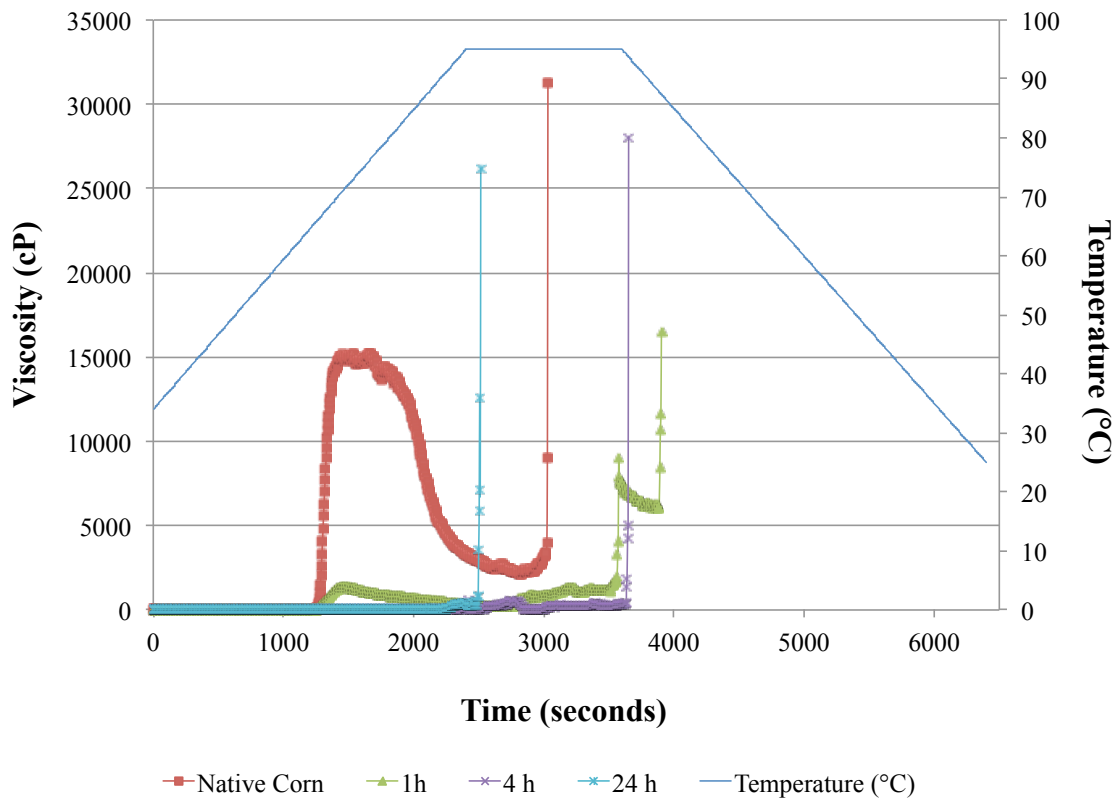


**Figure 3.5 – Viscosity profiles of native normal corn starch and acid hydrolysed starches in water (1, 4 and 24 hours) (Originally in colour)**

Further hydrolysis reduces the peak viscosity to less than 100 cP after 4 and 24 hours of the treatment (*Figure 3.6*). *Figure 3.7* shows the pasting viscosity of modified starches in ethanol and a similar result is observed with peak viscosity decreasing with hydrolysis time. After 1 day of treatment the peak viscosity decreases from 15,000 cP to approximately 1,700 cP.

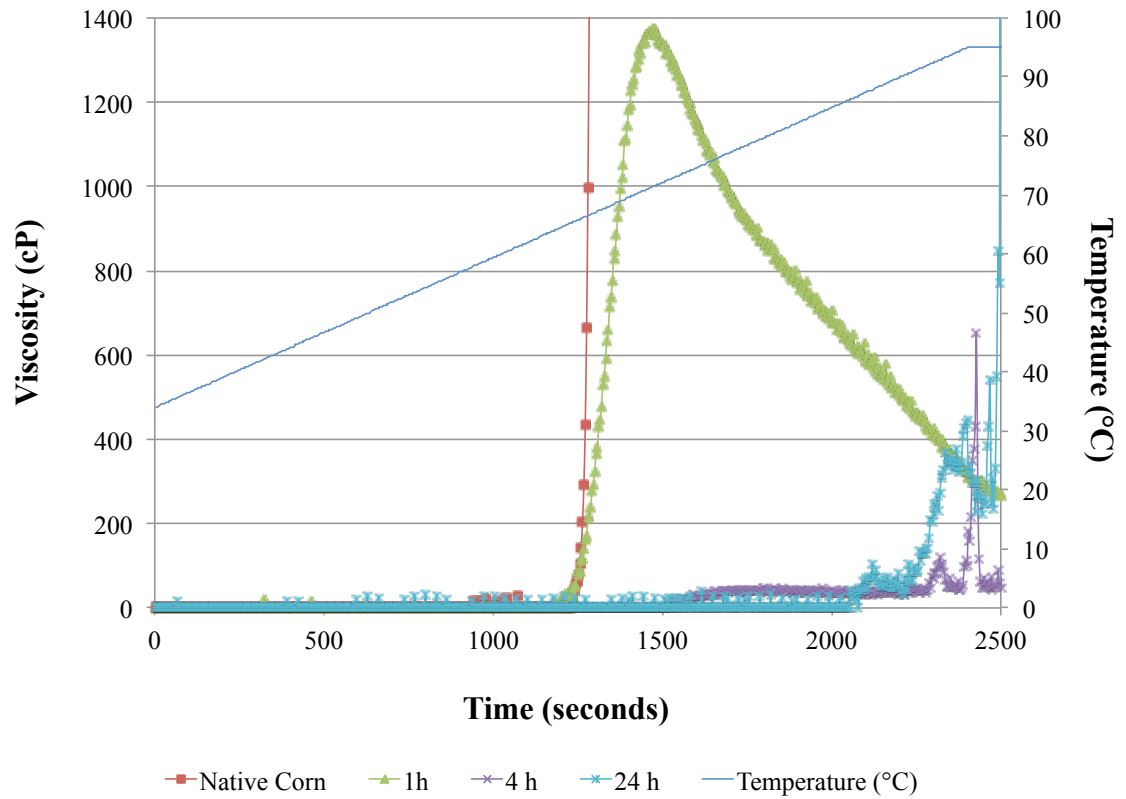


**Figure 3.6 – Viscosity profiles of native normal corn starch and acid hydrolysed starches in water (1, 4 and 24 hours) – enlarged from Figure 3.5 (Originally in colour)**

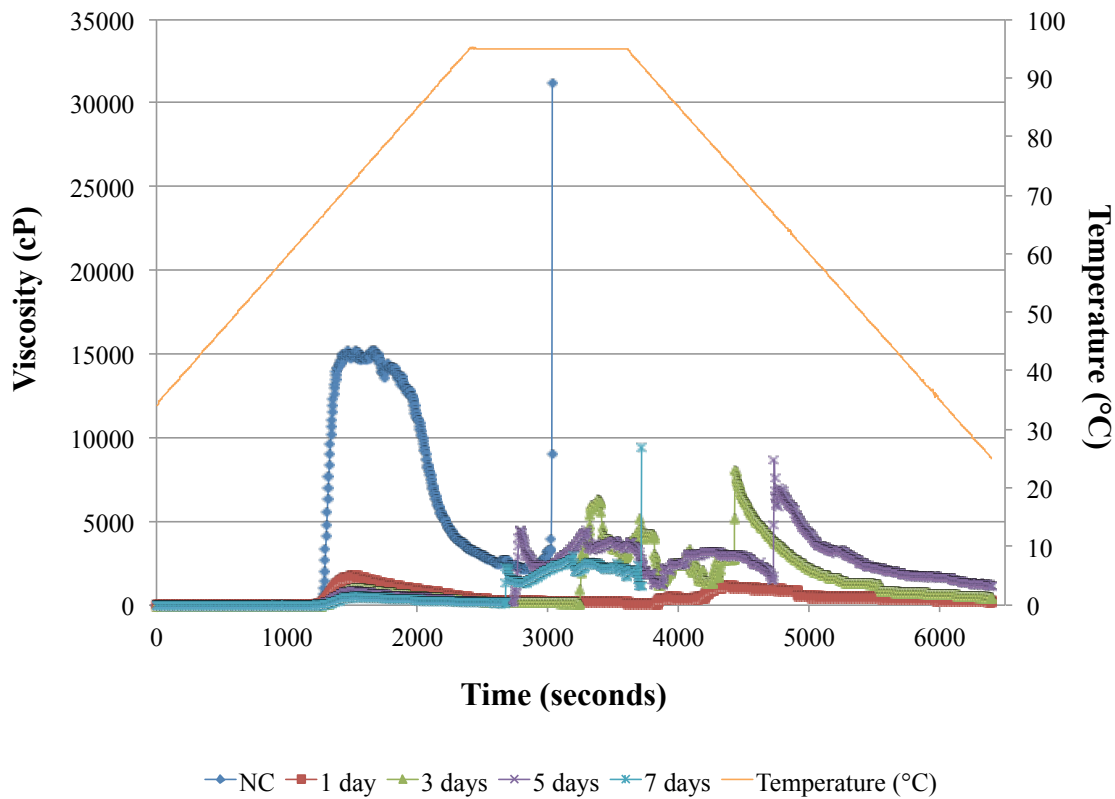


**Figure 3.7 – Viscosity profiles of native normal corn starch and acid hydrolysed corn starches in ethanol (1, 3, 5 and 7 days) (Originally in colour)**

Figure 3.8 demonstrates that the peak viscosity decreases further to 1000, 800 and 500 cP after 3, 5 and 7 days respectively. Lin *et al.* also observed a drop in pasting viscosity of the acid-alcohol treated maize and potato starches with some of the samples showing the peak viscosity lower than 100 cP.<sup>220</sup> As the 24-hour treated starch paste from method 1 (reaction in water) gives a lower peak viscosity than one from method 2 with the same treatment time, suggesting the higher degree of hydrolysis is obtained from method 1, confirming the data acquired from the solubility test in the previous section.

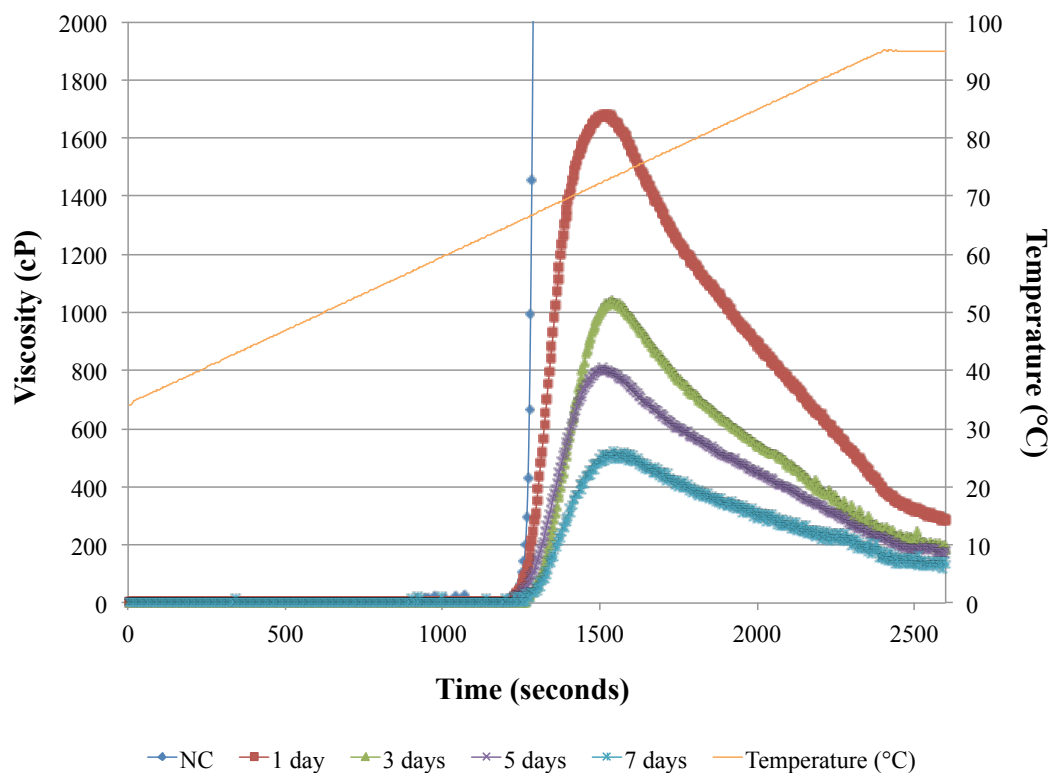


**Figure 3.8 – Viscosity profiles of native normal corn starch and acid hydrolysed corn starches in ethanol (1, 3, 5 and 7 days) – enlarged from Figure 3.7 (Originally in colour)**

### 3.3.3 Thermal properties

Thermogravimetric analysis (TGA) is a conventional and widely used technique in studies of thermal stability and thermal decomposition of starch materials.<sup>224</sup> Herein, the thermal properties of native and modified starch were examined in a Stanton Redcroft STA 625 (TG/DSC). Starch samples were heated from 25 °C to 500 °C at a heating rate of 10 °C/minute. Thermal degradation of starch has been described as an endothermic process, which appears as an exotherm in the presence of air due to the ignition of the material.<sup>225</sup> Therefore, the characterisations were performed under inert atmosphere (nitrogen) in order to simplify interpretation of the results.

Two major weight loss phases were observed in all TGA traces (*Figure 3.9-3.10*).

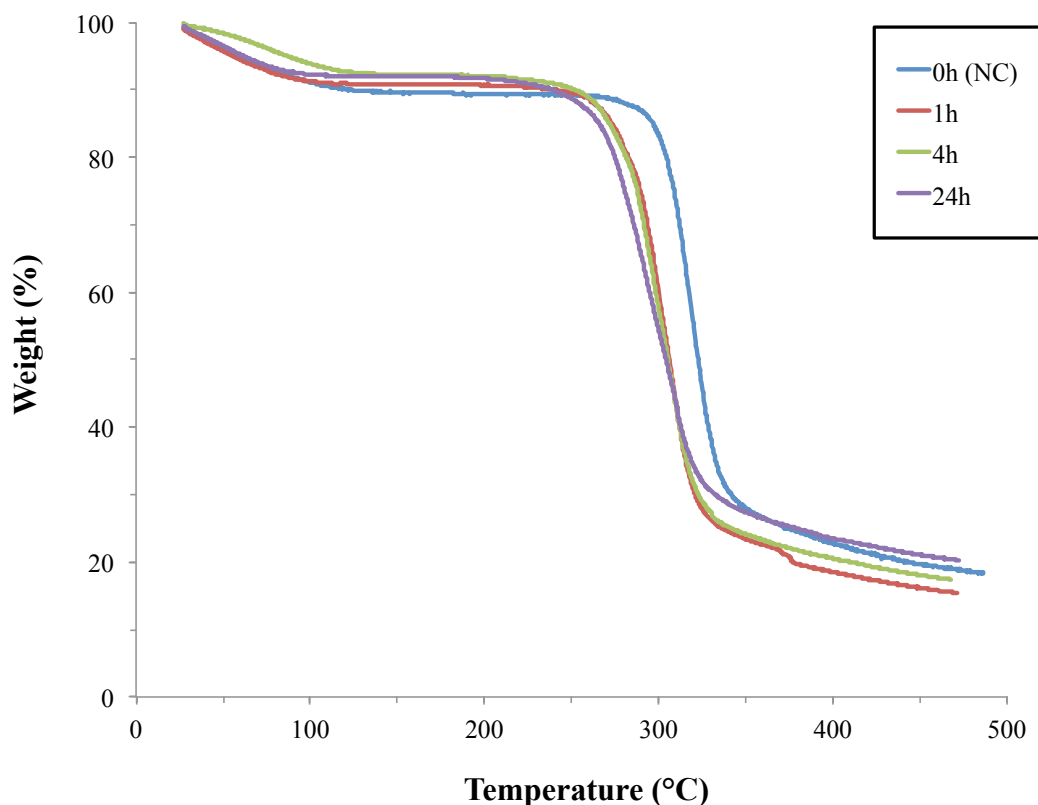


**Figure 3.9 – TGA thermograms of native normal corn starch and acid hydrolysed starches in water (Originally in colour)**

The first weight loss occurs almost instantly at the beginning of the heating and terminates just after 100 °C. This corresponds mainly to the evaporation of water and other volatile solvents, e.g. ethanol present in starch samples, which account for approximately 10% of the total weight. No significant mass loss is observed between 150-200 °C. The principal weight loss, correlating to the thermal decomposition of starch material, starts at around 260°C in normal corn starch. Acid hydrolysed starches in water (method 1) have the principal mass loss start at slightly lower temperature at 220 °C for the 1-hour and 4-hour hydrolysis and around 200 °C in the 24-hour modification. Regarding the modified starch from the method 2 (with ethanol), the second weight loss starts around 250 °C, regardless of the hydrolysis time, suggesting that the method 2 modification does not significantly alter the decomposition temperature of starch, and hence, less hydrolysis has occurred. This early decomposition temperature is attributed to a greater number of free chain ends, resulting from the hydrolysis process.<sup>226</sup> In conclusion, this study reveals that the acid treatment using method 1 (hydrolysis in water) affects the thermal stability of modified starch



more than one using method 2 (hydrolysis in ethanol) and this is likely to be induced by higher degree of hydrolysis.

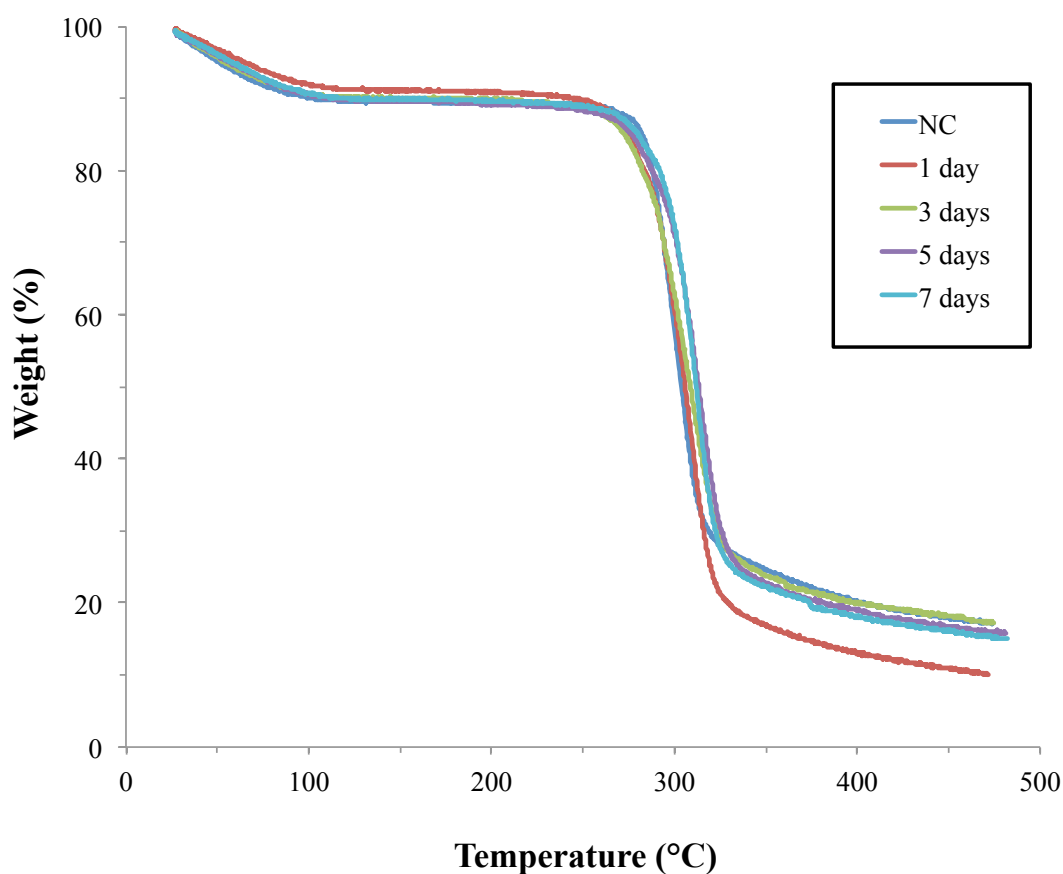


**Figure 3.10 – TGA thermograms of native normal corn starch and acid hydrolysed starches in ethanol (Originally in colour)**

The decomposition temperature was determined using DTG trace (*Figure 3.11*), which represents the rate of mass loss versus temperature.<sup>227</sup> DTG curves clearly show peak(s), which illustrates the temperature(s) at which the weight loss is at its maximum.<sup>228</sup>

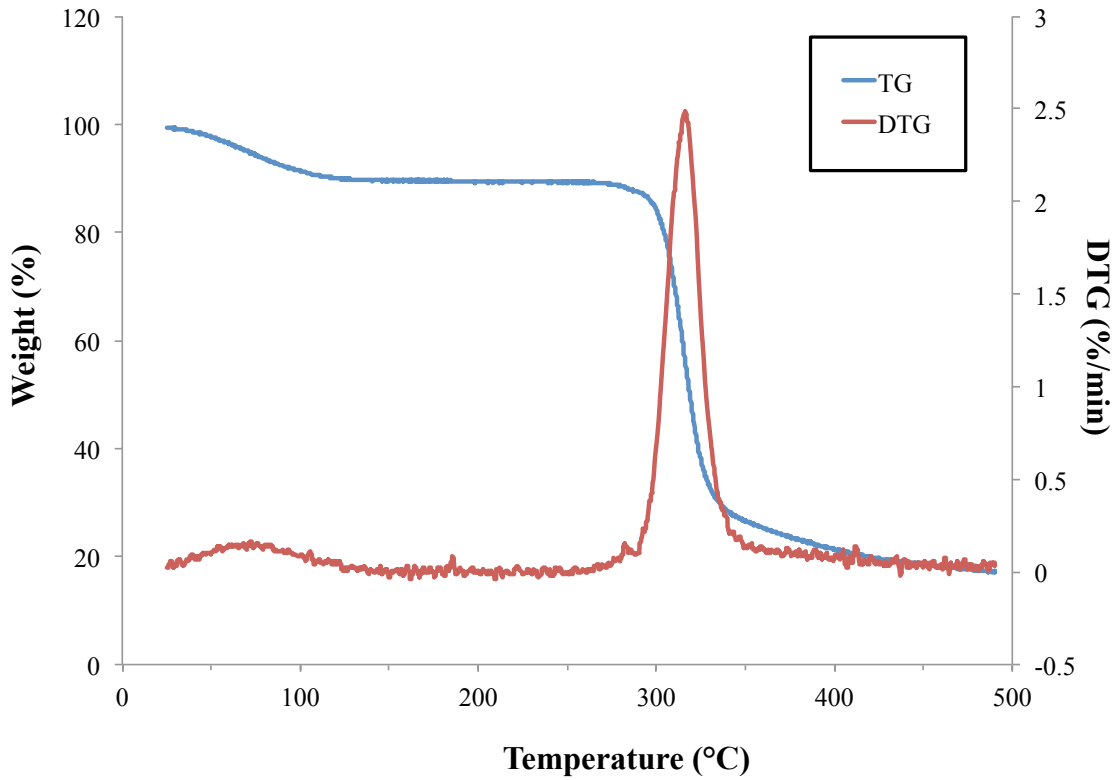


**Figure 3.11 – TG and DTG traces of native normal corn starch (Originally in colour)**

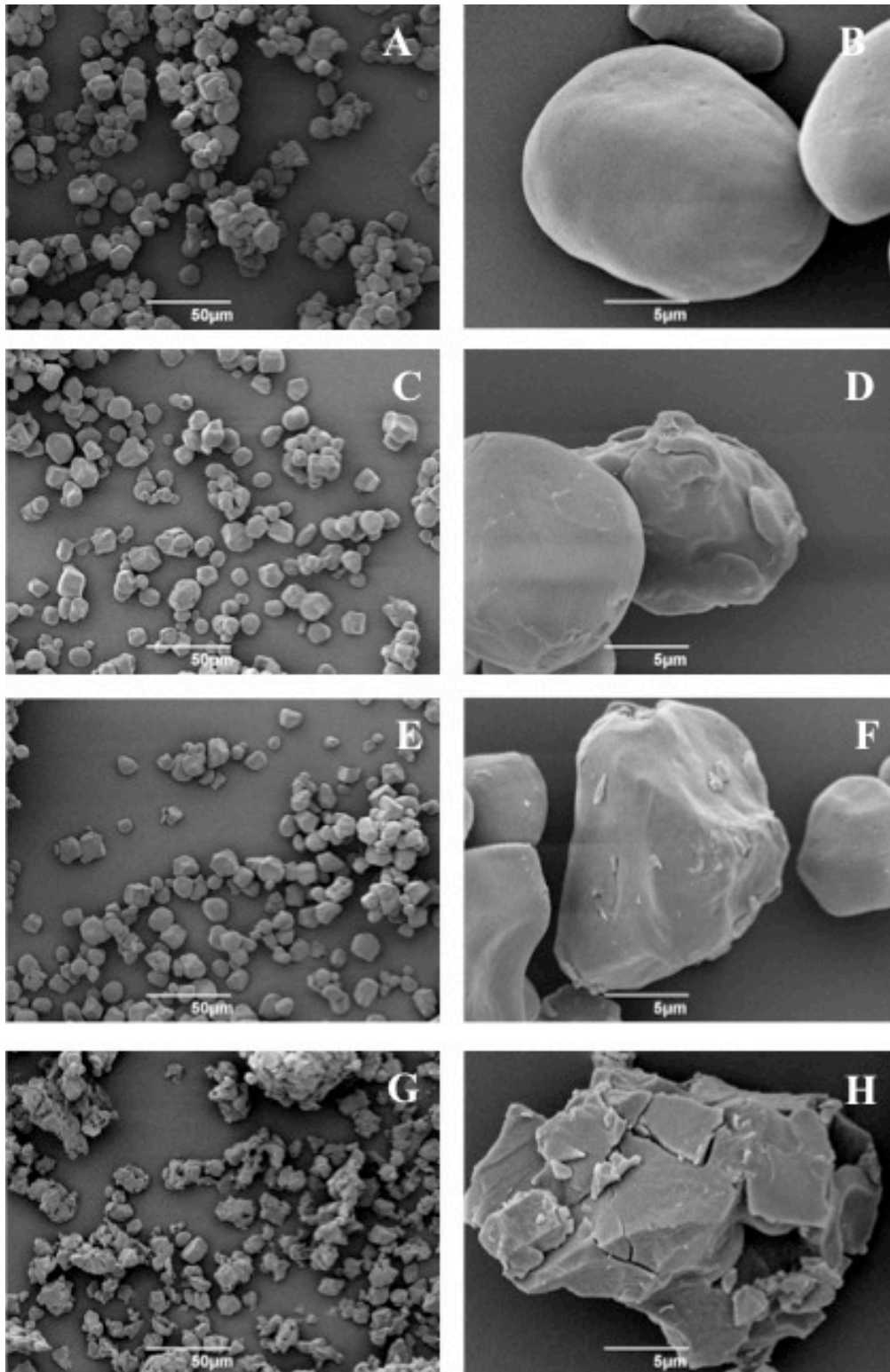
The decomposition of starch samples are summarised in *Table 3.1*. The acid treatment has a minor effect on the decomposition temperature of starch, which varies less than 5 °C before and after the modification. Approximately 20% wt. of starch residue is obtained after the rapid weight loss, which accounts around 72-82% wt.

**Table 3.1 – Degradation temperature of acid hydrolysed starches**

Hydrolysis time (Method)	Weight loss (%) (150-500 °C)	Decomposition temperature (°C) (DTG peak)
0 hours (1)	72.5	316.4
1 hour (1)	75.6	317.7
4 hours (1)	75.1	318.6
24 hours (1)	72.4	313.1
1 day (2)	81.4	315.1
3 days (2)	73.0	315.4
5 days (2)	73.9	319.4
7 days (2)	74.9	320.8

### 3.3.4 Morphological properties

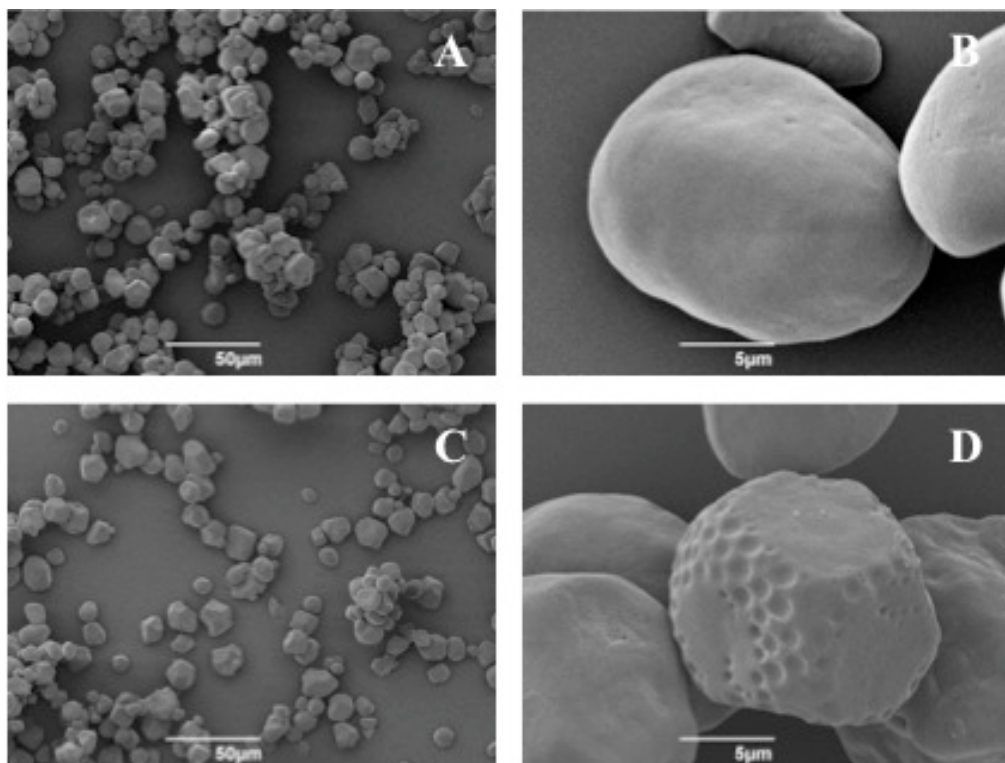
Native corn starch granules have a polygonal and irregular shape. The surface of the granules is relatively smooth and very small pores only present in some of the granules (*Figure 3.12 A-B*). After 1 or 4 hours of the treatment with method 1, although, no significant changes such as fragmentation or obvious fissures or cavities are observed, some starch granules have a rough surface with visible signs of corrosion on the granule exterior (*Figure 3.12 C-F*). After 24 hours of hydrolysis, obvious cracking and indentations are noted on the surface of the granules (*Figure 3.12 G-H*).



**Figure 3.12 – Scanning electron micrographs (magnification X500 and X5000) of native normal corn starch (A, B) and acid hydrolysed starches in water with various reaction times: 1 hour (C, D), 4 hours (E, F) and 24 hours (G, H)**

The cracks facilitate the penetration of acid into the internal part of the granules and causes endo-corrosion.<sup>229</sup> The granule shape changes dramatically with noticeable fragmentation, suggesting the structural disruption of starch granules during the hydrolysis process. It is well known that the amorphous regions in starch granules are more susceptible to the acid hydrolysis than the crystalline regions, which usually degrade in later stage of the treatment.<sup>137</sup> These SEM images show fractures after 24 hours of hydrolysis, suggesting that hydrogen ions start to attack the crystalline regions after 4 hours of the acid hydrolysis.<sup>230</sup>

Acid treatment in ethanol using method 2 causes a drastic change on the granule surface. The smooth surface of native starch granules (*Figure 3.13 A-B*) becomes rough with clearly visible holes and some surface fissures can be observed in some of the granules. (*Figure 3.13 B, D, F, H, and J*). However, the granules show no significant configuration changes, such as swelling or fragmentation after the treatment (*Figures 3.13 C, E, G and I*), suggesting that the crystalline regions are not greatly interrupted as seen in the product obtained after 24 hours of method 1 hydrolysis. These different granule surfaces and shapes of modified starches from the two methods confirm the postulation, which states that the acid-ethanol hydrolysis affects different linkages to the acid-water treatment.<sup>214</sup>



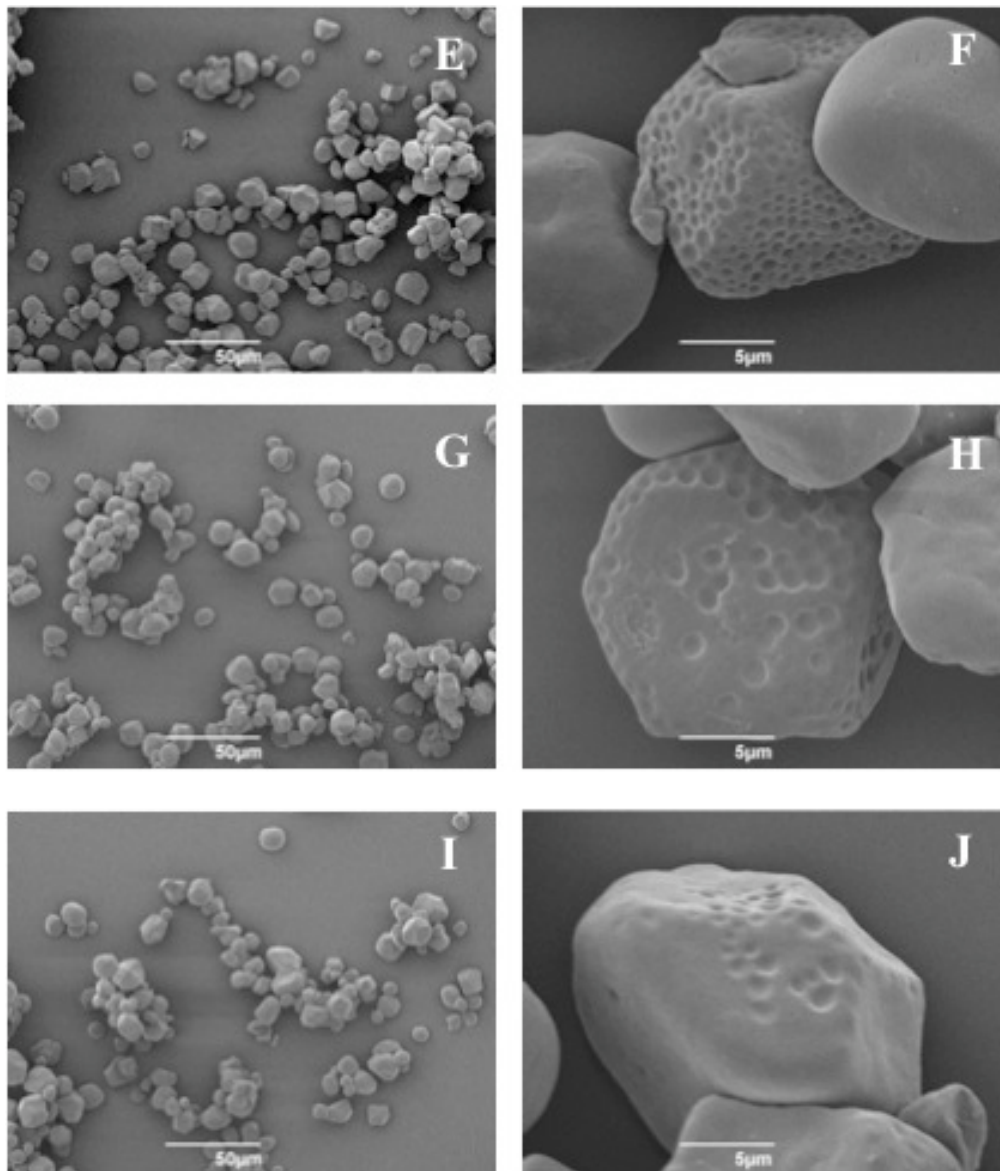


**Figure 3.13 – Scanning electron micrographs (magnification X500 and X5000) of native normal corn starch (A, B) and acid hydrolysed starches in ethanol with various reaction times: 1 day(C, D), 3 days (E, F), 5 days (G, H) and 7 days (I, J)**

### **3.4 Films containing normal corn starch and its acid hydrolysed derivatives**

The films are prepared according to the method described in section 7.3.5. The mechanical tests were performed at least in triplicate and the average values reported.

Normal corn starch and acid hydrolysed starches using both method 1 and method 2 were included in the standard formulation comprising of ELO, Pripol and DMAP, which is obtained from the optimisation of the formulation in chapter 2. In each film, 20% w/w of starch is present in the formulation. The production procedure is described in section 7.3.5. After curing, the reaction mixtures yield semi-transparent yellow films with good flexibility as shown in *Figure 3.14*. It is noted that the film produced from native corn starch (*Figure 3.14 A*) has pale yellow colour, whilst acid hydrolysed starch films give slightly darker films (*Figure 3.14 B-E*). This is possibly due to the slightly less thermally stable hydrolysed starch present in the films. Another possible explanation of the darker colour in the films could be the acid residues present in modified starches.

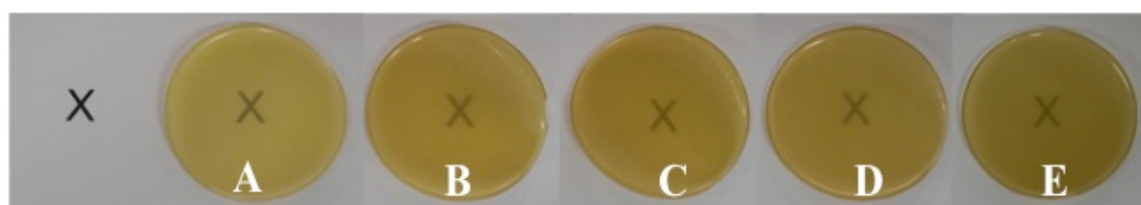


**Figure 3.14 – Native normal corn starch film (A) and acid-alcohol treated starch films with various reaction times (B-1 day, C-3 days, D-5days and E-7days) (Originally in colour)**

### 3.4.1 Mechanical properties

Tensile tests were performed in order to investigate the effect of starch and acid treated starch on the mechanical properties of resulting films. The values presented are the average values of at least three tests.

*Figure 3.15* shows the results obtained which reveal that the inclusion of starch or acid hydrolysed starch moderately improve the tensile strength of the films by 3.3-21.1%. The elongation at break and Young's modulus increase by 9.2% and 44.8% respectively on the addition of normal corn starch to the formulation. The films with acid treated starches from method 1 (indicated by M1-reaction time) have relatively similar tensile strength to that of the normal corn starch film however, a slight decrease in elongation at break is observed. It is noted that the Young's modulus of the films with method 1

starch increases with the hydrolysis time. The 24-hour hydrolysed starch yields a film with 71.1% enhancement in Young's modulus. The disrupted structure of the starch generated by acid hydrolysis with method 1, resulted in cracks and misshaped granules, leading to higher surface area, which can potentially enhance the interfacial contact between the granules and the polymer matrix. This consequently results in improved Young's modulus of the film. Although the films with acid hydrolysed starches from method 2 (indicated by M2-reaction time) give the Young's modulus in the same region as that of the 24-hour hydrolysed starch, a drop in elongation at break is clearly noticeable. As the preferred product should have satisfactory results in all three parameters, the film with overall good mechanical properties is the one produced from acid treated starch from method 1.

In conclusion, method 1 yields a hydrolysed starch that is better suited to produce films with enhanced mechanical properties. Hence, further experiments were undertaken to investigate the acid treatment (using method 1) of high amylose corn starch and the effect of this type of starch on the resulting properties of the films.

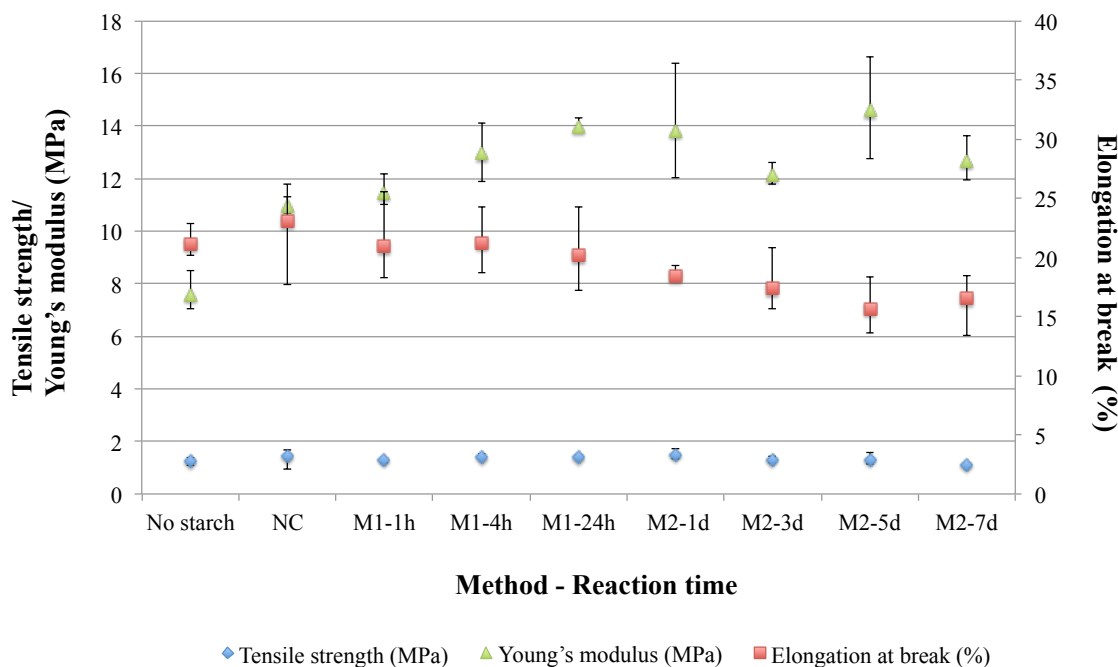


**Figure 3.15 – Mechanical properties of films based on ELO, Pripol and normal corn starch or acid hydrolysed starch (Originally in colour)**



### 3.5 Acid hydrolysis of high amylose corn starch

Normal corn starch typically contains approximately 25% of amylose. In 1946, R.L. Whistler and H.H. Kramer genetically modified corn starch and increased the amount of amylose content to 65%.<sup>231</sup> Today, commercially available high amylose starches usually have amylose content between 50-70%.<sup>232</sup> These starches possess unique properties such as rapid gelling, which makes them useful for enhancing food texture, and good film forming ability, which leads to the investigation of the uses of these starches in degradable plastics.<sup>231</sup> High amylose starch was found to be less susceptible to acid hydrolysis than normal starch, owing to the presence of lipid-complexed amylose (V-type polymorph), which is resistant to hydrolysis.<sup>233</sup> For lipid free-amylose, it was suggested that the partial hydrolysis occurs at the early stages but the resulting fragments retrograde into double helices that are resistant to hydrolysis.<sup>233</sup> Herein, high amylose corn starches were acid treated using method 1 (section 7.3.1), characterised and used in bio-based film preparation.

#### 3.5.1 Solubility and swelling power

The solubility of high amylose starch granules increases with the hydrolysis time (*Figure 3.16*). However, it only varies between 10-40% with the maximum solubility observed from 24-hour acid treated starch at 85 °C. This is significantly inferior to the value obtained from normal corn starch (100% solubility at the same hydrolysis time and temperature). The poor solubility in modified high amylose starch may be due to the lower extent of acid hydrolysis. Li *et al.* observed that the extent of acid hydrolysis in high amylose starch is lower than that of normal or waxy starch.<sup>234</sup> It is also noted that the solubility is almost independent of the temperature as the percentage of soluble starch barely changes when the temperature increases, with the exception of the 24-hour acid modified starch, which shows higher solubility when the temperature rises.

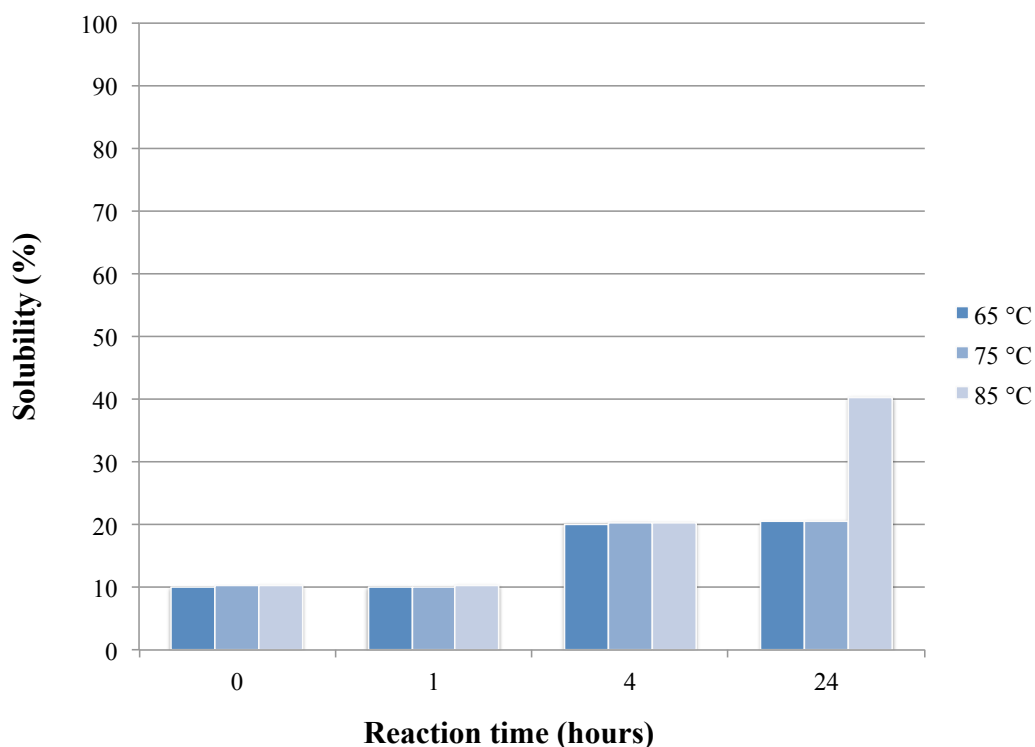


**Figure 3.16 – Effect of temperature and reaction time on solubility of acid hydrolysed high amylose corn starch (Originally in colour)**

The swelling power of high amylose starch and its derivatives is demonstrated in *Figure 3.17*. Temperature and hydrolysis time are found to have no obvious effect on swelling power of acid treated starches. This is in contrast to normal starch, which demonstrates a significant decrease in swelling power as a function of hydrolysis time. All native and acid treated high amylose starches exhibit relatively close values of the swelling power in the region of 2.5-4 g/g. Native high amylose starch granules exhibit lower swelling power (4-4.4 g/g at 65-85 °C) than those of native corn starch (6.9-11.7 g/g at 65-85 °C). This is in agreement with the data reported by other researchers.<sup>134, 235</sup> The difference in the swelling power can be attributed to several factors. Firstly, the amylose-lipid complex chains, that are present in high amylose starch, have been demonstrated to inhibit granular swelling.<sup>233</sup> Secondly, Morrison *et al.* reported that the swelling power is a property of amylopectin content; hence low molar proportion of amylopectin chains affects the swelling of high amylose starch granules.<sup>236</sup> Thirdly, hydrogen bonding between starch chains in both amorphous and crystalline regions

reduces the number of available hydroxyl groups to interact with water, resulting in poor granular swelling in starches with very low or very high crystallinity.<sup>134</sup>

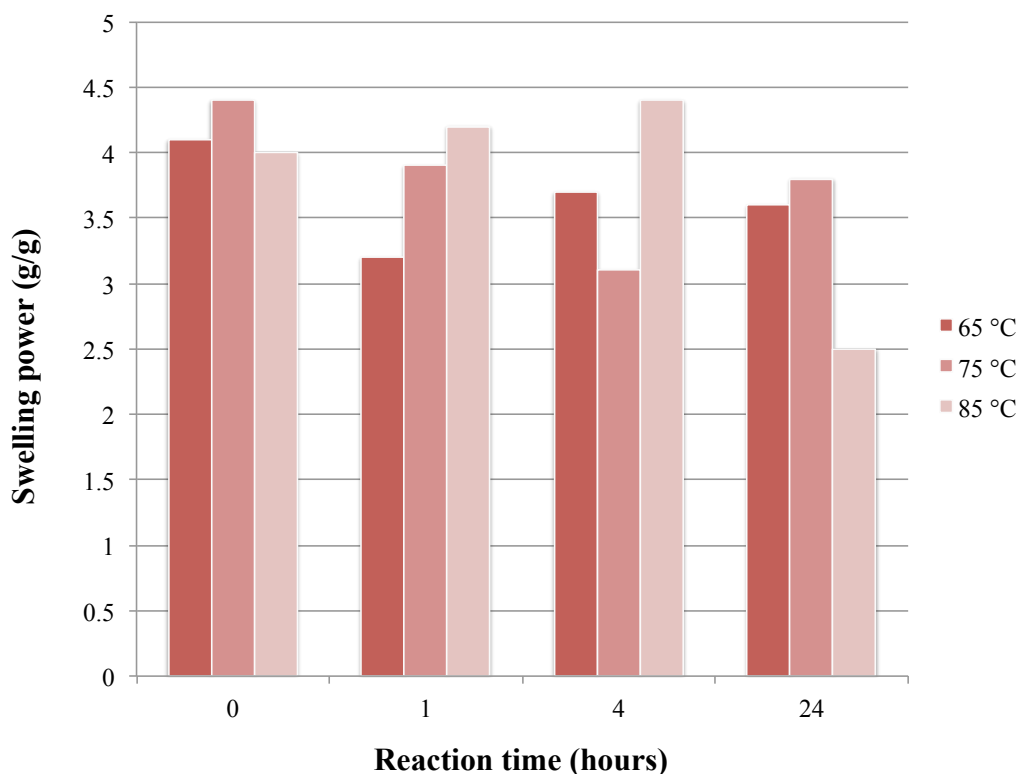


**Figure 3.17 – Effect of temperature and reaction time on swelling power of acid hydrolysed high amylose corn starch (Originally in colour)**

### 3.5.2 Pasting properties

Unmodified high amylose corn starch (HAS) shows peak viscosity in the region of 2200 centipoises (cP), which is considerably lower than that of unmodified corn starch at 15000 cP (*Figure 3.18*). The pasting temperature of native high amylose starch is 90.1 °C, which is higher than that of normal corn starch at 66.7 °C. It has been observed that the changes of peak viscosity and pasting temperature depend on the amount of amylose in starch granules.<sup>234, 237</sup> This is attributed to the complex of lipid-amylose, which restricted the granular swelling, resulting a lower peak viscosity and a higher pasting temperature in high amylose starch.<sup>237</sup> The decrease of pasting viscosity of acid treated high amylose starches compared to that of unmodified one is also observed in this case

(Figure 3.19). After 1 hour of acid hydrolysis, the peak viscosity decreases from 2200 cP to approximately 1000 cP and further treatment decreases the viscosity further to around 700 cP. The reduction of peak viscosity observed confirms shorter chains of starch are obtained after the acid hydrolysis.<sup>211</sup>

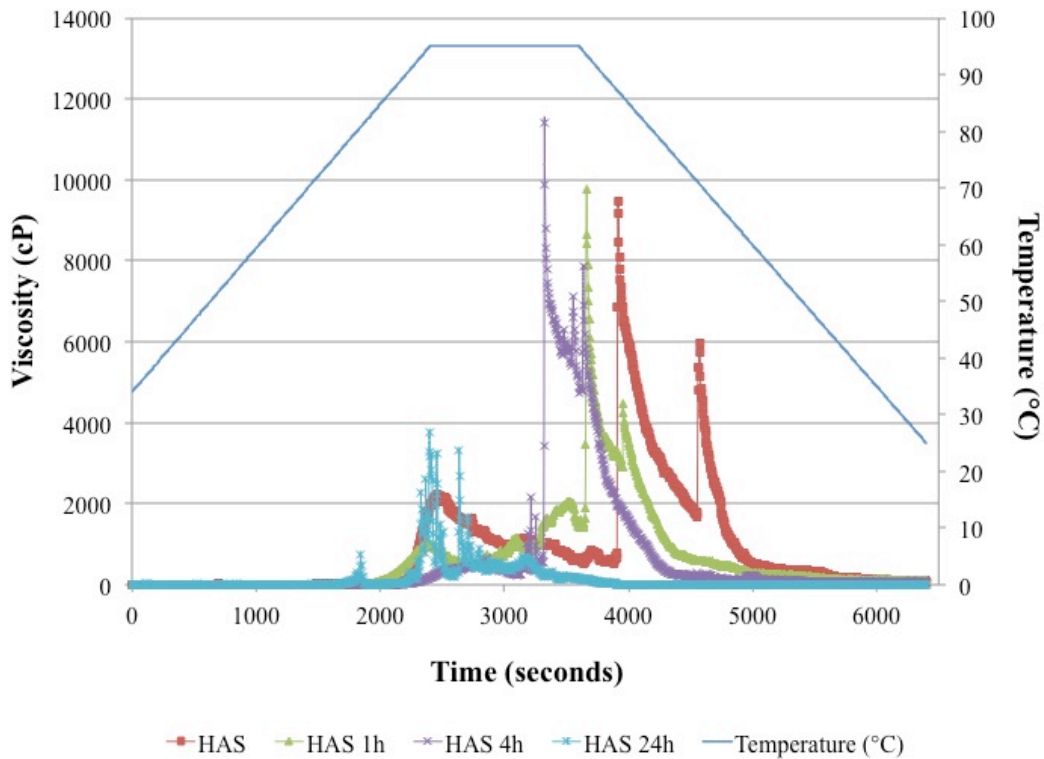


**Figure 3.18 – Viscosity profiles of high amylose corn starch and acid hydrolysed high amylose corn starches (1, 4 and 24 hours) (Originally in colour)**

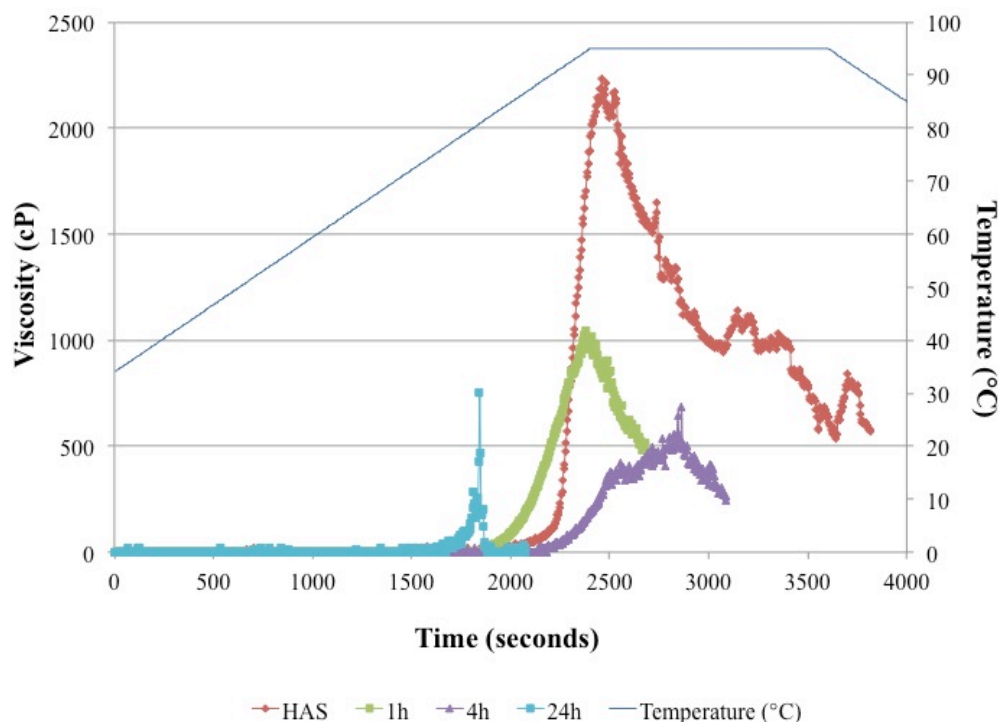


**Figure 3.19 – Viscosity profiles of high amylose corn starch and acid hydrolysed high amylose corn starches (1, 4 and 24 hours) – enlarged from Figure 3.18 (Originally in colour)**

### 3.5.3 Thermal properties

Thermogravimetric analysis of native high amylose starch and its acid hydrolysed derivatives also display two significant mass losses (*Figure 3.20*). The evaporation of water is observed almost immediately after the heating starts until the temperature reaches 100 °C and this corresponds to the first weight loss, accounting for approximately 10% of the total weight. It is noted that the 4-hour hydrolysed starch has slightly higher percentage of the first weight loss than other samples at 12%. There is no or very little weight change between 150-200 °C. The second weight loss phase in native high amylose starch begins at around 260 °C, similar to that of native normal corn starch. All the acid hydrolysed derivatives show the start of the mass loss at around 220 °C, which is in the same region as that of acid treated normal corn starch as seen in section 3.3.3.

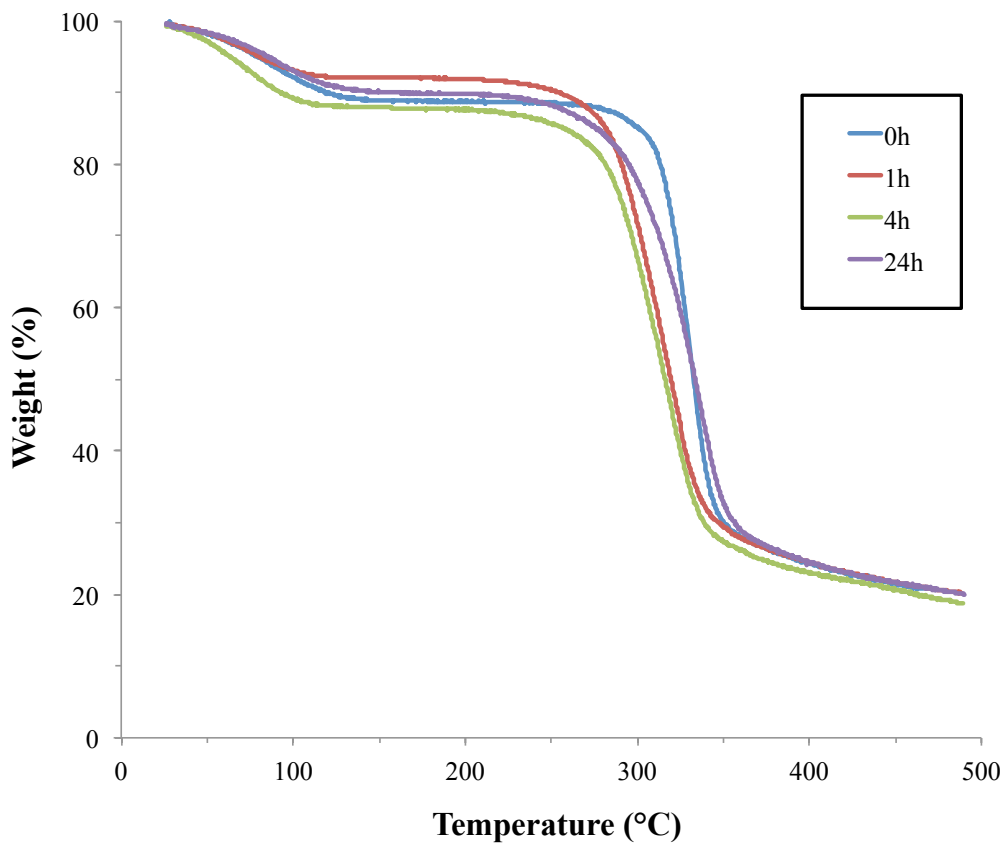


**Figure 3.20 – TGA thermograms of native high amylose corn starch and acid hydrolysed high amylose starches (Originally in colour)**

The residue of starch after heating accounts for approximately 20% of the total mass and this is not significantly affected by acid hydrolysis. Acid hydrolysis scarcely affects the decomposition of high amylose starch materials; a similar observation is also made for normal corn starch (*Table 3.2*).

**Table 3.2 – Degradation temperature of acid hydrolysed high amylose starch in water (method 1)**

Hydrolysis time	Weight loss (%) (150-500 °C)	Decomposition temperature (°C) (DTG peak)
0	70.9	316.0
1 hour	71.9	318.6
4 hours	69.2	316.4
24 hours	71.1	320.4

### 3.5.4 Morphological properties

High amylose corn starch has various granule shapes ranging from spherical, oval and rod-shape (*Figure 3.21 A, B*). The surface of the granules is smooth without pores or obvious fissures. After 1 and 4 hours of hydrolysis, no obvious changes in granular shape are observed however, the surface of the granules become rougher compared to that of the native granules (*Figure 3.21 C-F*). After 24 hours of hydrolysis, the granular configuration is significantly altered, similar to the previous observation in modified normal corn starch (*Figure 3.21 H*). This indicates that the granule structure is also disrupted in this case. It is noted that different size aggregates can be observed for 24-hour acid treated high amylose starch (*Figure 3.21 G*).

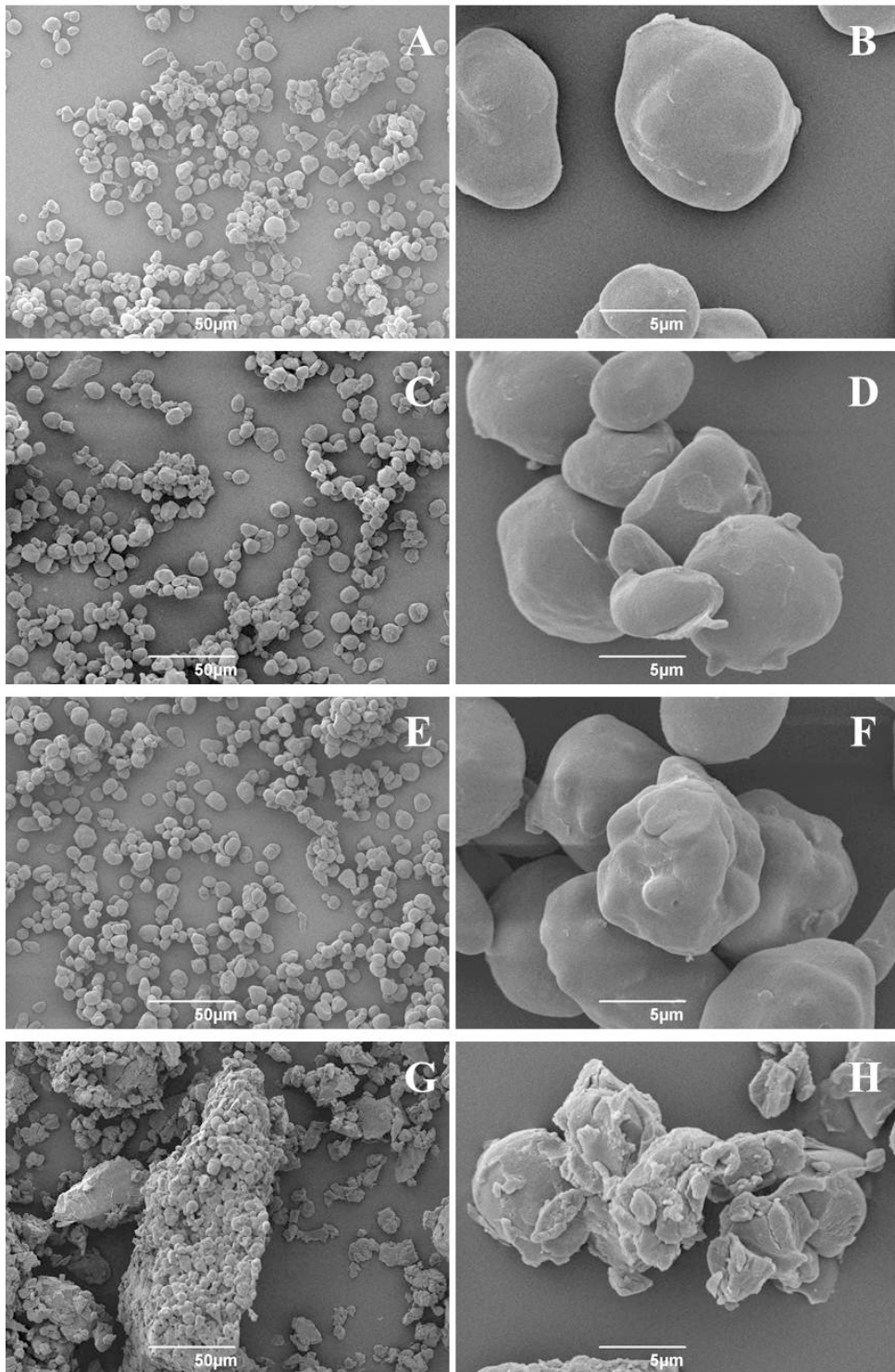


**Figure 3.21 – Scanning electron micrographs (magnification X500 and X5000) of native high amylose corn starch (A, B) and acid hydrolysed high amylose corn starches with various reaction times: 1 hour (C, D), 4 hours (E, F) and 24 hours (G, H)**



### 3.5.5 $^{13}\text{C}$ cross polarisation (CP) magic angle spinning (MAS) solid state nuclear magnetic resonance

Study of granular structure and molecular order of native and acid hydrolysed starches were performed using  $^{13}\text{C}$  solid state NMR. *Figure 3.22* shows the NMR spectra of native normal corn starch and its acid treated derivatives. Spectra were acquired by Dr David Apperley of solid-state NMR service at the University of Durham.

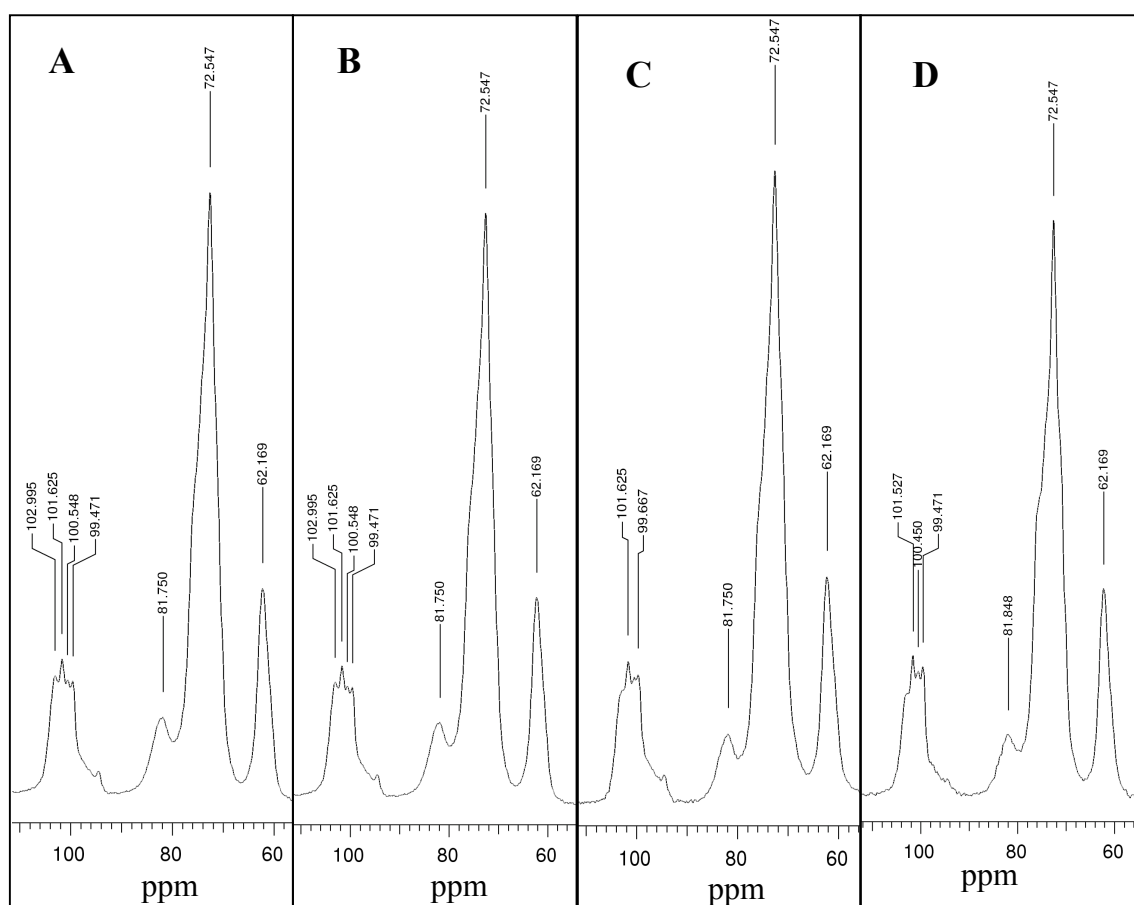


**Figure 3.22 –  $^{13}\text{C}$  CP MAS NMR of native normal corn starch (A) and acid hydrolysed normal corn starches with various reaction times: (B) 1 hour, (C) 4 hours and (D) 24 hours**

The signals in the region of 106–92 ppm are attributed to the resonance of C-1 of the anhydroglucose. The signals at 99.5, 100.5 and 101.6 ppm correspond to the double helical crystallites of C-1, confirming the three-peak pattern of A-type starch.<sup>238</sup> The

broad peaks at 103 and 95 ppm are correlated to the amorphous material in C-1, whilst the signal at 82 ppm arises from amorphous material in C-4.<sup>239</sup> The large peak between 69-77 ppm is attributed to C-2, C-3 and C-5 and the signal at 62 ppm correspond to C-6 of the anhydroglucose units.<sup>238</sup> An obvious change is observed on the amorphous resonances at 103, 95 and 82 ppm gradually decreases with the hydrolysis time and the signal at 95 ppm almost disappears after 24 hours of acid treatment. This indicates that the amorphous regions in starch granules are susceptible to the acid hydrolysis and this is in agreement with previously reported research.<sup>240</sup> Furthermore, the three characteristic peaks of A-type polymorph (99.5, 100.5 and 101.6 ppm) become better resolved, indicating an increase in crystallinity of the modified starch granules. Amorphous materials give much broader peaks than crystalline materials, owing to the distribution of local molecular environments, which causes a broad distribution of chemical shifts.<sup>239</sup>

The signals of C-1 in high amylose starch are different to that of normal corn starch as a well-resolved peak is observed at 103 ppm and two less resolved peaks are noted between 99-101 ppm, revealing the characteristic features of B-type starch (*Figure 3.23*). The signal at 103 ppm corresponds to the V-type polymorph, which is comprised of single helices of amylose-lipid complex.<sup>241</sup> Similar observation is made for the acid hydrolysed high amylose starches where the signals from the amorphous domains at 103, 95 and 82 ppm progressively reduce the intensity as the hydrolysis time increases. This becomes very obvious on the 24-hour treated starch spectrum, which shows the disappearance of the peak at 103 ppm. However, the 1-hour acid hydrolysed starch spectrum shows a relatively well-resolved peak at 103 ppm with a broadened doublet between 99-101 ppm. This is possibly due to the resistance to acid hydrolysis of the amylose-lipid complex as mentioned earlier in this chapter, causing a delay in the hydrolysis process.<sup>233</sup>

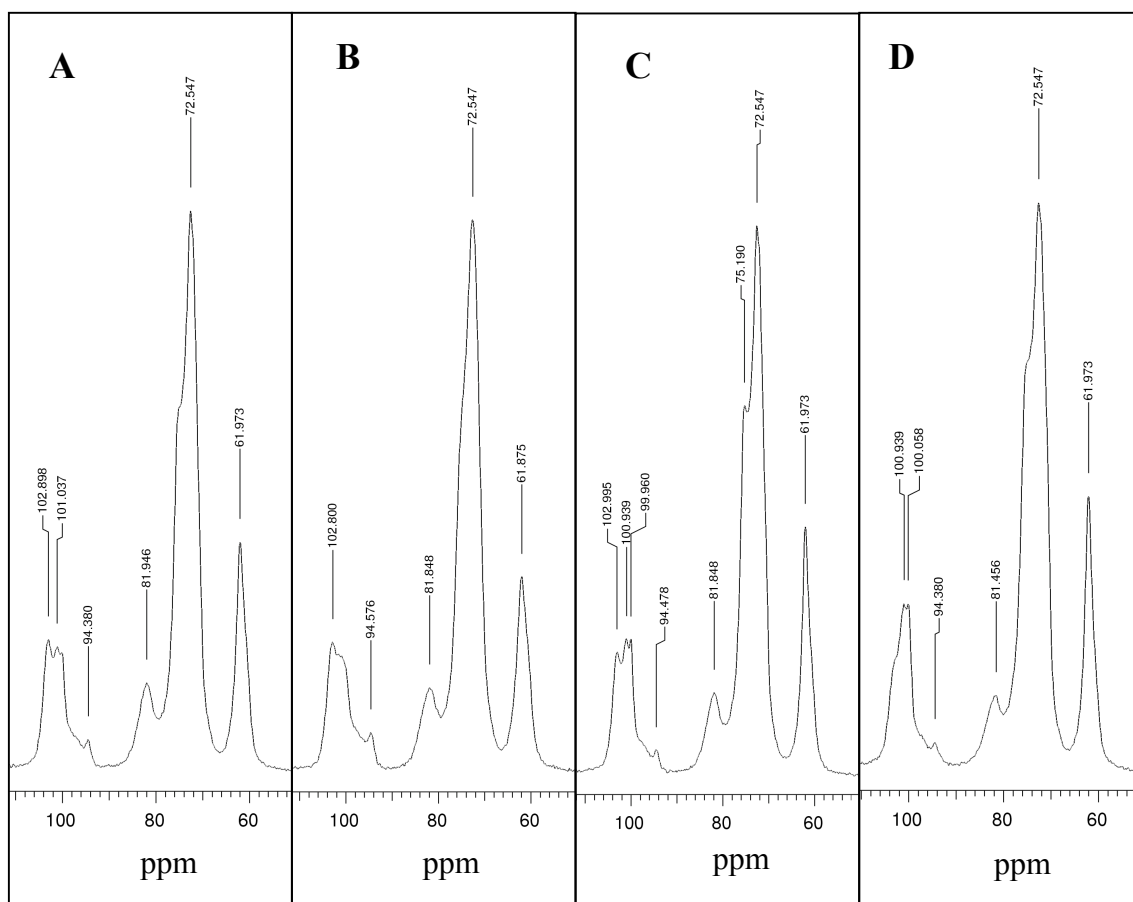


**Figure 3.23 –  $^{13}\text{C}$  CP MAS NMR of native high amylose starch (A) and acid hydrolysed high amylose starches with various reaction times: (B) 1 hour, (C) 4 hours and (D) 24 hours**

*Table 3.3* summarises the chemical shifts of native starches and their acid hydrolysed derivatives.

**Table 3.3 –  $^{13}\text{C}$  CP MAS NMR peak assignment of native starches (NC – Normal corn starch and HAS – High amylose corn starch) and their acid hydrolysed derivatives (type of starch-hydrolysis time)**

Sample	Chemical shift (ppm)			
	C-1	C-4	C-2, 3, 5	C-6
NC	106-92	81.750	72.547	62.169
NC-1 h	106-92	81.750	72.547	62.169
NC-4 h	106-92	81.750	72.547	62.169
NC-24 h	106-92	81.848	72.528	62.169
HAS	106-92	81.946	72.747	61.973
HAS-1h	106-92	81.848	72.547	61.973
HAS-4h	106-92	81.848	72.547, 75.190	61.973
HAS-24h	106-92	81.456	72.547	61.973

## 3.6 Films containing high amylose corn starch and its acid hydrolysed derivatives

### 3.6.1 Mechanical properties

Films containing high amylose starch and acid hydrolysed high amylose starches were prepared using the same method as one prepared from normal corn starch. The mechanical properties of resulting films are demonstrated in *Figure 3.24*. The native starch yields a film with the greatest tensile strength. The use of acid hydrolysed starches decreases the tensile strength of the films by up to 50.9% (4-hour hydrolysis starch). The elongations at break of all the films are in the region between 18.6-22.4%,

except for the one containing 4-hour acid treated starch, which yields a low elongation at break at 16.4 %. This is possibly due to the slightly higher moisture present in the granules, evidenced in the TGA thermograms in section 3.5.3. Water is not miscible with the other components in the formulation, leading to poor compatibility of starch granules with the polymer matrix, which as a result worsens the mechanical properties of the resin.

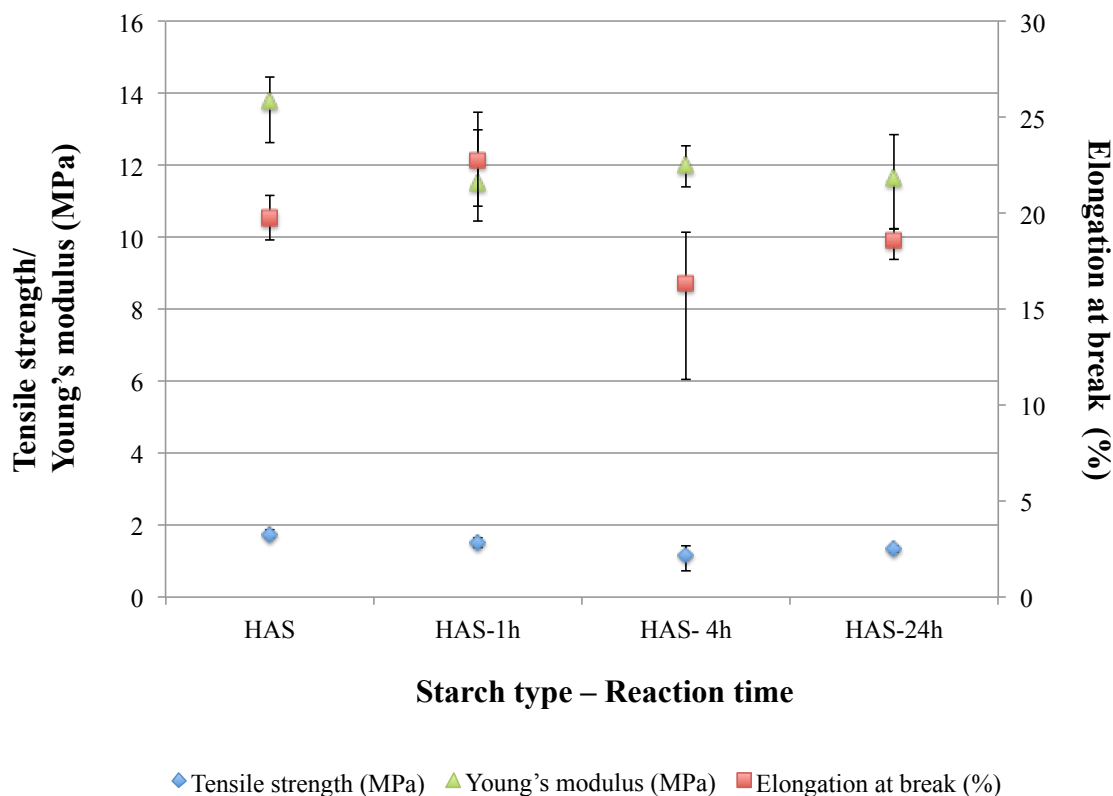


**Figure 3.24 – Mechanical properties of films based on ELO, Pripol and native high amylose starch or acid hydrolysed high amylose starch (Originally in colour)**

The mechanical properties of the films with normal corn starches and high amylose starches are compared in *Figure 3.25*. The native normal corn starch added film displays inferior tensile strength and Young's modulus than those of native high amylose starch film. This may be due to the smaller granules size of high amylose starch, which has the average granule diameter of 8.5  $\mu\text{m}$ , whilst the normal corn starch granules are approximately 13.9  $\mu\text{m}$  in diameter. The small granules have high surface area, which improve the contact surface between the starch filler and the polymer

matrix, resulting in better mechanical properties.<sup>242, 243</sup> The film containing native high amylose starch exhibits the greatest tensile strength, 42.3 % higher than that of the film with no starch added. The highest Young's modulus is obtained from the film with 24-hour hydrolysed normal corn starch at 13.96 MPa however, the tensile strength of this film is 25% lower than that of native high amylose starch film, which actually yields a reasonable Young's modulus at 13.78 MPa. These two films are therefore subjected to further investigation using scanning electron microscopy.

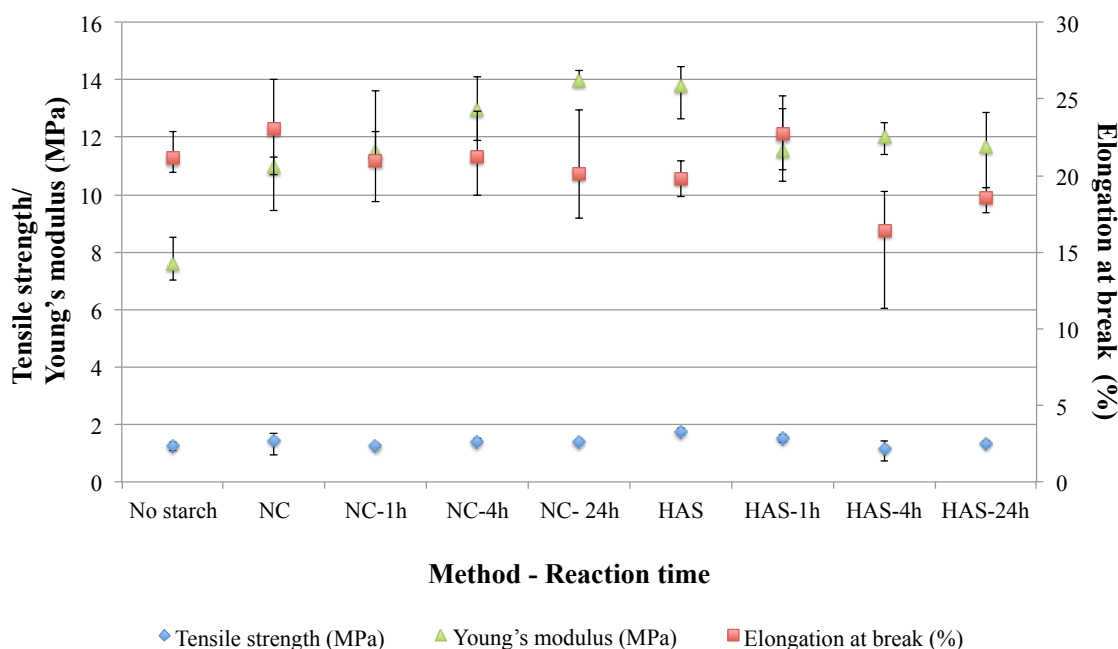


**Figure 3.25 – Mechanical properties of films based on ELO, Pripol and native normal corn (NC) or high amylose corn (HAS) starches or acid hydrolysed starches (Originally in colour)**

### 3.6.2 Morphological study

The two films, which have shown the best mechanical properties, were further investigated through scanning electron microscope. The cross-section of both films shows a phase separation (*Figure 3.26 A* and *Figure 3.27 A*). One side of the film shows rough surface with a high concentration of starch granules, whilst the other side is smooth with less starch granules present (*Figure 3.26 B-C* and *Figure 3.27 B-C*). *Figure 3.26 B* reveals a number of small voids between starch granules in the film with 24-hour

hydrolysed normal corn starch, however, these voids cannot be seen on the film with high amylose starch. This suggests that high amylose starch granules integrate better in the polymer matrix than those of the modified normal corn starch, owing to its smaller granule size.

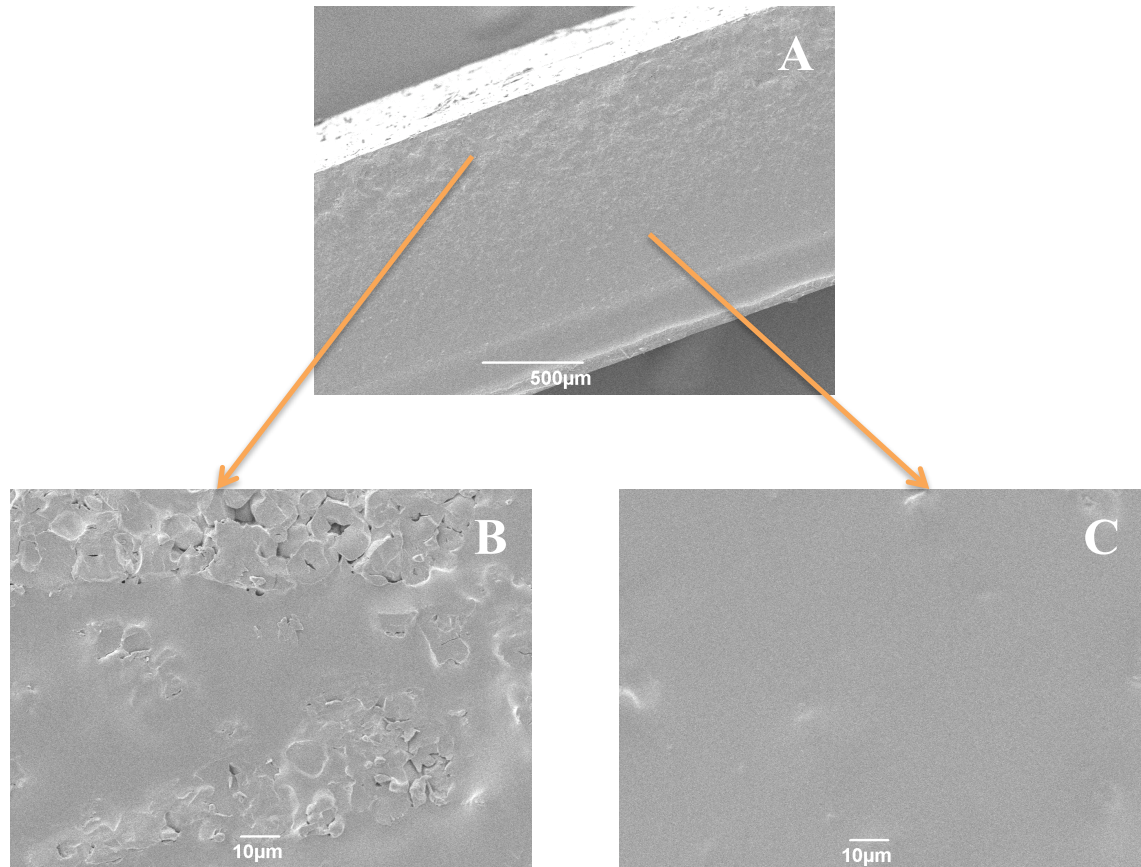


**Figure 3.26 – Scanning electron micrographs (magnification X50 and X1000) of the cross-section of film with acid hydrolysed starch – A) whole film, B) bottom of the film and C) front of the film**

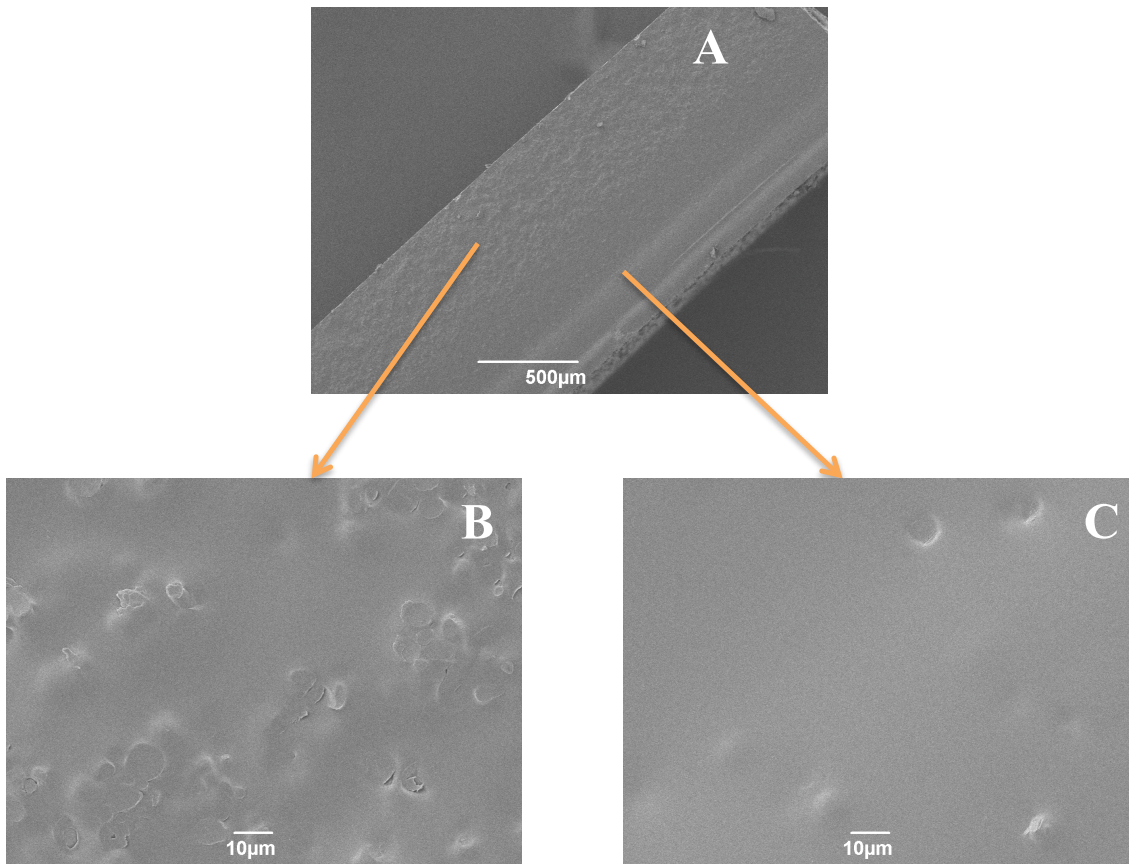


**Figure 3.27 – Scanning electron micrographs (magnification X50 and X1000) of the cross-section of film with native high amylose starch– A) whole film, B) bottom of the film and C) front of the film**

### 3.7 Conclusions

Normal corn starch was modified by acid treatment via two different methods in order to study their incorporation as fillers in films and subsequently determine the better hydrolysis method. The properties of modified starches studied including the solubility and swelling power tests, which revealed that the granule solubility increased with the hydrolysis time, whilst the swelling power inversely correlated with the hydrolysis time. Regarding the pasting property, the acid modified starch pastes showed a decline in the peak viscosity after acid hydrolysis. These features confirmed the altered properties of starch due to the changes in structure of starch granules after the acid treatment. Thermal stability of acid hydrolysed starch was slightly affected by the treatment as the TGA thermograms showed that the modified starch started to decompose at slightly



lower temperature than that of native starch, in particular the 24-hour acid hydrolysed starch obtained from method 1. The scanning electron microscopy also supported this finding as the SEM images revealed the disrupted structure of the granules after 24-hour hydrolysis with method 1. All the analysis data suggested that method 1 treatment yielded products with higher degree of hydrolysis for the same reaction duration. Furthermore, the tensile test demonstrated a moderate decrease in elongation at break in the films containing the method 2-hydrolysis material. Therefore, method 1 hydrolysis was applied to high amylose corn starch in further experiments. The acid hydrolysed high amylose starches were characterised by performing the solubility and swelling power tests, the pasting property test, thermal analysis, morphological study and NMR analysis. The results indicated the altered properties after hydrolysis however; the high amylose starch was more resistant to the acid hydrolysis than the normal corn starch. The mechanical test revealed that the films obtained from native high amylose starch had greater tensile strength, compared to that of native normal corn starch, owing to the bigger granule size of the latter. The 24-hour acid hydrolysed starch showed the highest Young's modulus, potentially due to the change in configuration and the appearance of cracks and fissures caused by the acid treatment. This increased the surface area of the granules, leading to better interfacial adhesion of the starch granules and the polymer matrix and resulted in improved mechanical properties. Further modification of starch by expansion could lead to improved film properties. SEM micrograms of the cross-section of these films showed a phase-separation and some voids were observed between the starch granules in the 24-hour hydrolysed starch film. However, no cavity was observed in the native high amylose starch film, indicating better miscibility of the high amylose starch granules in the polymer matrix. Therefore, the further work will be looking at the physical modification of the high amylose starch in order to increase the surface area of the granules and consequently enhance the mechanical properties of the products.



# Chapter 4

## *Expanded starch in bio-based thermoset composites*



## 4.1 Chapter 4 - Summary

Native high amylose corn starch and its gelatinised and retrograded derivatives are used in combination with ELO and bio-derived diacid Pripol 1009 in the presence of DMAP catalyst to yield bio-based thermoset composites. Firstly, gelatinised and retrograded starches were characterised using scanning electron microscopic and porosimetric methods in order to investigate their textural properties. Their thermal stability and chemical structure were also determined using thermogravimetric analysis and solid-state nuclear magnetic resonance, respectively. Other methods including X-ray diffraction and infrared spectroscopy were also used in order to collect additional information on the starch structure. The inclusion of starch in the thermosetting resin significantly improves the mechanical properties of the product. The tensile strength of the film improves by the maximum of 227% with 20% gelatinised starch added to the resin. The enhancement of the Young's modulus by 166% was also obtained from the same formulation. Phase separation was observed in the film with native starch as the filler. However, the films with modified starches show equally distributed starch granules dispersed without visible phase separation. Thermal and spectroscopic analysis were performed to study the curing reactions. Thermal analysis reveals a retardation in the cure process in the presence of starch, but the presence of hydroxyl groups within the starch are likely to promote a more extensive curing process, as indicated by the higher total enthalpy of reaction obtained.

## 4.2 Introduction

Starch possesses inherently numerous hydroxyl functionalities; however, the accessibility of these functionalities is limited due to the dense packing of the polysaccharide chains within the starch granules. The gelatinisation process opens up the compact structure and enables chemical modifications, resulting in a higher degree of substitution when modified.<sup>244</sup> Gelatinisation of starch occurs when starch granules are heated in excess of water. During this phenomenon, starch granules swell whilst the transition of ordered to disordered state occurs.<sup>245</sup> Atkin *et al.* observed the process of gelatinisation using a variety of microscopic techniques and reported that dry starch granules in excess of water at room temperature expand radially. The diameter of the granules increases up to 80% due to the hydration, resulting in a six-fold volume

increase. When the temperature rises to 65 °C, the granules swell further to reach the maximum diameter of 200% of its original value or 25 times of its original volume.<sup>246</sup> During and after the gelatinisation, linear amylose diffuses out of the swollen granules and creates the continuous gel matrix outside the granule.<sup>247</sup> The semi-crystalline structure of starch exhibits birefringence when visualised under crossed polarisation lenses. Gelatinised starch granule loses its birefringence, indicating the loss of crystallinity of starch structure.<sup>248</sup> Upon cooling, polysaccharide chains in gelatinised starch start to reassociate to an ordered structure.<sup>248</sup> This recrystallisation process is known as retrogradation, which causes effects such as precipitation, gelation, and changes in consistency and opacity.<sup>247</sup> Figure 4.1 illustrates the gelatinisation and retrogradation of starch granules.

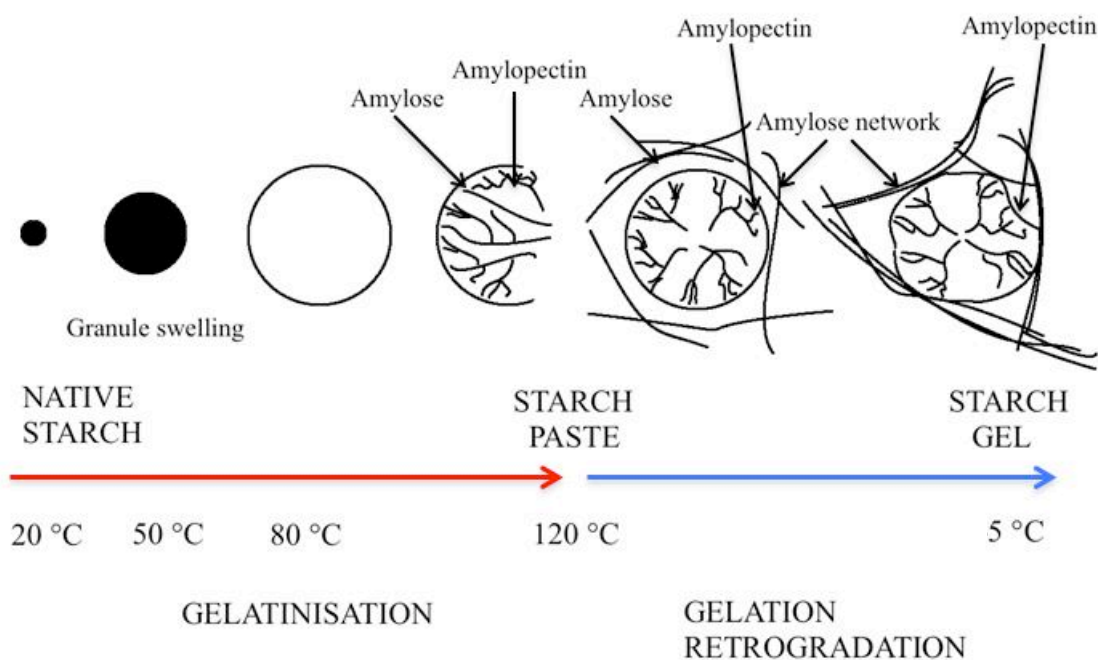


**Figure 4.1 – Gelatinisation and retrogradation of starch granules (Originally in colour)**

The method of expansion of starch was developed by Glenn *et al.* by gelatinising starch in water, followed by retrogradation at 5 °C. This gel is then solvent exchanged with ethanol, and dried, resulting in a microcellular foam (also known as expanded starch).<sup>249, 250</sup> Solvent exchange is crucial for preserving the high surface area of expanded starch. As the drying proceeds, the starch network becomes stiffer and the

surface tension of the liquid in the pores increases correspondingly. If water is removed directly, the capillary forces affect the starch porous structure, eventually causing it to collapse (*Figure 4.2*).<sup>251</sup> The replacement of water with a lower surface tension solvent (or sometimes a succession of solvents), such as ethanol, helps protect the structure of the modified starch.<sup>252</sup> Doi investigated the preparation of high amylose corn starch, normal corn starch and waxy corn starch. Despite the higher gelatinisation temperature of high amylose starch, it is found to be the most advantageous for the production of high surface area starch materials due to its rapid retrogradation time compared to the other two starches.<sup>253</sup>

### Pore in starch gel network

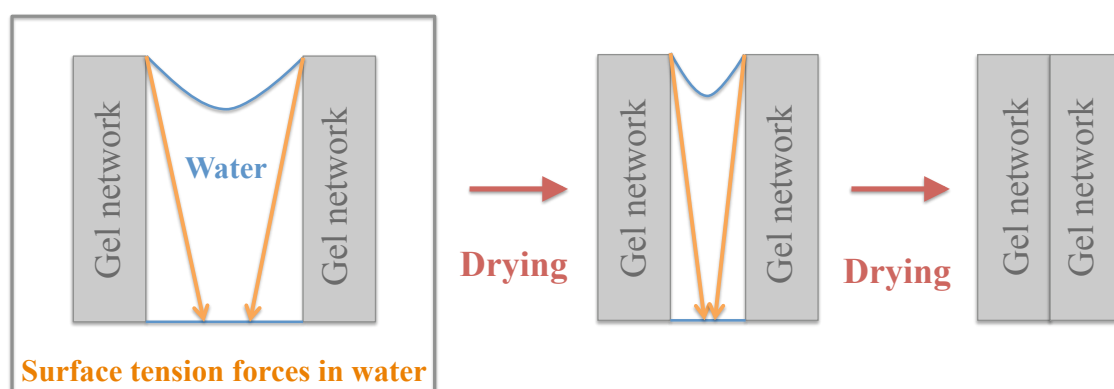


**Figure 4.2 – Collapse of pore structure in starch gel network due to surface tension forces in water during drying process (Originally in colour)**

Expanded starch finds its uses in various applications. Recent research include the use of expanded starch as support media in heterogeneous catalysis.<sup>244, 254</sup> Budarin *et al.* reported the use of expanded starch as stationary phase for column chromatography.<sup>255</sup> Expanded starch was also utilised as base material to produce a bio-derived switchable adhesive for carpet tiles.<sup>126</sup> Gelatinised starch has been blended with poly lactic acid (PLA) to produce biodegradable materials. SEM micrographs showed that gelatinised starch particles were held in the polymer matrix. The interfacial adhesion was enhanced and mechanical properties of gelatinised starch/PLA blend were also superior compared to those of native starch/PLA.<sup>256</sup> Gelatinised starch has been blended with modified polycaprolactone (PCL). PCL was grafted to glycidyl methacrylate (GMA) and then

blended with gelatinised starch and glycerine. The mechanical properties of the product improved with the amount of GMA. The author suggested that the reaction between starch and grafted GMA was more probable in the presence of higher concentrations of GMA. This improves the interfacial stability between starch and the matrix and also induces the formation of crosslinking.<sup>257</sup>

Doi reported that gelatinised and retrograded high amylose starches gave high surface area materials,<sup>253</sup> which could be advantageous for the resin product. As such, in this current work high amylose starch (HAS) was selected for use in the ELO/Pripol/DMAP formulation. The gelatinised and retrograded starches were characterised and subsequently incorporated in the formulation with epoxidised linseed oil and Pripol to yield the thermosetting films.

## 4.3 Characterisation of expanded starch

### 4.3.1 Morphological study

Gelatinisation and retrogradation of starch open up the structure of starch granules. SEM analysis shows changes on the granules after the modification process. High amylose starch granules possess different granules shapes, ranging from spherical, oval or rod-like (*Figure 4.3 A-B*). The surface of the granules is smooth without obvious pores or fissures. After gelatinisation and retrogradation, the morphology of starch granules dramatically changes. Gelatinised starch (*Figure 4.3 C-D*) and retrograded starch (*Figure 4.3 E-F*) granules show porous surfaces. Porous modified starch particles show irregularity in their size and shape. In fact, these particles are the remaining residues of the starch granule structures that have collapsed after the amylose migration during gelatinisation. The porous structure enables better contact between the granules and the polymer matrix. Moreover, the opened-up structure of starch after modification allows the natural high functionality of starch to undergo a variety of chemical modification.<sup>244</sup> In this work, this may enable chemical interaction between starch filler and ELO and/or Pripol in the film formulation and consequently improve the mechanical properties of the product.



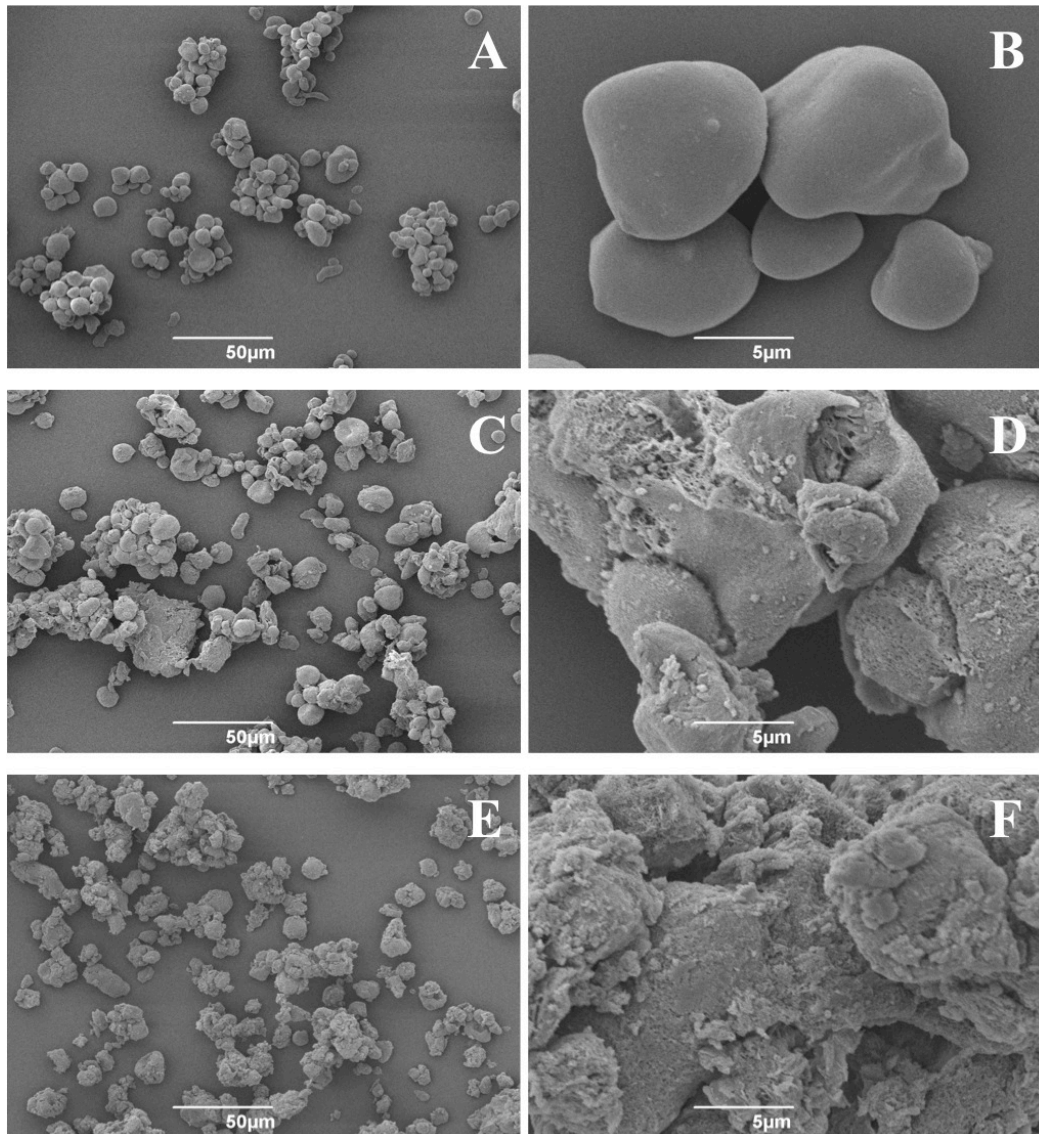


**Figure 4.3 – Scanning electron micrographs (magnification X500 and X5000) of native high amylose corn starch (A, B), gelatinised high amylose corn starch (C, D) and retrograded high amylose corn starch (E, F)**

### **4.3.2 Porosity of expanded starch**

As previously indicated from the SEM micrographs, gelatinisation and retrogradation of starch leads to significant changes in the morphology of the materials. The modification process also imparts dramatic changes to the physical properties of starch granules, including the formation of a porous network, leading to an expanded starch material

with a high surface area. This porosity was characterised using porosimetry (adsorption isotherm).

Nitrogen adsorption studies have shown native starch granules to typically possess a low surface area ( $<1 \text{ m}^2/\text{g}$ ) (Table 4.1). Gelatinisation and retrogradation processes significantly increase the surface area of starch. Ethanol and toluene were used to dehydrate the modified starch according to the procedure described in section 7.4.1.1. The use of toluene in the solvent exchange process seems to increase surface area compared to the use of ethanol alone. This may be explained by the fact that toluene is less polar than ethanol, which results in weaker interfacial adhesion between hydroxyl-rich starch molecules and the non polar solvent. As a result, the pore structure remains intact after the drying process. Doi also investigated the effect of dehydration solvents on the surface area of the gelatinised starch.<sup>253</sup> Ethanol was found to be the most effective solvent to preserve the porous structure of gelatinised starch, followed by *t*-butanol and 2-propanol. After the retrogradation process, the surface area increased to  $154 \text{ m}^2/\text{g}$ . In further experiments, gelatinised starch (GS) and gelatinised then retrograded starch (RS) suspended in toluene were utilised in film production.

**Table 4.1 – Surface area of native, gelatinised starch (GS) and retrograded starch (RS)**

Starch	Surface area ( $\text{m}^2/\text{g}$ )
Native	$<1$
GS <sub>ethanol</sub>	74
GS <sub>toluene</sub>	110
RS	154

### 4.3.3 $^{13}\text{C}$ cross polarisation (CP) magic angle spinning (MAS) solid state nuclear magnetic resonance

$^{13}\text{C}$  Solid state NMR has been widely used to study structural changes and molecular order of starch due to the convenience of analysing starch in solid state and it is essentially a non-destructive technique.<sup>258-260</sup> Figure 4.4 demonstrates the  $^{13}\text{C}$  CP MAS NMR spectra of native high amylose starch and its gelatinised and retrograded forms. Spectra were acquired by Dr David Apperley of solid-state NMR service at the University of Durham.

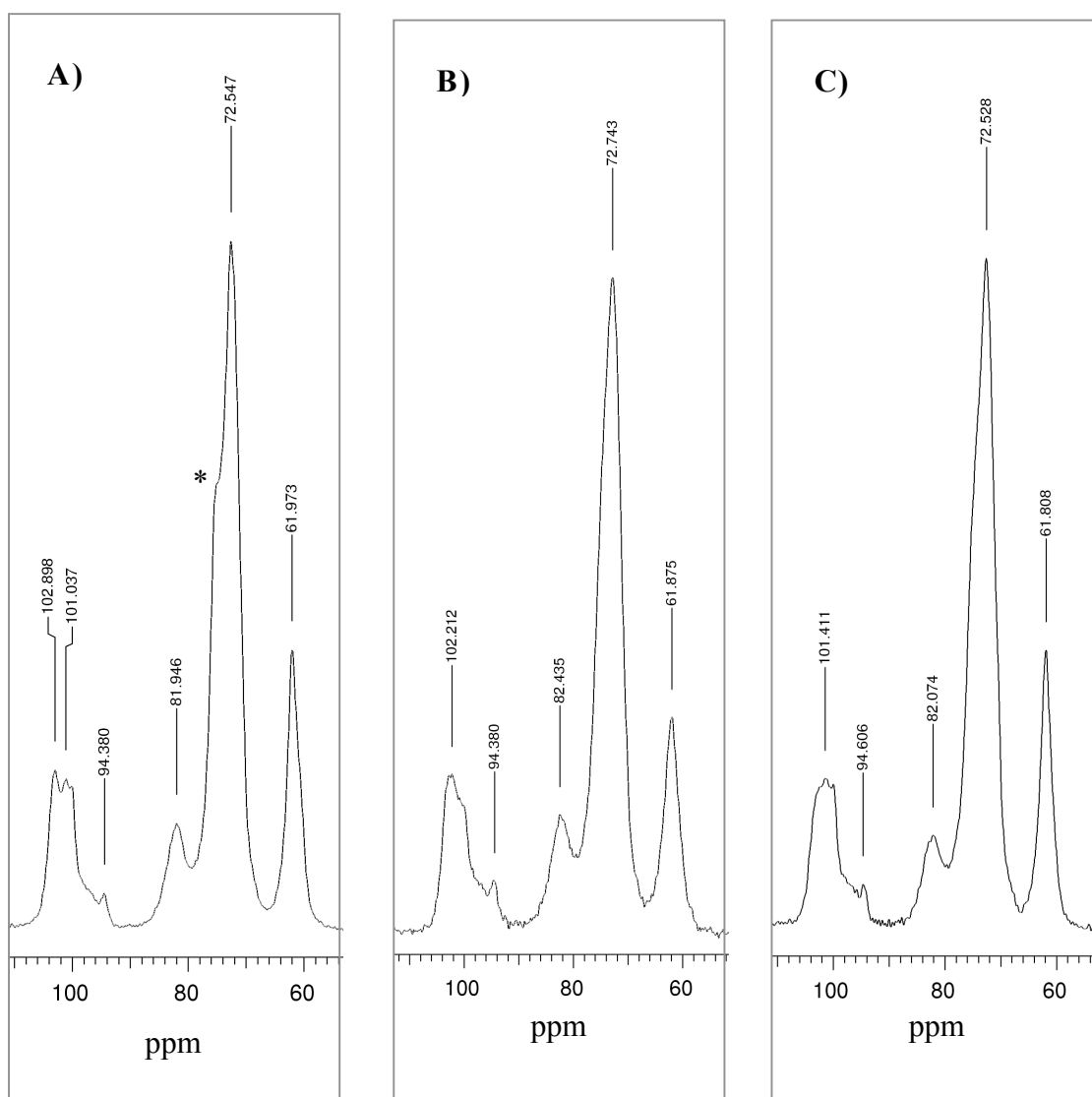


**Figure 4.4 –  $^{13}\text{C}$  CP MAS NMR of native high amylose starch (A), gelatinised starch (B) and retrograded starch (C)**

The signals in the range of 106-92 ppm correspond to the resonance of C-1 in the anhydroglucose unit. It is well known that the multiplicity and chemical shifts of C-1 atoms may provide information regarding the glycosidic conformation and polymorphism of starch.<sup>260, 261</sup> A-type starch spectra give the C-1 resonance region as a triplet whilst a doublet can be observed in the B-type form spectra.<sup>260</sup> Native high amylose starch spectra show a well-resolved peak at 103 ppm and less clearly resolved peaks in the region of 101-99 ppm, indicating the characteristics of a B-type polymorph (*Figure 4.4 A*).

The peak at 103 ppm is correlated to the V-type crystalline phase due to single helices of amylose-lipid complex present in the material.<sup>241</sup> Similar features were noted in B-type amylose, which is known to comprise of double helices packed in a hexagonal unit cell.<sup>262</sup> The broad shoulders in the region of  $\delta = 103$  and 95 ppm are believed to originate from the non-crystalline material for C-1.<sup>239</sup> The signal at 82 ppm is assigned to the non-crystalline components of C-4 carbons.<sup>259</sup> After gelatinisation, the peaks in the region of 101-99 ppm notably reduce in relative intensity, whilst the peaks at 103, 94 and 82 ppm, which are characteristics of amorphous material, become more noticeable in both intensity and resolution. This confirms that the crystallinity in starch granules is disrupted during gelatinisation. After retrogradation, the peak at 103, 94 and 82 ppm decreases the intensity, suggesting recrystallisation has occurred during gelation, and the previous single helices amylose complex may recrystallise into the double helical form.

The large signal between 73-70 ppm corresponds the C-2, C-3 and C-5 and the signal at 62 ppm is associated to the hydroxymethyl C-6 of the anhydroglucose units.<sup>263</sup> Resolution of the resonance near 73 ppm (indicated by \* in *Figure 4.4 A*) is not observed in gelatinised and retrograded starches. This is evidence of peak broadness in the resonance of C-2, C-3 and C-5, which occurs when the system becomes less ordered after the modifications. Extreme regularity in crystalline domain give rise to narrow and sharp resonance, whilst the distribution of the local molecular environment in non-crystalline materials allow allocation of chemical shifts, as a result, broad resonances are obtained.<sup>239</sup> *Table 4.2* summarises the peak assignment of the NMR spectra.

**Table 4.2 –  $^{13}\text{C}$  CP MAS NMR peak assignment of native high amylose starch, gelatinised starch (GS) and retrograded starch (RS)**

Sample	Chemical shift (ppm)			
	C-1	C-4	C-2, 3,5	C-6
Native HAS	106-92	81.946	72.547	61.973
GS	106-92	82.435	72.734	61.875
RS	106-92	82.074	72.528	61.808

#### 4.3.4 X-ray diffraction

The X-ray diffraction (XRD) pattern of high amylose starch shows the peaks at 5, 15, 17, 20, 22-23 ° ( $2\theta$ ), which is typical pattern obtained from the combination of B- and V- type polymorph (*Figure 4.5*).<sup>211, 232</sup> The strong peak at  $2\theta$  of 20 ° indicates that a highly crystalline structure of amylose-lipid complex can be found in the starch granules.<sup>232</sup> This peak significantly reduces its intensity after gelatinisation and retrogradation, suggesting the loss of the V-type crystalline form of the amylose complex. This is in agreement with the previous result obtained from the  $^{13}\text{C}$  CP MAS NMR. After gelatinisation, starch gives a smooth curve, indicating the loss of crystallinity of the starch granules.<sup>264</sup> It is well known that during retrogradation, the crystallinity of starch partly recovers.<sup>265</sup> TEM and DSC studies reported by Keetels *et al.* indicates that long range order present in native starch granules is not regained after gelatinisation and retrogradation, suggesting that during the recrystallisation (in retrogradation process), only short branches of amylopectin reform the ordered double helices within the crystalline domain.<sup>266</sup> This is also evidenced by broader peaks on the X-ray diffractogram of retrograded starch compared to those of native starch. The XRD measurements were carried out with assistance from Emma Cooper.

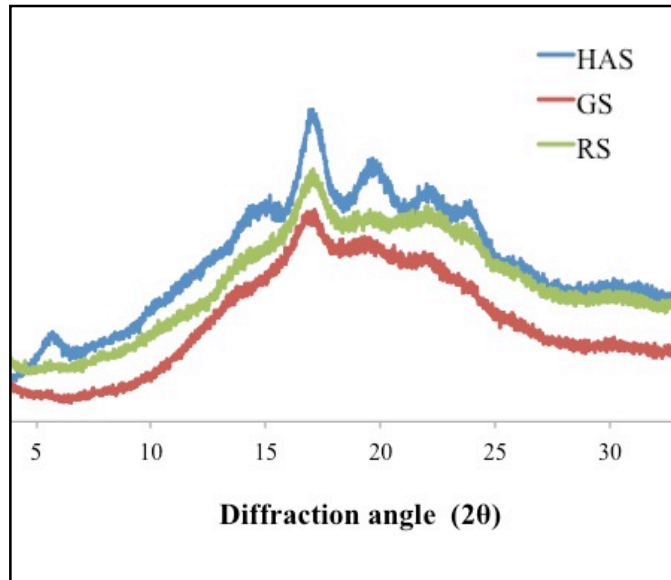


**Figure 4.5–Diffractograms of high amylose starch (HAS), gelatinised starch (GS) and retrograded starch (RS) (Originally in colour)**

#### 4.3.5 Thermal characterisation

TGA traces of all samples show two significant weight loss phases (*Figure 4.6*). The first phase occurs almost immediately after the samples are heated and finishes at around 100 °C. This corresponds to the evaporation of water or other volatile components such as traces of exchanging solvents, representing approximately 10% of sample total weight. There is little or no mass loss in the region of 150-230 °C. The second weight loss appears from approximately 260 to 330 °C and represents the thermal decomposition of the materials. After the rapid decrease in mass, there is approximately 20% of starch residue left at 500 °C.

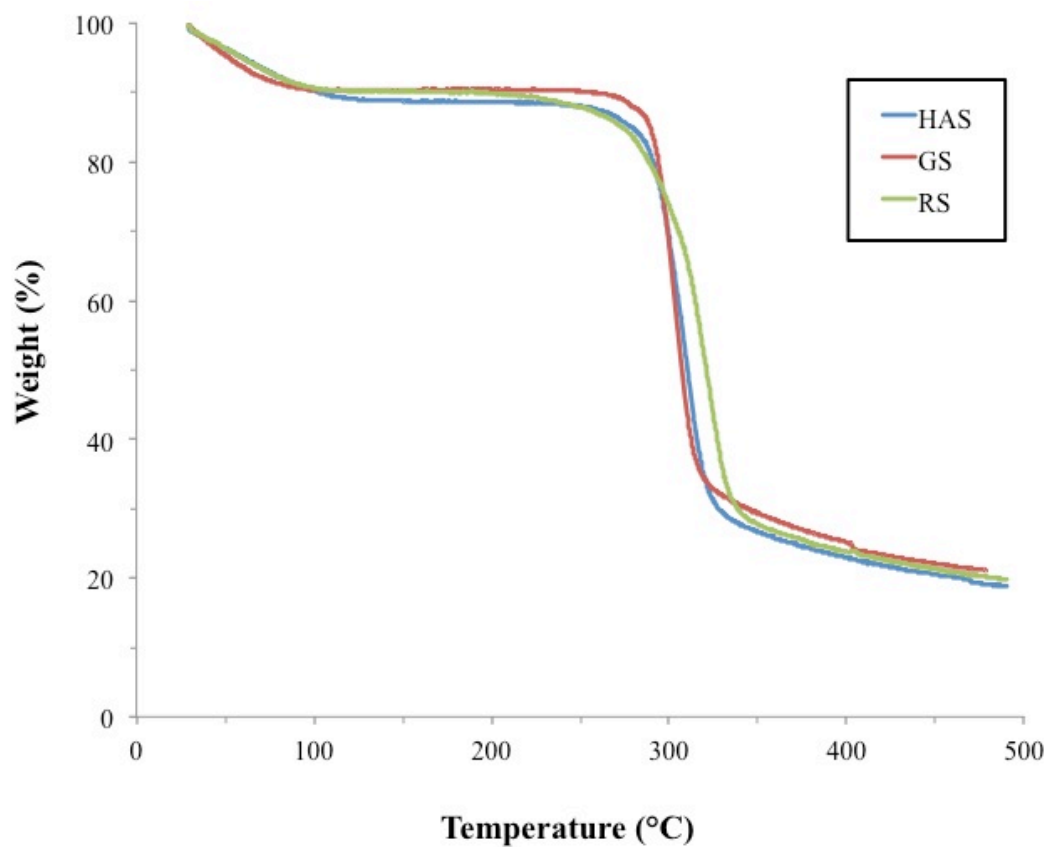


**Figure 4.6 – TGA thermograms of unmodified, gelatinised and retrograded starches (Originally in colour)**

The decomposition temperatures of all samples are assigned by determining the peak temperature of DTG traces and summarised in *Table 4.3*. The decomposition temperatures of all starch samples are comparable, however the retrograded starch shows a slightly higher temperature of degradation relative to the other starches.

**Table 4.3 – Thermal characteristics of native, gelatinised and retrograded starches**

Starch type	Weight loss (%) (150-500 °C)	Decomposition temperature (°C) (DTG peak)
HAS	70.9	316.4
GS	69.3	314.9
RS	70.6	323.0

The chemical reactions occurring during the thermal decomposition of starch were studied by Zhang *et al.* using  $^{13}\text{C}$  high resolution solid-state NMR spectroscopy.<sup>267</sup> Thermal condensation and dehydration occur around 300 °C to generate ether and ethylene segments. At higher temperatures, aromatic rings such as phenol/benzene and furan structures are formed with methylene and ether linkages. A similar observation was reported by White *et al.* with expanded starch samples, however in this case, the decomposition occurs at lower temperatures.<sup>268</sup>

## 4.4 Films with expanded starch

As described in chapter 2, the combination of ELO and bio-derived diacid (Pripol 1009) yields flexible and transparent film after curing at high temperature. A catalytic amount of DMAP in the formulation not only considerably reduces the curing time, but also increases the mechanical performance of the product. In this section, native and modified starches (gelatinised and retrograded) were added in this standard formulation in order to investigate the effect of starch on the properties of the films.

### 4.4.1 Mechanical properties

The films are prepared according to the method described in section 7.4.4. The mechanical tests were performed at least in triplicate and the average values reported.



#### 4.4.1.1 Effect of different types of starch

Native high amylose starch, gelatinised starch and retrograded starch were added to the standard formulation of ELO and Pripol using DMAP as catalyst. The amount of starch used in the formulation was set at 10% the weight of the thermosetting resin. The tensile results show that gelatinised starch moderately improves the mechanical properties of the film produced with a respective increase of 47%, 11% and 3%, for tensile strength, Young's modulus and elongation at break (*Figure 4.7*). After retrogradation, the modified starch yields a slight increase in tensile strength, compared to the one of the native starch (approximately 6%). However, Young's modulus and elongation at break decrease by 4% and 9%, respectively. This suggests that the opened structure of the modified starch slightly affects the tensile strength of the films. Research concerning the use of porous starch as filler in polymer is fairly limited, however, starch nanoparticles have been utilised as reinforcement in thermoplastic.<sup>269</sup> Nanoparticles fillers are known to enhance the mechanical properties of composites, partly due to the high surface area of the materials in relative with other typical fillers.<sup>270</sup> The same idea may also be applied on the high surface area in expanded starch and this is evidenced by the improvement of tensile strength of the modified starch films.

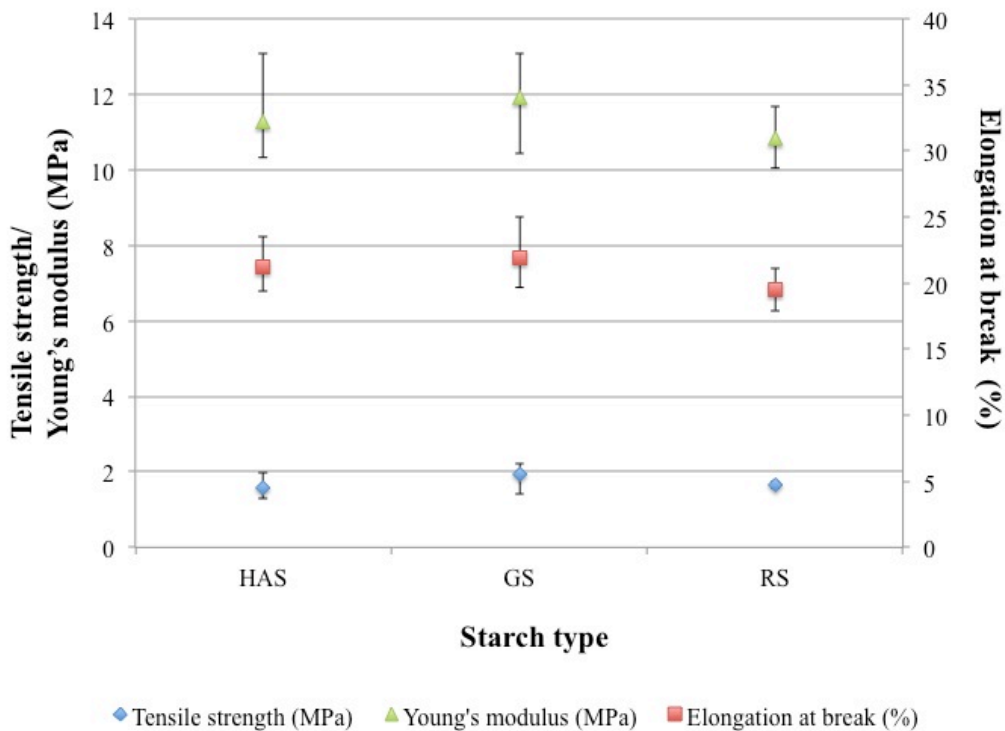


**Figure 4.7 – Mechanical properties of films based on ELO, Pripol and unmodified or gelatinised or retrograded starch (Originally in colour)**

#### 4.4.1.2 Effect of different amounts of starch

Various amounts of gelatinised starch were added into the standard mixture in order to study the influence of starch concentration on the mechanical properties of the resulting films (*Figure 4.8*). The addition of starch clearly improves the tensile strength of the films with a maximum of 227% enhancement seen when 20% wt. of starch is added. The Young's modulus also increases with the quantity of starch added. Formulation with 20% wt. starch yields films with 166% Young's modulus improvement. At low starch concentrations (10% wt.), the elongation at break is scarcely affected. However, at the higher starch loadings, the elongations at break decrease by 13% with 20% of starch, and a considerable decrease is seen (90%) with loadings of 23% starch. The addition of filler typically decreases the elongation at break of composites, sometimes at very low loading.<sup>271, 272</sup> Increasing of amount of starch filler gives rise to the decline of elongation at break of the materials. This deterioration is attributed to the different polar characteristics of starch and the polymer matrix, which induces poor interfacial

adhesion between the two components.<sup>273</sup> It is also noted that the maximum amount of starch that can be included in the formulation is 23% wt. as more starch leads to very viscous mixtures, which were found to be impossible to cast as films.

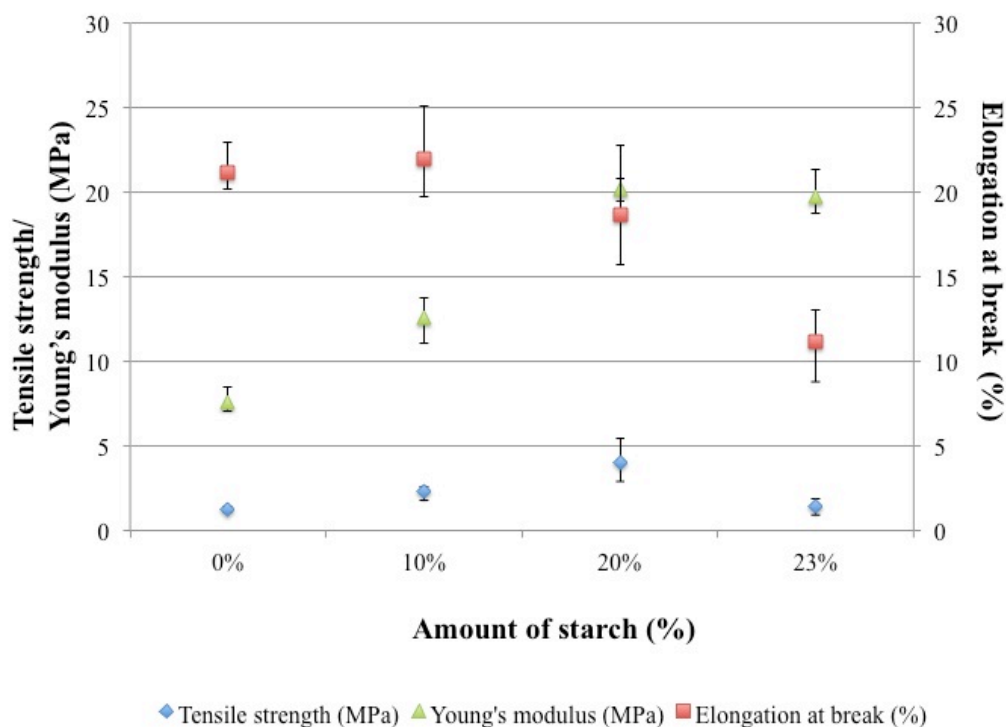


**Figure 4.8 – Effect of amount of gelatinised starch on the mechanical properties of films (Originally in colour)**

#### 4.4.1.3 Effect of curing temperature

It has been reported that the curing temperature can affect the mechanical properties of thermosetting polymers.<sup>274</sup> Hill *et al.* studied the reactivity of etherified melamine-formaldehyde resins with polyol binders at various curing temperatures, which was found to influence the properties of the product.<sup>275</sup> As such three different curing temperatures were investigated using the formulation, which is comprised of ELO, Pripol and 10% wt. of gelatinised starch in the presence of DMAP, in order to optimise the film production process. The resulting data is shown in *Figure 4.9*. The highest tensile strength is obtained when the film was cured at 140 °C, at which the resulting film shows 23% and 50% enhancement compared to the ones cured at 160 °C and 180 °C, respectively. The highest Young modulus is achieved at curing temperature of 160

°C, however, a 44% drop in elongation at break is observed compared to the film prepared at 140 °C. The film cured at 180 °C yields the weakest product out of the three curing temperatures. Despite giving a slightly better Young's modulus, the film obtained at 160 °C has low elongation at break. Therefore, the best curing temperature of the films prepared with starch is at 140 °C.

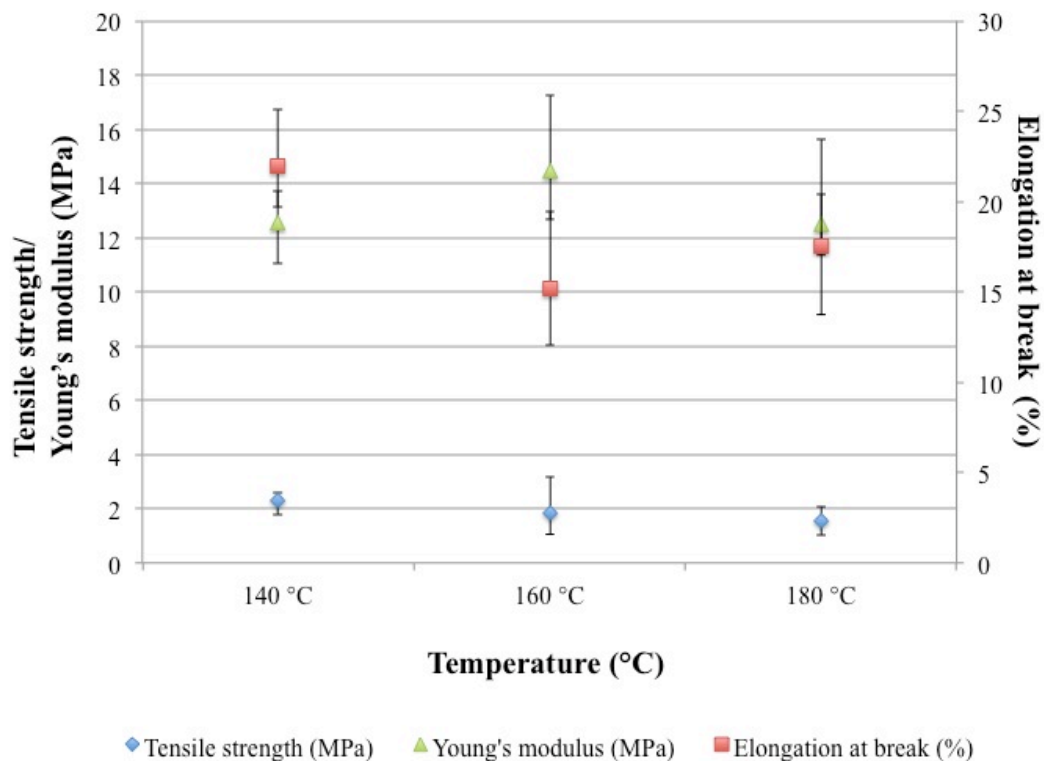


**Figure 4.9 – Effect of curing temperature on mechanical properties of resulting films (Originally in colour)**

Moreover, higher curing temperatures resulted in significant colouration films as shown in *Figure 4.10*. The yellowing of the ELO based films is a result of autoxidation of non-epoxidised unsaturation in linoleic acid present in the oil, and the rate of oxidation was shown to increase with the temperature.<sup>276</sup> Dell'Erba *et al.* also observed darkening of epoxy resins using DMAP as catalyst and explained that the colouration was due to the segments of the polymerised chains that have the initiator with conjugated double bonds attached to one of the chain ends.<sup>199</sup>

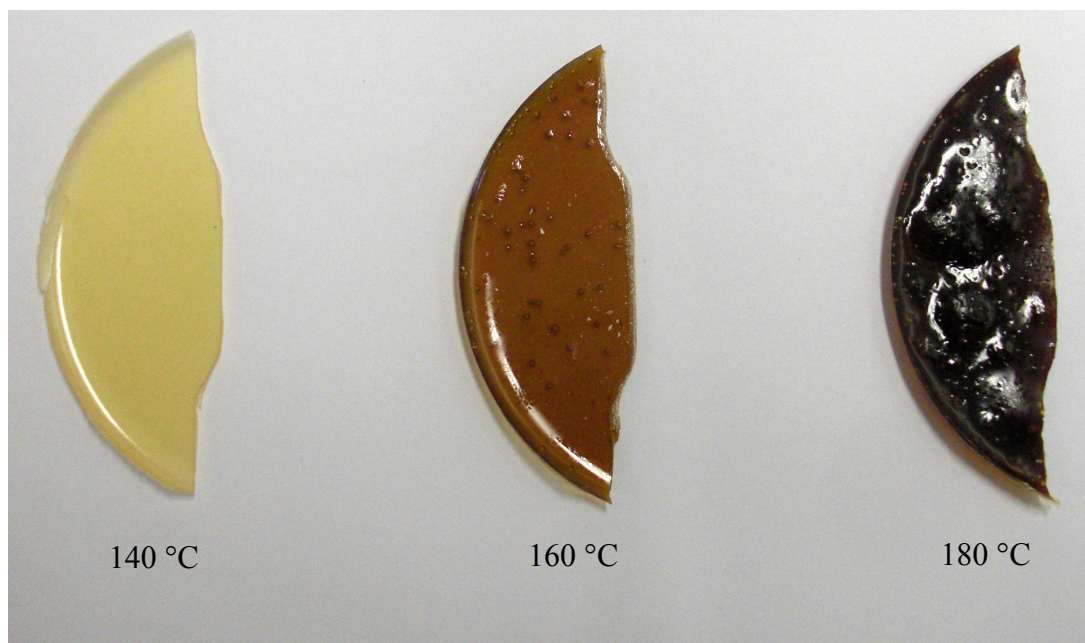


**Figure 4.10 – Films made of ELO, Pripol, gelatinised starch and DMAP cured at various temperatures (Originally in colour)**

#### **4.4.2 Morphological study**

The cross-section of starch-included films were viewed using SEM, with phase separation clearly seen with the native HAS films (*Figure 4.11 A*). The enlarged images of the film show that one side of the film (*Figure 4.11 B*) is filled with a much greater amount of starch granules than the other (*Figure 4.11 C*).

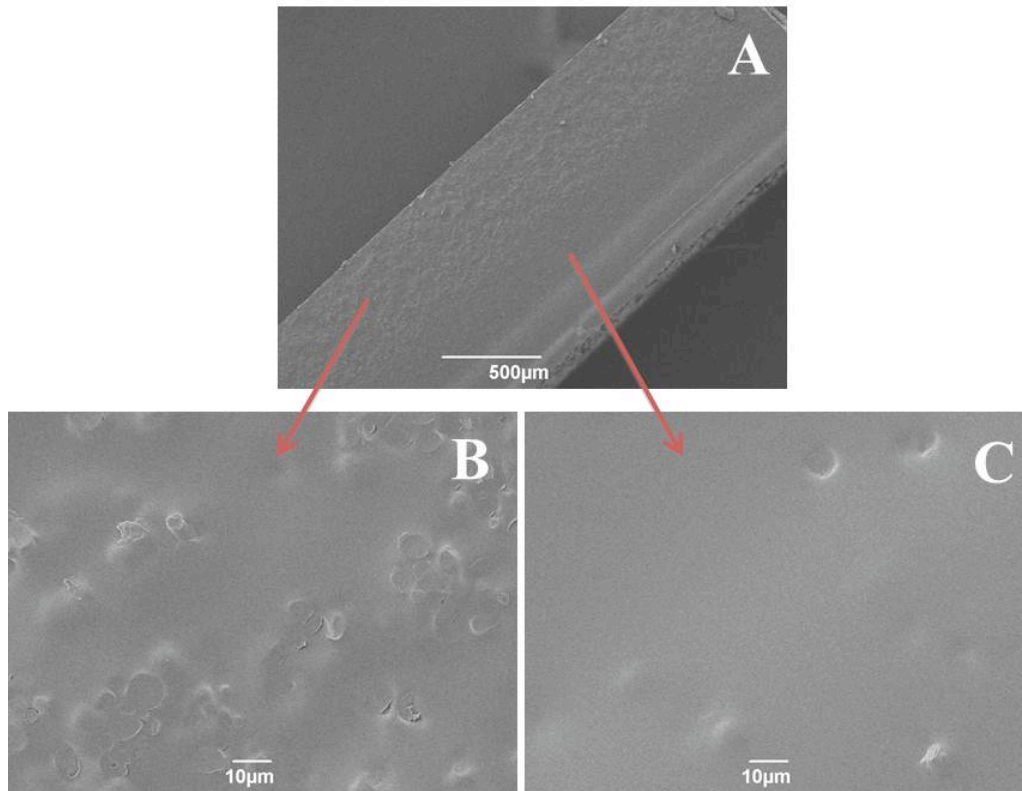


**Figure 4.11 – Scanning electron micrographs (magnification X50 and X1000) of the cross-section of film with native high amylose starch– A) whole film, B) bottom of the film and C) front of the film**

The films from gelatinised and retrograded starches revealed a homogenous cross-section and exhibited no noticeable phase separation (*Figure 4.12 A*). Furthermore, the starch granules are equally distributed throughout the film (*Figure 4.12 B-C*). This suggests that gelatinised and retrograded starch granules disperse better in the polymer matrix than native granules, possibly due to the porous structure in the modified starches, which allows the monomers to penetrate into the granules and consequently enables a uniform dispersion. It is also noted that the size of starch remains in the region of 5-10 μm, which indicates that no swelling had occurred during the cure.

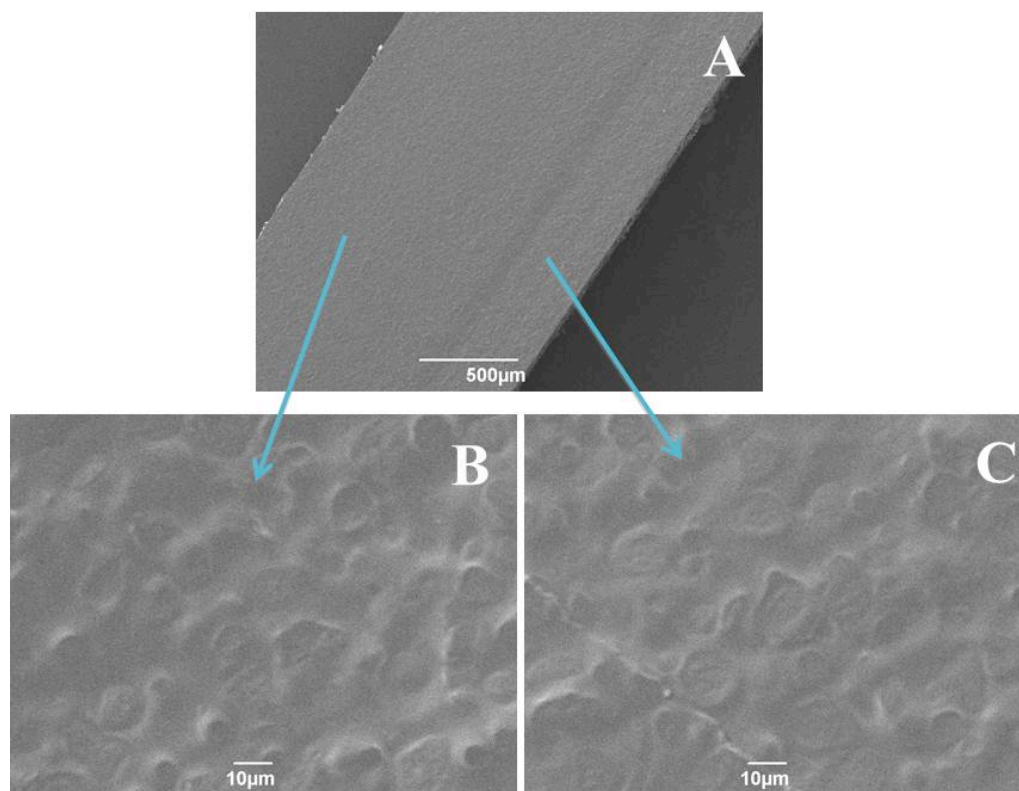


**Figure 4.12 – Scanning electron micrographs (magnification X50 and X1000) of the cross-section of film with gelatinised starch– A) whole film, B) bottom of the film and C) front of the film**

#### **4.4.3 Water uptake**

The water uptake test performed was the same method previously mentioned in section 2.4.2.2.

The average water uptake of the resins with starch shows the water uptake between 2-3% (*Figure 4.13*). The film with native starch gives slightly higher value than the modified ones. As shown in the morphological study, the films with gelatinised and retrograded starches reveal uniform granules dispersion, indicating good interfacial adhesion between the filler and polymer matrix, which leads to better coverage of the granules and consequently reduces the water uptake of the resin.<sup>277</sup>

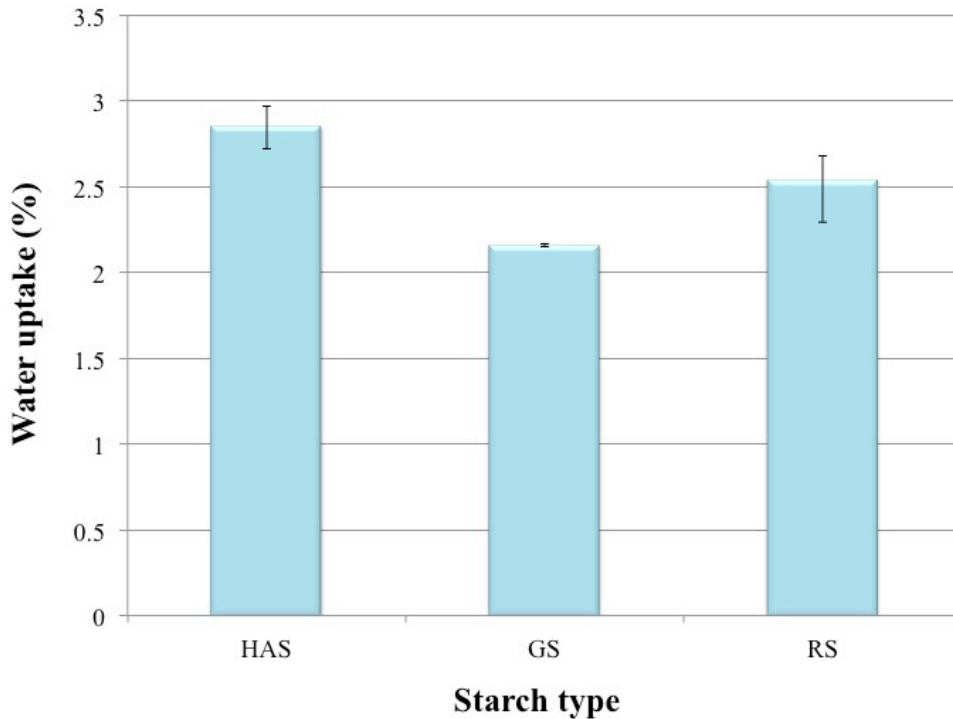


**Figure 4.13 – Effect of different types of starch on water uptake of films – high amylose starch (HAS), gelatinised starch (GS) and retrograded starch (RS) (Originally in colour)**

Figure 4.14 shows the water uptake increases with the amount the starch added to the resin. The film without starch absorbs water less than 0.5% of the resin weight after 24 hours of submersion, whilst the water uptake of the film with 20% wt. gelatinised starch rises to nearly 4%. By increasing starch loading from 20% wt. to 23% wt., the difference of water uptake of the films becomes notably significant. The high content of starch may lead to filler agglomeration that might have occurred during the mixing process, which could generate additional voids in the polymer texture, leading to some surface roughness in the film with 23% wt. starch and resulting in greater than expected increase in the water uptake of the film.<sup>277</sup> The water uptake of the films can be potentially reduced by using chemically modified starches with higher degree of hydrophobicity, such as acetylated starch.<sup>278</sup>



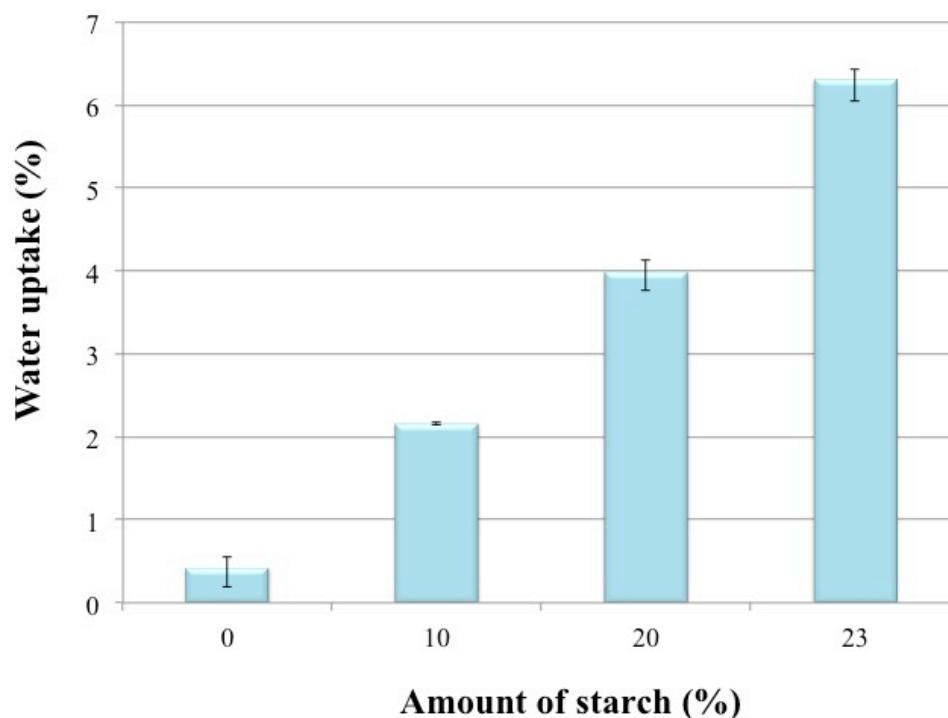


**Figure 4.14 – Effect of different amounts of starch on water uptake of the films (Originally in colour)**

#### 4.4.4 Thermal properties

The thermal properties of resulting films were studied using thermogravimetric analysis (TGA). The samples were heated from 25 °C to 500 °C at a heating rate of 10 °C/min.

##### 4.4.4.1 Effect of different amounts of starch

TGA thermograms of all samples reveal practically no weight loss up to 150 °C. Between 150-250 °C, a slight reduction in mass can be observed for the samples that contain starch (*Figure 4.15*). The resin without starch displays a single significant weight loss starting around 350 °C. However the DTG curve of this material clearly shows that the resin experiences two-stage thermal decomposition (*Figure 4.16*). The first stage, which is the main thermal event, occurs in the temperature range of 380-420 °C and the second stage takes place between 440-460 °C. The first stage of the decomposition could be partially attributed to the unreacted ELO as neat ELO shows a decomposition peak at 380 °C (*Appendix A – Figure A.4.1*). This is also observed by

previous thermal decomposition study of epoxidised soybean oil based thermoset, which stated that unreacted components in the resin are responsible for the decomposition at lower temperature than that of the polymerised resin.<sup>50</sup> The first stage decomposition, which peaks at 405 °C is mainly assigned to the crosslinked polymer. A part of the material that decomposes at the second stage, suggests that more crosslinking might be present in some regions of the resin, hence the decomposition at higher temperature is observed. Li *et al.* reported that high degree of crosslinking improved the thermal stability in polystyrene beads.<sup>279</sup> The resins with starches display two major weight losses on the TGA thermograms (*Figure 4.15*).

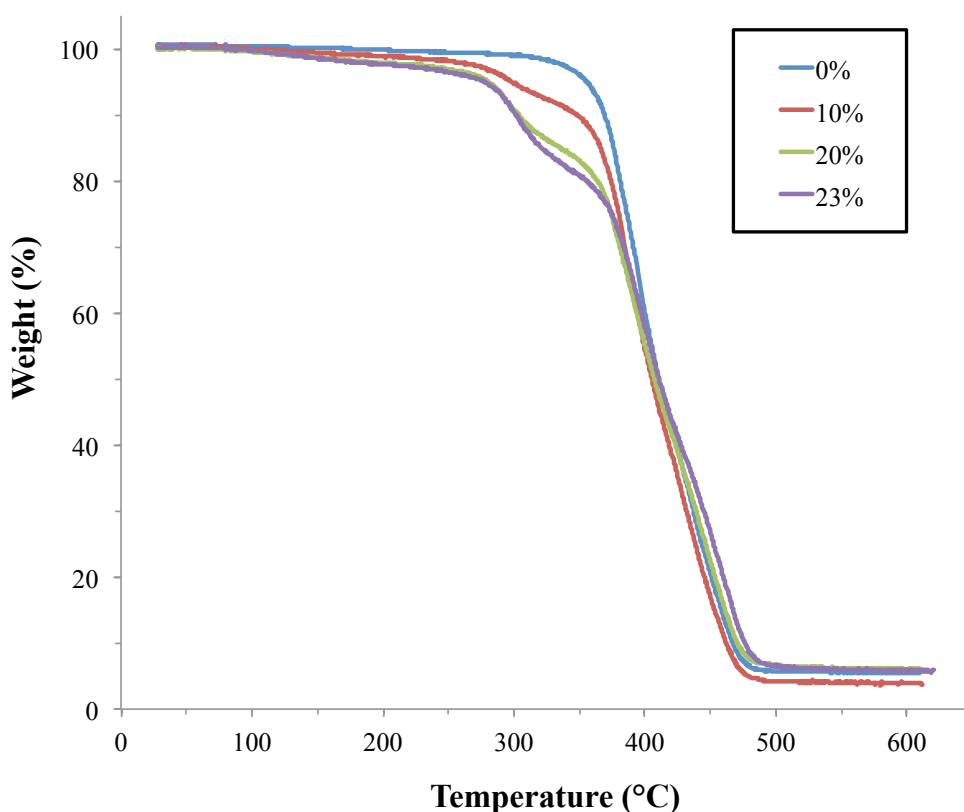


**Figure 4.15 – TGA thermograms of films with different amounts of added starch (Originally in colour)**

The first weight loss phase commences at approximately 280 °C and is more significant with greater starch presence within the formulation. This is in good agreement with the DTG curves, which shows a transition in temperature range of 280-320 °C and this becomes more significant when more starch is added (*Figure 4.16*). The second weight loss begins at around 350 °C and finishes at 500 °C, which is in the same region as

170

decomposition observed for the resin without starch. The DTG curves also display two-stage decomposition for this second mass loss, similar to that of the film without starch. Interestingly, the DTG curves demonstrate that the ratio of second stage to the first stage of the decomposition becomes more significant as the amount of starch added rises. This suggests that the presence of starch in the formulation potentially promotes additional crosslinking in the resin; hence an increase in the proportion of highly crosslinked material is observed. In conclusion, the first weight loss phase corresponds to the decomposition of starch. The crosslinked polymer decomposes at higher temperatures and can be witnessed as the second weight loss on the TGA thermograms. It is noted that the inclusion of starch slightly affects the thermal stability of the polymerised resin and a modest decrease in the second decomposition peak is observed in the films containing starch (*Table 4.4*).

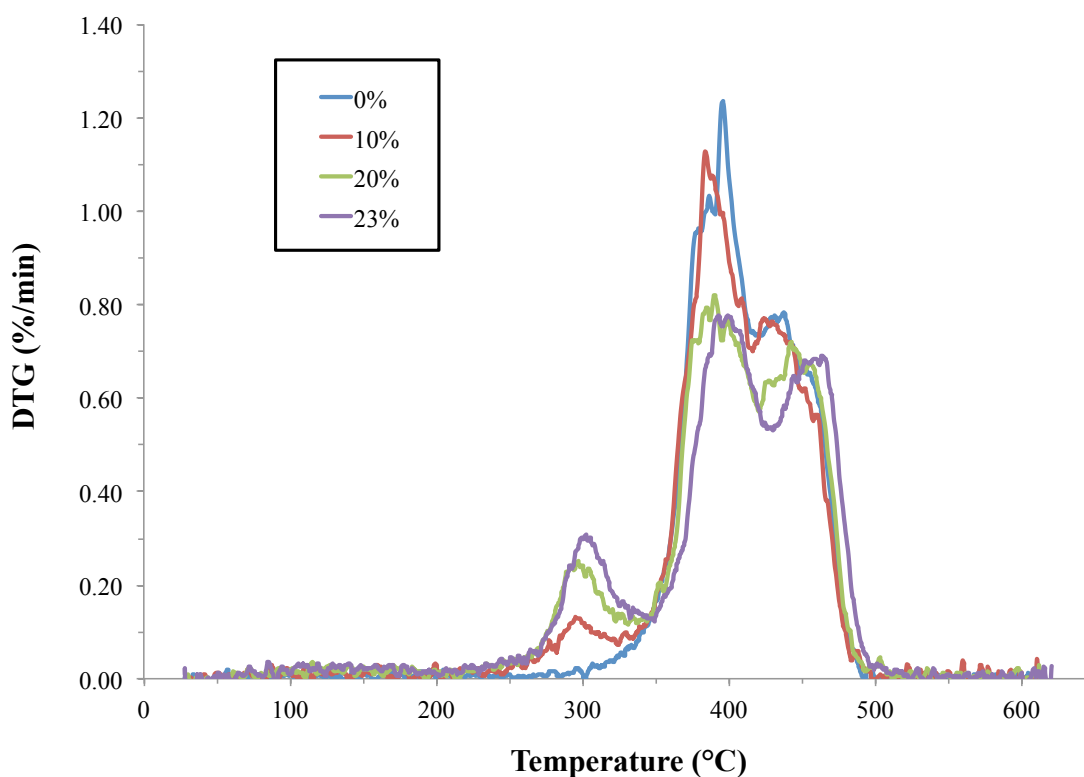


**Figure 4.16 – DTG curves of films with different amounts of added starch (Originally in colour)**

**Table 4.4 – Summary of TGA results of films with various amounts of starch**

Amount of starch (%)	Weight loss (%) (150-600 °C)	Decomposition temperatures (°C) (DTG peaks)
0	94.7	405.0
10	95.6	303.5, 393.5
20	92.6	303.9, 396.9
23	92.7	302.0, 393.0

#### 4.4.4.2 Effect of starch expansion by gelatinisation or retrogradation

The thermal stability of films with native, gelatinised and retrograded starches are summarised in *Table 4.5*.

**Table 4.5 – Summary of TGA results of films with native or gelatinised or retrograded starch**

Starch type	Weight loss (%) (150-600 °C)	Decomposition temperature (°C) (DTG peak)
HAS	95.3	323.9, 400.8
GS	95.6	303.5, 393.5
RS	91.2	302.1, 398.4

Different types of starch scarcely affect the decomposition temperature of resulting films. The decomposition temperatures, determined from the peak temperature of DTG traces, are approximately 300 °C and 400 °C, with the film with native starch showing slightly higher first decomposition temperature than those of modified starch films. The

thermograms of these films all show two weight loss phases at relatively close temperature; the first one being at around 280 °C and the second one at around 350 °C (*Appendix A – Figures A.4.2-4*).

## 4.5 Expanded starch in the formulation

### 4.5.1 Thermal study

Modulated DSC was used to characterise thermal events during the curing process of the reaction mixtures. The formulations are comprised of ELO, Pripol and DMAP (0.5% of total weight) with native, gelatinised or retrograded starch. Non-reversible heat flow traces of the formulations with starches show two overlapping exothermic transitions between 75 °C to 200 °C, whilst the formulation without starch gives only one transition in that region (*Figure 4.17*). It is also noted that the transition peaks are broadened when starch is included in the formulation, suggesting a retardation of the curing process. The first transition of HAS formulation occurs at 125.6 °C, whilst the ones of GS and RS formulations happen at 127.4 °C and 132.0 °C, respectively (*Table 4.6*). The second transitions occur at higher temperatures at around 150 °C. These are slightly higher than that of formulation without starch (133.4 °C). The same observation is made for the onset temperatures. This indicates that the addition of starch decelerates the rate of polymerisation or curing. The inclusion of starch in the formulation decreases the glass transition temperatures of the cured products, in particular, in the case of HAS. Numerous studies reported an increase in  $T_g$  with the amount of starch filler incorporated in the composites. They associated the rise of the  $T_g$  to the hydrogen bonding between starch particles and in some occasions, between the filler and the polymer matrix.<sup>218, 280, 281</sup> However, the falloff of the  $T_g$  has also been observed and was believed to be due to the poor interaction of the polymer with the filler particles, which is likely to be the case of these ELO based resins with the starch filler.<sup>282</sup> The total heat of cure increases moderately in the presence of the starch. A similar observation was made by Wu *et al.* in their calorimetric study of the effect of carbon fillers on the curing of epoxy resin.<sup>283</sup> The total heat of reaction is typically related to degree of cure of the polymer.<sup>51, 284</sup> The fact that the heat of reaction of formulations with starch is greater than that of the standard formulation may be attributed to the presence of starch filler in

the polymer matrix, though further investigation is needed to understand the role of starch in the formulation.

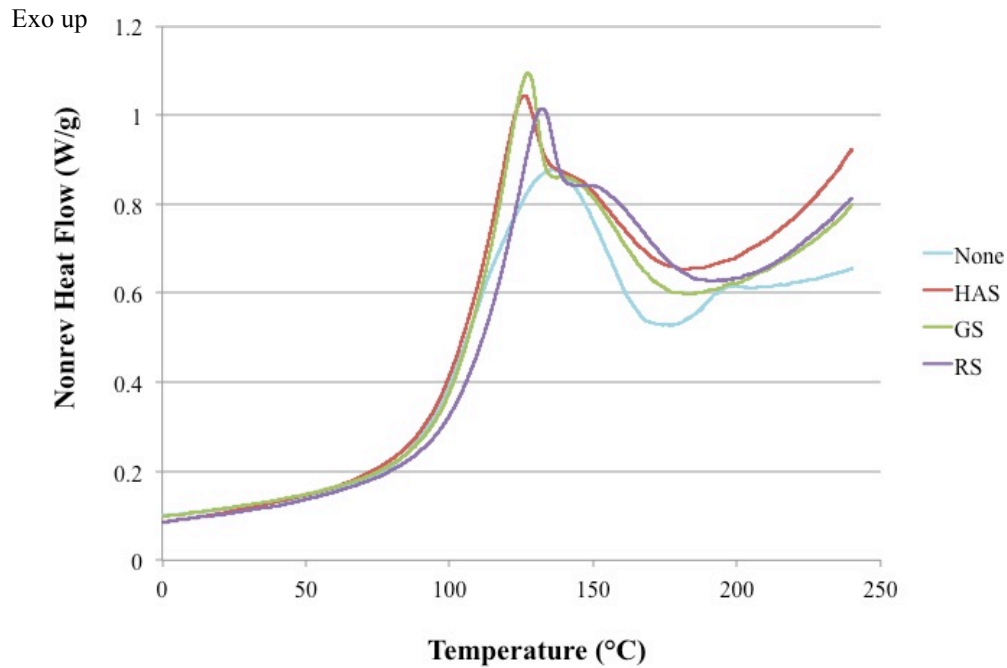


**Figure 4.17 – Thermograms of formulations comprised of ELO, Pripol, DMAP and different types of starch (Originally in colour)**

**Table 4.6 – MDSC results of starch formulations**

Starch type in the formulation	Total heat of reaction (J/g)	Onset temperature (°C)	Peak temperature (°C)	T <sub>g</sub> (°C)
None	131.9	92.61	133.36	-13.33
HAS	156.7	100.98	125.61	-29.61
GS	156.6	104.07	127.35	-19.28
RS	162.6	107.81	132.0	-17.19

In order to investigate further into this matter, the same experiments were conducted for these following mixtures:

- 1) ELO
- 2) ELO and DMAP
- 3) ELO, Gelatinised starch and DMAP
- 4) Pripol, Gelatinised starch and DMAP

The resulting MDSC traces of these formulations and ones of previous cases (ELO+PP+GS+DMAP and ELO+PP+DMAP) were overlaid as shown in *Figure 4.18*. The thermogram from neat ELO has exothermic transition with two visible peaks at 142.2 °C and 159.8 °C. The first peak is likely to correspond to the ring opening of the oxirane rings and the smaller peak at higher temperature is attributed to the possible subsequent etherification reaction. By adding DMAP to ELO, both transitions can still be seen but occur at slightly higher temperatures, however, the heat of reaction increases significantly. This suggests that DMAP promotes the curing reaction, resulting in a higher degree of polymerisation of the resin. Homopolymerisation of epoxy resin using DMAP as catalyst was previously studied by Dell'Erba *et al.* and they found that the product using DMAP as initiator had a considerably higher  $T_g$  than those using conventional tertiary amine catalysts.<sup>199</sup> They ascribed this to a higher crosslink density in resin with DMAP. The addition of starch (gelatinised) in the mixture of ELO and DMAP slows down the curing reaction by increasing the maximum exothermic heat flow temperature to 172.14 °C. However, the total enthalpy of reaction moderately increases, suggesting additional curing has occurred in the presence of starch filler. This is in good accordance with the thermal decomposition study of the cured films in section 4.4.4, which suggested that additional crosslinking occurred in the presence of starch in the formulation. With hemp fibre and epoxidised oil Boquillon *et al.* reported that the change in the cure mechanism was due to hydroxyl group presence of the vegetable fibre.<sup>285</sup> In our case, the increase of total enthalpy of reaction in the presence of starch could be explained by the hydroxyl groups in starch, which can facilitate the ring-opening of epoxide rings, hence, promotes the polymerisation. This is also confirmed by the significantly greater  $T_g$  (*Table 4.7*). The formulation comprised of Pripol, starch and DMAP also shows an exothermic peak at 136.11 °C. However, the

total heat of reaction of this formulation is relatively low, suggesting minimal reaction had occurred between the two components in the presence of DMAP.

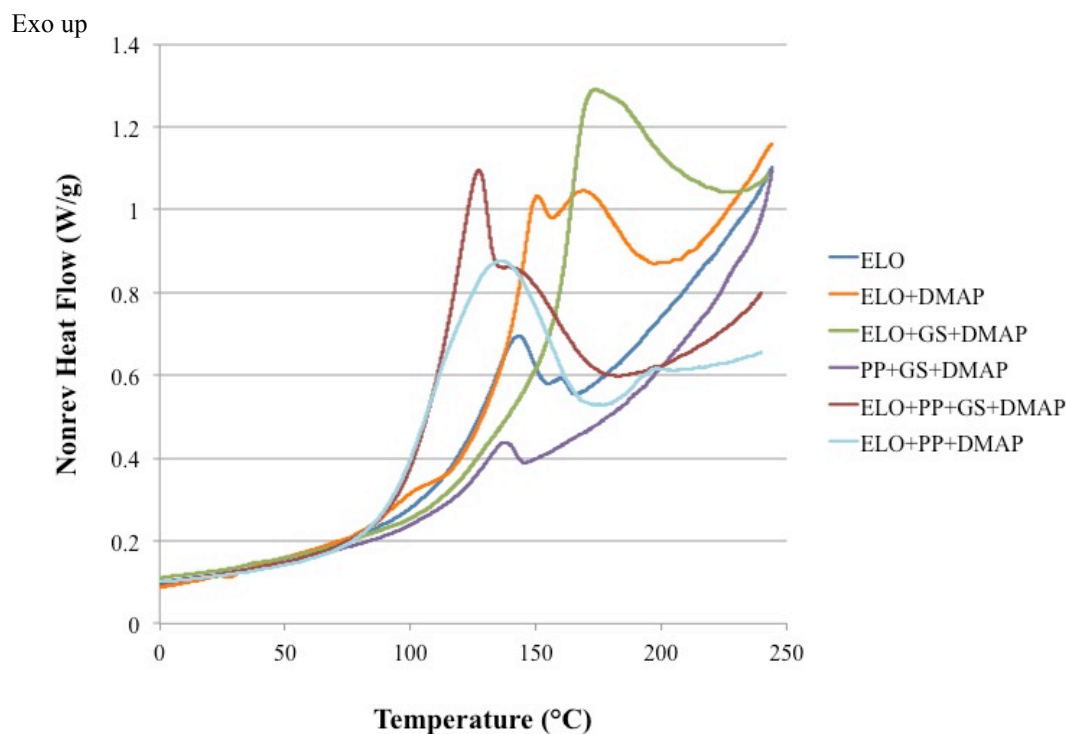


**Figure 4.18 – Thermograms of various formulations 1) ELO, 2) ELO and DMAP, 3) ELO, GS and DMAP, 4) Pripol, GS and DMAP, 5) ELO, Pripol, GS and DMAP and 6) ELO, Pripol and DMAP (Originally in colour)**

According to these experiments, the two exothermic peaks observed in the formulation of ELO, Pripol, starch and DMAP are presumably due to heterogeneity of the mixture. The first transition corresponds to the reaction of ELO and Pripol in the vicinity where starch is less present. Whereas the region where more starch is present, the steric hindrance caused by the starch granules slows down the reaction between ELO and Pripol, resulting in higher maximum exothermic heat flow temperature. The greater enthalpy of reaction obtained from formulation with starch is ascribed to the presence of hydroxyl functionalities in starch granules, which assists the ring-opening of ELO and thus induces more crosslinking to take place. However, there is no obvious evidence that starch is chemically bonded to any components in the polymer matrix. The glass transition temperature of the formulation with gelatinised and retrograded starch is quite



similar to one without starch (*Table 4.6*). However, the formulation with HAS gives much lower  $T_g$  than other formulation. This indicates poor miscibility of native starch granules in the polymer matrix, compared to that of modified ones.<sup>286</sup> This matter is supported by the SEM observation in previous section.

**Table 4.7 – MDSC results of various formulations 1) ELO, 2) ELO and DMAP, 3) ELO, GS and DMAP, 4) Pripol, GS and DMAP**

Formulation	Heat of reaction (J/g)	Onset temperature (°C)	Peak temperature(s) (°C)	$T_g$ (°C)
ELO	37.0	119.30	142.22, 159.80	-37.90
ELO+DMAP	110.1	136.34	150.84, 168.99	-42.28
ELO+GS+DMAP	148.9	155.95	172.14	-18.31
PP+GS+DMAP	7.1	120.51	136.11	-49.91

## 4.5.2 Rheological properties

### 4.5.2.1 Effect of different types of starch (native vs expanded)

The viscosity study of the formulations consisted of ELO, Pripol and DMAP with different types of starch (unmodified, gelatinised and retrograded) was conducted to examine the progress of polymerisation and the gel point of these reaction mixtures. The steady shear rate was applied to all samples, which were cured at 140 °C. The rise of viscosity can be noted at the beginning of the observation when starch is present in the formulation, in particular gelatinised and retrograded starches (*Figure 4.19*). The initial viscosity slightly increases from 2000-3000 cP in neat mixture to 4000-5000 cP in unmodified starch mixture. The mixtures with modified starch show even higher initial viscosity at 12000-18000 cP. The augmentation of the viscosity of formulations

with filler is expected as the suspended particles perturb the flow of the material, resulting in an increase of dissipated energy and viscosity increase.<sup>287</sup>

The gel point of formulation without starch is determined at around 700 seconds of curing. The addition of starch clearly decelerates the resin to gel as the starch mixtures gel at approximately 1200 seconds after being heated. This is in accordance with the thermal analysis, which reveals that the presence of starch slows down the polymerisation of the resin.

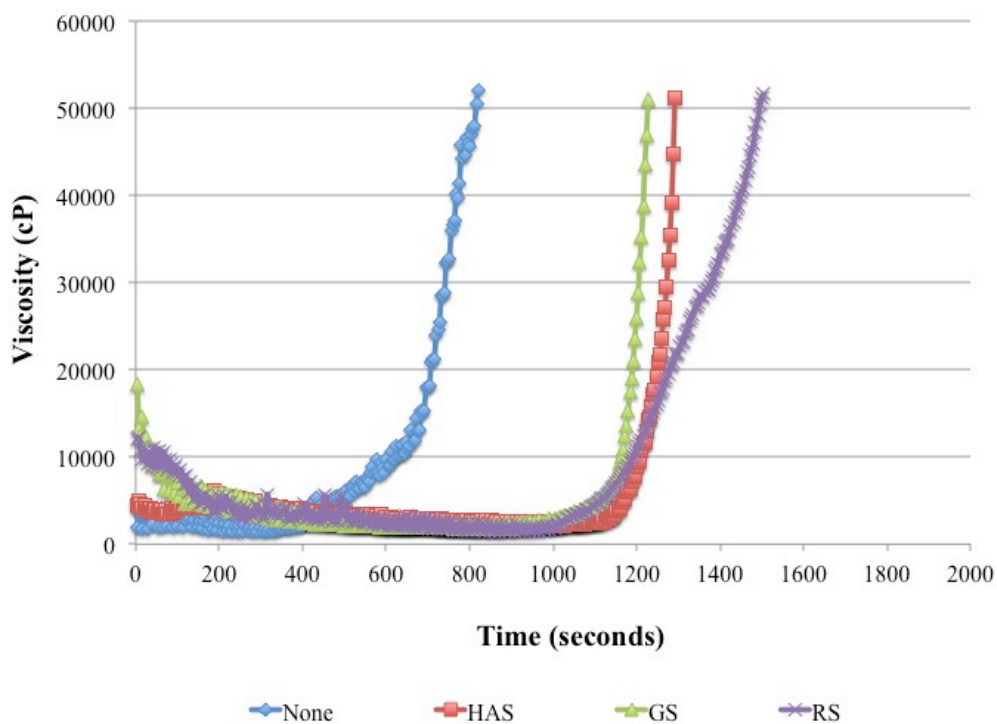


**Figure 4.19 – Viscosity of reaction mixtures of ELO, Pripol and DMAP with 1) no starch, 2) unmodified starch (HAS), 3) gelatinised (GS) and 4) retrograded starch (RS) (Originally in colour)**

#### 4.5.2.2 Effect of different amounts of starch

As stated in the previous section, the added starch retards the curing process of the ELO based resin. Herein, different amounts of gelatinised starch were included into the standard formulation and the development of the viscosity at 140 °C with steady shear

rate was pursued. As anticipated, the gel time of the reaction mixture increases in correlation with the amount of starch included in the formulation (*Figure 4.20*). The neat mixture starts to gel at around 700 seconds. By incorporating 10% wt. of starch in the mixture, the gel time rises near 1200 seconds. Whilst starch-loading increase to 20% wt. and 23% wt., the gel points increase further to around 1500-1600 seconds, which double the gelling time of formulation without starch ( $\approx 700$  seconds).

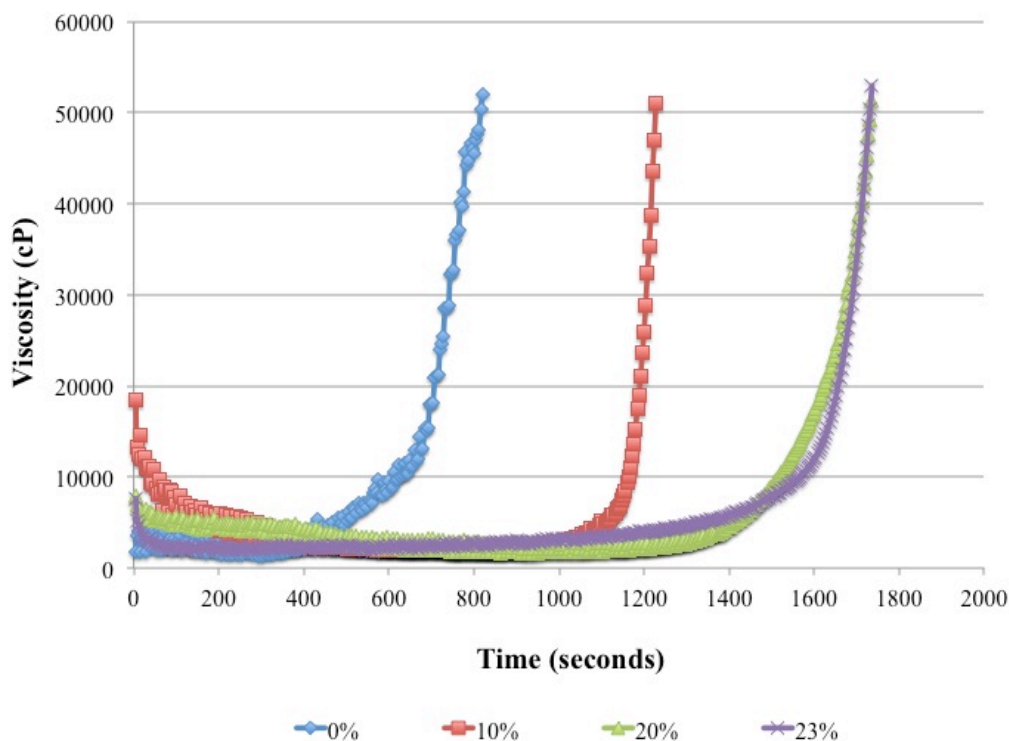


**Figure 4.20 – Viscosity of reaction mixture of ELO, Pripol and DMAP with different amounts of gelatinised starch (Originally in colour)**

### 4.5.3 Infrared spectroscopic study

In order to investigate the chemical reactions of the components present in the thermoset composite formulation, an infrared spectroscopic study was carried out during the curing process. The mixtures of two components were conducted in order to facilitate the interpretation of spectra. The IR study of the mixture of ELO and Pripol in the presence of DMAP catalyst was described in chapter 2 (section 2.5.1). In this section, the IR study of a mixture of expanded starch (in toluene suspension, as toluene

is good at dispersing expanded starch and is compatible with all the components) and ELO, and a second formulation of expanded starch (in toluene suspension) and Pripol, both of which contained DMAP, were heated at 140 °C, and samples were taken every 30 minutes. *Figure 4.21* shows the spectra of ELO and expanded starch in the presence of DMAP at 0, 30, 60 and 90 minutes. At the onset of the observation (0 min), traces of toluene are observed. These bands disappear after 30 minutes, indicating the evaporation of the solvent. The characteristic band of the hydroxyl group in starch is observed at 3323 cm<sup>-1</sup> in dried expanded starch. When starch is suspended in toluene, this band slightly shifts to 3333 cm<sup>-1</sup> (*Appendix A – Figure A.4.5*). ELO and Pripol show no bands in this area. At the onset of the observation, a broad band at 3433 cm<sup>-1</sup> can be clearly seen on the spectrum of this reaction mixture. This may arise from possible hydrogen bonding between epoxide in ELO and the hydroxyl presented in starch, which assists the ring-opening reaction and leads to the formation of a new hydroxyl group. The alcohol assisted ring-opening reaction of epoxides have been mentioned in many occasions in the literature.<sup>288, 289</sup> This postulation is in agreement with the result from the thermal analysis, which reveals the higher heat of curing reaction is obtained from the mixture with starch. At 30 minutes, a low-intensity band is observed at 3456 cm<sup>-1</sup>. This band shifts overtime to 3464 and 3476 cm<sup>-1</sup> after 60 and 90 minutes, respectively. The band is likely due to the end-chain hydroxyl group from homopolymerisation of ELO (*Appendix A – Figure A.4.6*). Furthermore, a band at 1742 cm<sup>-1</sup>, corresponding to the C=O bond of ester functionality in the triglyceride is noted at the beginning of the observation. A minimal shift (1740 cm<sup>-1</sup>) is perceived after 90 minutes of curing. This is also observed in the homopolymerisation of ELO in the presence of DMAP. Zhang *et al.* studied a preparation of composite comprised of polyester and solid epoxy and also observed a slight change in their IR spectra regarding the original PLA ester band, compared to the new ester band of the composite.<sup>290</sup>

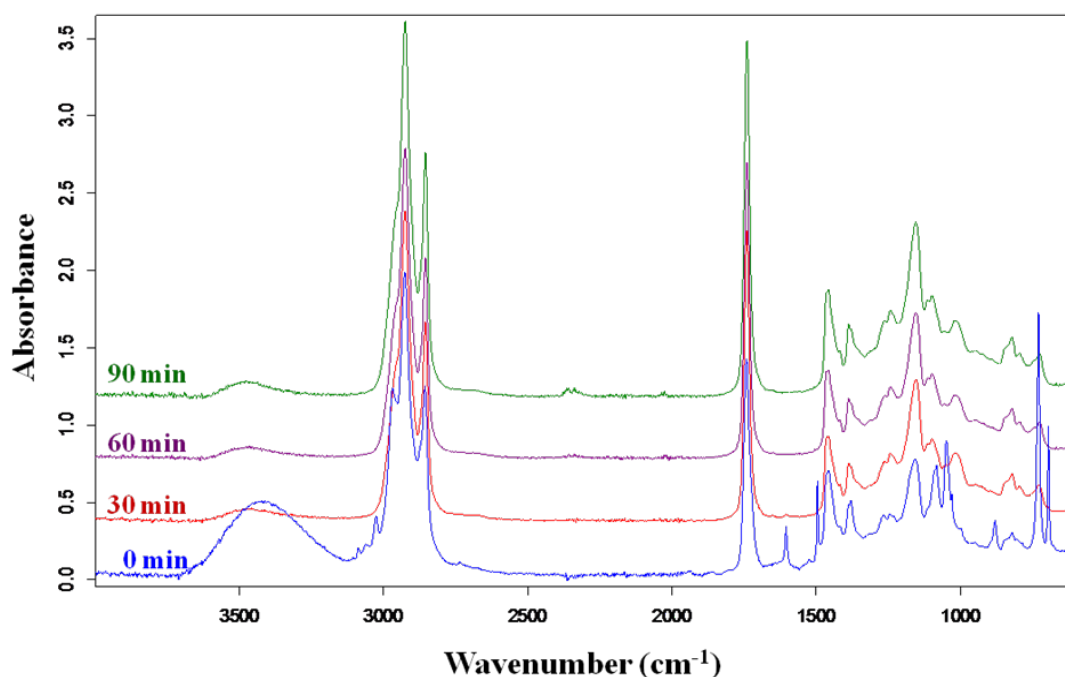


**Figure 4.21 – Infrared spectra of ELO and expanded starch mixture (0.5% of total weight DMAP catalyst) cured at 140 °C (Originally in colour)**

The spectra of the mixture consisted of Pripol, expanded starch and DMAP are demonstrated in *Figure 4.22*. Similar observation can be made at the beginning of the experiment. Bands from toluene are noted at 0 minute, and disappear after 30 minutes of heating, due to solvent evaporation. The stretching of hydroxyl in starch is also detected at around 3400 cm<sup>-1</sup> at the onset of the reaction. After 30 minutes, there are no evident changes in the spectra until the end of the observation.

In conclusion, IR data indicates that starch potentially plays an important role within the formulation through hydrogen bonding and subsequently facilitates the ring opening of the epoxides. This leads to a greater heat of reaction and resulting in a stronger more crosslinked film.

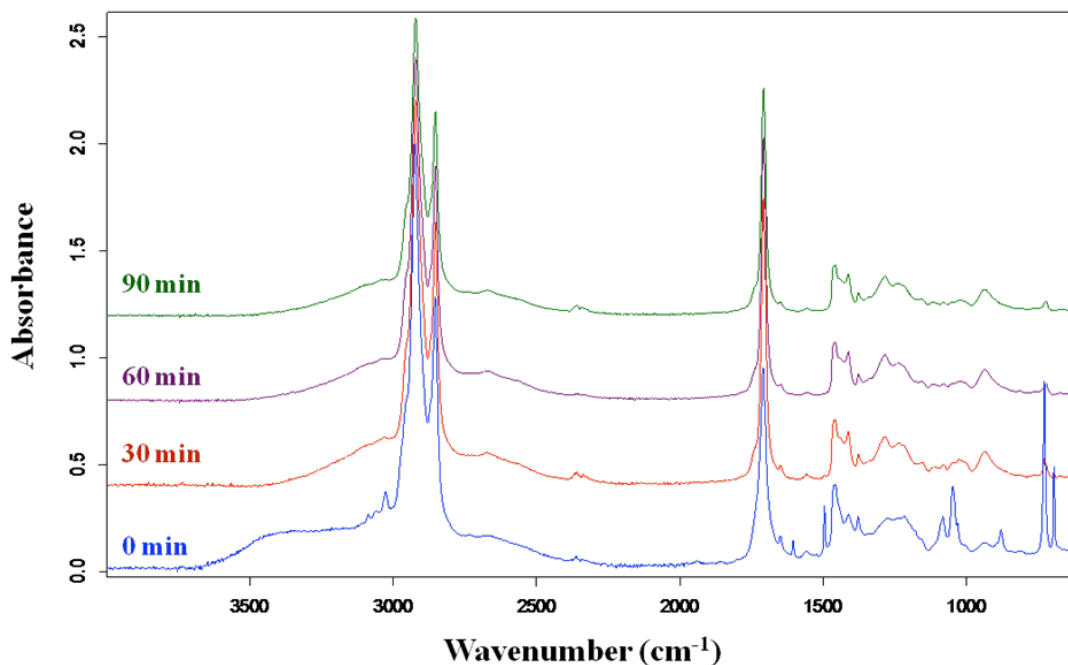


**Figure 4.22 – Infrared spectra of Pripol and expanded starch mixture (0.5% of total weight DMAP catalyst) cured at 140 °C (Originally in colour)**

## 4.6 Role of starch in the formulation

According to the analysis of the formulation mixtures and resulting films with added starch, it can be clearly seen that the inclusion of starch improves the mechanical properties of the resins, in particular the modified porous starches. However, limited amount of starch can be included in the formulation as high loading of starch leads to a very viscous mixture, which makes the casting of the film impractical. Gelatinised and retrograded starch granules disperse uniformly in the polymer matrix, whilst the native starch causes phase separation in the film. Thermal analysis by MDSC demonstrates that despite starch retarding the curing process, the higher enthalpy of the formulation with starch indicates a higher degree of crosslinking. This is likely to be caused by the hydroxyl functionality in starch, which can promote the curing of the polymer. According to the IR study, this might happen through the assistance of starch in the epoxide ring opening reaction, leading to a higher degree of crosslinking and results in films with better mechanical properties. However, no obvious evidence of a chemical reaction between starch and Pripol is observed. Furthermore, the thermal analysis of the

cured resin reveals that starch decomposes at lower temperature than the crosslinked polymer, suggesting that starch may not be chemically attached to the resin. However, as starch is a high molecular weight polymer, a fraction of chemical bonding would not significantly affect the decomposition of the bulk polymer, resulting in starch breaking down at its actual decomposition temperature.

## 4.7 Conclusions

High amylose corn starch was gelatinised and retrograded to yield a high surface area material. Gelatinisation and retrogradation alter the properties of starch including the morphological property and crystallinity of the granules. The surface area of starch significantly increased after the modification. It was noted that the solvent used in dehydration process of the product played an important role in determination of surface area. The crystallinity of starch granules reduced after gelatinisation and partly restored after retrogradation. This was witnessed by X-ray diffraction and  $^{13}\text{C}$  CP MAS NMR analysis. The thermal properties of native and modified starches were studied using TGA, which revealed that all starch samples had relatively similar decomposition temperatures at around 320 °C. The tensile testing of the resulting films showed that starch considerably improved the mechanical properties of the films. The optimum formulation was achieved when 20% wt. of gelatinised starch was present in the mixture. This formulation yielded a film with 227% improvement in tensile strength and 166% enhancement in Young's modulus, compared to those with no added starch. Curing temperature also affected the mechanical properties of the films. The optimum curing temperature of these films was 140 °C, at which the highest tensile strength and lowest colouration were obtained. SEM micrographs showed uniform dispersion of gelatinised and retrograded starch granules in the polymer matrix, whilst the cross-section of film with native starch showed a phase separation. This was attributed to the porous structure of modified starch, which allowed possible monomer penetration in the polymer matrix, leading to better dispersion. This porous structure gave rise to better coverage of the granules by the polymer resulting in lower water uptake of modified starch films compared to that of native starch film. A positive correlation was observed between the water uptake of the films and the filler content. Thermogravimetric study of the resulting films revealed two major mass losses. The first weight loss starting at around 280 °C was attributed to the decomposition of starch filler and the second

weight loss was at around 390 °C corresponds to the decomposition of the crosslinked polymer. DTG curves demonstrated that the polymerised resin undergo two-stage decomposition. The first stage was associated with unreacted ELO and some parts of crosslinked polymer. The second stage was related to the parts of the resin that highly crosslinked and therefore decomposed at relatively high temperature. The infrared spectroscopy and thermal analysis studies showed no obvious evidence of the attachment of starch to the resin. Thermal study and the gel time investigation of reaction mixture with starch unveiled the role of starch in the formulation. The presence of starch in the mixture delayed the curing reaction, possibly caused by the steric hindrance. DSC thermograms showed two superimposed peaks. This was believed to cause by the heterogeneity of the mixture. The first transition occurring at lower temperature was assigned to the region in the polymer matrix where starch was less present and the second broader peak at higher temperature was ascribed to the region, which contained more starch. However, higher heat of reaction was obtained when starch was present in the formulation, indicating greater degree of crosslinking and as a result superior mechanical properties were obtained with starch films. This was in good agreement with the decomposition study of starch films, which suggested that higher proportion of highly crosslinked material was observed when starch was present in the formulation. Infrared spectra showed that starch might promote the curing process via aiding with the ring-opening reaction.



# Chapter 5

## *Esterified starches and their use in bio-based thermoset composites*



## 5.1 Chapter 5 - Summary

Attempts to enhance the properties of ELO/starch based films were undertaken through esterification of expanded starches using various anhydrides including acetic anhydride, maleic anhydride, succinic anhydride and itaconic anhydride. Replacing the hydrophilic hydroxyl groups by more hydrophobic groups can potentially increase the interfacial adhesion between starch and polymer matrix, resulting in enhancement of the resin properties, including water resistance and mechanical features. The modified starches were characterised by infrared spectroscopy and nuclear magnetic resonance technique to ascertain that the esterification has taken place, and titration used quantitatively to determine the degree of substitution. The thermal stability of the esterified starch was determined through thermogravimetric analysis, which demonstrated that the acetylated starch decomposed at higher temperatures compared to the unmodified starch. However, other esterified starches were observed to decompose at temperatures lower than that of the native starch and typically a two-phase decomposition was observed. The thermogravimetric analysis coupled with Fourier transform infrared spectroscopy was conducted in order to investigate further the decomposition process of these starches. The results obtained showed that the first phase of the decomposition corresponded to the introduced ester group on the starch backbone, resulting in release of carbonyl containing compounds. The second phase of the decomposition was associated with that of the starch material. The esterified starches were subsequently utilised in the standard formulation of ELO, Pripol and DMAP to produce thermoset composites. The film containing acetylated starch exhibited better transparency and a comparable Young's modulus compared to those of native starch. However, the tensile strength of the film slightly decreased compared to that of unmodified starch. Other esterified starches demonstrated no improvement in mechanical properties. The water uptake of the films significantly reduced when replacing native starch with esterified starch. This was due to the better hydrophobicity of the modified starches compared to that of unmodified starch. In particular, the films with acetylated starch and succinic anhydride modified starch showed the water uptake as low as 0.7% and 0.8% respectively. These values are very close to that of the film with no starch added, which showed 0.4% water uptake. Interestingly, all resulting films showed good thermal stability, despite the lowered decomposition temperature of some of the esterified starches. The TG traces of all films showed that the weight loss starts at approximately

250 °C, except for the film with acetylated starch, where the decomposition point begins after 300 °C.

## 5.2 Introduction

Native starch has several disadvantages, which limits its uses in many applications. As a hydrophilic filler, the abundant hydroxyl groups in the native starch granules cause poor compatibility with the polymer matrix, which typically has a hydrophobic nature. This leads to low interfacial adhesion between the starch and the polymer matrix, resulting in poor mechanical properties.<sup>291, 292</sup> Therefore chemical modifications of starch, including esterification, have been intensively studied to overcome this drawback. Esterified starch has been demonstrated to improve the compatibility of starch and other component(s) in the composites and consequently enhances the mechanical properties of the materials.<sup>293, 294</sup>

Esterification of starch can be conveniently achieved due to a great number of hydroxyl groups present in starch. Modification can occur at the C2, C3 or C6 hydroxyl position of the anhydroglucose unit, thus a maximum degree of substitution of three can be attained. These three available hydroxyls however have different reactivities. The primary hydroxyl at C6 is more reactive than the two secondary ones and can be readily esterified, due to the low steric hindrance.<sup>295</sup> The properties of esterified starch significantly differ to that of the native starch starting material. These changes from the native material typically depend on the degree of substitution and the new substituent group. One of the most intensively applied esterification methods for starch is acetylation. Acetylation changes some properties of starch including paste clarity, resistance to retrogradation, freeze-thaw stability and hydrophobicity, depending considerably on the degree of substitution (DS).<sup>131, 296</sup> The degree of acetylation in starch depends on different factors, including the starch source, reaction time, reactant concentration and reaction media. A low DS acetylated starch (DS = 0.01-0.2), is commonly prepared by esterification of starch with acetic acid in aqueous medium,<sup>132</sup> whilst higher DS can be obtained with strong polar solvents such as pyridine or DMSO.<sup>295, 297</sup> Unlike water, these solvents will not interfere with the esterification reaction, hence the side reactions are minimised and a high DS can be obtained. The acetylated starch can usually be prepared by the reaction with acetic anhydride,<sup>132</sup> vinyl

acetate<sup>298</sup> or acetic acid.<sup>299</sup> However, a standard laboratory method involves the use of acetic anhydride and pyridine due to its convenience, versatility and ability to alter the degree of substitution.<sup>129</sup> The mechanism of this system is shown in *Figure 5.1*.

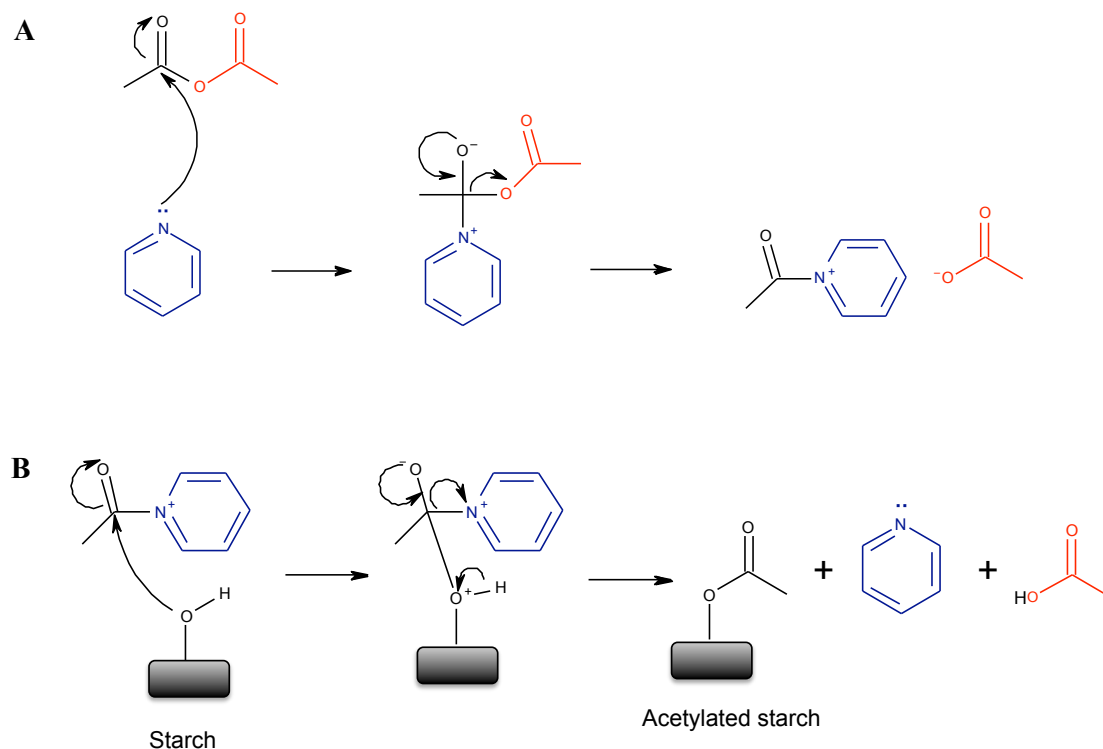


**Figure 5.1 – Mechanism of acetylation of starch using acetic anhydride and pyridine A) formation of acetyl-pyridine complex, B) formation of acetylated starch (adapted from reference 126) (Originally in colour)**

Doi investigated the use of this method on expanded starch in order to study the effect of the modification on the surface area of the material and found that the surface area of the acetylated starch decreased from 107 m<sup>2</sup>/g to 3 m<sup>2</sup>/g.<sup>253</sup> However, the use of toluene as solvent in the reaction caused less hindrance to the original surface area of the acetylated product (64 m<sup>2</sup>/g). Shuttleworth further developed the method by replacing pyridine with 4-dimethylaminopyridine (DMAP), which maintained the high surface area of the acetylated starch.<sup>126</sup> Moreover, DMAP is a more effective catalyst than pyridine, owing to its greater nucleophilicity, consequently the first step of the acetylation is more rapid using DMAP catalyst.<sup>300</sup> Also, the intermediate acetyl-DMAP benefits from the resonance stabilisation, which results in greater conversion of the

acetylated product (*Figure 5.2*).<sup>300</sup> In this chapter, expanded starch (gelatinised then retrograded starch) is modified via this procedure using acetic anhydride and maleic anhydride and also with other anhydrides including succinic anhydride and itaconic anhydride, which can be derived from biomass.<sup>301</sup> Expanded starch was chosen, as the preferred high degree of modification is more easily achieved using this starting material.<sup>253</sup> After the esterified starches are characterised, they are added into the standard formulation of ELO, Pripol and DMAP and the resulting films properties are investigated.

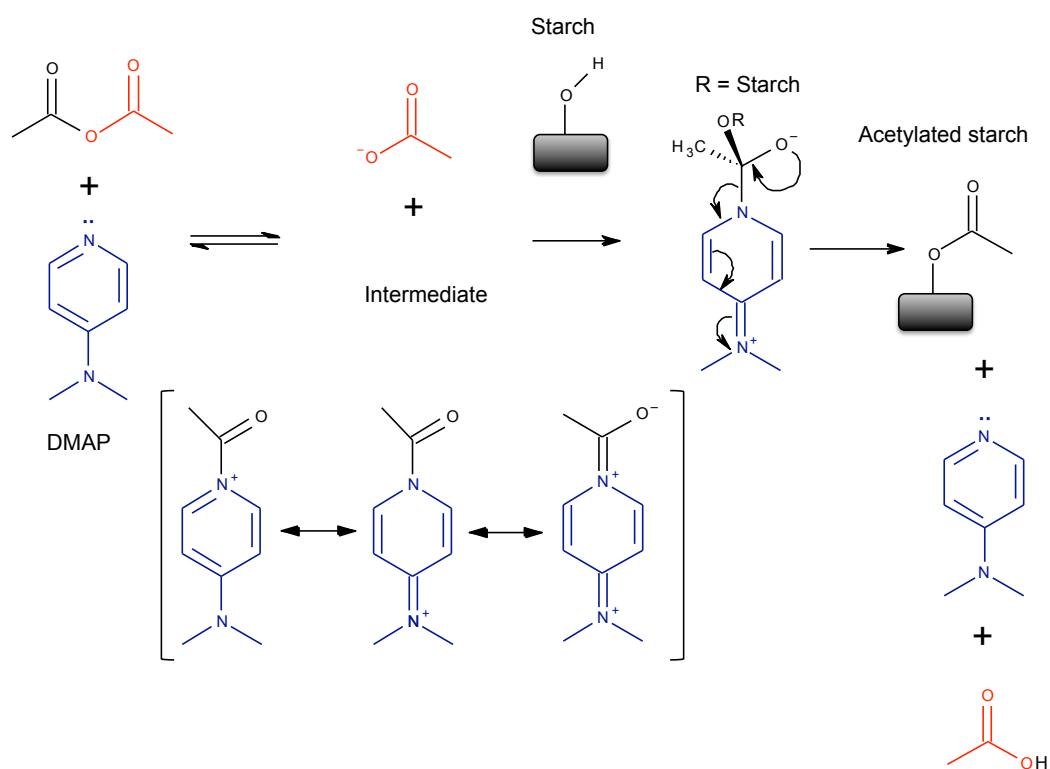


**Figure 5.2 – Mechanism of acetylation of starch using acetic anhydride and DMAP (adapted from reference 126) (Originally in colour)**

## 5.3 Characterisation of modified starches

### 5.3.1 Physical appearance

Acetic and succinic anhydride modified starches are white powdery materials, whilst maleic and itaconic anhydride modified starches are cream/yellowish in colour (*Figure 5.3*). The appearance of dark brown colour was observed during the esterification while

DMAP was added into the reaction slurry. The fact that only maleic and itaconic anhydrides reaction mixtures yield the brown colour suggests that the unsaturation in the anhydride could be the cause of the colouration. Simms *et al.* demonstrates that the unsaturation in the anhydride only promotes colour when it is conjugated with the anhydride ring, therefore, the development of colour could be attributed to the base-catalysed rearrangement of the anhydrides.<sup>302</sup> The base-catalysed rearrangement of itaconic anhydride to citraconic anhydride is demonstrated in *Figure 5.4*.



**Figure 5.3 – Acetylated starch (Ace), maleated starch (Mal), succinic anhydride modified starch (Suc) and itaconic anhydride modified starch (Ita) (Originally in colour)**

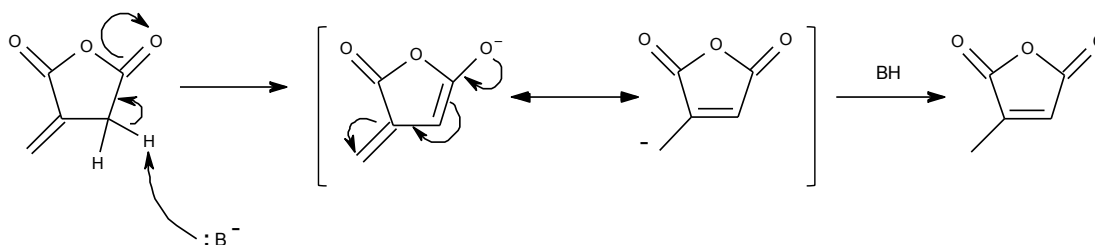


**Figure 5.4 – Base-catalysed rearrangement of itaconic anhydride to citraconic anhydride (adapted from reference 303)**

### 5.3.2 Infrared spectroscopy

Infrared spectra of the modified starches were recorded using attenuated total reflectance (ATR) technique in order to confirm the modification. The testing procedure is described in experimental section 7.7.5.

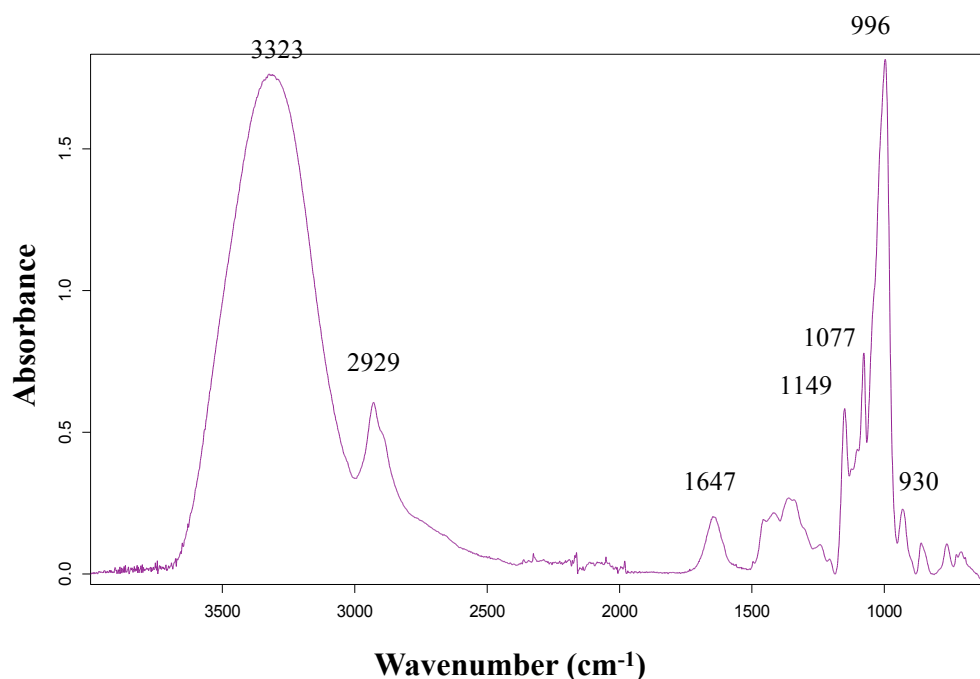


**Figure 5.5 – Infrared spectrum of unmodified expanded starch**

Figure 5.5 shows IR spectrum of unmodified expanded starch. Bands below  $800\text{ cm}^{-1}$  are assigned to skeletal modes of the pyranose rings. The skeletal mode vibrations of  $\alpha$ -1, 4 – glycosidic linkages (C-O-C) corresponds to the band observed at  $930\text{ cm}^{-1}$ .<sup>304</sup>



Strong bands are noted at 996 and 1077  $\text{cm}^{-1}$  are associated with the C-OH bending, with the band at 996  $\text{cm}^{-1}$  relating to the intramolecular hydrogen bonding of the hydroxyl of C-6 of the anhydroglucose.<sup>305</sup> The bands at 1021 and 1047  $\text{cm}^{-1}$  are reported to be characteristic of amorphous and crystalline structures in starch granules respectively, however they are seen as a shoulder of the strong band at 996  $\text{cm}^{-1}$  in this case.<sup>305, 306</sup> The band at 1149  $\text{cm}^{-1}$  corresponds to the stretching of C-O and C-C bonds.<sup>304, 307</sup> The fingerprint region between 1200-1500  $\text{cm}^{-1}$  shows several overlapped bands, but by enlarging the spectrum, some characteristic bands of native starch can be identified. The band at 1340  $\text{cm}^{-1}$  is associated with  $\text{CH}_2$  twisting and C-O-H bending, whilst the one at 1360  $\text{cm}^{-1}$  is assigned to the  $\text{CH}_2$  scissoring and C-H and C-O-H deformation.<sup>304, 308</sup> The bands at 1415 and 1456  $\text{cm}^{-1}$  are attributed to CH and  $\text{CH}_3$  bending respectively.<sup>307</sup> The band at 1647  $\text{cm}^{-1}$  is related to the tightly bound water present in starch.<sup>309</sup> The asymmetric and symmetric stretching of C-H is observed at 2929  $\text{cm}^{-1}$ .<sup>307</sup> The characteristic band of O-H stretching of starch and water is noted in the region of 3000 - 3500  $\text{cm}^{-1}$  with the band centred at 3323  $\text{cm}^{-1}$ .

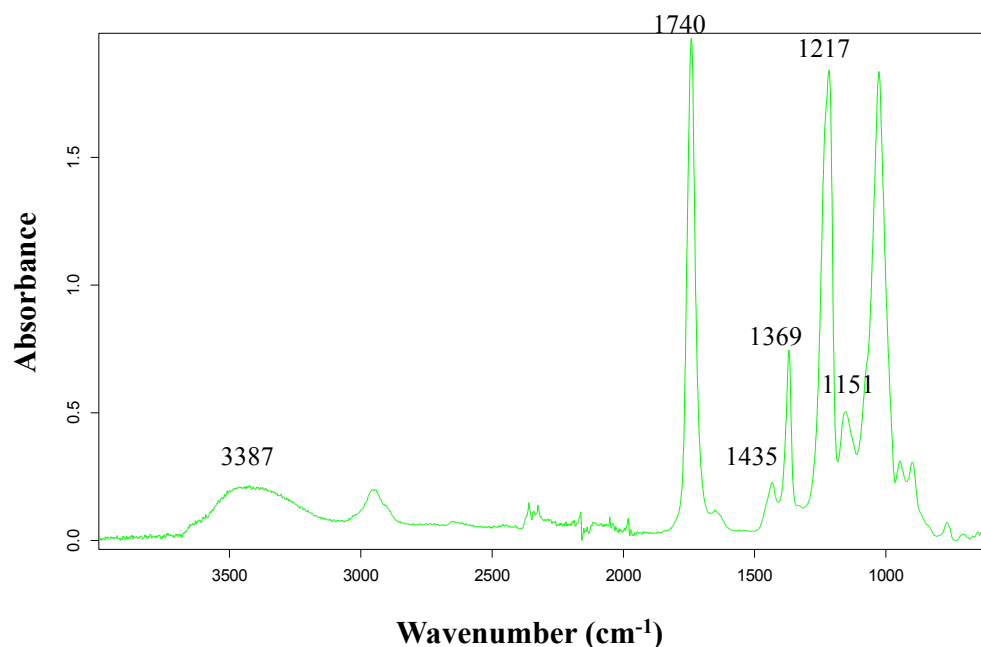
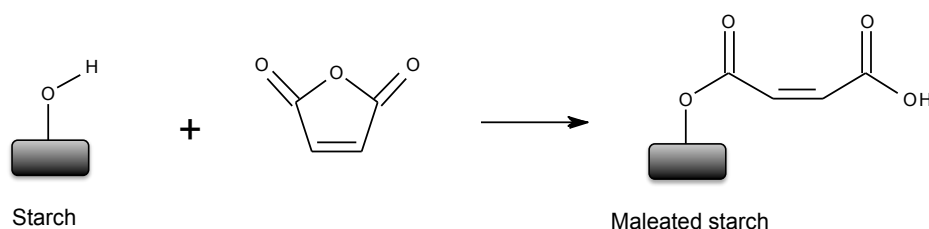


**Figure 5.6 – Infrared spectrum of acetylated starch**

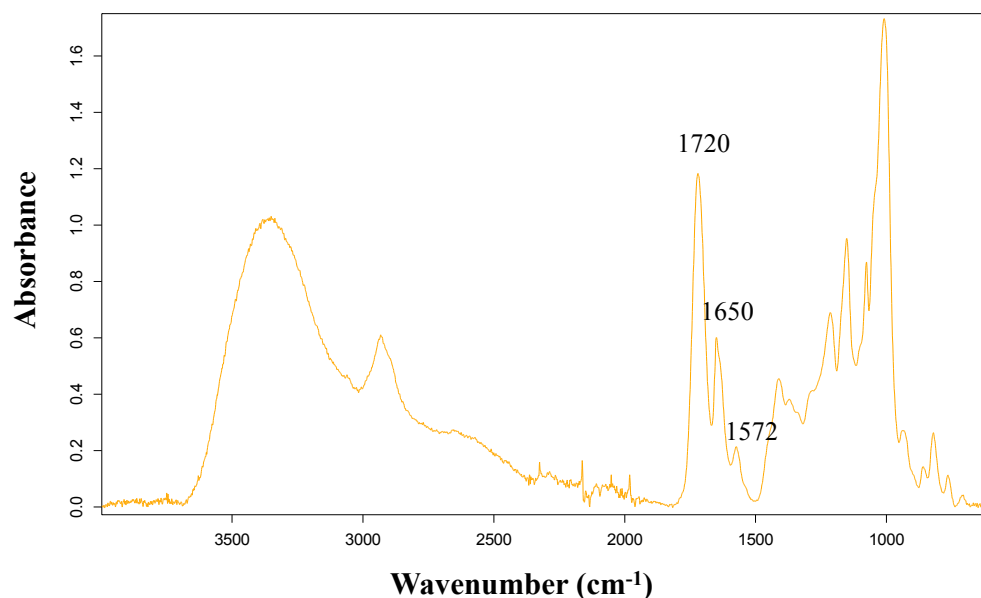
After acetylation, new strong absorption bands are noted at 1217 and 1740  $\text{cm}^{-1}$ , corresponding to the vibration of C-O and C=O of the acetyl group (*Figure 5.6*).<sup>310</sup> Other changes includes the significant decrease in intensity of the O-H band, which also

shifts to  $3387\text{ cm}^{-1}$ , indicating the modification of the O-H in starch molecules which results in less hydroxyl available for hydrogen bonding. The intensity reduction of the band at  $1647\text{ cm}^{-1}$ , which is associated to tightly bound water, is noted, suggesting that less water can be bound to starch chains when acetylation has been achieved to the starch. Also, the bands at  $1077$  and  $1151\text{ cm}^{-1}$  decrease the intensity. As previously stated, these bands are related to the stretching and bending of C-OH in the unmodified expanded starch. The well resolved bands at  $1369$  and  $1435\text{ cm}^{-1}$ , which correspond to asymmetric and symmetric deformation of  $\text{CH}_3$  respectively, are observed.<sup>311</sup> Moreover, the spectrum of acetylated starch shows no bands relating to the residue of acetic anhydride, whose characteristic bands are noted at  $1850$  and  $1750\text{ cm}^{-1}$  (*Appendix A – Figure A.5.1*) or acetic acid by product, which has a characteristic band at  $1700\text{ cm}^{-1}$  (*Appendix A – Figure A.5.2*).

Maleic anhydride treatment of starch is conducted using the same procedure as acetylation but the acetic anhydride is replaced with maleic anhydride (*Figure 5.7*). The spectrum of maleated starch is demonstrated in *Figure 5.8* and the characteristic bands are observed at  $1720\text{ cm}^{-1}$ , corresponding to the carbonyl ester.<sup>128</sup> Novel bands at  $1572$  and  $1650\text{ cm}^{-1}$  are assigned to the C=C from the maleate moiety with the latter arising from the stretching of the double bond overlapping with vibration of tightly bound water.<sup>312</sup> The absence of the anhydride characteristic bands at  $1774$  and  $1855\text{ cm}^{-1}$  suggests that the maleic anhydride ring was opened and reacted during the modification (*Appendix A – Figure A.5.3*).<sup>312, 313</sup> A noticeable decrease of the O-H band intensity is also observed in this case, suggesting the replacement of hydroxyl groups of starch with maleate group.



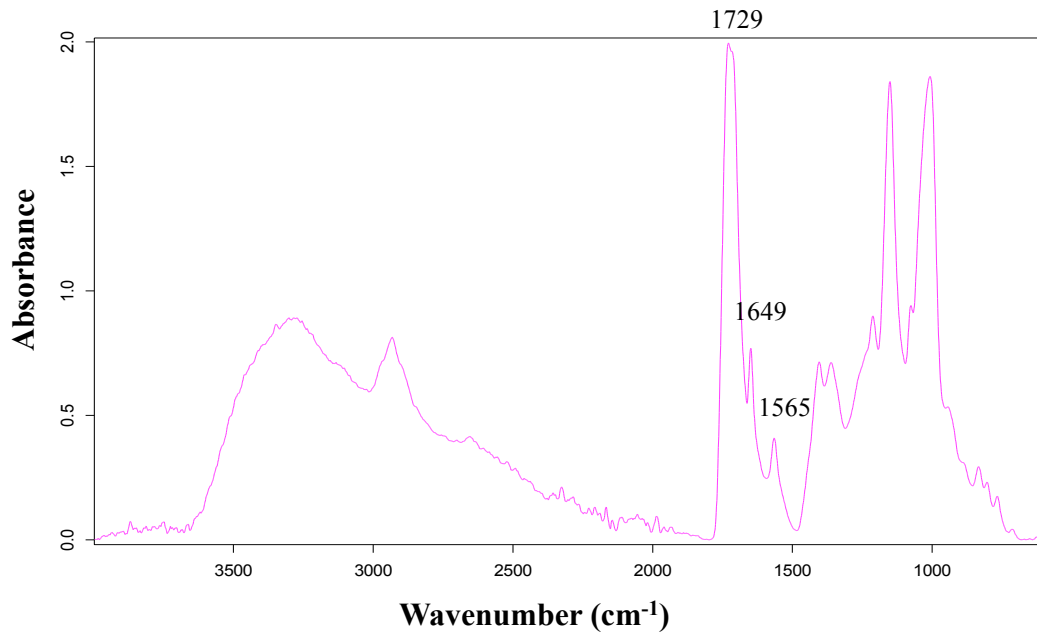
**Figure 5.7 – Reaction of maleic anhydride and starch**



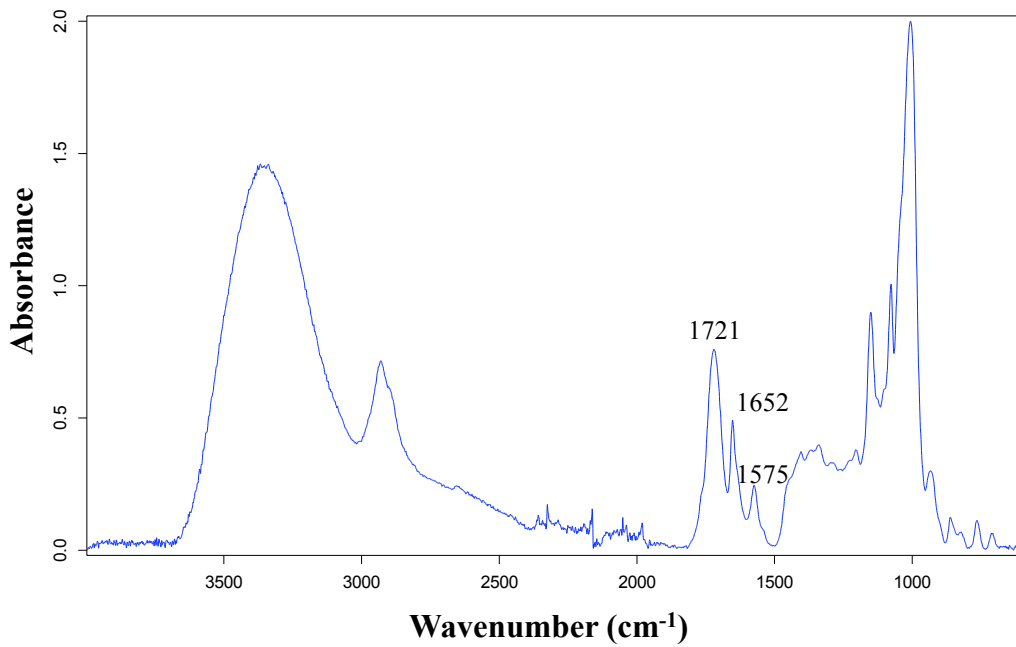
**Figure 5.8 – Infrared spectrum of maleated starch**

Compared to unmodified starch, succinic anhydride modified starch shows a new band at  $1729\text{ cm}^{-1}$ , which is attributed to the ester carbonyl, suggesting the formation of succinylated starch (Figure 5.9).<sup>314</sup> In general, the ester carbonyl band is observed at  $1750\text{ cm}^{-1}$  and the acid carbonyl band locates at  $1712\text{ cm}^{-1}$ , but in this case the two bands strongly overlap, resulting in the centred band at  $1729\text{ cm}^{-1}$ .<sup>315</sup> The band  $1565\text{ cm}^{-1}$  is probably related to intermediate carboxylate anions and the one at  $1649\text{ cm}^{-1}$  corresponds to tightly bound water in starch granules.<sup>316, 317</sup> The disappearance of the anhydride characteristic bands at  $1778$  and  $1860\text{ cm}^{-1}$  also confirms the modification of starch with succinic anhydride (Appendix A – Figure A.5.4).

Regarding the itaconic anhydride modified starch; the carbonyl ester band is noted at  $1721\text{ cm}^{-1}$ , indicating the modification has taken place (Figure 5.10). The carbonyl absorption bands of the anhydride at  $1764$  and  $1843\text{ cm}^{-1}$  are absent in the modified starch spectrum (Appendix A – Figure A.5.5) Similar features of the previous spectra including the bands at  $1575$  and  $1652\text{ cm}^{-1}$  and the decrease in intensity of the O-H absorption band are also observed in this case.



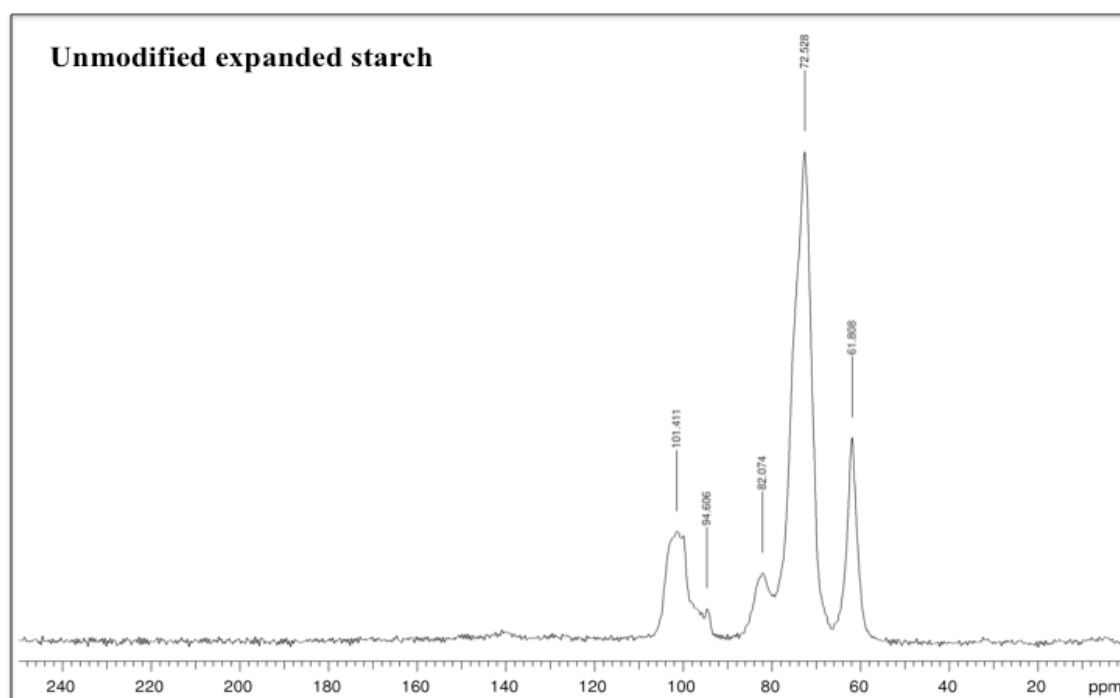
**Figure 5.9 – Infrared spectrum of succinic anhydride modified starch**

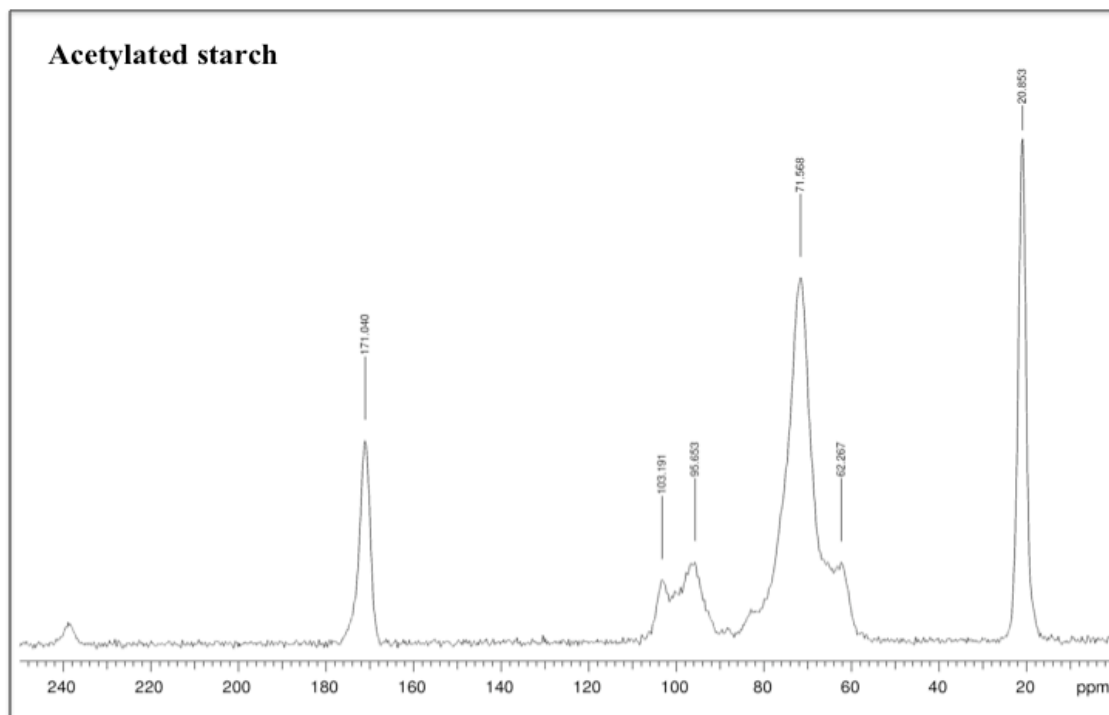


**Figure 5.10 – Infrared spectrum of itaconic anhydride modified starch**

### 5.3.3 $^{13}\text{C}$ cross polarisation (CP) magic angle spinning (MAS) solid state nuclear magnetic resonance

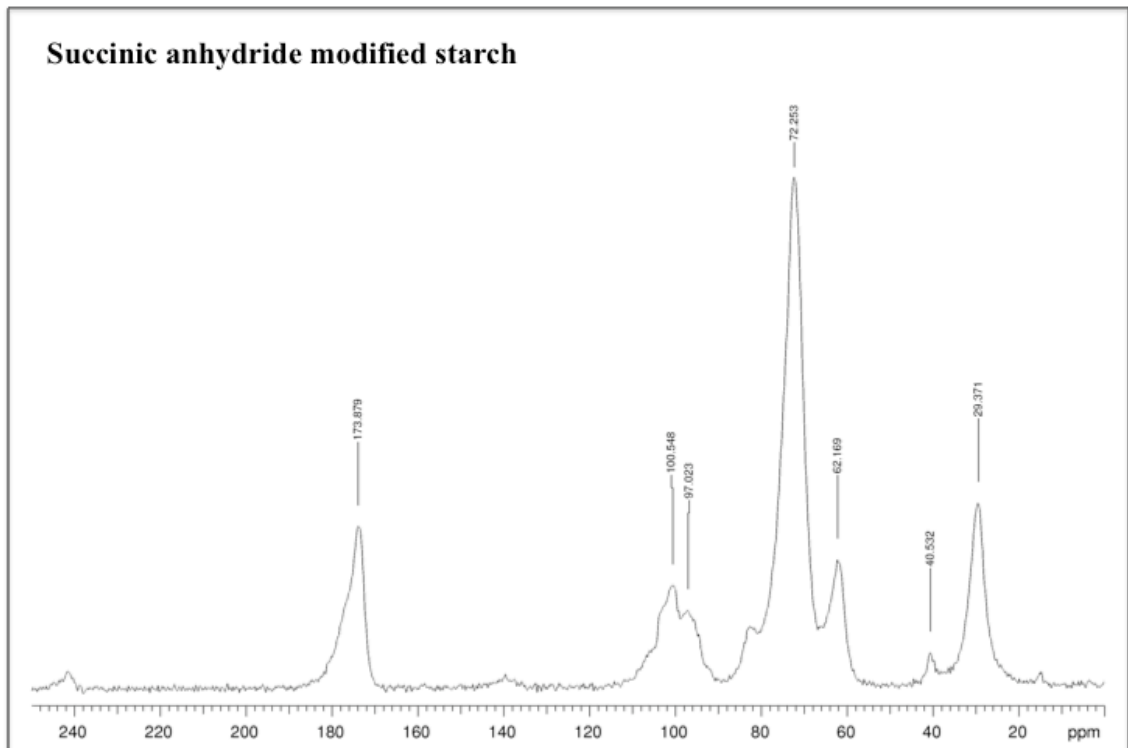
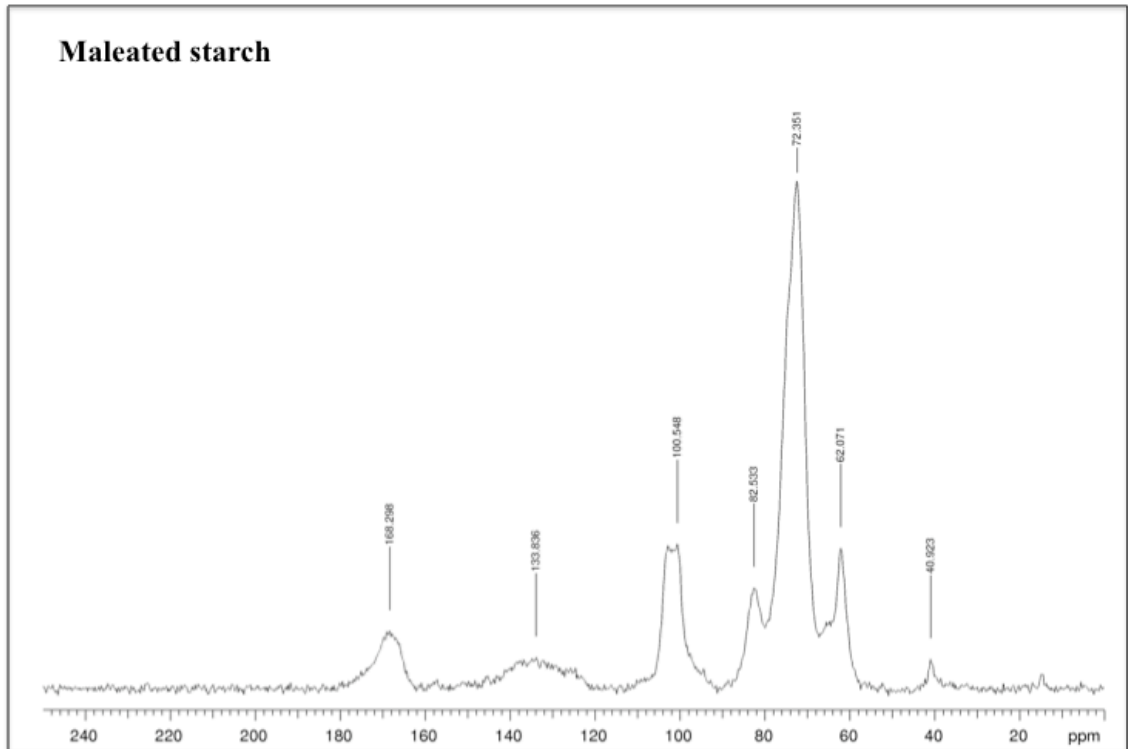
The CP MAS  $^{13}\text{C}$  NMR spectra of unmodified expanded starch and acetylated starch are demonstrated in *Figure 5.11*. The spectra were acquired by Dr David Apperley of solid-state NMR service at the University of Durham. The signals between 106-92 ppm correspond to the resonance arising from C-1 of the anhydroglucose units. The peak at 82 ppm is attributed to the non-crystalline components of C-4. The large peak between 73-70 is assigned to C-2, C-3 and C-5 and the signal at 62 ppm is associated to the hydroxymethyl C-6 starch. The spectrum of the acetylated starch shows the characteristic peaks of the acetyl group at 171 and 21 ppm, corresponding to the carbonyl group and methyl group of the esterified starch respectively.<sup>318</sup> In addition, a decrease in intensity of C-6 peak at 62 ppm is notable, suggesting the acetylation might have occurred at this position of the anhydroglucose.<sup>319</sup> The signal of C-2, C-3 between 73-70 ppm also modestly decreases the intensity, although less obvious than the C-6 signal, implying the modification preferably takes place at the C-6 position. These results are in good agreement with ATR-FTIR data and as such confirm the acetylation of starch by acetic anhydride.





**Figure 5.11 –  $^{13}\text{C}$  CP MAS NMR of unmodified expanded starch and acetylated expanded starch**

Regarding the maleated starch spectrum, characteristic peaks of the carbonyl group are observed at 168.3 ppm (*Figure 5.12*). The signal at 133.8 ppm is assigned to the alkene group. The succinic anhydride modified starch spectrum shows the carbonyl signal at 173.9 ppm and the signal at 29.4 ppm is attributed to  $\text{CH}_2$  carbon. A decrease in intensity of the C-6 signal at 62 ppm is noted in both spectra of maleic and succinic anhydride modified starches, whilst the change in intensity of the large signal of C-2 and C-3 is unnoticeable. This confirms that C-6 is the most reactive position for esterification due to the low steric hindrance.<sup>295</sup> This result is also in good agreement with ATR-FTIR data indicating that the modification was successful. In regard to the spectrum of itaconic anhydride modified starch, a broad signal at 135.2 ppm, which is ascribed to the alkene carbon, is observed. The carbonyl signal at 172.9 ppm is clearly lower in intensity compared to the other two starches, suggesting lower degree of substitution in this starch ester, although it is recognised that these NMR peaks cannot be used to precisely quantify the degree of esterification.



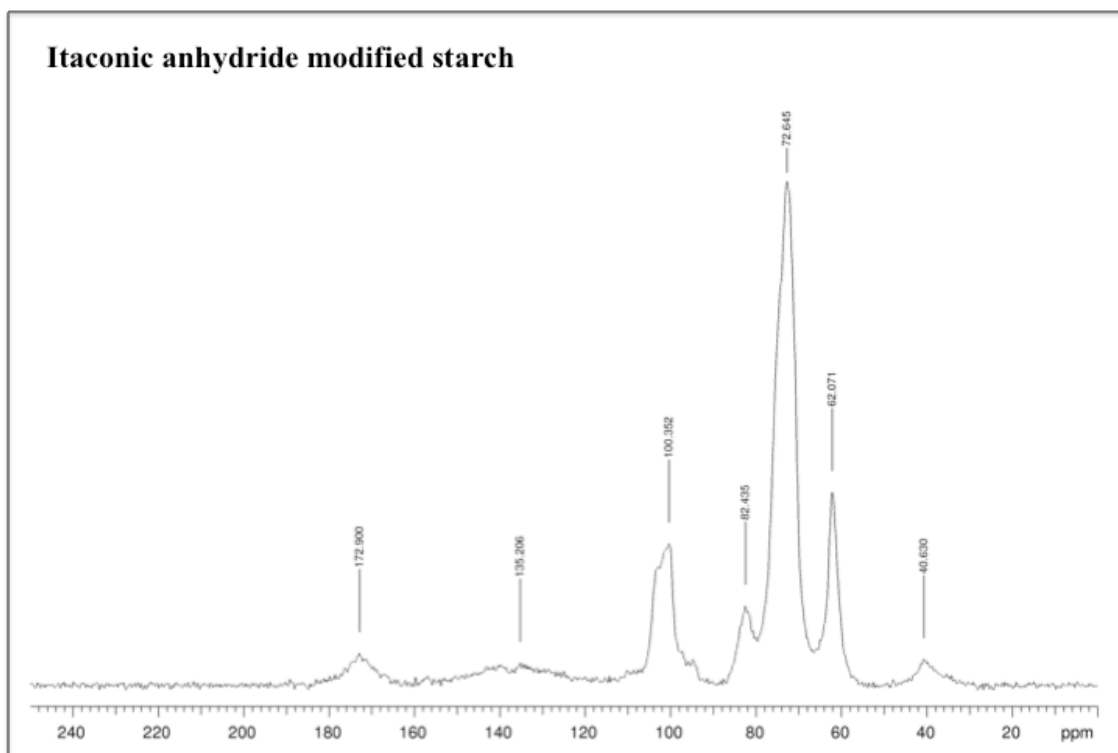


**Figure 5.12 –  $^{13}\text{C}$  CP MAS NMR of maleated starch, succinic anhydride modified starch and itaconic anhydride modified starch**

### 5.3.4 Determination of degree of substitution

The hydrophobic characteristic of modified starch are more pronounced at higher degrees of substitution, which should improve the miscibility of the starch with the polymer matrix.<sup>130</sup> Also, in the case of maleic, succinic and itaconic anhydride modified starches, a number of carboxylic acid end groups is advantageous as this might lead to reaction of the modified starch with ELO and enhance the mechanical properties of the resin. As such the molar ratio of starch to anhydride used was 1:3 in attempt to achieve the highest theoretical degree of substitution of 3. The degree of substitution (DS) of acetylated starch was determined by titration according to the standard procedure of Wurzburg described in section 7.5.2.<sup>320</sup> The DS was calculated according to the following *equation 5.1*.



$$DS = \frac{(162 \times \text{Acetyl}\%)}{(4300 - [42 \times \text{Acetyl}\%])}$$

**Equation 5.1**

Where 162 is the molecular weight of glucose unit, 4300 is the molecular weight of acetyl group multiplied by 100 and 42 is the actual molecular weight increase per acetyl group added starch. The acetyl% is calculated according to the *equation 5.2*.

$$\text{Acetyl}\% = \frac{[\text{Blank}(\text{cm}^3) - \text{Sample}(\text{cm}^3)] \times \text{Molarity of HCl} \times 0.043 \times 100}{\text{Sample weight}(g)}$$

**Equation 5.2**

Where *Blank* and *Sample* are the volume of HCl used to titrate unmodified starch and acetylated starch respectively. The value 0.043 is the molecular weight of the acetyl group in 1 cm<sup>3</sup>.

The DS of other esterified starches was determined using the same method with modification of the molecular weight of the ester group added.<sup>321, 322</sup> The following equations were used for each esterified starches.

Maleated starch:

$$DS = \frac{(162 \times M\%)}{2(9800 - [98 \times M\%])}$$

**Equation 5.3**

$$M\% = \frac{[\text{Blank}(\text{cm}^3) - \text{Sample}(\text{cm}^3)] \times \text{Molarity of HCl} \times 0.098 \times 100}{\text{Sample weight}(g)}$$

**Equation 5.4**

Succinic anhydride modified starch:

$$DS = \frac{(162 \times S\%)}{2(10000 - [100 \times S\%])}$$

**Equation 5.5**

$$S\% = \frac{[Blank(cm^3) - Sample(cm^3)] \times \text{Molarity of HCl} \times 0.1 \times 100}{\text{Sample weight}(g)}$$

**Equation 5.6**

Itaconic anhydride modified starch:

$$DS = \frac{162 \times I\%}{2(11200 - [112 \times I\%])}$$

**Equation 5.7**

$$I\% = \frac{[Blank(cm^3) - Sample(cm^3)] \times \text{Molarity of HCl} \times 0.112 \times 100}{\text{Sample weight}(g)}$$

**Equation 5.8**

The degree of substitution of esterified starches obtained from titration is shown in *Table 5.1*.

**Table 5.1 – Degree of substitution of esterified starches**

Modified starch	Degree of substitution
Acetylated starch	2.62
Maleated starch	0.86
Succinic anhydride modified starch	1.12
Itaconic anhydride modified starch	0.64

The highest DS is obtained from the reaction with acetic anhydride, owing to not only its liquid state, which allows good miscibility in the reaction slurry, but also the good accessibility of the carbonyl, which facilitate the addition of the nucleophile in the first step of the substitution reaction (*Figure 5.2*). Although both steps of the nucleophilic acyl substitution (addition of nucleophile and elimination of a leaving group) can influence the overall rate of reaction, the addition of nucleophile is the rate-limiting step. Therefore, the reactivity of the carbonyl substantially affects the reaction.<sup>28</sup> Comparing the cyclic anhydrides, the carbonyl of succinic anhydride is electronically the most reactive due to the absence of the double bond in its structure. Thus, the reaction of succinic anhydride yields the products with higher DS than the other cyclic anhydrides. The unusually low DS of itaconic anhydride modified starch is attributed to poor solubility of the anhydride in toluene.

### 5.3.5 Thermal characterisation

Thermogravimetric analysis (TGA) of unmodified and esterified starches was conducted using Stanton Redcroft STA 625 (TG/DSC). Samples were heated from 25 °C to 500 °C at 10 °C/min under an inert atmosphere. Esterification considerably affects the decomposition of starch. Unmodified starch shows two major mass losses where the first one starts almost immediately after heating begins and finishes at around 100 °C. This is mainly attributed to the evaporation of water present in starch material. Acetylated starch shows no weight loss at this region, indicating that very little moisture is present in the modified starch, owing to its increased hydrophobicity. The second

weight loss in unmodified starch, which corresponds to the decomposition of the material, starts at approximately 260 °C. The decomposition of acetylated starch commences comparatively at higher temperatures (over 300 °C), indicating better thermal stability of acetylated starch compared to native starch (*Figure 5.13*).

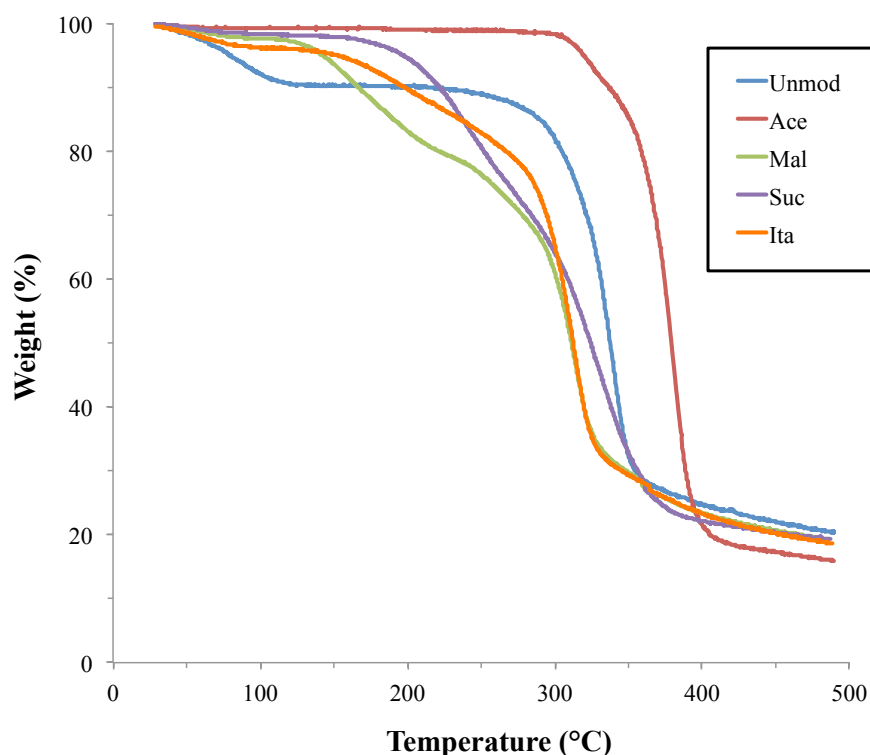


**Figure 5.13 – TGA thermograms of unmodified expanded starch and esterified starches (Originally in colour)**

Similar observation was made by Zhang *et al.*, however, they found that good thermal stability can only be achieved at high DS as starch with lower degree of acetylation (0.09, 0.50 and 1.51) start to decompose at lower temperature than that of unmodified starch.<sup>323</sup> Maleic, succinic and itaconic anhydride modified starches thermograms also show lower water loss than that of unmodified starch ( $\leq 5\%$ ), demonstrating that they become more hydrophobic after the modification. These cyclic anhydride modified starches undergo two stages of decomposition. Their initial decomposition temperatures are lower than that of native starch (260 °C). Maleated starch major weight loss starts at around 110 °C, whilst succinic and itaconic anhydride modified starches start to decompose around 160 °C and 130 °C respectively. This first step of decomposition gradually causes weight loss up to about 260 °C, then the rapid second weight loss

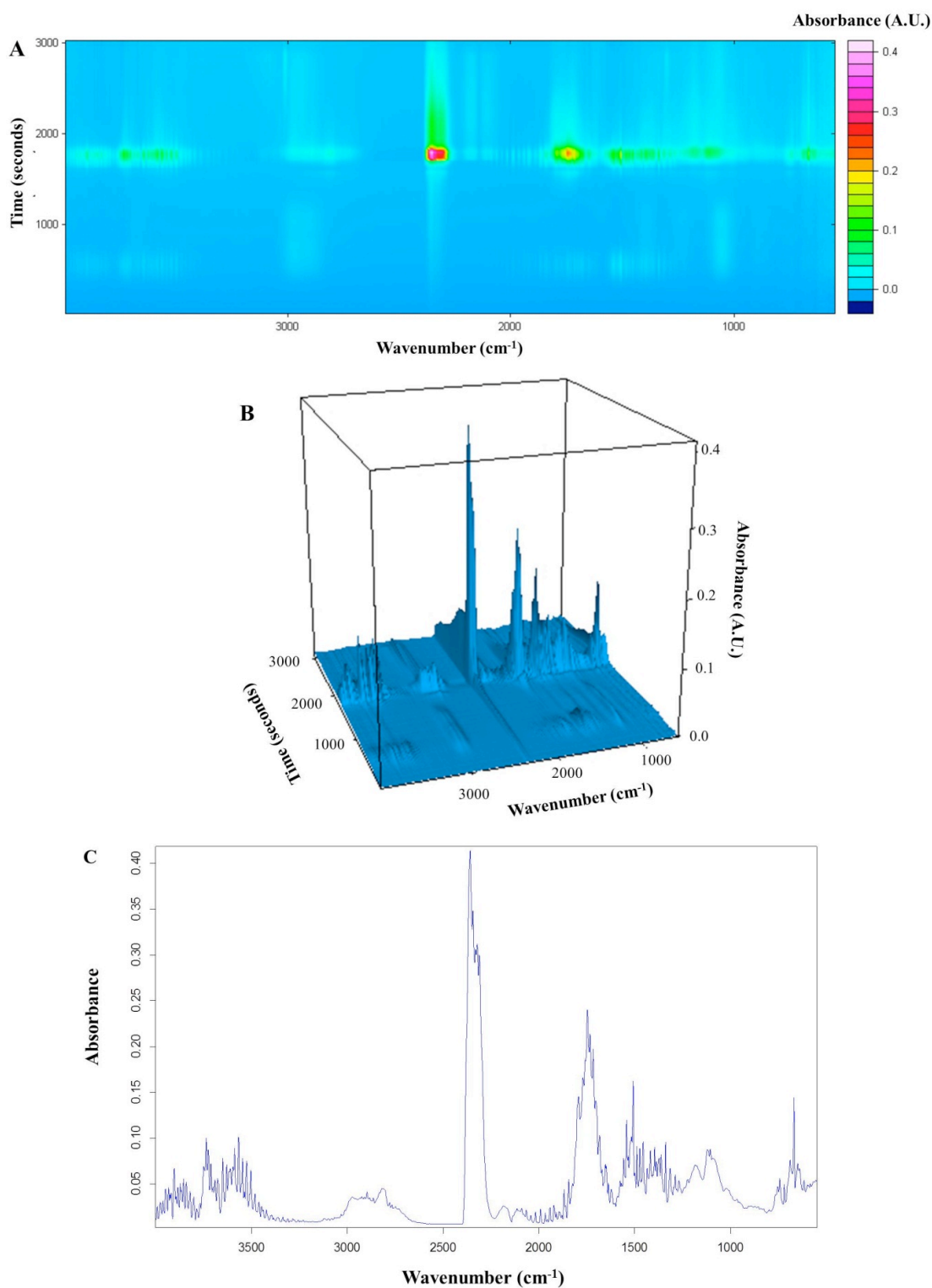
occurs between 260-400 °C. The decrease in thermal stability of these modified starches is attributed to the disintegration of intramolecular interactions such as hydrogen bonding in the starch chains and the poor thermal stability of carboxylic group introduced onto the polymer after the esterification.<sup>324, 325</sup> Approximately 20% wt. of starch residue is obtained after heating to 500 °C. The temperature at which 50% of weight loss occurs and the decomposition temperature determined by DTG are summarised in *Table 5.2*.

**Table 5.2 – Thermal characteristics of unmodified expanded starch and esterified starches**

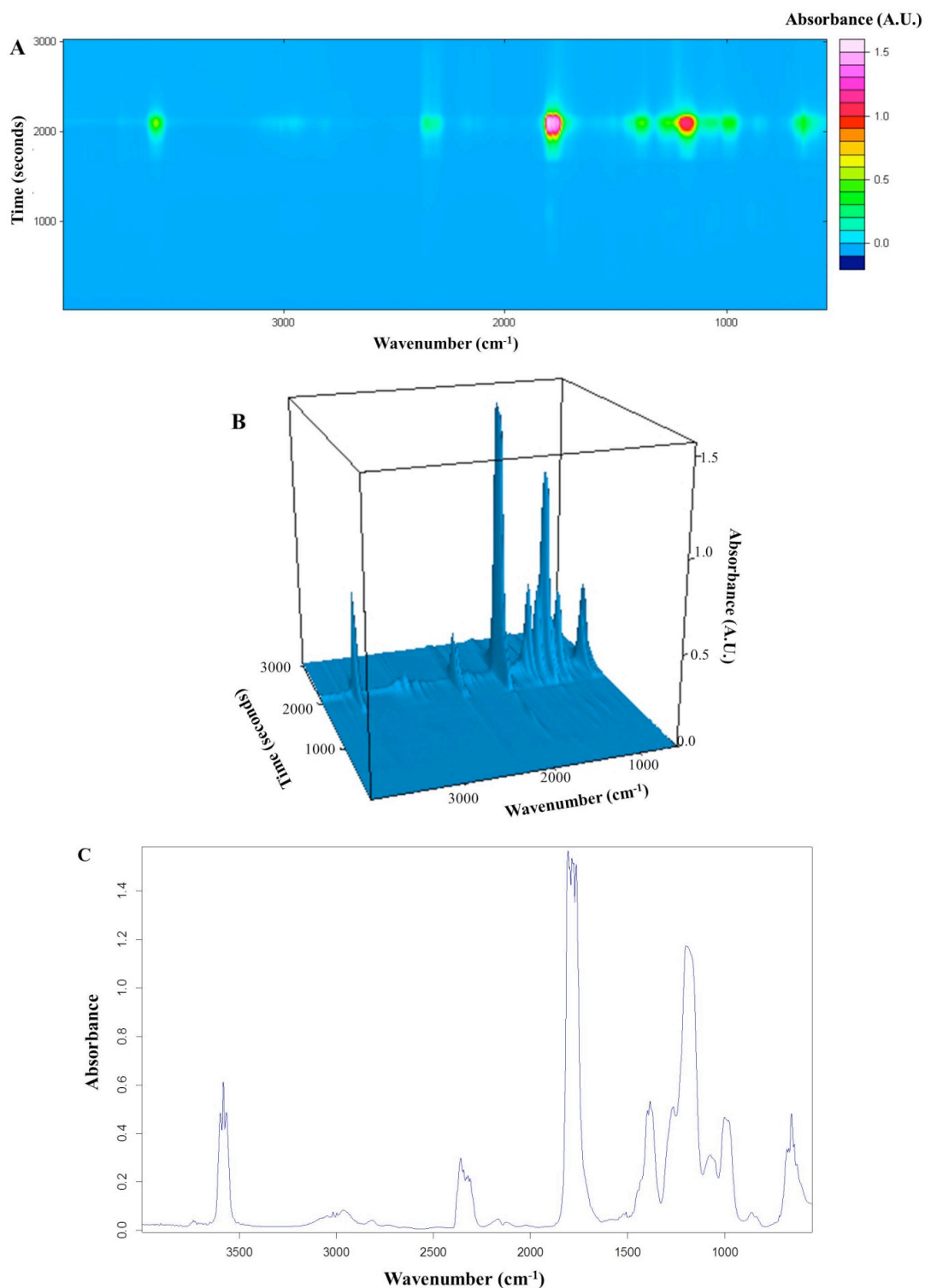
Starch type	50 % Weight loss temperature (°C)	Decomposition temperature (°C) (DTG peak)
Unmod	337	323.0
Ace	379	323.7, 381.9
Mal	310	153.2, 312.1
Suc	323	245.1, 324.5
Ita	312	200.0, 313.0

### 5.3.6 Thermogravimetric - Fourier transform infrared spectroscopy (TG-FTIR)

Thermogravimetric-infrared spectroscopy (TG-FTIR) was performed in order to study the composition of the volatiles produced during the decomposition process of native and modified starches. The surface plots of unmodified starch (*Figure 5.14 A*) and that of acetylated starch (*Figure 5.15 A*) show one main thermal event where the gas release is at its maximum, corresponding to the greatest rate of decomposition.

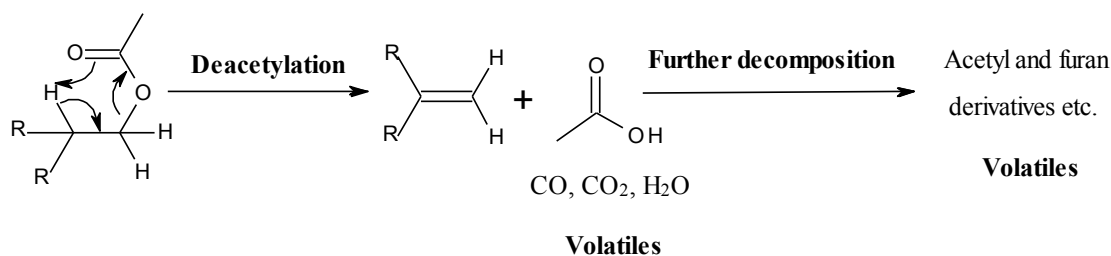


**Figure 5.14 – A) surface plot of volatiles released during decomposition of unmodified starch, B) 3D plot of IR spectra obtained during TG-FTIR experiment, C) IR spectrum taken at the maximum rate of decomposition (Originally in colour)**



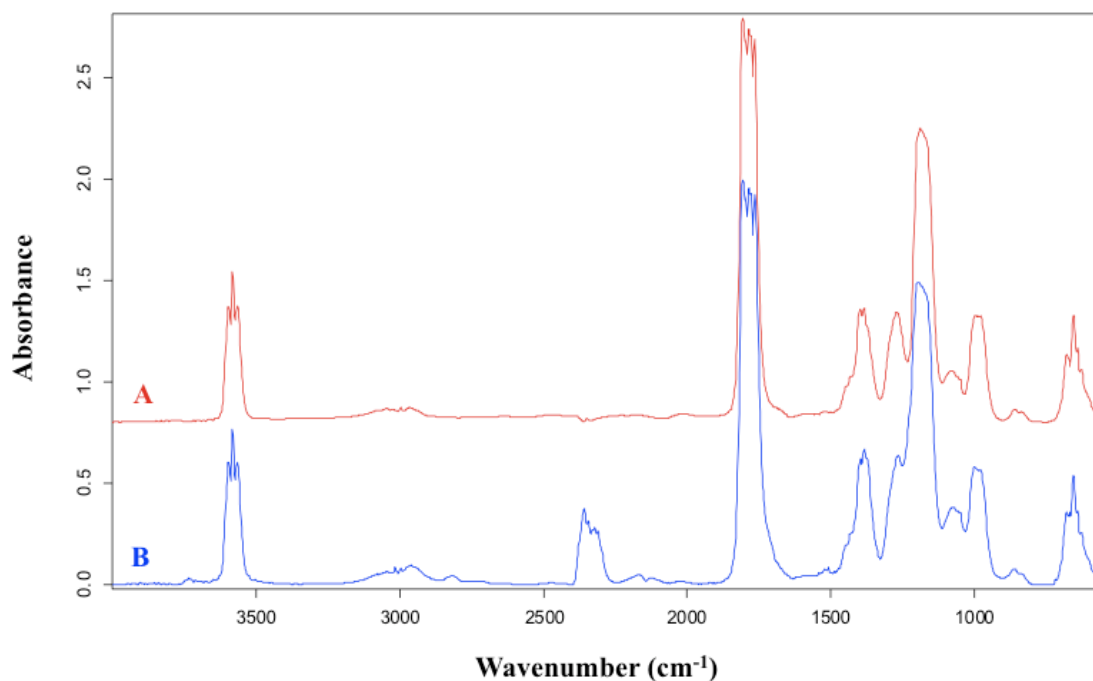
**Figure 5.15 – A) surface plot of volatiles released during decomposition of acetylated starch, B) 3D plot of IR spectra obtained during TG-FTIR experiment, C) IR spectrum taken at the maximum rate of decomposition (Originally in colour)**

The unmodified starch exhibits its main decomposition at 1790 seconds or at the temperature of 323 °C (calculation described in section 7.5.4). Acetylated starch decomposition occurs later at 2093 seconds or at 374 °C. These results are in agreement with the TGA data obtained in section 5.3.5. The gas products obtained from the decomposition of native starch are low molecular weight compounds, such as CO<sub>2</sub> and CO, which show their characteristic bands at 2359 cm<sup>-1</sup> and 2164 cm<sup>-1</sup> respectively (Figure 5.14 C). The band at 1746 cm<sup>-1</sup> is related to carbonyl compounds and the bands between 3400-3800 cm<sup>-1</sup> are associated with the stretching of O-H. This is in good agreement with previous results.<sup>326, 327</sup> Figure 5.15 C displays the IR spectrum of acetylated starch at the highest concentration of the volatiles (374 °C), which shows a large band at 1806 cm<sup>-1</sup>. This band is attributed to the carbonyl stretching of the acetic acid, produced during the thermal decomposition.<sup>328</sup> The mechanism of decomposition of cellulose acetate was proposed by Gaan *et al.*, which reported that the first step of the decomposition involves deacetylation of cellulose acetate to release CO<sub>2</sub>, acetic acid and some water (Figure 5.16). Further decomposition of the residue of the material yields several furan and acetyl derivatives, however, these are too complex to detect by FTIR.<sup>328</sup> The same phenomenon is likely to occur in acetylated starch as the TG-FTIR results from both materials demonstrate a great similarity. In order to ascertain this postulation, a TG-FTIR of pure acetic acid was performed. The characteristic bands of gaseous acetic acid match those of evolved gas obtained from the acetylated starch sample (Figure 5.17). This confirms that the carbonyl band at 1806 cm<sup>-1</sup> observed during the decomposition of acetylated starch corresponds to that of gaseous acetic acid.



**Figure 5.16 – Proposed mechanism of decomposition of cellulose acetate (adapted from reference 328)**

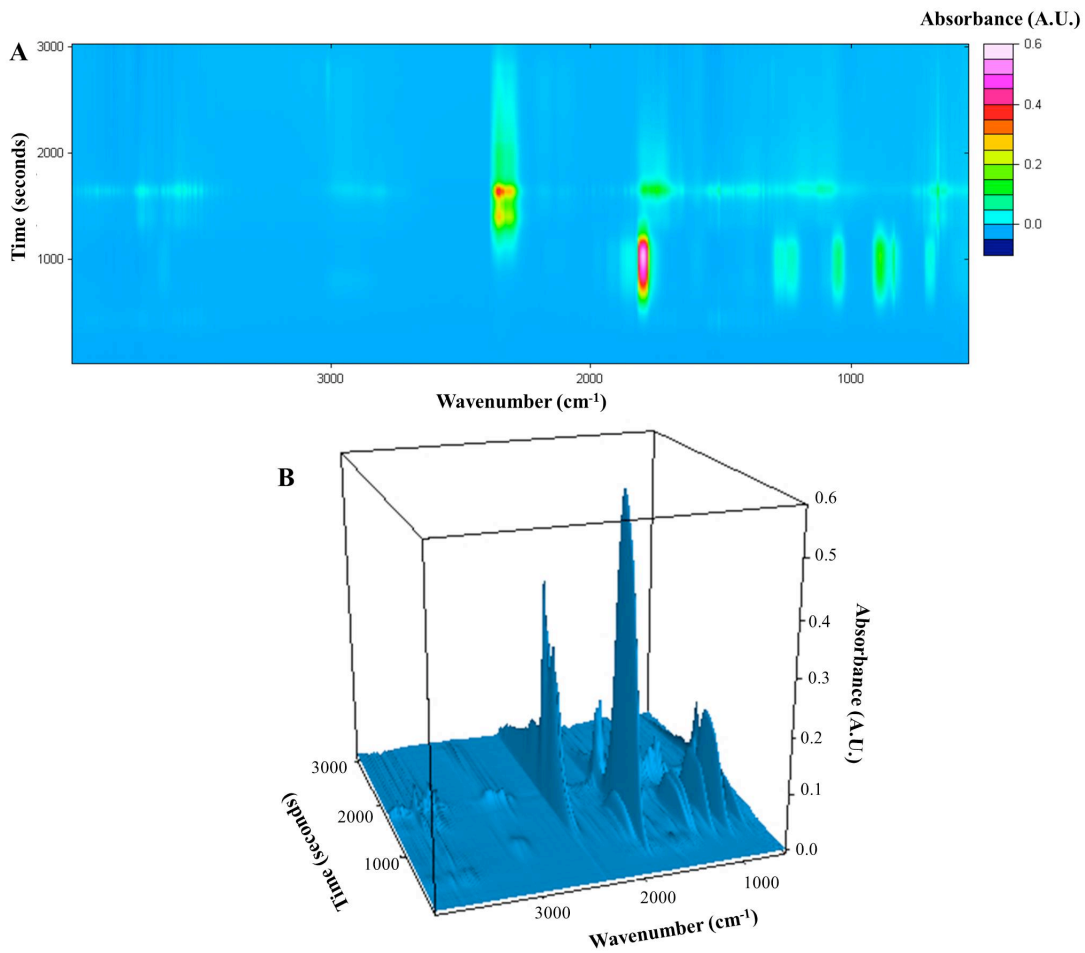


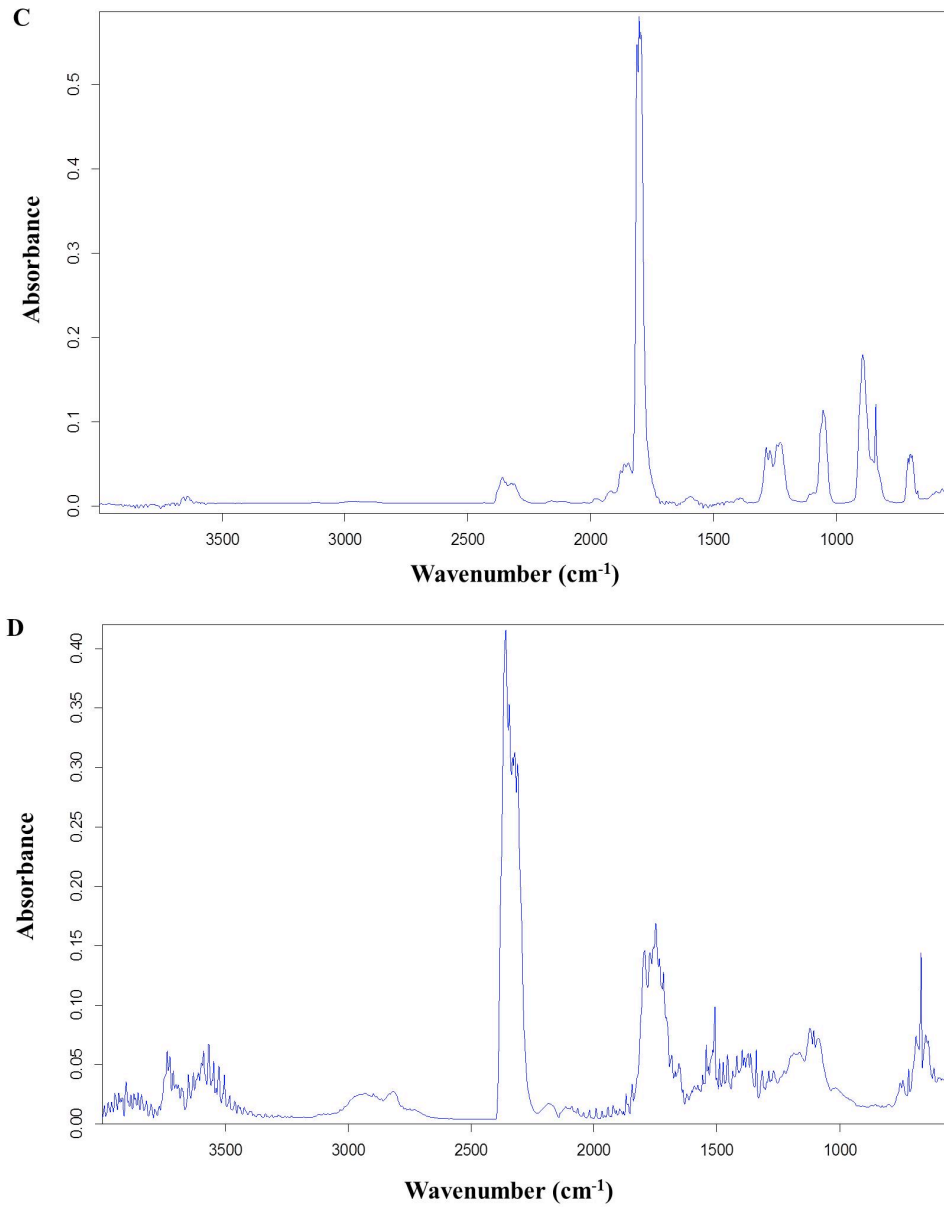


**Figure 5.17 – IR spectra of evolved gases from TG-FTIR analysis of A) acetic acid and B) acetylated starch (Originally in colour)**

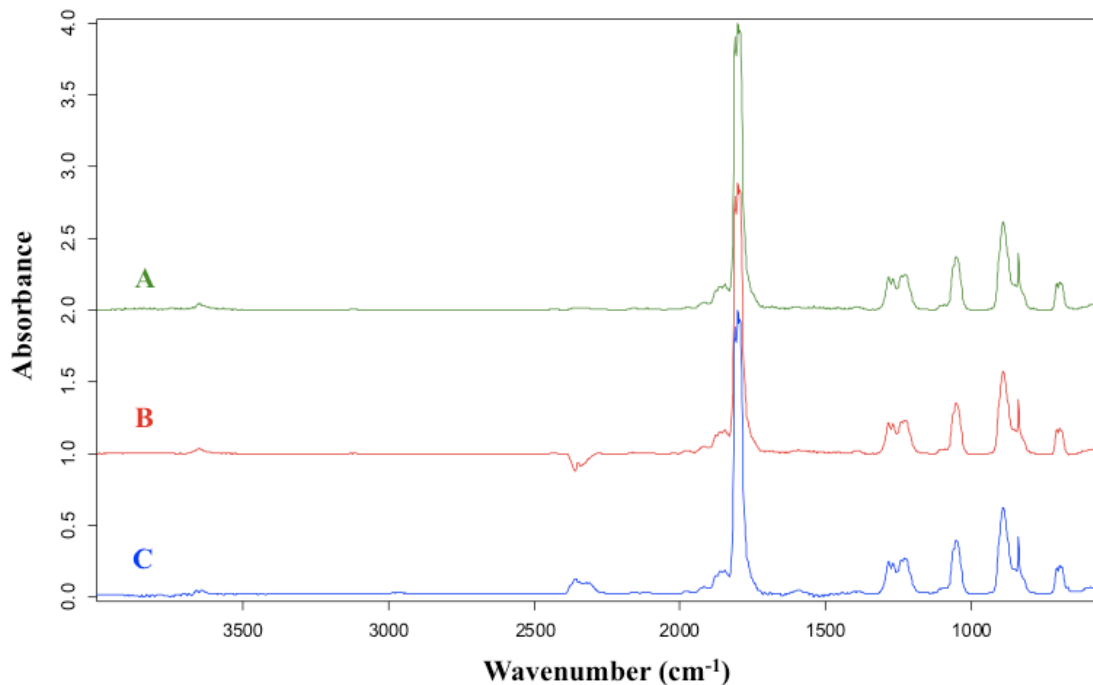
In contrast to the unmodified and acetylated starches, the surface plot of maleated starch demonstrates two major events, corresponding to the two phases of decomposition of the material that was also detected in section 5.3.5 (*Figure 5.18*). The first gas release starts at 460 seconds after the heating commences (101 °C) and reaches its maximum at 1003 seconds (192 °C). The IR spectrum of the former is displayed in *Figure 5.18 C*. A large band at 1810 cm<sup>-1</sup> and a small band at 1592 cm<sup>-1</sup> are associated with C=O and C=C of the maleate groups respectively. It was speculated that the mechanism of decomposition of maleated starch is similar to that of acetylated starch. Therefore, a TG-FTIR of maleic acid, which was believed to be released during the decomposition of the modified starch, was conducted. The IR spectrum of evolved gas from the first stage of the decomposition of maleated starch is identical to that of maleic acid (*Figure 5.19 B-C*). However, it was reported that maleic acid decomposes before its boiling point to generate the anhydride through dehydration.<sup>329-331</sup> The IR spectrum of gaseous maleic anhydride, which is presented in *Figure 5.19 A*, shows similar characteristic bands to the spectra of released gas from the maleated starch and maleic acid. This suggests that the maleic acid, which is decomposed into the anhydride by heat, was

released during the first stage of decomposition of maleated starch. This could potentially occur through hydrolysis of the starch ester due to the moisture present in the starch. The second phase of the decomposition takes place at 1689 seconds (307 °C) (*Figure 5.18 D*) and the spectrum resembles the spectrum of unmodified starch, indicating that this corresponds to the decomposition of the starch backbone.



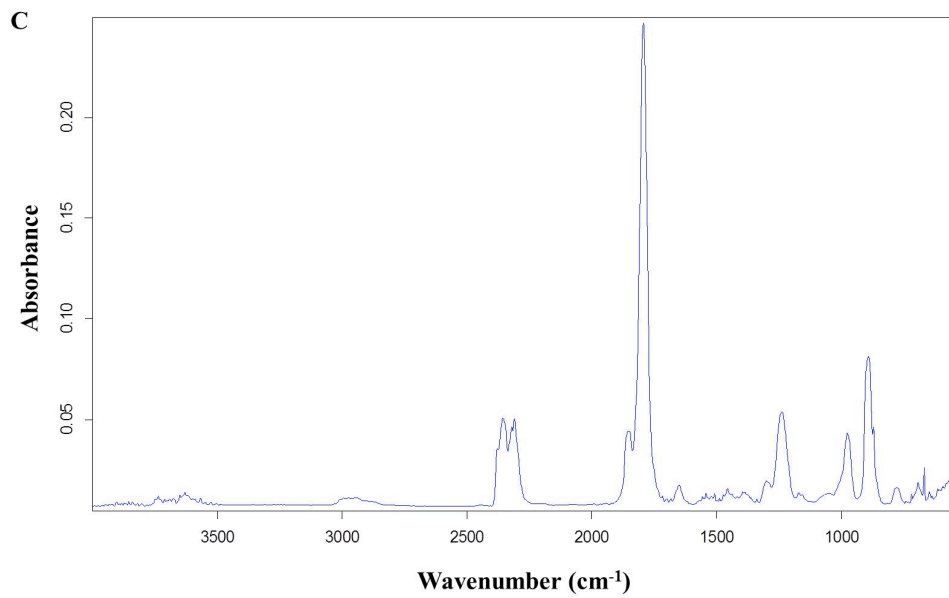
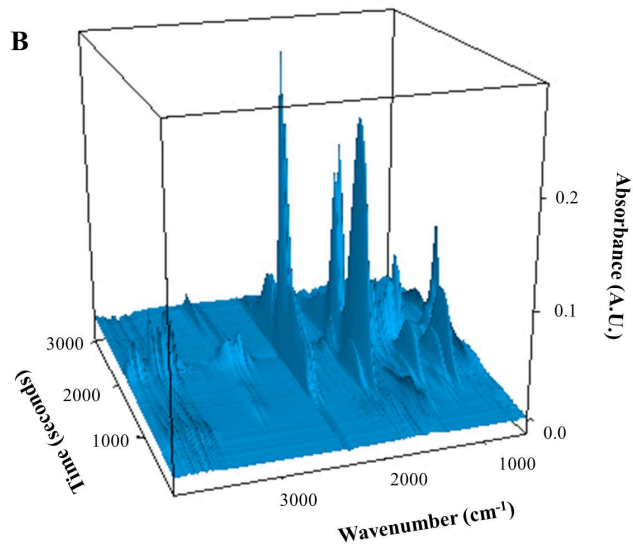
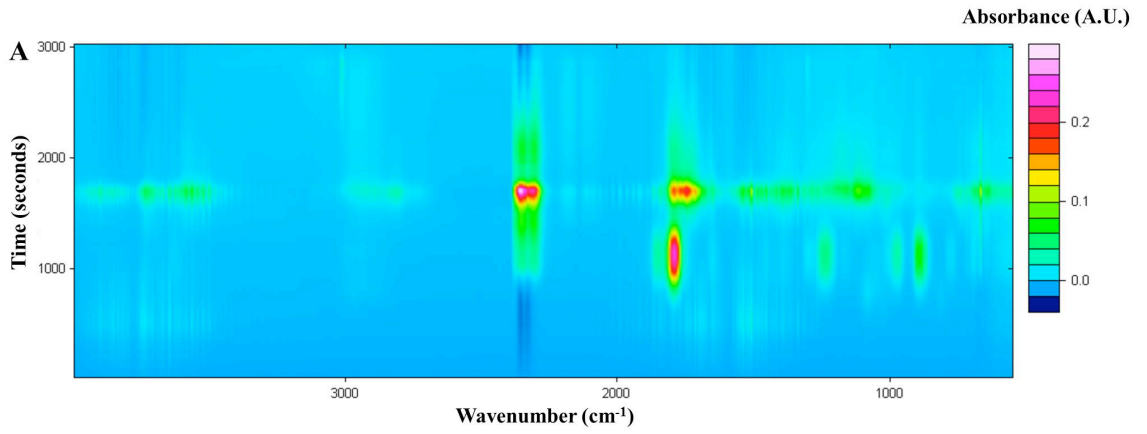


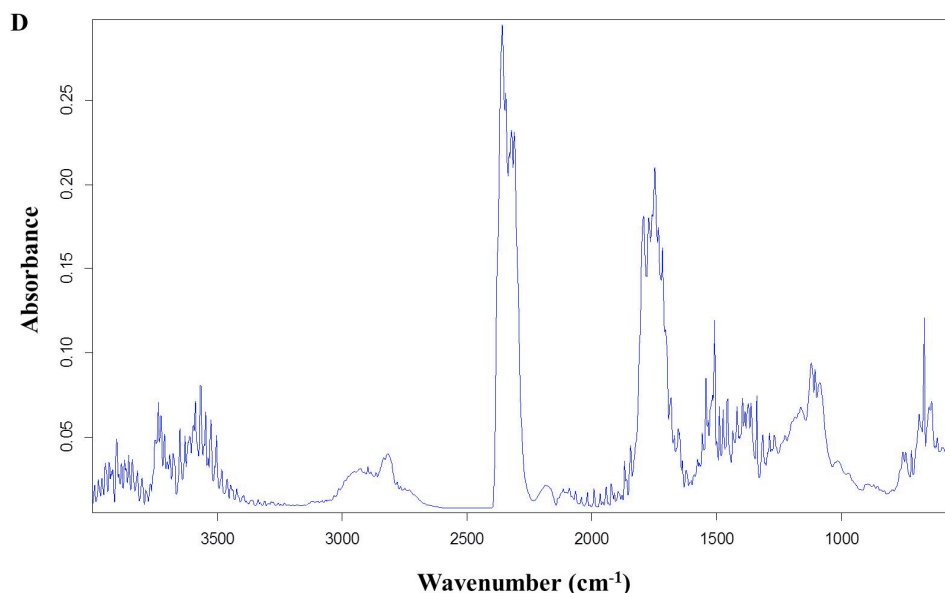
**Figure 5.18 – A) surface plot of volatiles released during decomposition of maleated starch, B) 3D plot of IR spectra obtained during TG-FTIR experiment, C) and D) IR spectra taken at the maximum rate of decomposition (Originally in colour)**



**Figure 5.19 – IR spectra of evolved gases from TG-FTIR analysis of A) maleic anhydride, B) maleic acid and C) maleated starch (Originally in colour)**

Itaconic anhydride modified starch also demonstrates two-phase decomposition process. The first gas evolution can be observed at 700 seconds into the heating (142 °C). The greatest concentration of the volatiles occurs at 1104 seconds (209 °C) and 1689 seconds (307 °C). The first spectrum (*Figure 5.20 C*) shows characteristic carbonyl bands at 1793 and 1849 cm<sup>-1</sup> associated with the itaconate modification. The IR spectrum of neat itaconic acid confirms that the acid was released from the modified starch during the first decomposition phase (*Appendix A – Figure A.5.6*). The second phase of the decomposition also corresponds to that of starch material (*Figure 5.20 D*).

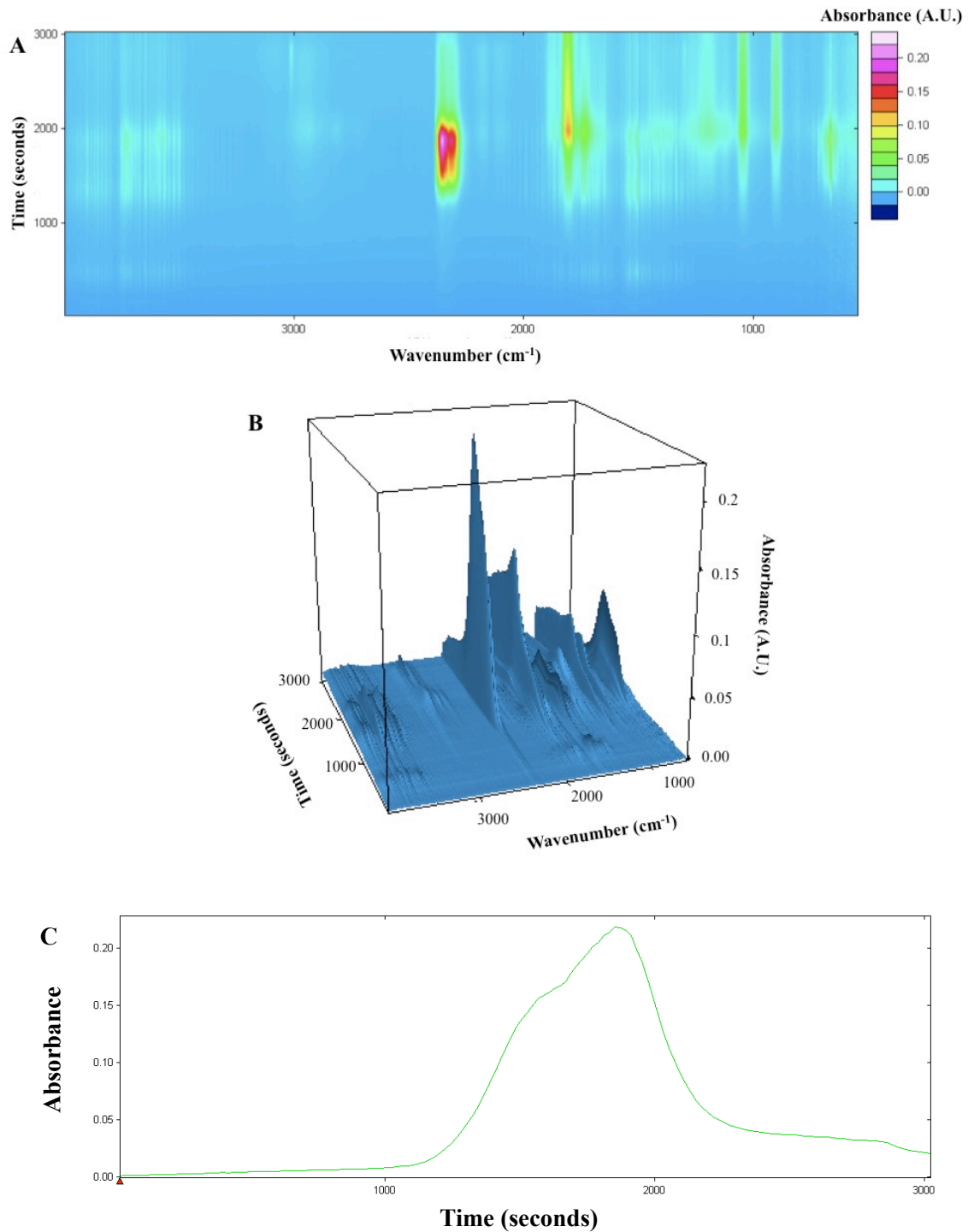




**Figure 5.20 – A) surface plot of volatiles released during decomposition of itaconic anhydride modified starch, B) 3D plot of IR spectra obtained during TG-FTIR experiment, C) and D) IR spectra taken at the maximum rate of decomposition (Originally in colour)**

According to the TGA results, succinic anhydride modified starch shows a two-step decomposition process. Although the two phases are difficult to evaluate on the surface plot as they occur at relatively close temperatures (*Figure 5.21 A*), these can be easily seen on the Gram-Schmidt trace (*Figure 5.21 C*). The gas evolution during the decomposition peaks at 1568 seconds (286.33 °C) and at 1851 seconds (333.5 °C). However, the two spectra are comparatively similar with the one at 333.5 °C demonstrates absorption bands with slightly greater intensity. This suggests that the maximum concentration of the volatiles of the two decomposition phases may overlap. Besides the characteristic bands of starch backbone, the carbonyl stretching is observed at 1810 cm<sup>-1</sup> on both decomposition spectra (*Figure 5.21 D* and *Appendix A – Figure A.5.7*). The IR spectra of evolved gases from TG-FTIR analysis of succinic acid and the succinic anhydride modified starch were presented in *Figure 5.22*. The characteristic bands of succinic acid are noted in the modified starch spectrum, suggesting that the acid was released during the decomposition of the modified starch. The bands at 2359 and 1746 cm<sup>-1</sup> correspond to the released gases of the starch backbone (*Figure 5.14 C*).

This indicates that the decomposition of the ester substituent group and that of the bulk starch occur at the same range of temperature.



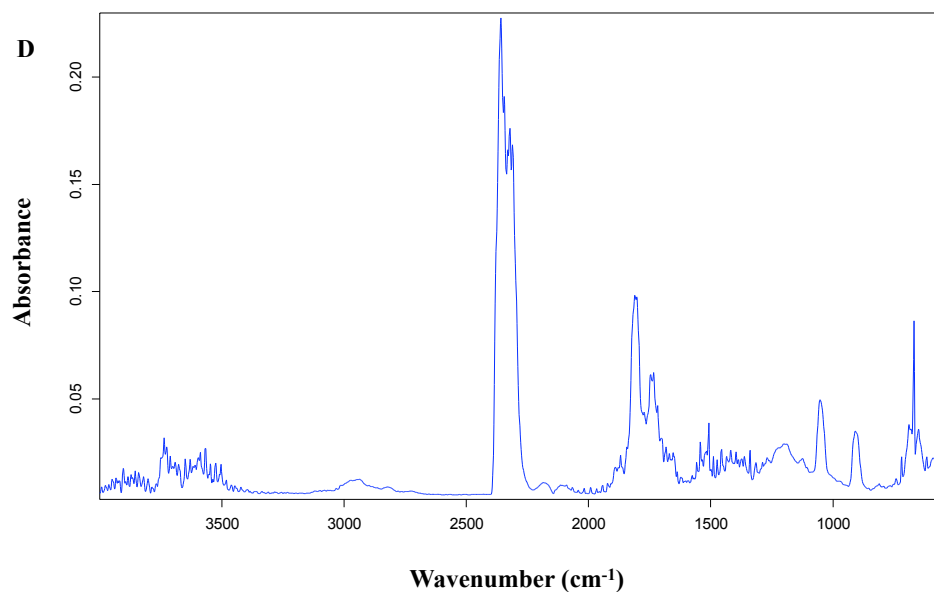


**Figure 5.21 – A) surface plot of volatiles released during decomposition of succinic anhydride modified starch, B) 3D plot of IR spectra obtained during TG-FTIR experiment, C) Gram-Schmidt trace and D) IR spectra taken at the maximum rate of decomposition (333.5 °C) (Originally in colour)**

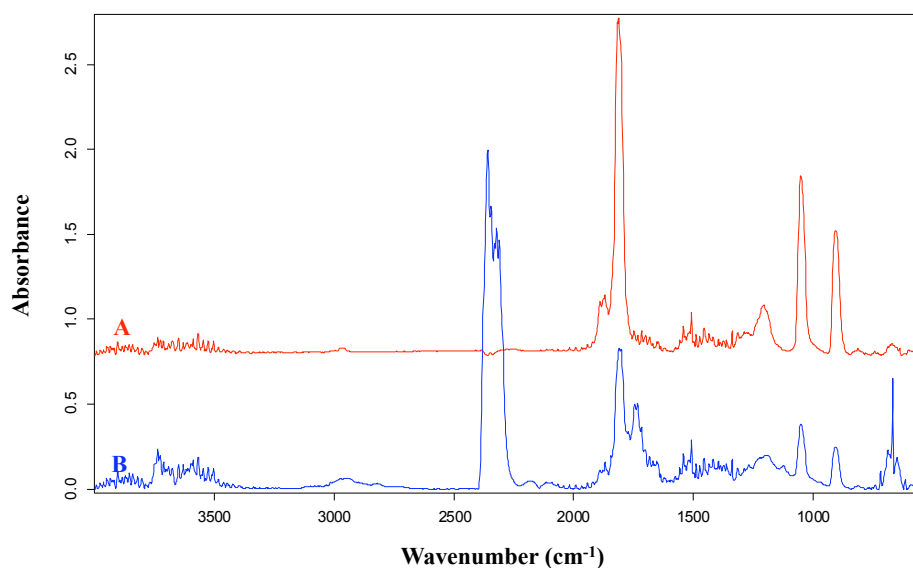
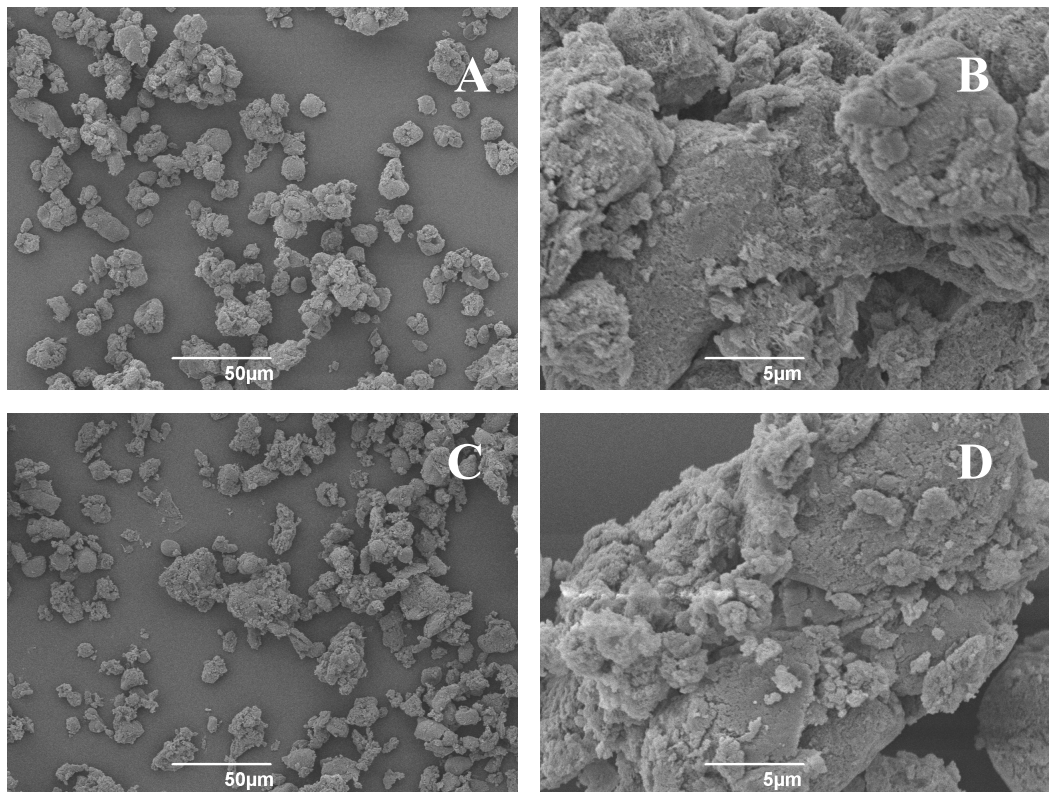


**Figure 5.22 – IR spectra of evolved gases from TG-FTIR analysis of A) succinic acid and B) succinic anhydride modified starch**



### 5.3.7 Morphological study

SEM micrographs of unmodified and esterified starches are shown in *Figure 5.23*. As stated in the previous chapter, the expansion of starch dramatically changes morphological properties of starch granules. The change in configuration of starch granules and small pores are observed on the surface of the granules. Esterification of starch may affect the morphology of the material.<sup>332</sup> The esterified starches were therefore viewed by SEM in order to investigate the granules after modification. There is no significant change in granule shape after the esterification, however the unmodified starch appears to have more uniform granules. Additionally, the porous structure of expanded starch can still be seen in all modified starches. This confirms that the modification scarcely affects the granule morphology and the esterified starches still have the porous structure, which was found to be advantageous for the subsequent production of thermosetting films.



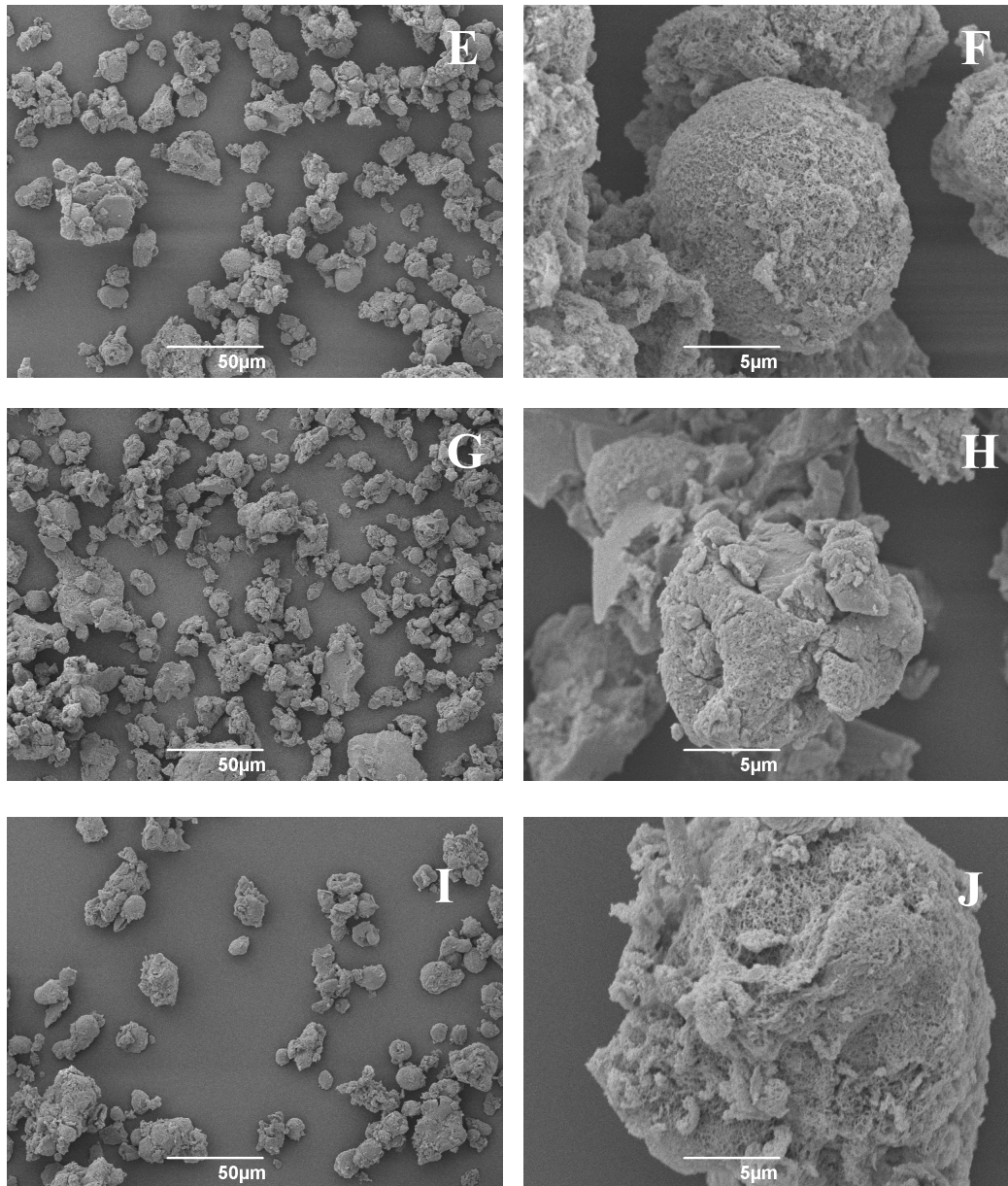


**Figure 5.23 – Scanning electron micrographs (magnification X500 and X5000) of unmodified expanded starch (A, B), acetylated starch (C, D), maleated starch (E, F), succinic anhydride modified starch (G, H) and itaconic anhydride modified starch (I, J)**

#### **5.4 Films with esterified starches**

The resulting films containing 20% wt. of esterified starches are shown in *Figure 5.24*. Unmodified starch film has a light yellow colour, whilst cyclic anhydride modified

starch films display slightly darker colour. This is likely caused by the relatively low decomposition temperature of the latter. The acetylated starch film shows better transparency compared to that of unmodified starch, which contains the same amount of starch. However, small brown spots were observed on the surface of the film, which can only be observed after the mixture has been heated. The maleated starch film, which takes 4 hours to cure, is semi-transparent. The film with succinic anhydride modified starch is more transparent than the previous case, whilst the film with itaconic anhydride modified starch is almost opaque with rough surface.

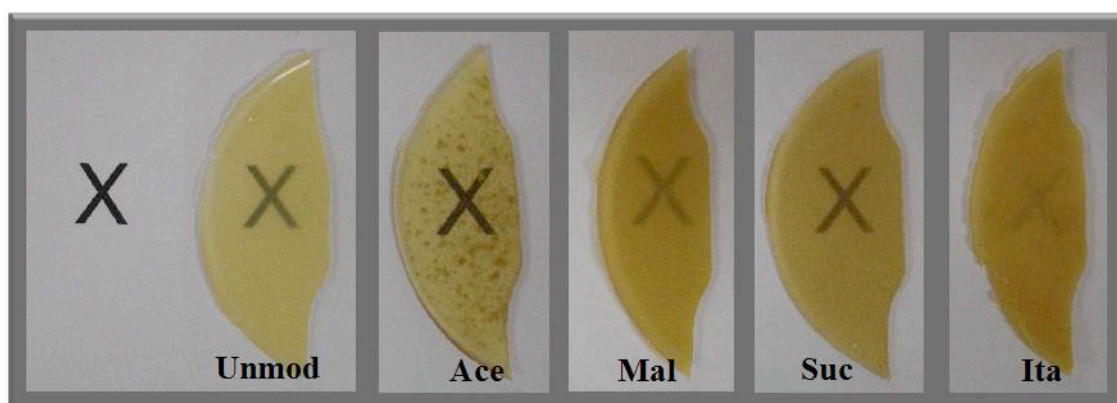


**Figure 5.24 – Films with esterified starches**

### **5.4.1 Mechanical properties**

Tensile strength of films with esterified starches decreases compared to that of unmodified expanded starch by 7.0-131.7% (*Figure 5.25*). The elongations at break of these films are also slightly lower than that of unmodified film by 12.1-33.1%. The film with acetylated starch yields a film with 4.2% enhancement in Young's modulus, whilst the film with itaconic anhydride modified starch exhibits 33.2% improvement in this parameter.

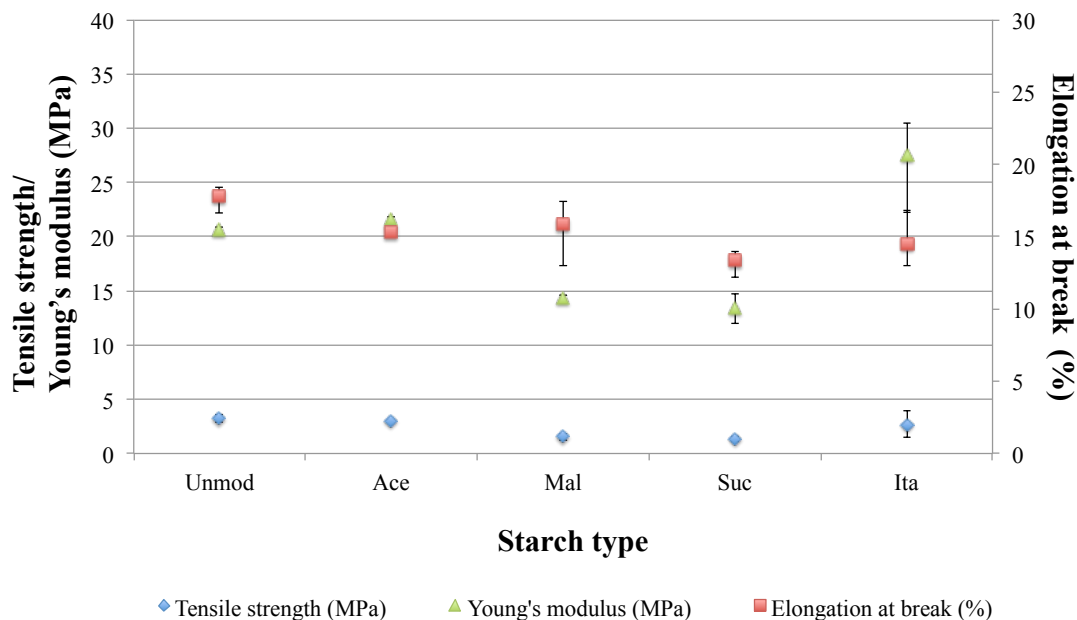


**Figure 5.25 – Mechanical properties of films with esterified starches**

#### 5.4.2 Morphological study

Scanning electron micrographs of the cross-section of esterified starch films are displayed in *Figure 5.26*. No phase separation is observed in any of the films, however small voids (marking in red circles) are noticed in the film with acetylated starch. This is likely to be caused by the DMAP catalyst, as the film without catalyst shows no dark spots. Possible explanation of this matter might be the residue of acetic acid by-product could potentially promote the decomposition of DMAP, however, more work is needed in order to ascertain the postulation. The presence of these brown spots may result in the small voids observed and consequently worsen the film mechanical properties. The film with itaconic anhydride shows some cavities inside the film, which is possibly caused by excessive loading of starch in the film. This suggests that lower amount of this modified starch can be incorporated in the film, compared to those of other starches.

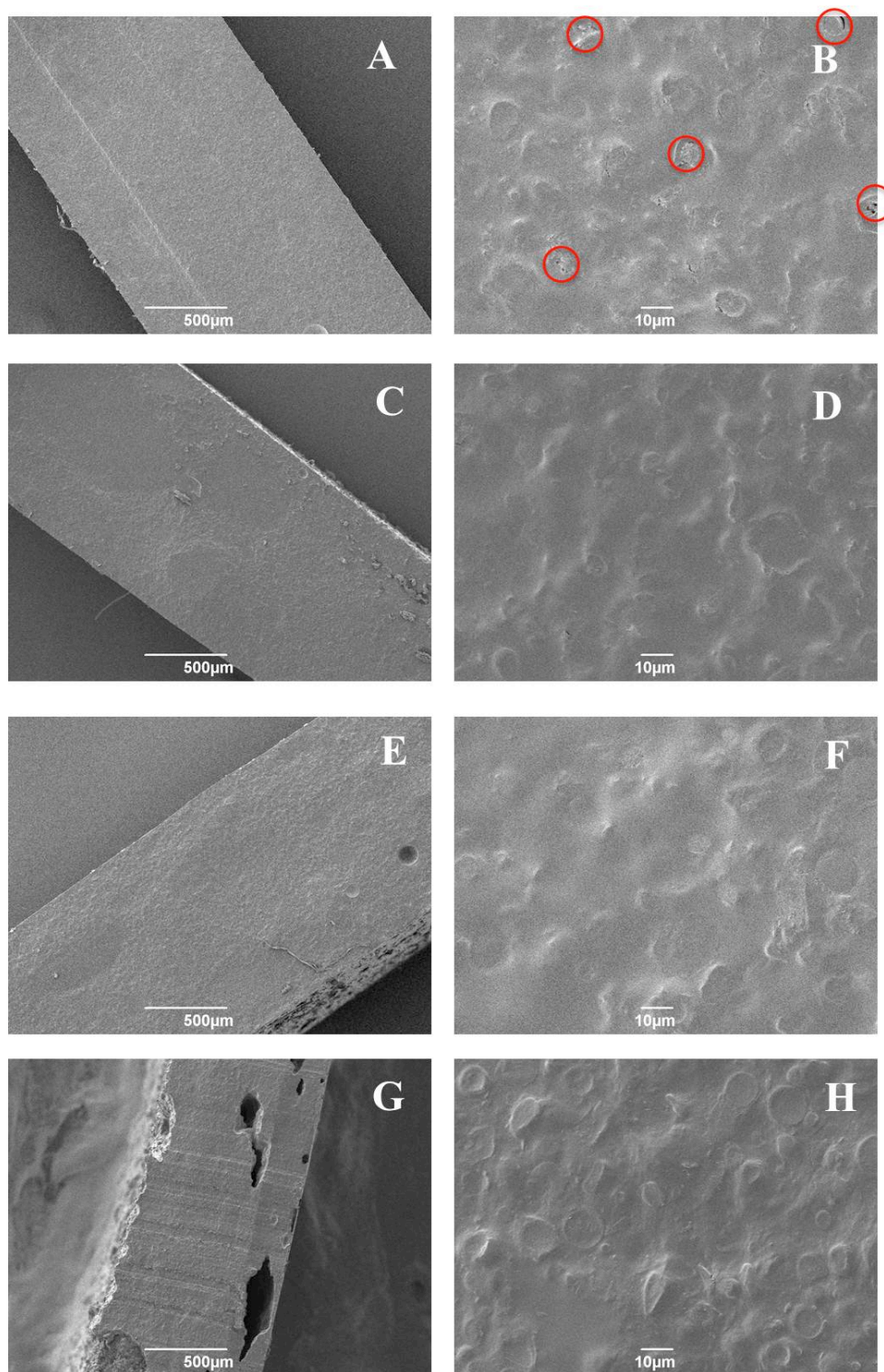


**Figure 5.26 – Scanning electron micrographs (magnification X50 and X1000) of the cross-section of films with esterified starches (A-B – acetylated starch, C-D – maleated starch, E-F – succinic anhydride modified starch, G-H – itaconic anhydride modified starch)**

### 5.4.3 Water uptake

The average water uptake of films with esterified starches was compared to that of the unmodified starch film in *Figure 5.27*. A decrease in water uptake is observed in the films containing esterified starch as anticipated. This is due to the increase in hydrophobicity of the modified starch as a result of the reduction of hydroxyl groups in starch after the modification. However, the film containing itaconic anhydride modified starch exhibits a slightly higher water uptake than that of unmodified starch. This is likely to be caused by the presence of the voids inside the cured resins, which increases the contact of the resin with water, resulting in augmentation of the water uptake. Acetylated starch and succinic anhydride modified starch films demonstrate 0.7% and 0.8% water uptake after 24-hour submersion in water respectively. These comparatively low values are due to the greater degree of substitution with acetic and succinic anhydride modified starches compared to other modified starches. The water uptake of these two films is in fact comparable to that of the film without starch added (0.4%) despite the inclusion of 20% wt. of starch in the resin.

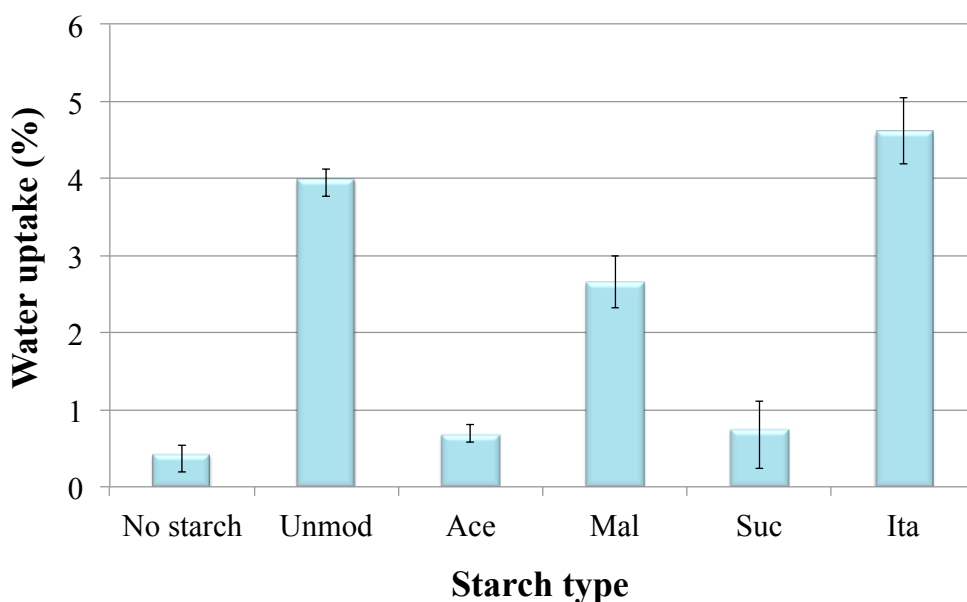


**Figure 5.27 – Water uptake of films with no starch, unmodified starch (Unmod), acetylated starch (Ace), maleated starch (Mal), succinic anhydride modified starch (Suc) and itaconic anhydride modified starch (Ita) (Originally in colour)**

#### 5.4.4 Thermal properties

TGA thermograms of all the films demonstrate no or minimal mass loss between 25 °C to 250 °C (*Figure 5.28*). The first weight loss then occurs in the region of 250-350 °C, which according to the study asserted in chapter 4, is attributed to the decomposition of starch. The principal weight loss, corresponding to the decomposition of the crosslinked polymer, is subsequently observed. However, there is an exception for the film with acetylated starch, which shows only one weight loss, starting at around 300 °C. This is likely due to the good thermal stability of the acetylated starch, which exhibits the initial decomposition at the temperature over 300 °C (*cf. section 5.3.5*). Interestingly, despite the low decomposition temperature of cyclic anhydride modified starches, the thermal stability of the films containing these starches is not affected as their weight losses start at the same temperature as the film with unmodified starch. *Table 5.3* demonstrates the percentage of weight loss between 150-600 °C and the decomposition temperature determined as the peak of DTG curves. The residue of the films accounts for approximately 7-8% of the total weight. DTG curves demonstrate a small transition peak around 300 °C, which is associated to the decomposition of starch. The main transition, which occurs around 390 °C corresponds to the decomposition temperature of the crosslinked polymer. It is noted that the first transition at around 300 °C is absent in the formulation with acetylated starch. This is also in agreement with the only one mass loss observed on the TG curve, owing to high decomposition temperature of the acetylated starch.

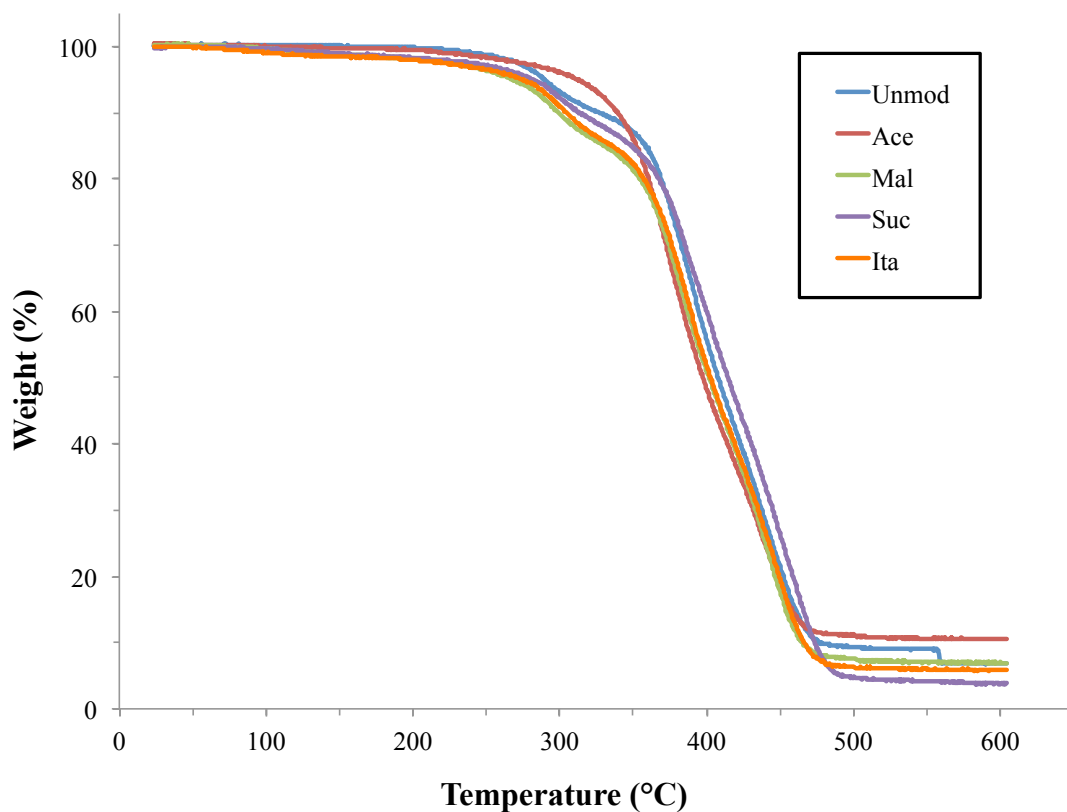


**Figure 5.28 – TGA thermograms of films with unmodified and modified starches (Originally in colour)**

**Table 5.3 – Thermal characteristic of films with unmodified expanded starch and esterified starches**

Starch type	Weight loss (%) (150-600 °C)	Decomposition temperature (°C) (DTG peaks)
Unmod	93.3	302.1, 403.7
Ace	93.9	389.8
Mal	93.0	301.9, 392.6
Suc	93.0	297.9, 389.6
Ita	92.1	304.8, 396.8



## 5.5 Study of curing reaction of the formulations with esterified starches

### 5.5.1 Thermal study

The thermal events occurring during the cure process of the formulations comprised of ELO, Pripol, 20% in weight of unmodified or esterified starch and DMAP are investigated using modulated DSC technique. The resulting thermograms are demonstrated in *Figure 5.29*.

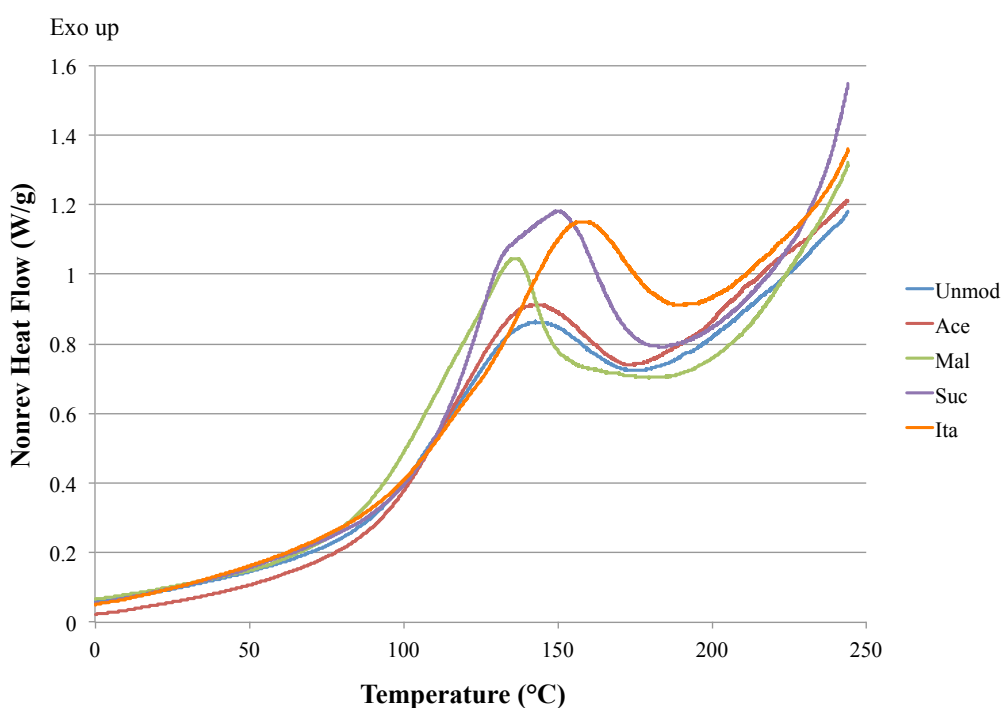


**Figure 5.29 – Thermograms of formulation comprised of ELO, Pripol, DMAP and esterified starches (Originally in colour)**

The thermogram of formulation with acetylated starch films shows an exothermic transition in the same temperature region as one from formulation with unmodified starch with slightly higher heat of reaction. The cured acetylated starch resin also displays a higher glass transition temperature (*Table 5.4*). These results suggest that more crosslinking has occurred in the formulation with the esterified starch, probably due to its hydrophobicity, which allows better dispersion of starch granules in the

formulation. Szymanowski *et al.* demonstrated that the alteration of hydrophobicity of starch filler enhances its miscibility in the polymer matrix and consequently improves the properties of the composite.<sup>333</sup> The exothermic transition of the cyclic anhydride modified starch formulations show comparatively higher enthalpy of reaction than the unmodified starch mixture with succinic anhydride modified starch formulation giving the highest heat of reaction. The  $T_g$  of the esterified starch cured resins are comparable to that of the unmodified starch, except for the resin containing maleated starch, which shows relatively low  $T_g$ . Despite the higher heat of reaction, formulations with esterified starches show similar or lower  $T_g$  and poorer mechanical properties compared to those of unmodified starch film. This may be explained by the low thermal stability of these esterified starches (sections 5.3.5 and 5.3.6). Maleated starch starts to decompose as low as 101 °C and 142 °C for itaconic anhydride modified starch. Although the decomposition is considered as an endothermic reaction under nitrogen atmosphere, the higher total heat of reaction of the formulation mixture may be attributed to the reaction of the first-phase decomposition products and other components present in the mixture. These reactions contribute to the total heat of the reaction, but do not contribute to the curing of the resin. Hence, the films with higher total heat of reaction show no improvement in mechanical properties. The low decomposition temperatures of esterified starch also affect the curing time of the resin as evidenced by formulation with maleated starch needed more time to cure than other formulations.

**Table 5.4 – MDSC of esterified starch formulations**

Starch type in the formulation	Total heat of reaction (J/g)	Onset temperature (°C)	Peak temperature (°C)	T <sub>g</sub> (°C)
Unmod	89.0	94.04	139.55	-19.12
Ace	97.9	95.96	139.30	-15.98
Mal	134.9	90.42	135.21	-31.48
Suc	157.4	108.60	149.06	-17.16
Ita	120.5	113.84	154.62	-19.88

### 5.5.2 Infrared spectroscopic study

The infrared spectra of the formulations with esterified starch were recorded during curing process at 140 °C for 2 hours and 4 hours for maleated starch formulations. The samples were taken every 30 minutes and the resulting spectra are displayed in *Figures 5.30-5.33*.

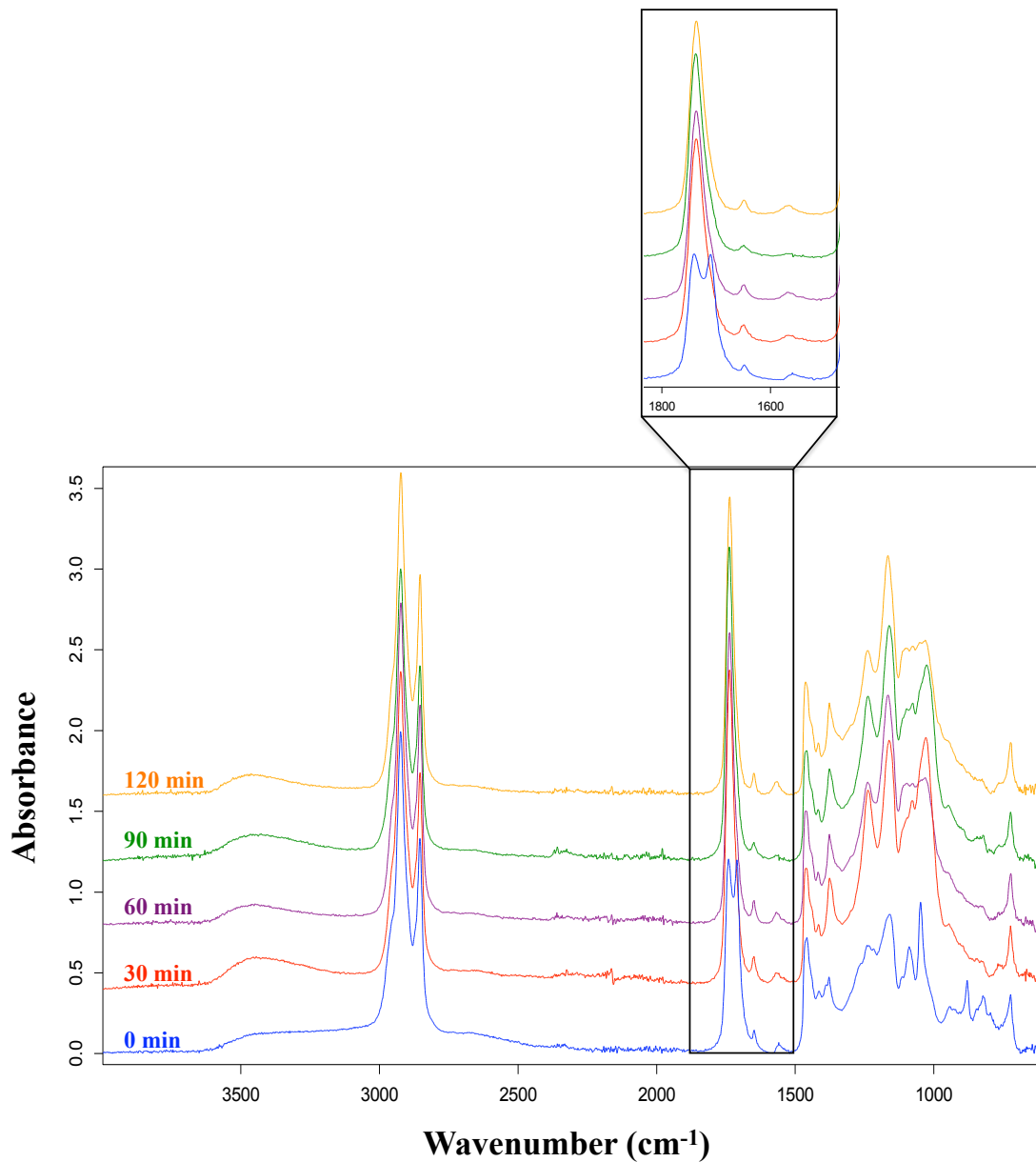


**Figure 5.30 – Infrared spectra of the formulation comprised of ELO, Pripol, acetylated starch and DMAP cured at 140 °C (Originally in colour)**

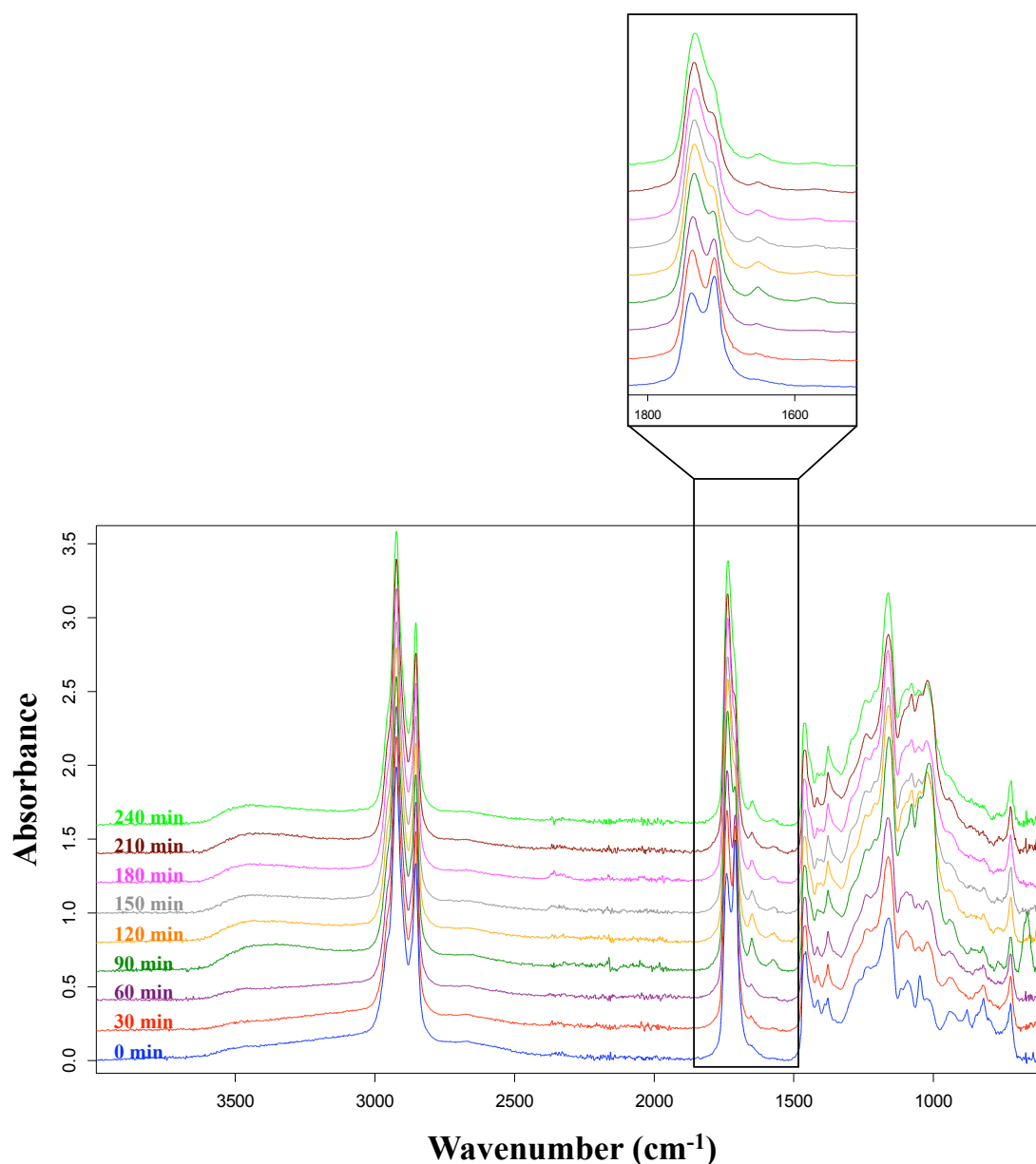


**Figure 5.31 – Infrared spectra of the formulation comprised of ELO, Pripol, maleated starch and DMAP cured at 140 °C (Originally in colour)**

The spectra of all the formulations show relatively similar changes as the curing time increases. The most obvious change involves the intensity decrease of the acid carbonyl band at 1709 cm<sup>-1</sup>, which disappears completely after 2 hours of curing. However, for the formulation with maleated starch, the band can still be seen as a shoulder of the adjacent band after 4 hours of heating, indicating slow crosslinking of this formulation. The characteristic carbonyl ester band at 1740 cm<sup>-1</sup>, shifts to 1736 cm<sup>-1</sup> at the end of the

observation, suggesting a new ester bond is formed during the curing process.<sup>186</sup> A development of a broad band in the region of 3600-3200  $\text{cm}^{-1}$  is noted overtime and the band is attributed to the hydroxyl group, resulted from the ring-opening of the epoxide. Moreover, the formation of bands at 1647 and 1570  $\text{cm}^{-1}$  are also observed in these formulations. These bands are assigned to the attached DMAP onto the polymer matrix, explained in details in section 2.5.1. The spectra of the esterified starch formulations exhibit a great similarity to that of unmodified starch, suggesting that the mixtures undergo the same curing reaction. However, the new functionality introduced by cyclic anhydrides onto starch has a characteristic band at the same region as that of ester and acid carbonyls of ELO and Pripol respectively, creating the difficulty to investigate the activity of this added group.

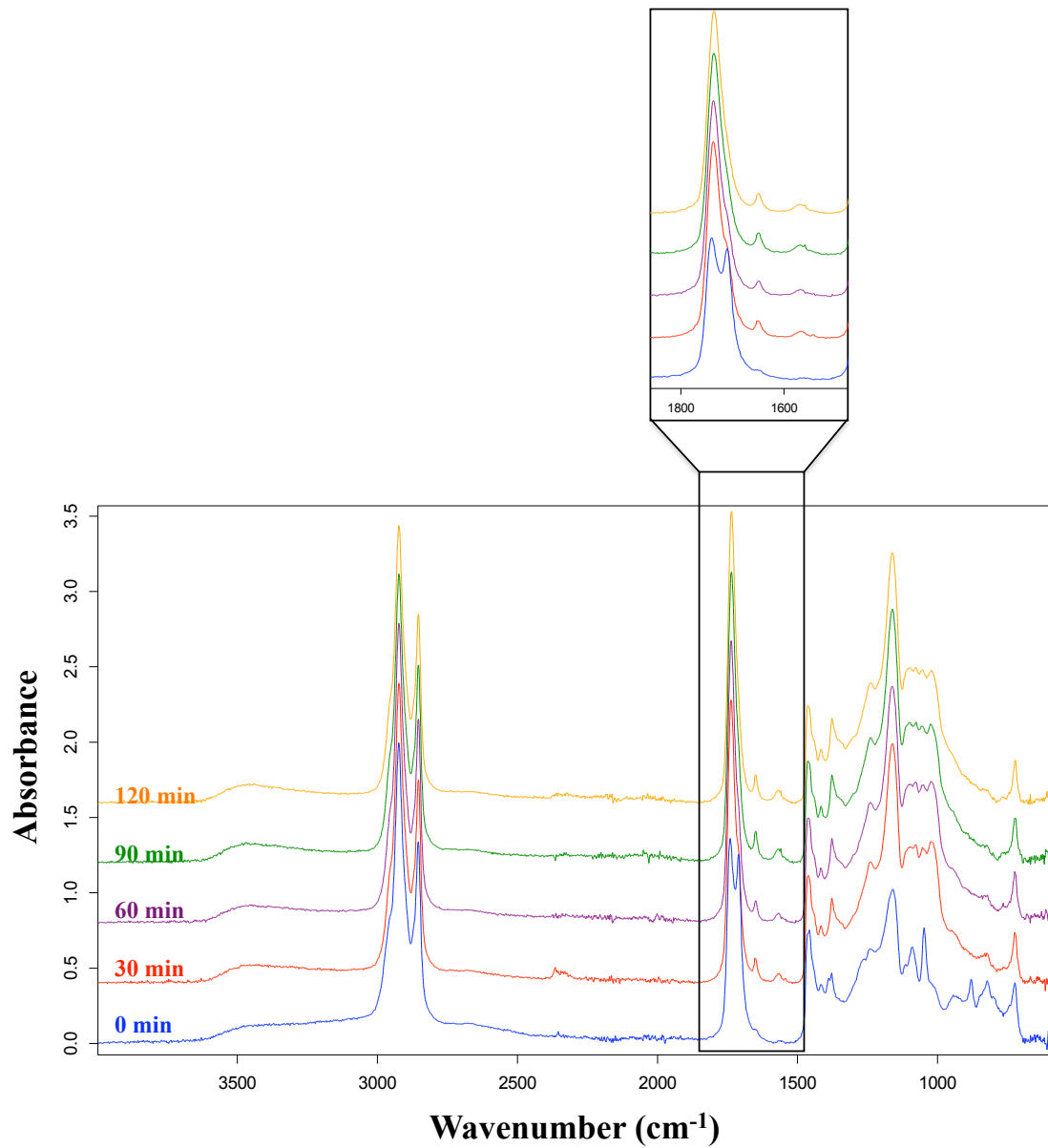


**Figure 5.32 – Infrared spectra of the formulation comprised of ELO, Pripol, succinic anhydride modified starch and DMAP cured at 140 °C (Originally in colour)**

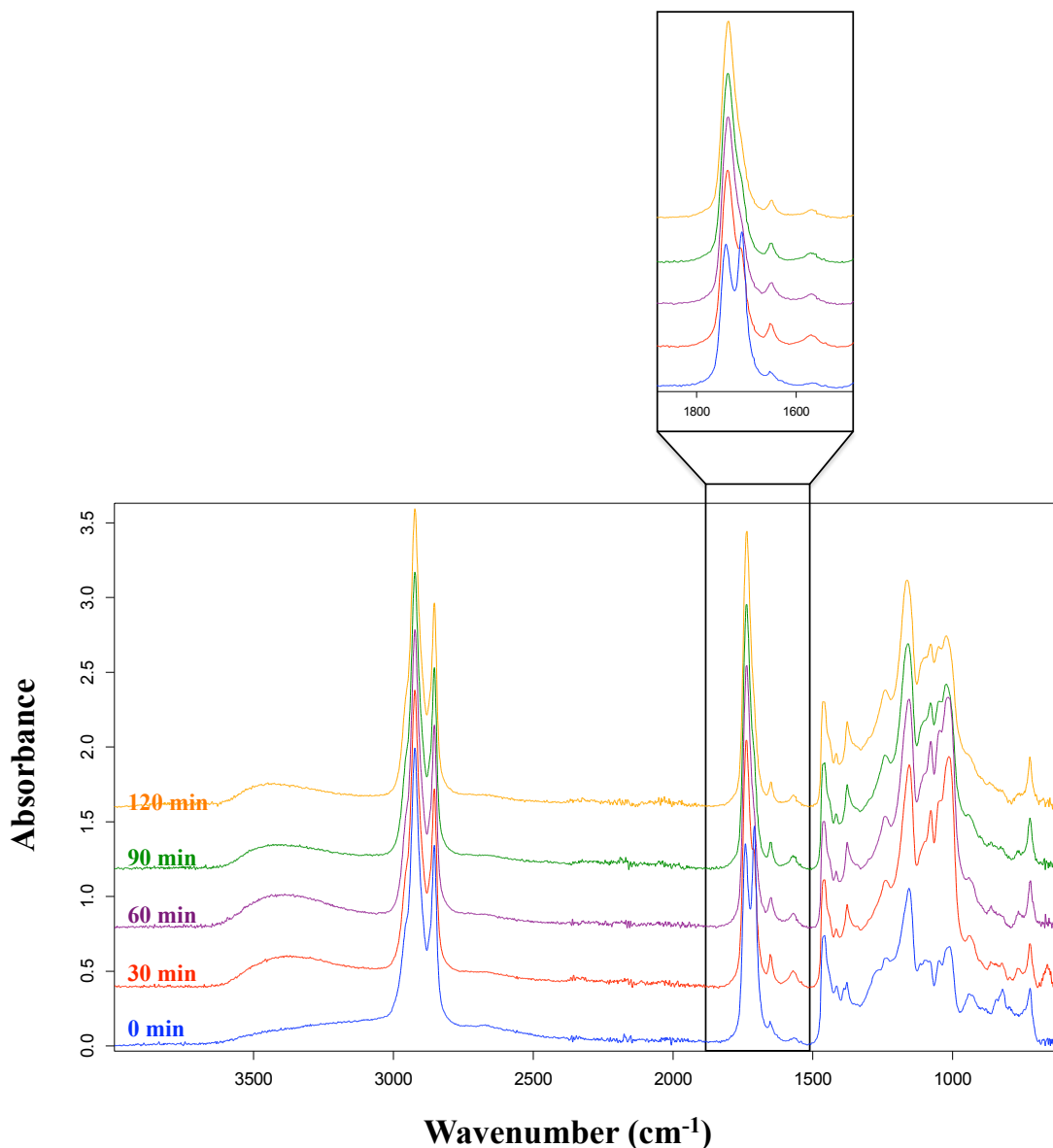


**Figure 5.33 – Infrared spectra of the formulation comprised of ELO, Pripol, itaconic anhydride modified starch and DMAP cured at 140 °C (Originally in colour)**

## 5.6 Conclusions

Esterification of expanded starch was performed with acetic, maleic, succinic and itaconic anhydrides. IR and NMR spectra of the products confirmed the modification and degree of substitution was determined using titration method. Acetylated starch demonstrated the highest DS, owing to good accessibility of the carbonyl carbon, which



facilitates the nucleophilic addition. The acetylated starch also showed better thermal stability than native starch, however other esterified starches exhibited lower decomposition temperatures. This is associated with the disintegration of intramolecular interactions such as hydrogen bonding in starch chains and the poor thermal stability of carboxylic group introduced onto the polymer after the esterification. TG-FTIR results revealed that two-phase decomposition of cyclic anhydride modified starches with the first step corresponding to the decomposition of the substituent groups and the second phase is assigned to the decomposition of starch backbone. The mechanical properties of esterified starch films demonstrated no significant improvement over native starch and in fact a decrease in tensile strength was observed for all the esterified starch films, however, the Young's modulus of acetylated starch and itaconic anhydride modified starch exhibited a slight improvement. The film with acetylated starch showed better transparency compared to that of unmodified starch. A significant improvement was observed in water resistance of the esterified starch films. The films with acetylated and succinic anhydride modified starches exhibited water uptake of 0.7% and 0.8% respectively. These values are comparable to that of the film without starch included (0.4%). All the films demonstrated good thermal stability with the acetylated starch films not starting to decompose until after 300 °C.



# Chapter 6

*Literature comparison and  
evaluation of the bio-based  
composites against PVC  
wearlayer*



## 6.1 Chapter 6 -Summary

Bio-based resins based on ELO, Pripol and starch were compared to resins produced from relatively similar system in the literature and also to common petroleum based polymer such as low density polyethylene and polyvinyl chloride wearlayer. The resin containing 20% w/w of gelatinised starch demonstrated comparable or greater mechanical properties compared to other epoxidised oil based resins. Although the mechanical properties of these bio-based films were relatively inferior compared to that of the PVC wearlayer, other properties including water resistance exhibited similar performance and the thermal stability was in fact superior. The resin containing acetylated starch showed 0.7% water uptake after 24-hour submersion in water and the value of 0.4% was obtained from PVC sample. Moreover, these bio-based composites remained thermally stable up to 280-310 °C, whilst PVC started to decompose at the temperature as low as 150 °C.

## 6.2 Introduction

The bio-based thermoset composites with extremely high content of bio-derived feedstocks were successfully prepared using up to 99.5% (by weight) renewable materials. Moreover, the films can be casted without the use of solvent, which is not only environmentally friendly but also could be a suitable production process of the wearlayer in vinyl flooring replacements. To better assess the suitability of the materials for various applications, their properties have been compared to literature values of other renewable films and commonly used polymers.

## 6.3 Mechanical properties

According to the work conducted in the thesis, the greatest tensile strength was observed from the formulation comprising of 20%wt. of gelatinised starch, ELO, Pripol and 0.5% DMAP (with respect to the total resin weight) (GS film). Other bio-based resins from the relatively similar system yielded films with comparable mechanical properties.<sup>334, 335</sup> Carter *et al.* investigated the use of epoxidised linseed oil to substitute linoleum or some parts of carpet manufacturing process.<sup>334</sup> A diacid crosslinker was synthesised from dipropylene glycol and maleic anhydride and was incorporated with

ELO without catalyst. The strongest film was obtained from the formulation with molar ratio (ELO:diacid) of 1:2. Carter's ELO+diacid film shows approximately 200% higher elongation at break than that of GS film however, Carter's films demonstrate a 101% decrease in tensile strength and 217% reduction in Young's modulus as compared to GS films. Luo *et al.* modified epoxidised soybean oil via allylation and esterification. The obtained product was incorporated with maleic anhydride in order to yield a thermosetting resin.<sup>335</sup> The mechanical properties were significantly influenced by the amount of maleic anhydride in the formulation. At 10 % loading, the resin demonstrated inferior mechanical properties compared to those of GS film. A decrease of 265%, 80% and 53% are noted for tensile strength, elongation at break and Young's modulus respectively in Luo's films as compared to GS film. Although the increased amount of the anhydride dramatically improved tensile strength and Young's modulus of the resin, a considerable decrease in elongation at break was observed. Moreover, the bio-content of the resin was reduced when more petroleum-derived maleic anhydride was present in the resin.

*Figure 6.1* compares the mechanical properties of these bio-based composites to those of petroleum-based polymer such as low density polyethylene (LDPE) and polyvinyl chloride (PVC).<sup>336</sup> GS film shows 132% lower in tensile strength than LDPE and 873% than PVC wearlayer. The elongation at break and Young's modulus of the bio-based resin are also obviously inferior compared to those of LDPE and PVC. Therefore, there is room for improvement to enhance the mechanical properties of these environmentally friendly composites. In which case, more research is needed to achieve the required properties.

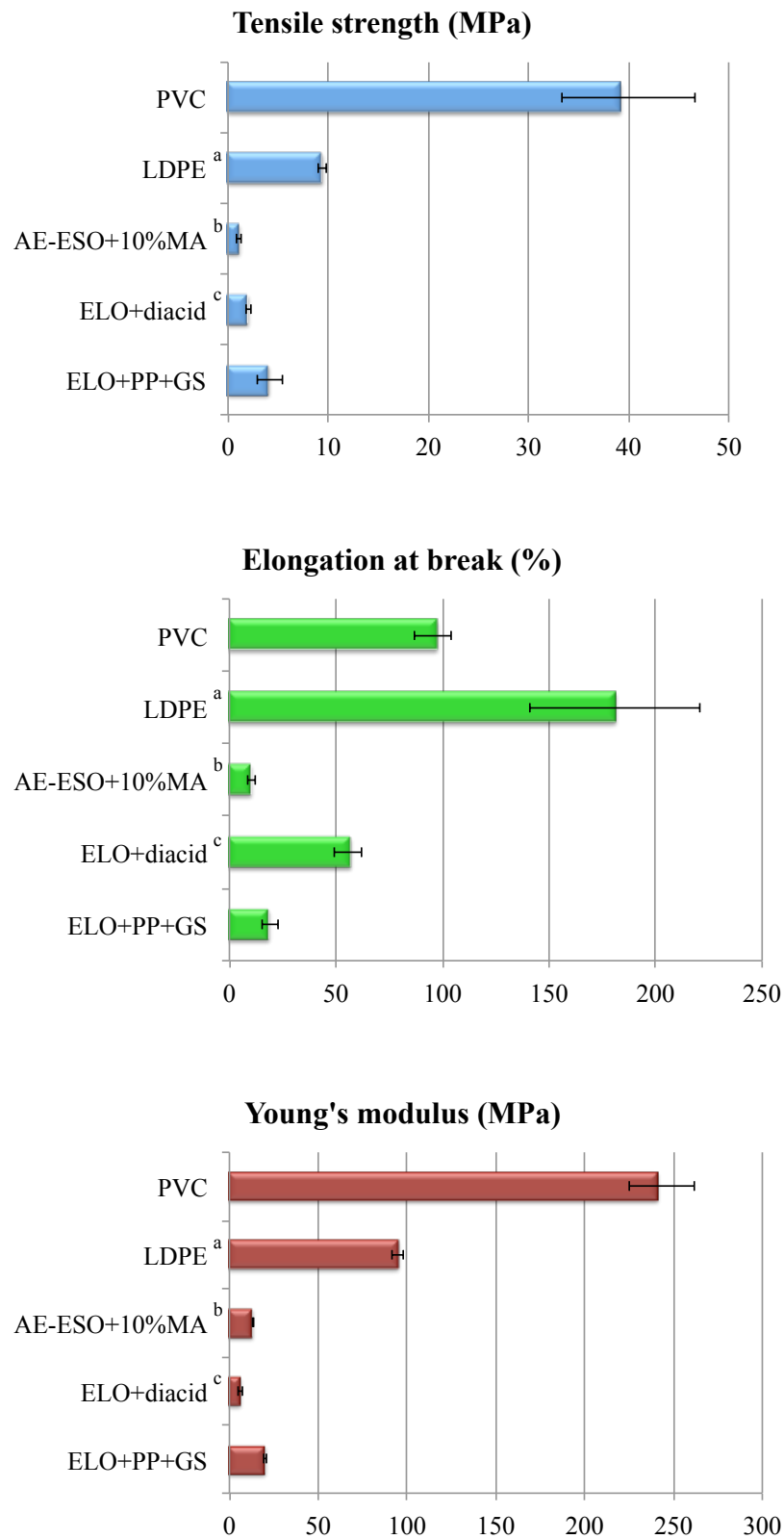


**Figure 6.1 – Mechanical properties of bio-based films compared to PVC wearlayer and LDPE (results obtained from the literature a) reference 336, b) reference 335 and c) reference 334) (Originally in colour)**

## 6.4 Water resistance

The water uptake of the PVC wearlayer is 0.4%, whilst the GS film shows higher water uptake at 4% after 24-hour submersion in water. However, acetylated starch film demonstrated comparable water uptake to that of PVC at 0.7%. Overall, the bio-based exhibit good water resistant property, which is essential in various applications such as flooring and coating.

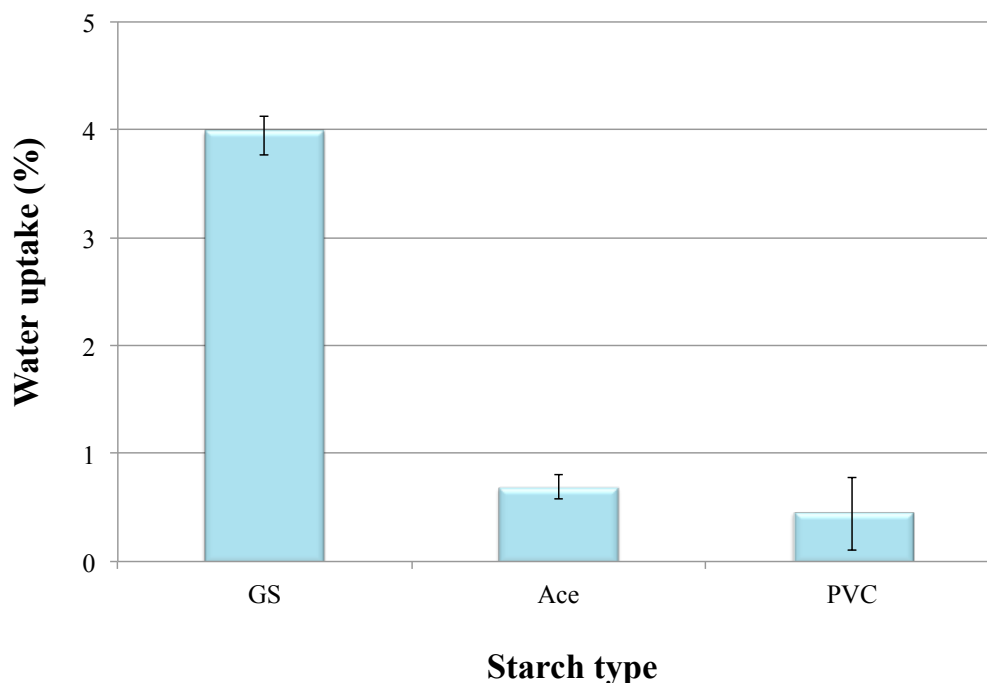


**Figure 6.2 – Water uptake of bio-based resins with gelatinised and acetylated starches compared to that of PVC wearlayer (Originally in colour)**

## 6.5 Thermal stability

TGA thermogram of PVC wearlayer displays two major mass losses (*Figure 6.3*). The first mass loss, which starts at around 150 °C, corresponds to the main decomposition of the material, accounting for approximately 70% of the weight loss. The second weight loss is observed in the temperature range of 400-525 °C. The DTG curve confirms the two stages of the decomposition observed in the TG curve. The peak temperatures of the two transitions are at 232.9 °C and 458.8 °C. The films with gelatinised and

240



acetylated starches demonstrated the first weight loss around 280 °C and 310 °C respectively (Figure 6.4). This indicates that ELO based resins are more thermally stable than PVC film, which is advantageous for future potential applications. Moreover, it is well known that the decomposition of the poor thermally stable PVC emits very toxic gases, such as hydrogen chloride and other chlorinated hydrocarbons.<sup>337, 338</sup> PVC can therefore present a serious health problem in the event of fire.

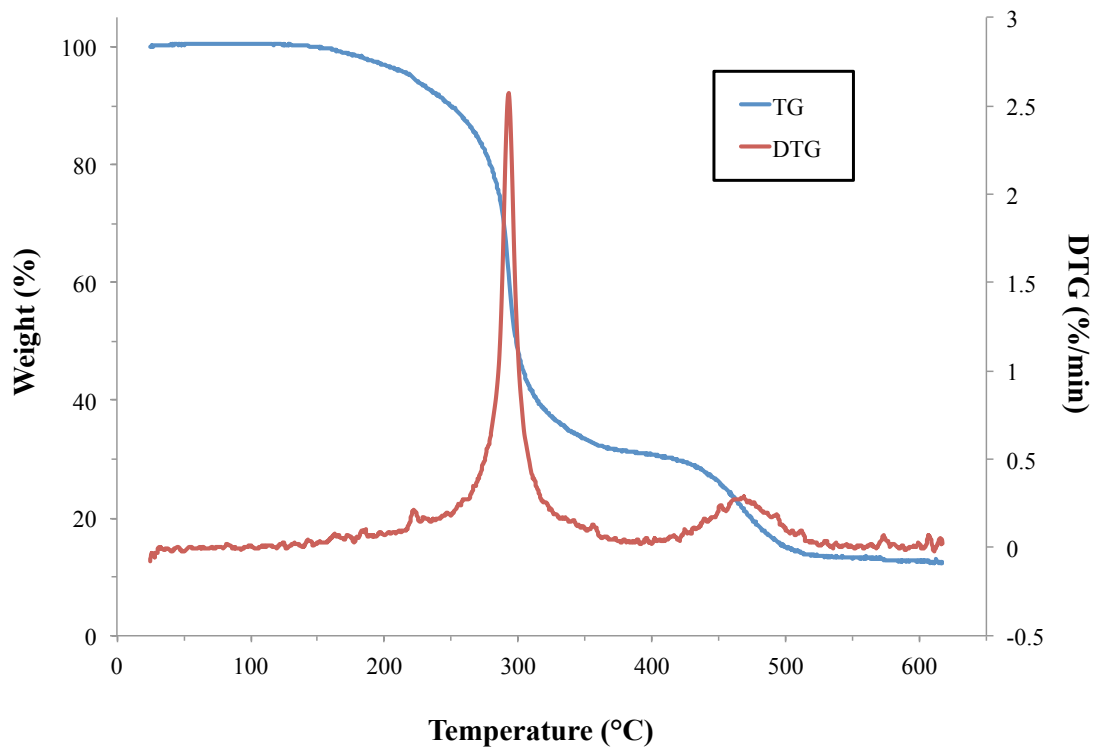


**Figure 6.3 – TG and DTG traces of PVC wearlayer (Originally in colour)**

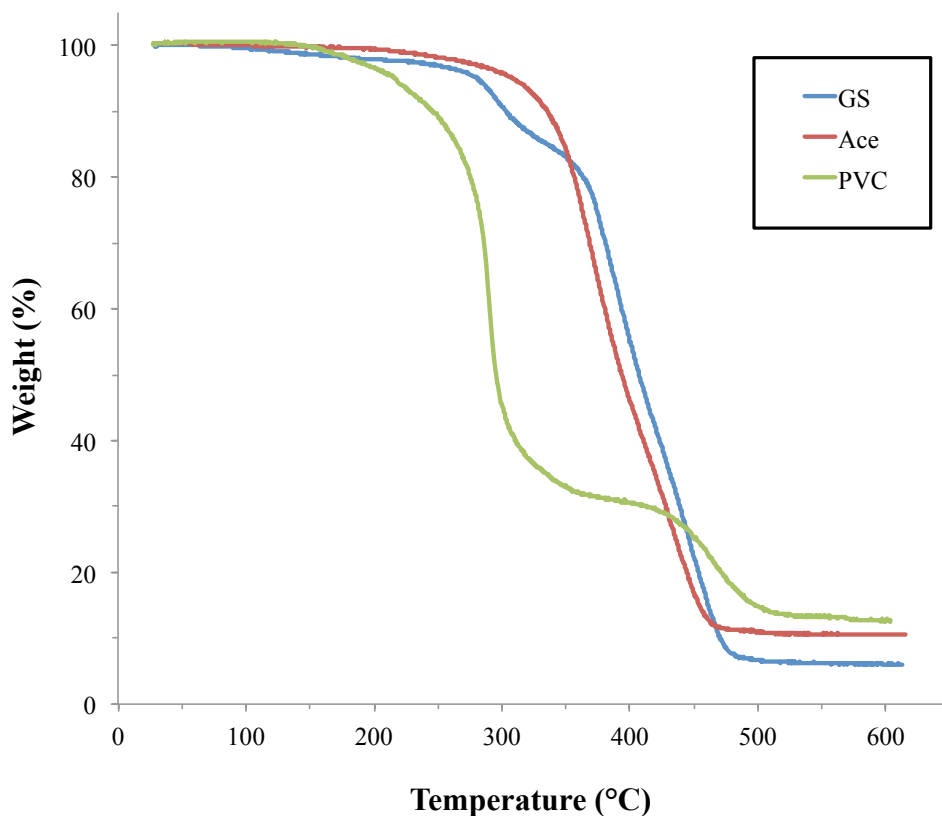


**Figure 6.4 – TGA thermograms of bio-based films with gelatinised and acetylated starches compared to that of PVC wearlayer (Originally in colour)**

## 6.5 Conclusions

The comparison of bio-based composites produced from ELO, Pripol and starch to the resins produced from relatively similar system in the literature and common petroleum based polymer such as LDPE and PVC wearlayer was presented. These ELO and starch films demonstrated comparable or slightly better mechanical properties compared to the composites from similar system. Despite the fact that the petroleum-derived products showed superior mechanical properties compared to the bio-derived products, other properties including water resistance and thermal stability of the bio-based composites demonstrated good performance. Acetylated starch film exhibited comparable water uptake to that of PVC wearlayer. Moreover, PVC has low thermal stability compared to the ELO based resins, which remain stable up to 280-310 °C. Overall, these bio-based

composites produced from ELO, Pripol and starch present a great potential as an environmentally friendly alternative to petrochemical polymers.



# Chapter 7

## *Experimental*



## 7.1 Chemicals

Epoxidised linseed oil under the trade name Lankroflex® L (oxirane oxygen = 9%) was purchased from Akcros Chemicals. Pripol 1009 was kindly supplied by Croda Ltd. Corn starch and high amylose starch (Hylon® VII) were kindly provided by National Starch & Chemical. Solvents were purchased from Fisher Scientific.

Chemical were purchased from Sigma-Aldrich, Fluka and Fisher Scientific and were used without further purification.

The following chemicals were purchased from Sigma-Aldrich:

1,8-diazabicyclo [5.4.0] undec-7-ene (DBU), triethylamine (TEA), 1-methylimidazole (1-MeIm), acetic anhydride, succinic anhydride, itaconic anhydride, itaconic acid, maleic acid and phenolphthalein

Hydrochloric acid, potassium hydroxide, ethanol and toluene were obtained from Fisher Scientific.

4-dimethylaminopyridine (DMAP), succinic acid and maleic anhydride were purchased from Fluka.

2-methylimidazole (2-MeIm) was obtained from Acros organics.

## 7.2 Experimental details and instrumentation for chapter 2

### 7.2.1 ELO and bio-derived crosslinkers film preparation

3 g of ELO and required weight of crosslinker (*Table 6.1*) were weighed into a 30 mL glass vessel and mixed with a high-speed mixer (2000 rpm) for 3 minutes at room temperature prior to be poured into a 70 mL aluminium tray (inner diameter = 70 mm). The mixtures were cured in an oven at 140 °C for required time (*Table 6.2*).

**Table 7.1 – Amount of crosslinkers in the formulation (molar ratio crosslinker:ELO = 2.5:1)**

Crosslinker	Amount (g)
Succinic acid	0.91
Itaconic acid	1.01
Succinic anhydride	0.77
Itaconic anhydride	0.87
Pripol 1009	4.36

**Table 7.2 – Curing time required for different formulations**

Formulation	Curing time (hours)
ELO + bio-derived crosslinkers	24
ELO + Pripol	6
ELO + Pripol + Catalyst	1 (except for TEA, 3.5)

For the films containing catalyst, 1% weight of total resin weight of catalyst was added into the formulation, unless otherwise stated. The films were cured at 140, 160 or 180 °C for 1 hour, except for the study of the effect of curing time on mechanical properties of the films. Different curing times applied were 15, 30, 45, 60, 90 and 120 minutes.

### 7.2.2 Simultaneous thermal analysis

Prior to the addition of catalysts in the formulations, the standard ELO and Pripol 1009 mixture was analysed using Simultaneous Thermal Analysis (STA) in order to determinate the optimum ratio of mixing for these two components. ELO and Pripol



1009 mixtures of different weight ratios were analysed in a Stanton Redcroft STA 625 (TG/DSC) under a nitrogen atmosphere (gas flow 60 mL/min) with the sample weight of 10–15 mg. The samples were heated from 25–500 °C at 10 °C/min. The enthalpy of the reaction was obtained by integrating the peak area of the exothermal transition on the thermogram using dedicated software for Stanton Redcroft STA 625.

## **7.3 Experimental details and instrumentation for chapter 3**

### **7.3.1 Preparation of acid hydrolysed starch in water**

Acid treated starch in water was prepared according to Wang *et al.* method with minor alterations.<sup>219</sup> A 40% slurry of starch (dry basis) was prepared by adding 80 g of corn starch (or high amylose corn starch) with 1 mol/L hydrochloric acid solution to a final weight of 200 g. The erlenmeyer containing the starch slurry was immersed in a water bath at a controlled temperature of 50 °C with continuous stirring. At various times (1, 4 or 24 hours), the reaction was stopped by adding 1 mol/L sodium hydroxide solution to raise the pH to 6-7. The slurry was washed with two-folded volume of distilled water then centrifuged at 3500 rpm for 5 minutes. This procedure was repeated three times and the product was subsequently dried in an oven at 40 °C overnight. The dried starch was ground and sieved using 125µm sifter.

### **7.3.2 Preparation of acid hydrolysed starch in ethanol**

Acid-alcohol modified starch was prepared by opting method reported by Lin *et al.*, however, ethanol was used instead of methanol in this case.<sup>220</sup> 25g of normal corn starch was suspended in 100 mL of ethanol in a 250 mL erlenmeyer flask. The reaction was started by adding 1 mL of concentrated hydrochloric acid (36% by weight) into the slurry, which was continuously stirred at room temperature for various times (1, 3, 5 or 7 days). The reaction was stopped by adding 14 mL of 1 mol/L sodium hydroxide solution, which raised the pH up to 6-7. The slurry was centrifuged at 3500 rpm for 5 minutes, and then washed with two-folded volume of 50% ethanol/water. The precipitate was dried in an oven at 40 °C overnight and the dried starch was ground and sieved using 125µm sifter.

### 7.3.3 Swelling power and solubility tests

Swelling power and solubility tests were measured using the method of Lin *et al.* and that of Lawal *et al.* respectively.<sup>220, 221</sup> Accurately weighed 0.1 g of acid-treated starch sample and 40 mL of distilled water were heated at various temperatures (65, 75 and 85 °C) in a water bath for 30 minutes with continuous stirring. The mixture was allowed to cool to room temperature, and then centrifuged at 4000 rpm for 10 minutes. The residual starch (with retained water) in the tube was weighed and the swelling power was calculated using equation below:

$$\text{Swelling power} = \frac{W_1 - W_2}{\text{weight of starch}}$$

where  $W_1$  is dry starch and centrifuge tube,  $W_2$  is wet starch after heating and centrifugation and centrifuge tube.

The supernatant obtained after centrifugation was decanted and the aliquot of the supernatant evaporated at 130 °C overnight and weighed. The solubility was obtained by divided the weight of the dried supernatant by the initial weight of the dry starch.

### 7.3.4 Pasting properties

Pasting properties of acid-treated starch samples were carried out using method of Wang *et al.*<sup>219</sup> 10% (dry basis) solution of acid hydrolysed starch in water was prepared by weighing 0.1 g of starch and water was added to achieve the final weight of 1 g. The starch slurry was vigorously mixed and the pasting properties were performed using a Brookfield R/S – CPS plus rheometer. The sample was heated from 35 °C to 95 °C at the heating rate of 1.5 °C/minute, held at 95 °C for 20 minutes and cooled down to 25 °C/minute at 1.5 °C/minute.

### 7.3.5 Film preparation

1.75 g of native or acid hydrolysed starch (ground and sieved) was added in to a 30 mL glass vessel, in which 3.5 g of ELO, 3.5 g of Pripol and 0.5% of the total resin weight

(0.044 g) of DMAP were subsequently added. The components were vigorously mixed with a high-speed overhead stirrer (2000 rpm) for 3 minutes at 120 °C to assure the dispersion of the catalyst into the polymer matrix. The mixture was then poured into a 70 mL aluminium tray (inner diameter = 70 mm) and cured at 140 °C for 1 hour.

## **7.4 Experimental details and instrumentation for chapter 4**

### **7.4.1 Expansion processes of starch**

#### **7.4.1.1 Gelatinisation**

Gelatinised starch was obtained by preparing a 10% of high amylose starch in water slurry (dry basis) in a glass pressure bottle and the mixture was heated at 120 °C in an oil bath for 2 hours with continuous stirring. A clear gel formed was allowed to cool down to room temperature prior to the addition of ethanol (equal volume to the gel). The mixture was vigorously stirred at room temperature for 10 minutes then centrifuged at 3500 rpm for 10 minutes. The supernatant was decanted and fresh ethanol was added into the starch residue. The solvent exchange process was repeated a further four times with ethanol and a further three times with toluene if required. The suspended starch in toluene was utilised in films production. The dried gelatinised starch utilised in analysis in order to investigate the properties of starch, was dried in a vacuum oven at 50 °C overnight.

#### **7.4.1.2 Retrogradation**

After gelatinisation process (section 7.4.1.1), the clear gel obtained was placed in a refrigerator at 4-5 °C for 4 days. The retrograded starch subsequently underwent the solvent exchange process with ethanol as described for the gelatinised starch in previous section. The solvent exchange with toluene adopts the similar method and the procedure was repeated three times. The drying of the starch was conducted in a vacuum oven at 50 °C overnight.

### 7.4.2 BET surface area measurement

Nitrogen adsorption/desorption isotherms were conducted using a Micrometrics ASAP 2010 volumetric adsorption analyser at 77 K. Prior to analysis, the samples were degassed at 65 °C for at least 3 hours under reduced pressure and mass differences were corrected after the experiment. The surface area of samples was automatically calculated by the Micrometrics ASAP 2010 volumetric adsorption analyser. The isotherm data were subjected to the BET method to obtain the BET specific surface area results ( $S_{\text{BET}}$ ).<sup>339</sup>

### 7.4.3 Powder X-ray diffraction

X-ray diffraction patterns of dried native and expanded starch were obtained using a Bruker-AXS D8 advance diffractometer, which is equipped with a Cu  $K_{\alpha}$  radiation source. Scans were taken across the angular range of 2.5–40  $2\theta$  with a 45 kV voltage and 20 mA current. The measurements were carried out with assistance from Emma Cooper.

### 7.4.4 Film preparation

Native or expanded starch suspended in toluene (dry weight = 1.75 g) was placed in a 30 mL glass vessel, followed by 3.5 g of ELO. The mixture was stirred with a high-speed overhead mixer (2000 rpm) at 120 °C until constant weight. Then 3.5 g of Pripol and 0.044 g of DMAP (0.5% of the total resin weight) were added into the mixture, which was mixed at 120 °C for a further 3 minutes. The mixture was subsequently poured into a 70 mL aluminium tray (inner diameter = 70 mm) and cured in an oven at 140 °C for 2 hours.

## 7.5 Experimental details and instrumentation for chapter 5

### 7.5.1 Esterification of starch

Acetylated starch was prepared by adding 5 g (30.9 mmol) of expanded starch in toluene (dry weight) in a 250 mL two-necked round bottom flask and to this, 70 mL of

toluene was added followed by the 8.74 mL (92.6 mmol) of acetic anhydride. The mixture was heated at 90 °C with stirring for 15 minutes then 0.4 g (3.28 mmol) of 4-dimethylaminopyridine (DMAP) was added. The reaction was maintained at 90 °C for 24 hours with continuous stirring. The mixture was allowed to cool down to room temperature and 50 mL of ethanol was added, and then the slurry was stirred for 3 minutes. The mixture was centrifuged at 3500 rpm for 10 minutes and the solvent exchange process was repeated for a further four times. Esterification with other anhydrides was performed using the same procedure and replacing the acetic anhydride with required anhydride. The same molar amount of anhydrides was added (9.08 g for maleic anhydride, 9.27 g for succinic anhydride and 10.38 g for itaconic anhydride) in an attempt to achieve the degree of substitution of three. The esterified starches were dried in a vacuum oven at 50 °C overnight.

### 7.5.2 Determination of degree of substitution by titration

The degree of substitution of esterified starches was determined using the titration method described by Wurzburg, which involves complete basic hydrolysis of the linkages, followed by the titration of excess alkali.<sup>320</sup> Finely ground esterified starch was accurately weighed (1 g) and placed in a 250 mL conical flask, in which 50 mL of 75% ethanol in distilled water was added. The slurry was stirred at 50 °C for 30 minutes and then cooled down to room temperature. 40 mL of potassium hydroxide solution (0.5 mol/L) was added into the mixture, which was left at room temperature for 72 hours with stirring. Excess alkali was back titrated by 0.5 mol/L hydrochloric acid using phenolphthalein as indicator. The mixture was allowed to stand for further 2 hours and additional alkali that probably leached from the sample was titrated. Unmodified starch, which was used as the starting material for the esterification, was treated in the same manner in order to obtain the blank value. The degree of substitution was then calculated using *Equations 5.1-5.8*.

### 7.5.3 Film preparation

1.75 g of unmodified or esterified expanded starch suspended in ethanol and 3.5 g of ELO were placed in a 30 mL glass vessel. The mixture was stirred with a high-speed overhead mixer (2000 rpm) at 120 °C until constant weight. Pripol (3.5 g) and DMAP

(0.044 g) (0.5% of the total resin weight) were subsequently added into the mixture, which was mixed at 120 °C for a further 3 minutes. The mixture was poured into a 70 mL aluminium tray (inner diameter = 70 mm) and cured in an oven at 140 °C for 2 hours, except for maleated starch film, which needed 4 hours of curing.

#### **7.5.4 Thermogravimetric-Fourier transform infrared spectroscopy (TG-FTIR)**

An accurately weighed sample (~100 mg for starch samples and ~20 mg for pure chemical samples) was placed in a dry and clean porcelain sample cup, which was heated from 25 °C to 500 °C (400 °C for pure chemical samples) at 10 °/min using a Netzsch 409 Simultaneous Thermal Analyser under N<sub>2</sub> at 100 mL/min. FTIR spectra of the volatiles are recorded using a Bruker EQUINOX-55 FT instrument equipped with a liquid N<sub>2</sub> cooled MCT detector with a resolution of 4 cm<sup>-1</sup> and 32 scans.

The crude results were obtained in seconds and were converted into temperature using the following equation:

$$Temperature(^{\circ}C) = \left\{ \left[ \frac{Time(sec)}{60} \right] \times 10 \right\} + initial\ temperature$$

## **7.6 Experimental details and instrumentation for chapters 2, 3 and 4**

### **7.6.1 Viscosity measurement**

The viscosity of the mixtures was studied using a Brookfield R/S – CPS plus rheometer. Isothermal measurements were performed at 140 °C with steady shear rate of 30 s<sup>-1</sup> until the extent of the reaction reached the limit of the instrument. The gap between the cone and the plate was set at 0.5 mm. The gel point was defined as the point at which the diverging steady state viscosity becomes infinite.<sup>203, 205</sup>

## 7.7 Experimental details and instrumentation for chapters 2, 3, 4 and 5

### 7.7.1 Mechanical Test

The resulting films were cut into standard dumbbell shapes (60 mm x 10 mm). Film thickness was in the region of 1–1.5 mm. Tensile studies were conducted in triplicate using an Instron 3367 universal testing machine fitted with 1000 N capacity load cell. The initial grip separation was set at 35 mm and the crosshead speed was 20 mm min<sup>-1</sup>. The results reported were the averages of the three measurements. However, two sets of three specimens were tested in some cases to ensure the accuracy of the test.

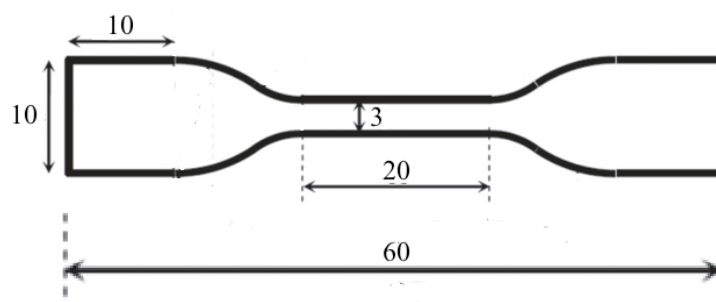


**Figure 7.1 – Dumbbell specimen for tensile test (scales are in millimetre)**

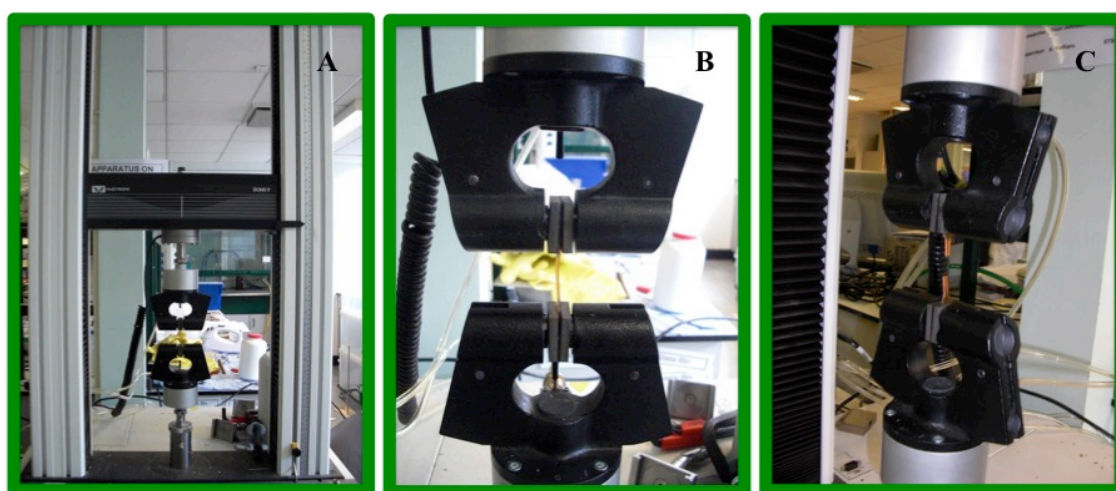


**Figure 7.2 – Instron 3367 universal testing machine (A), sample before the test (B) and after the test (C) (Originally in colour)**

### 7.7.2 Water uptake

All the resulting films were cut into approximate 50 mg sample pieces, which were suspended in distilled water at room temperature for 24 hours and then dried and re-weighed. The average water uptake was determined from at least three experiments and calculated using the formulation:

$$\text{Water uptake} = \frac{W_f - W_i}{W_i} \times 100\%$$

where,  $W_i$  is the initial weight of the film and  $W_f$  is the final weight of the film after drying.

### 7.7.3 Thermal decomposition temperature of cured films

The decomposition temperature was determined using a Stanton Redcroft STA 625 (TG/DSC). The samples were heated at 10 °C/minute from 25 °C to 625 °C under a nitrogen atmosphere. The gas flow was set at 60 mL/min. The sample was accurately weighed in the region of 10-15 mg in an aluminium STA pan. All measurements were recorded against an empty aluminium reference pan. The analysis was performed using the dedicated software for the Stanton Redcroft STA 625. The decomposition temperature was determined as the peak temperature of the DTG curves.

### 7.7.4 Modulated differential scanning calorimetry

The thermal events during the curing of the reaction mixtures were investigated using a TA Q2000 modulated differential scanning calorimeter (MDSC). The mixtures were accurately weighted (10 mg) into high pressure stainless steel pans, sealed and subjected to a heat-cool cycle from -80 °C to 250 °C at 1 °C min<sup>-1</sup>. The samples were then cooled down to -80 °C once more prior to heating to 250 °C. The analysis was performed using TA Universal Analysis 2000 program. The heat of reaction was determined from the area under the cure thermogram. Peak and onset temperatures were automatically generated whilst the heat of reaction was established. The glass transition



temperature was determined from the second heating cycle using the TA installed program. An empty pan was used as reference for all the measurements.

### **7.7.5 Infrared spectroscopy**

Infrared spectra were recorded using a Bruker Vertex 70 Spectrometer in attenuated total reflectance (ATR) mode, using a resolution of  $2\text{ cm}^{-1}$  and 32 scans. All spectra were normalised using OPUS software as provided by the instrument manufacturer.

In order to follow the curing reaction for each formulation, all components in the formulation were pre-mixed using a high-speed overhead stirrer (2000 rpm) in a 30 mL glass vessel ( $20\text{ }^{\circ}\text{C}$ ). Their initial spectrum was recorded ( $t = 0\text{ s}$ ) and then the mixture was cured in an aluminium tray at  $140\text{ }^{\circ}\text{C}$  with spectra recorded at required time.

## **7.8 Experimental details and instrumentation for chapters 3, 4 and 5**

### **7.8.1 Scanning electron microscopy**

Samples were mounted on alumina sample holders using double sided tape. Film samples were cut into small pieces of approximate dimension of  $2 \times 10\text{ mm}$  and the cross-section of the films can be seen on the top view. Prior to analysis samples were coated in a thin film of gold using a high resolution sputter SC-7640 coating device at a sputtering rate of  $1500\text{ V/min}$ . The samples were viewed on an JEOL JSM-6490LV (JEOL, Japan) at the Department of Biology, the University of York, under the supervision of Meg Stark and Karen Hodgkinson.

### **7.8.2 Solid-state $^{13}\text{C}$ CP MAS NMR analysis**

Solid-state  $^{13}\text{C}$  CP MAS NMR measurements were conducted by Dr David Apperley of solid-state NMR service at the University of Durham. The spectra were obtained using a Varian VNMRS spectrometer operating at  $100.56\text{ MHz}$  for  $^{13}\text{C}$ . Spectral referencing is with respect to neat tetramethylsilane. All measurements were conducted at ambient temperature.



# Chapter 8

## *Conclusions and further work*



## 8.1 Conclusions

Bio-based thermoset composites were prepared from epoxidised linseed oil and bio-derived crosslinkers, including succinic anhydride, succinic acid, itaconic anhydride, itaconic anhydride and long-chain dimer fatty acid, Pripol 1009. The resin containing Pripol yielded a transparent film with good flexibility and thus was chosen for further studies. Thermal analysis revealed that the optimum ratio of ELO and Pripol was 50:50% wt. This formulation exhibited the highest enthalpy of the curing reaction, which indicated the greatest degree of polymerisation in the resin. It was demonstrated that the use of an amine catalyst not only accelerated the curing process but, also enhanced the mechanical properties of the products. The use of a relatively small amount of DMAP as catalyst in the formulation (0.5-1% with respect to the total weight of the resin) gave the products with the greatest mechanical properties. The production of the film was optimised and the mixture cured at 160 °C for 1 hour yielded a film with the best mechanical properties. Moreover, the resulting films showed excellent water resistance and good thermal stability. The reaction mechanism of the system was investigated using infrared spectroscopy and thermal analysis. The IR data suggested the formation of carboxylate anion, resulting from the deprotonation of the acid group(s) in Pripol, occurring at the beginning of the reaction. The carboxylate ion then acted as a nucleophile in the ring-opening of the epoxide resulting in an alkoxide, which could be protonated to form an alcohol. The alcohol formed continued to react with more epoxide and consequently created the polymerised network. The base catalysts assisted the proton transfer in the system. This was in agreement with the thermal analysis using modulated differential scanning calorimetry. The thermograms showed that the curing process occurred in two steps, assigned to the formation of alkoxide from the epoxide ring opening and the etherification of alcohol formed in the first reaction and oxirane ring.

The optimised formulation comprised of ELO, Pripol and 0.5% DMAP was subsequently combined with native or modified starches in order to improve the composite properties. Modifications of starch included acid hydrolysis, expansion and esterification. Normal corn starch and high amylose corn starch were acid treated and the subsequent investigation of the starch properties, including solubility, swelling power and pasting, confirmed that the modification had occurred. The tensile tests

revealed that the inclusion of starch significantly enhanced the mechanical properties of the resins. The native high amylose starch film exhibited greater tensile strength, compared to that of native normal corn starch, owing to the smaller granule size of the high amylose starch. The 24-hour acid hydrolysed starch showed a 71.1% enhancement in Young's modulus compared to that of the film with no added starch. This is potentially due to the change in configuration and the appearance of cracks and fissures caused by the acid treatment. This increased the surface area of the granules, leading to better interfacial adhesion of the starch granules and the polymer matrix and resulted in improved mechanical properties. SEM micrograms of the cross-section of these films showed a phase-separation and some voids were observed between the starch granules in the 24-hour hydrolysed starch film. However, no cavity was observed in the native high amylose starch film, indicating better miscibility of the high amylose starch granules in the polymer matrix. This result suggested that the small granules of high amylose starch benefited the film properties. Moreover, the high surface area also helped improve the mechanical properties of the resin. Therefore, the further work was dedicated to the expansion of starch, which opened up the starch granules and yielded a high surface area material.

High amylose corn starch was gelatinised and retrograded, followed by the characterisation of the products. The porous structure of the gelatinised and retrograded starches was revealed by SEM and the surface area of these starches was confirmed using porosimetry (adsorption isotherm). Native, gelatinised and retrograded starches were added in to the formulation with ELO, Pripol and DMAP. The tensile testing of the resulting films showed that gelatinised and retrograded starches significantly enhanced the mechanical properties of the films. The influence of the amount of starch added on the properties of the films was studied and the optimum features was achieved with 20% wt. of gelatinised starch in the formulation. This mixture yielded a film with 227% improvement in tensile strength and 166% enhancement in Young's modulus, compared to those with no added starch. In contrast to the film with native starch, which showed a phase-separation on to cross-section, the films with expanded starch demonstrated uniform dispersion of starch granules in the polymer matrix. This was attributed to the porous structure of modified starch, which improved the interfacial adhesion between starch filler and the polymer matrix, leading to homogeneous resins. Moreover, this porous structure gave rise to better coverage of the granules by the

polymer, resulting in lower water uptake of modified starch films compared to that of native starch film. A positive correlation was observed between the water uptake of the films and the filler content. Thermogravimetric study of the resulting films with starch revealed two major mass losses, whilst the film without starch demonstrated a single significant mass loss. DTG curves displayed the first weight loss observed on the TG thermogram at around 300 °C, which became more significant when more starch was present in the formulation. This indicated that this weight loss corresponded to the decomposition of starch. The second weight loss in starch films occurred at similar temperature range as that of the film without starch, suggesting this major weight loss corresponded to the decomposition of the crosslinked resin. Additionally, DTG curves revealed that the resin with no starch added in fact experienced two-stage decomposition. The first stage was partially associated with unreacted ELO but mainly related to the polymerised material. The second stage was attributed to the highly crosslinked parts of the resin, which was reported to have good thermal stability. Interestingly, the second stage of the resin decomposition became more significant when starch was present in the formulation, suggesting that the proportion of highly crosslinked became greater in the presence of starch. This was in good agreement with the thermal study of the curing process, which demonstrated that higher enthalpy of the reaction and higher  $T_g$  were obtained when starch was present in the mixture, indicating greater degree of crosslinking could be achieved with starch. Infrared spectra showed that starch might promote the curing process by aiding the ring-opening reaction. Thermal study and the gel time investigation of reaction mixture demonstrated that the presence of starch in the mixture delayed the curing reaction, possibly caused by the steric hindrance.

The preparation of esterified starches was conducted using acetic, maleic, succinic and itaconic anhydrides. The modification was ascertained using IR and NMR characterisation and degree of substitution was determined using titration method. Acetylated starch demonstrated the highest DS, owing to good accessibility of the carbonyl carbon, which facilitate the nucleophilic addition in the first step of substitution reaction. The acetylated starch also showed better thermal stability than native starch, however other esterified starches decomposed at relatively low temperature. The low thermal stability of these esterified starches was due to the disintegration of intramolecular interactions such as hydrogen bonding in starch chains and the poor thermal stability of carboxylic group introduced onto the polymer after the

modification. TG-FTIR results revealed that two-phase decomposition of cyclic anhydride modified starches. The first phase of the decomposition corresponded to that of the substituent groups and the second phase was assigned to the decomposition of starch backbone. The mechanical properties of esterified starch films demonstrated no significant improvement over native starch. A decrease in tensile strength was observed for all the esterified starch films. However, the films with acetylated starch and itaconic anhydride modified starch exhibited a modest enhancement in Young's modulus. Moreover, the acetylated starch film showed better transparency compared to that of unmodified starch. The water resistance of the films considerably improved when esterified starches were incorporated in the films instead of native starch. The films with acetylated and succinic anhydride modified starches demonstrated the water uptake of 0.7% and 0.8% respectively. These values were comparable to that of the film without starch included (0.4%). All the films demonstrated excellent thermal stability, in particular the film with acetylated starch, which was thermally stable up to the temperature of 310 °C.

These bio-based thermoset composites with extremely high content of bio-derived materials were subsequently compared to thermoset resins obtained from relatively similar system and commonly used petroleum derived polymers, such as LDPE and PVC. The film produced from the formulation comprising of 20%wt. of gelatinised starch, ELO, Pripol and 0.5% DMAP (with respect to the total resin weight) exhibited comparable or superior mechanical properties to the resins of similar system. Although more work is needed to improve the mechanical properties of these bio-based films to match those of the petroleum-derived polymers, other properties including water resistance and thermal stability demonstrated promising results. ELO based composites showed good water resistance despite the presence of 20% w/w of starch. The water uptake of the film with acetylated starch was comparable to that of PVC wearlayer. Moreover, in contrast to PVC, the ELO based resins exhibited excellent thermal stability. These composites remained stable up to the temperature of 310 °C, whilst PVC started to decompose at around 150 °C and produced hazardous gases such as hydrogen chloride. The use of these renewable resources helps move the composites towards greener and more sustainable products.



## 8.2 Further work

Production process plays an important role in determining the performance of materials, hence other manufacturing methods such as extrusion presents an interesting approach in attempt to improve the mechanical properties of the products.

Other modifications of starch, which introduces hydrophobic groups to the starch backbone, can improve the compatibility of the starch filler in the polymer matrix, resulting in better mechanical properties. Modification of starch with fatty acid is an interesting technique as fatty acids can be derived from renewable resources and these modified starches have demonstrated a good thermal stability.<sup>340</sup> Surface modification of starch would be another interesting method to increase the compatibility of starch filler.

It would be of interest to use other biopolymers such as cellulose and lignin or naturally derived plant fibres as fillers in the formulation. These materials have exhibited an excellent reinforcement in composites in many occasions.<sup>341-343</sup> However, the products would be suitable for applications in which transparency is not required.

It would be of interest to investigate the behaviour of other vegetable oils in the similar system. For instance, epoxidised soybean oil, which is abundantly available, and tung oil, which processes high degree of unsaturation that can potentially give rise to a great degree of crosslinking.



# Appendix A



## A.2 Chapter 2

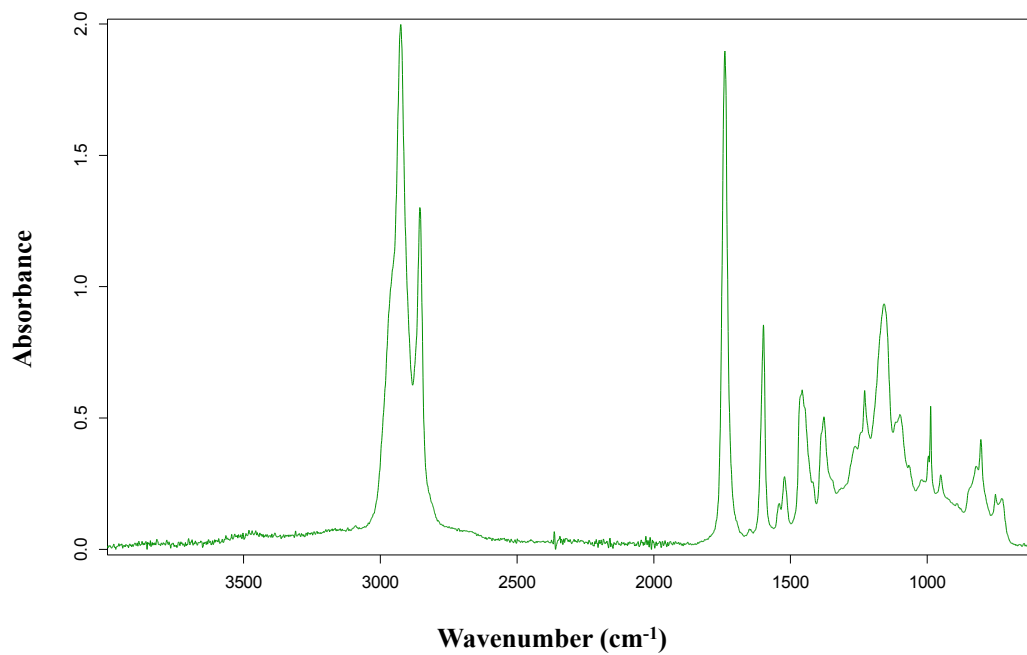


**Figure A.2.1 – Infrared spectrum of ELO and DMAP before curing**

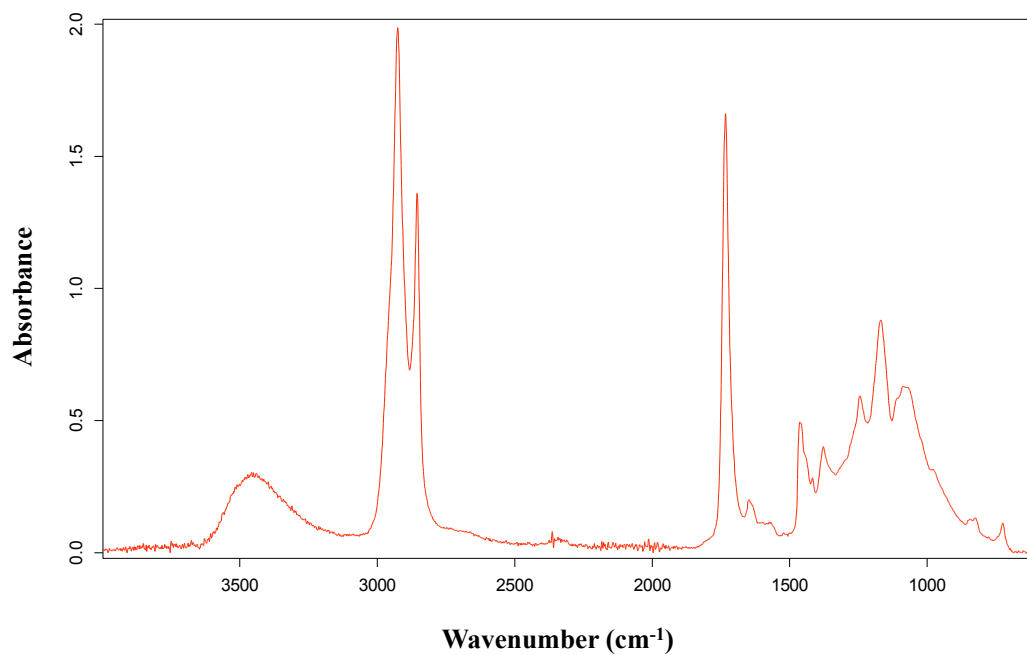


**Figure A.2.2 – Infrared spectrum of ELO and DMAP after curing**

## A.4 Chapter 4

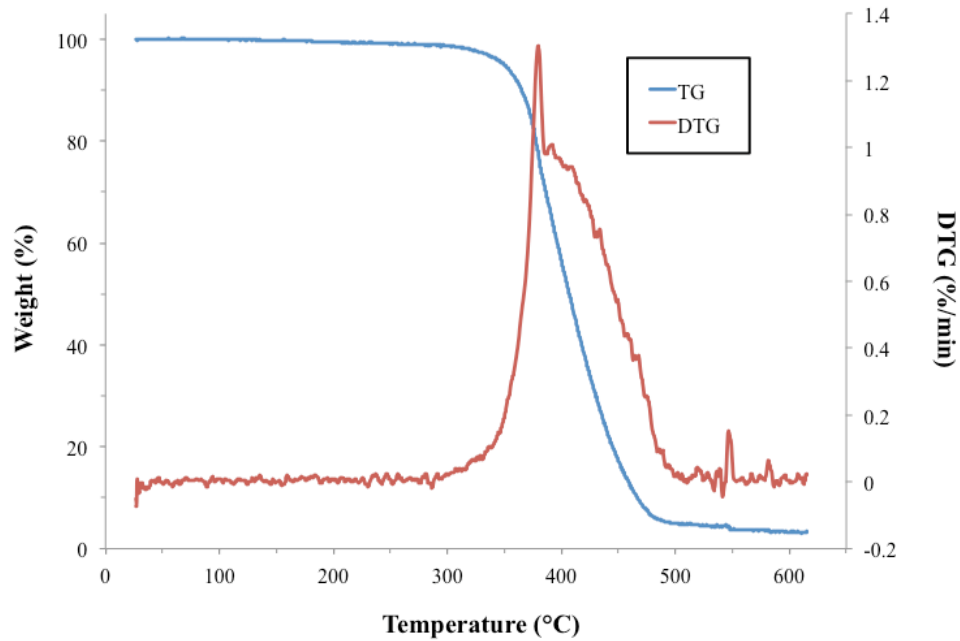


**Figure A.4.1 – TG and DTG curves of epoxidised linseed oil (25-625°C, 10 °C/min)**

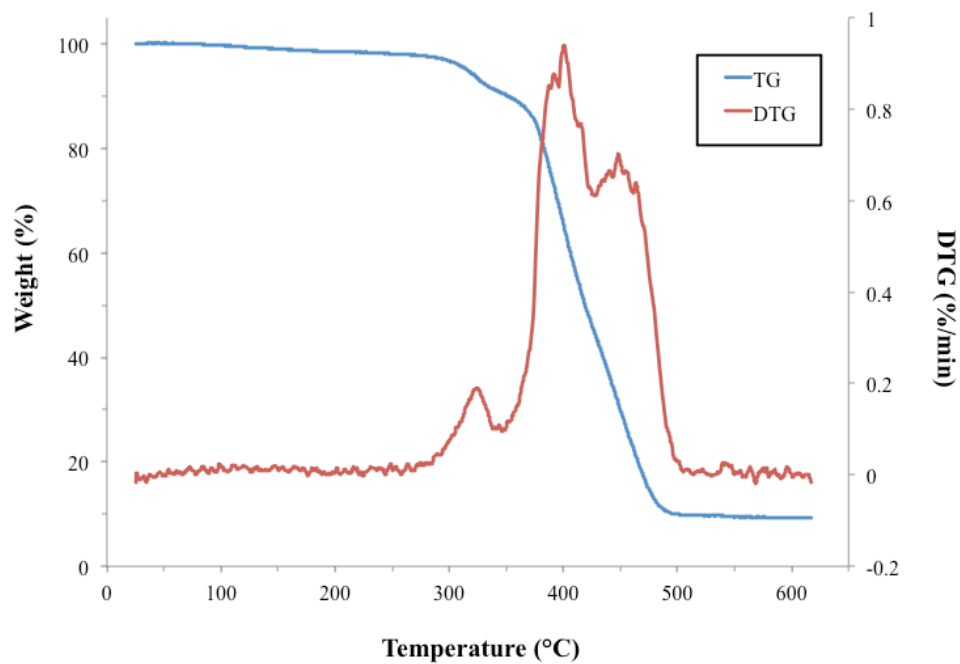


**Figure A.4.2 – TG and DTG curves of film with native high amylose starch (25-625°C, 10 °C/min)**

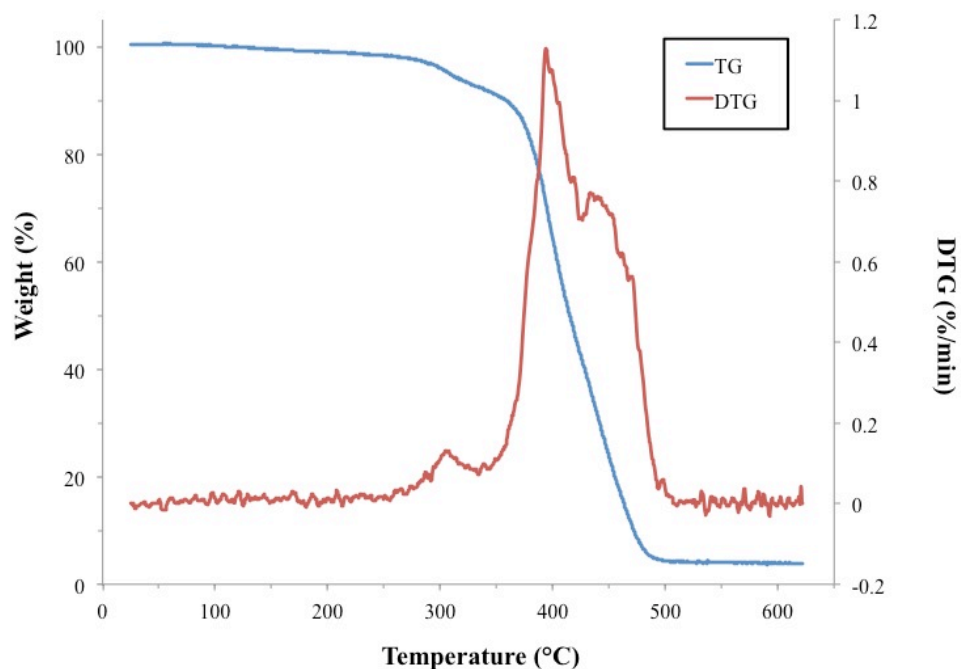


**Figure A.4.3 – TG and DTG curves of film with gelatinised high amylose starch (25-625°C, 10 °C/min)**

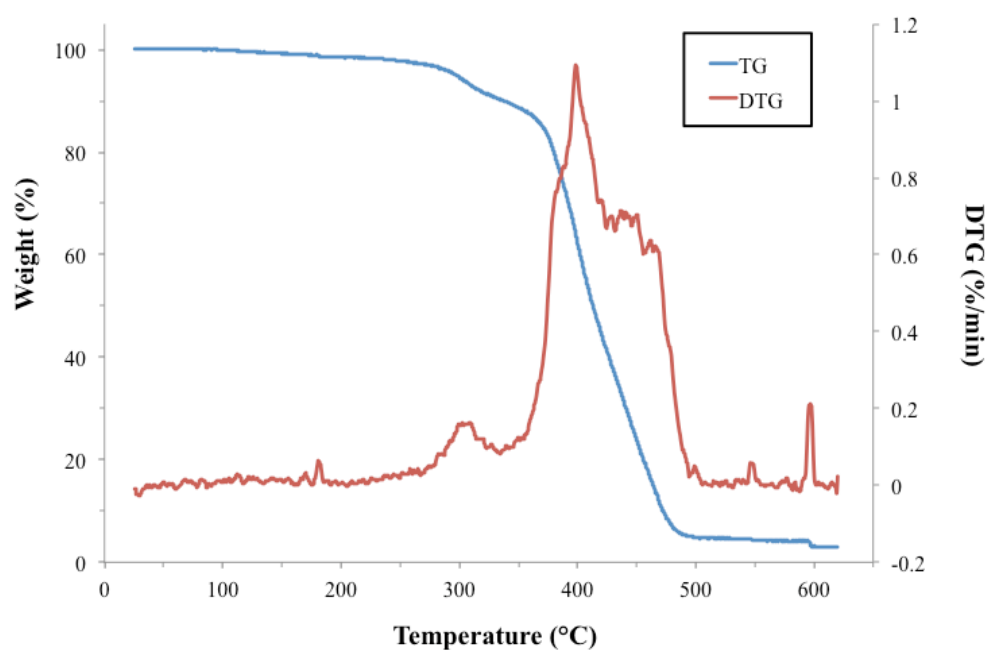


**Figure A.4.4 – TG and DTG curves of film with retrograded high amylose starch (25-625°C, 10 °C/min)**

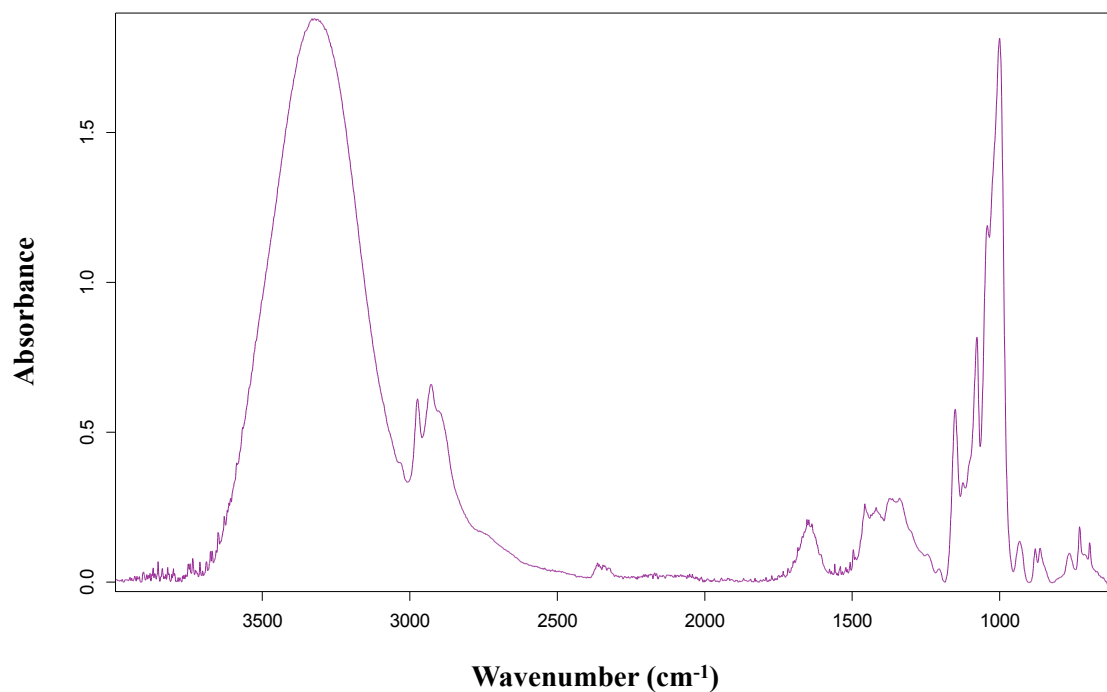


**Figure A.4.5 – Infrared spectrum of expanded starch in toluene**

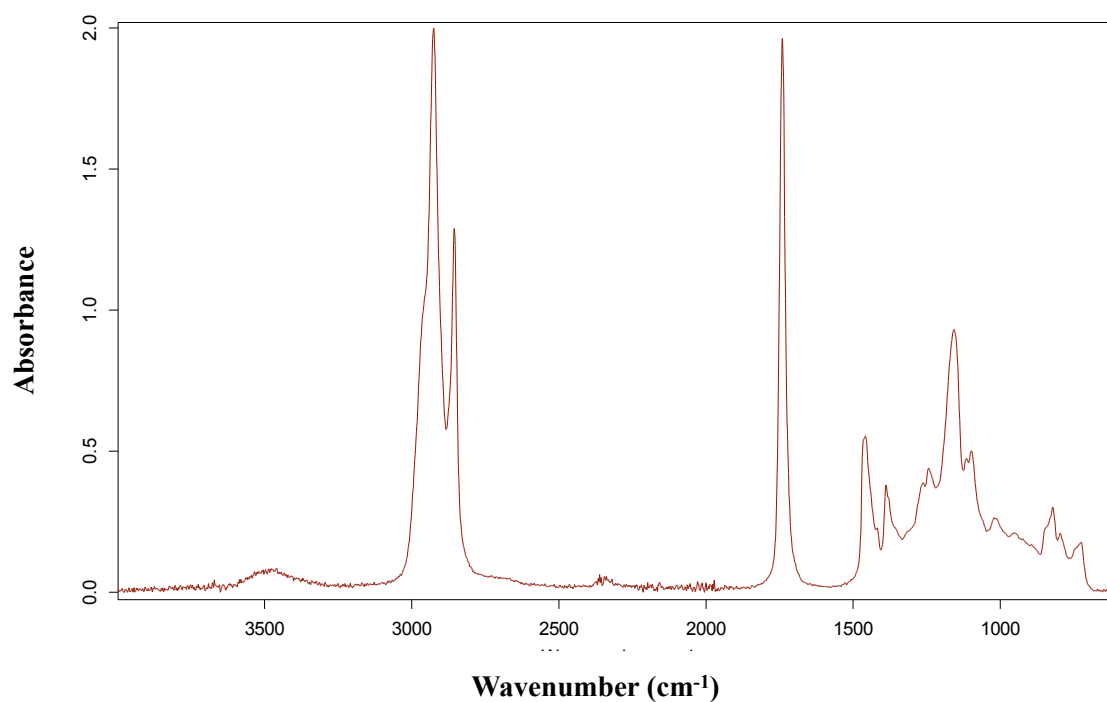


**Figure A.4.6 – Infrared spectrum of homopolymerisation of ELO**



## A.5 Chapter 5

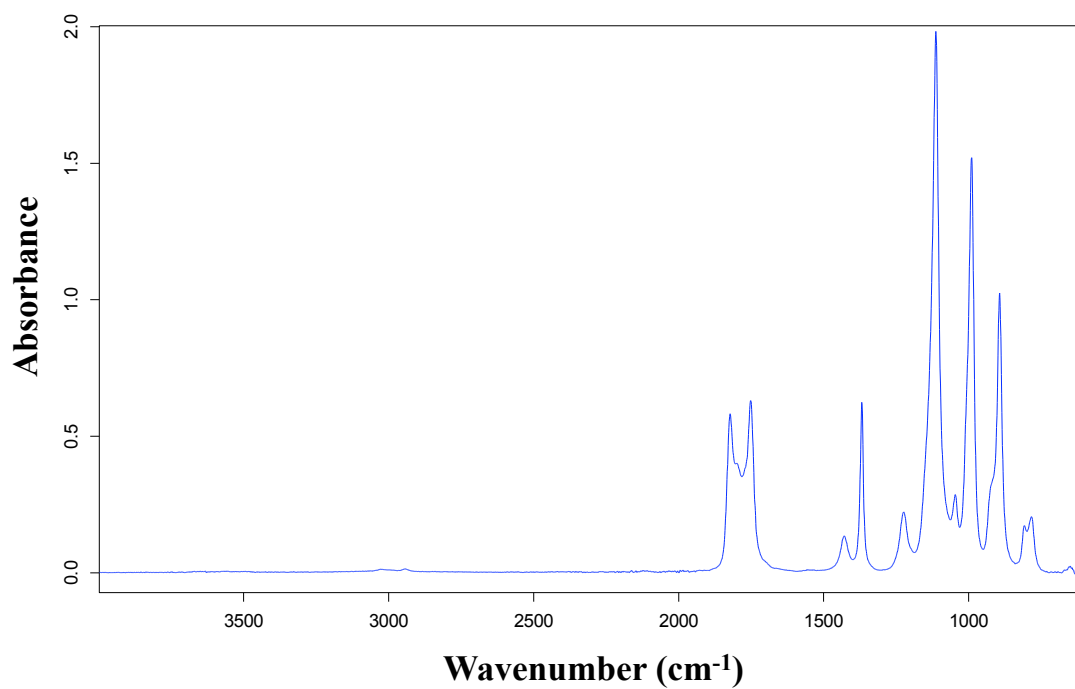


Figure A.5.1 – Infrared spectrum of acetic anhydride

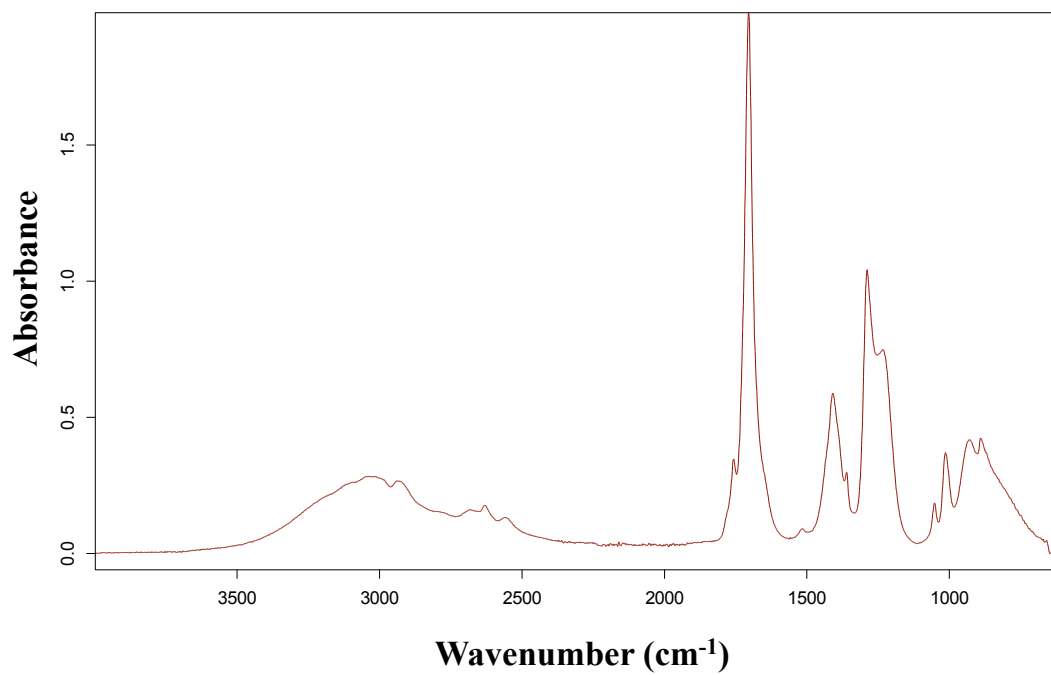
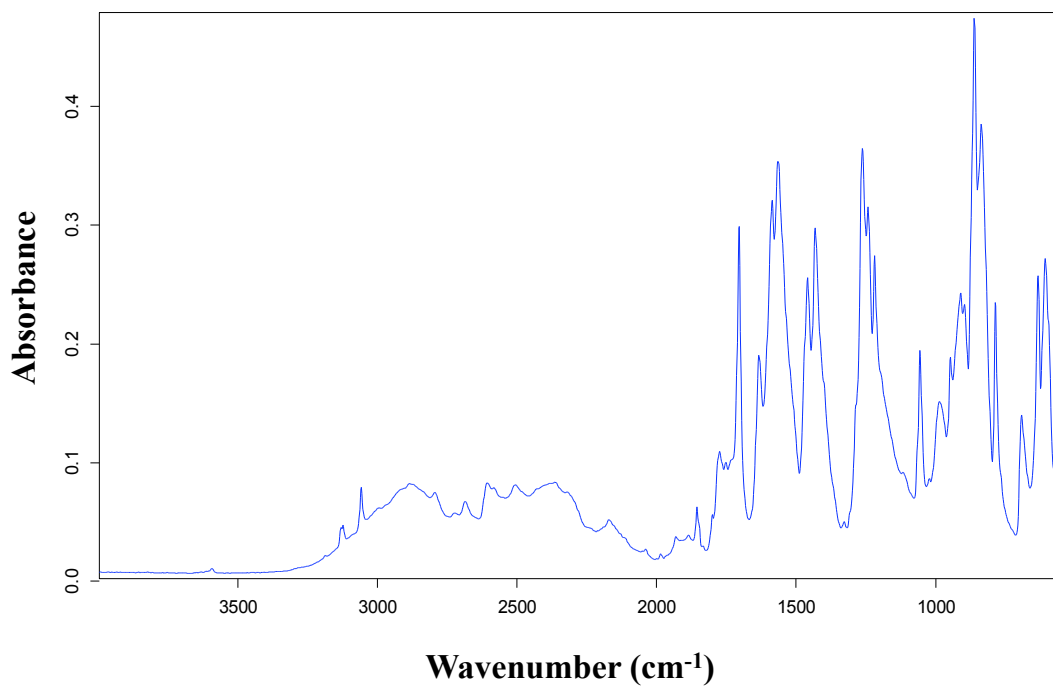
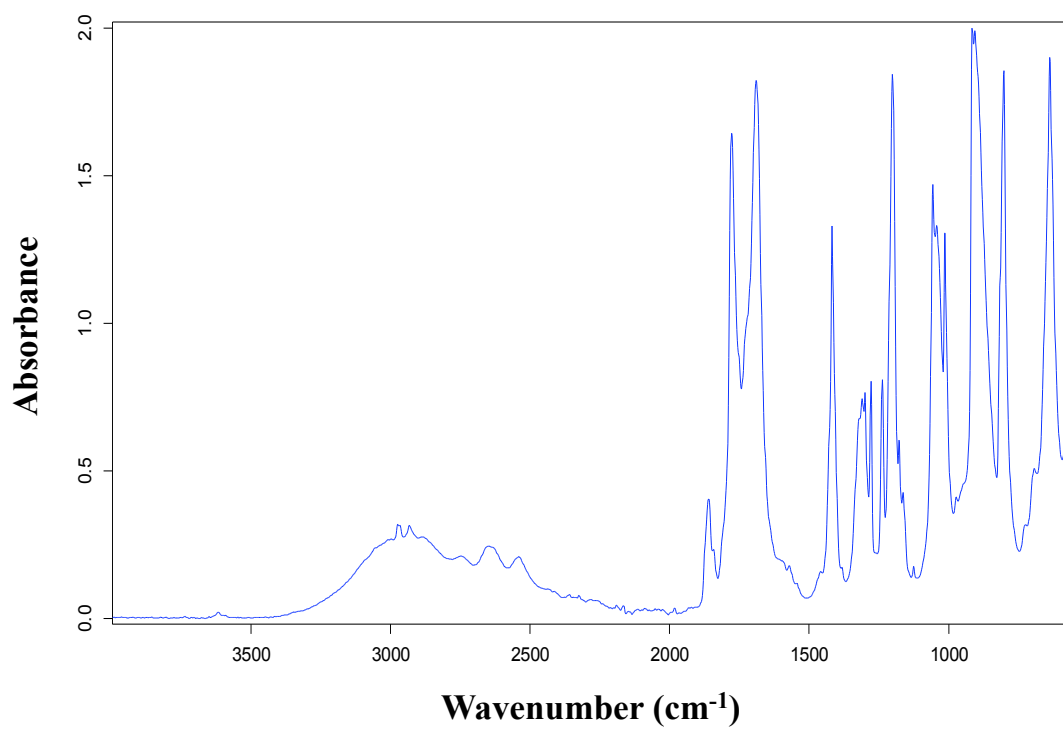


Figure A.5.2 – Infrared spectrum of acetic acid



**Figure A.5.3 – Infrared spectrum of maleic anhydride**



**Figure A.5.4 – Infrared spectrum of succinic anhydride**

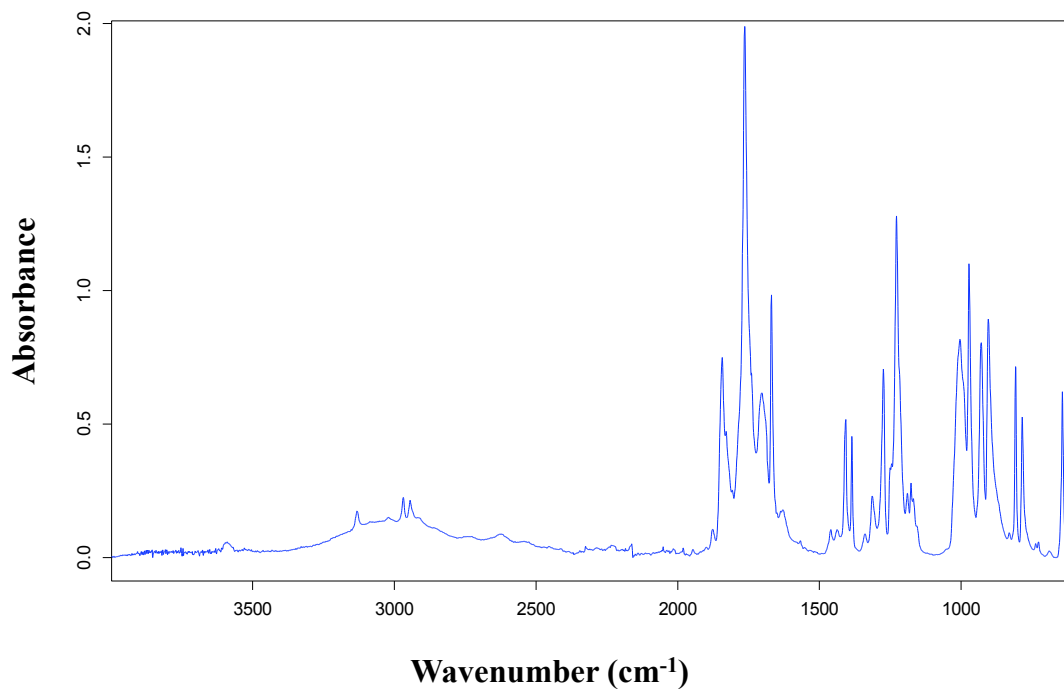


**Figure A.5.5 – Infrared spectrum of itaconic anhydride**

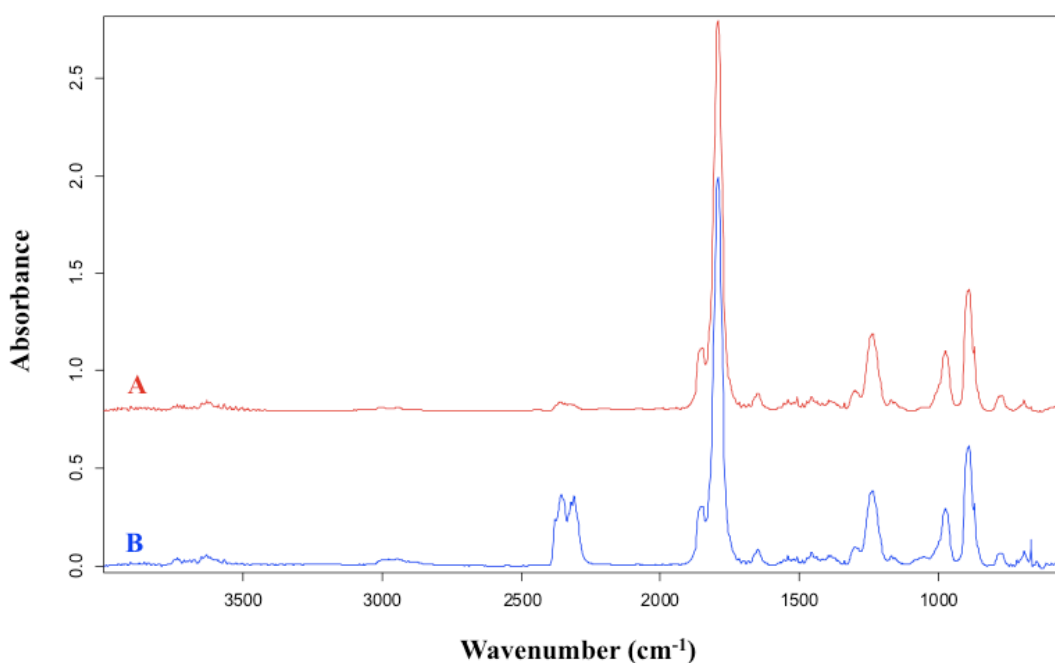


**Figure A.5.6 – IR spectra of evolved gases from TG-FTIR analysis of A) itaconic acid and B) itaconic anhydride modified starch**

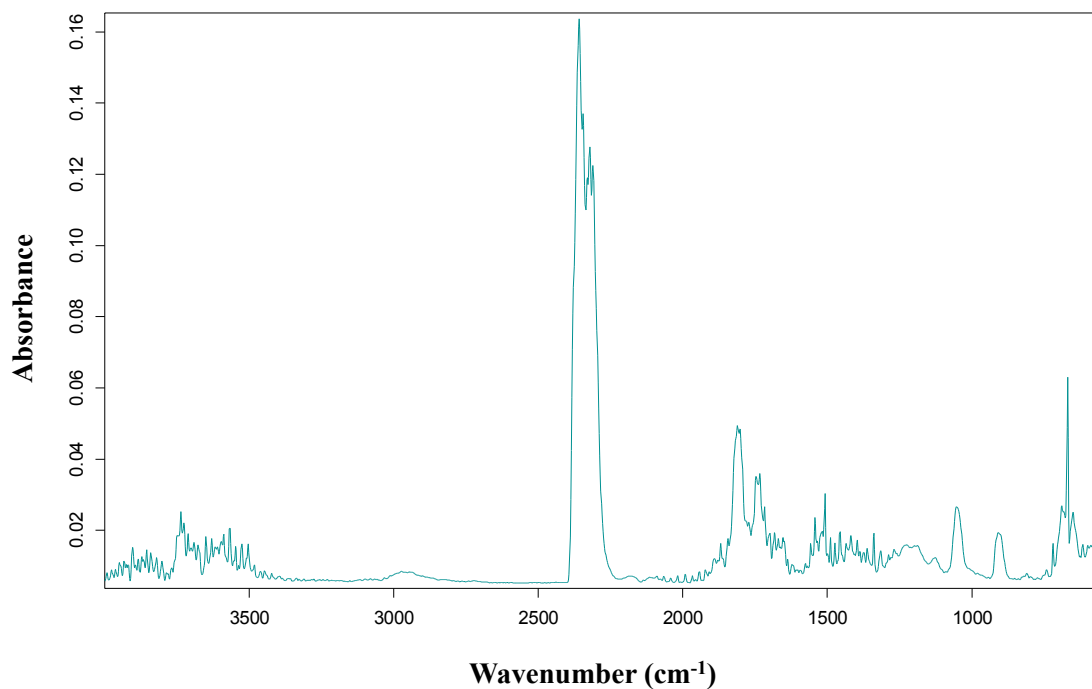


**Figure A.5.7 – Infrared spectrum of succinic anhydride modified starch taken at the maximum rate of decomposition (286.33 °C)**

# Glossary



---

1-MeIm	-	1-methylimidazole
2-MeIm	-	2-methylimidazole
Ace	-	Acetylated starch
AFM	-	Atomic force microscopy
AIER	-	Acidic ion exchange resin
ATR	-	Attenuated total reflectance
BPH	-	<i>N</i> -benzylpyraziniumhexafluoroantimonate
CP MAS NMR	-	Cross polarisation Magic angle spinning solid state Nuclear magnetic resonance
cP	-	Centipoise
Da	-	Dalton
DBU	-	1,8-diazabicyclo [5.4.0] undec-7-ene
DGEBA	-	Diglycidyl ether of bisphenol-A
DMAP	-	4-dimethylaminopyridine
DS	-	Degree of substitution
DSC	-	Differential scanning calorimetry
DTG	-	Derivative thermogravimetry
ECO	-	Epoxidised castor oil
ELO	-	Epoxidised linseed oil
EPO	-	Epoxidised plant oils
ESO	-	Epoxidised soybean oil
FTIR	-	Fourier transform infrared
G-POSS	-	3-glycidylpropylheptaisobutyl-T8-polyhedral oligomeric silsesquioxane
GS	-	Gelatinised starch
HAS	-	High amylose corn starch
HDPE	-	High-density polyethylene

---

IR	-	Infrared spectroscopy
Ita	-	Itaconic anhydride modified starch
J	-	Joule
LDPE	-	Low-density polyethylene
LO	-	Linseed oil
Mal	-	Maleated starch
MDSC	-	Modulated differential scanning calorimetry
MMT	-	Million metric tonnes
mmol	-	millimoles
mol/L	-	moles per litre
PCL	-	Polycaprolactone
PET	-	Polyethylene terephthalate
PHA	-	Hydroxyl alkanoate
PHB	-	Poly (3-hydroxybutyrate)
PHBV	-	Poly (hydroxybutyrate-co-valerate)
PLA	-	Polylactic acid
PP	-	Pripol
ppm	-	Parts per million
PU	-	Polyurethane
PVA	-	Polyvinyl alcohol
PVC	-	Polyvinyl chloride
PVC	-	polyvinyl chloride
rpm	-	Revolutions per minute
RS	-	Retrograded starch
SEM	-	Scanning electron microscopy
STA	-	Simultaneous thermal analysis
Suc	-	Succinic anhydride modified starch



TEA	-	Triethylamine
$T_g$	-	Glass transition temperature
TG	-	Thermogravimetry
TPS	-	Thermoplastic starch
W	-	Watt
XRD	-	X-ray diffraction



# References



1. N. Munier, *Introduction to Sustainability: Road to a Better Future*, Springer, Dordrecht, 2005, p. 1.
2. J. Blewitt, *Understanding sustainable development*, Earthscan, Padstow, 2008, pp. 15-16.
3. United Nations World Commission on Environment and Development, *Our Common Future (Brundtland Report)*, Oxford, 1987.
4. S. I. Rodriguez, M. S. Roman, S. C. Sturhahn and E. H. Terry, *Sustainability Assessment and Reporting for the University of Michigan's Ann Arbor Campus*, University of Michigan, Ann Arbor, 2002.
5. The United Nations, *Report of the United Nations Conference on Environment and Development*, New York, 1993.
6. J. Schummer, B. Bensaude-Vincent and B. v. Tiggelen, *The Public Image of Chemistry*, World Scientific Publishing, Singapore, 2007, p. 1.
7. P. T. Anastas and J. C. Warner, *Green Chemistry: Theory and Practice*, Oxford University Press, New York, 1998, p. 30.
8. R. B. Seymour and C. E. Carraher, *Polymer Chemistry: An introduction*, Marcel Dekker Inc., New York, 1981, p. 1.
9. A. D. McNaught and A. Wilkinson, *IUPAC Compendium of Chemical Terminology (the "Gold Book")*, 2nd edn., Oxford, 1997, p. 2289.
10. N. Karak, *Fundamentals of Polymers: Raw Materials to Finish Products*, PHI, New Delhi, 2009, p. 101.
11. A. Ashori, *Bioresource Technol.*, 2008, **99**, 4661-4667.
12. M.-S. Lin, C.-C. Liu and C.-T. Lee, *J. Appl. Polym. Sci.*, 1999, **72**, 585-592.
13. P. P. Klemchuk, *Polym. Degrad. Stabil.*, 1990, **27**, 183-202.
14. M. Fliieger, M. Kantorová, A. Prell, T. Řezanka and J. Votruba, *Folia Microbiol.*, 2003, **48**, 27-44.
15. M. A. R. Meier, J. O. Metzger and U. S. Schubert, *Chem. Soc. Rev.*, 2007, **36**, 1788-1802.
16. R. P. Wool and X. S. Sun, *Bio-based polymers and composites*, Elsevier Academic Press, 2005, pp. 56-113.
17. United States Department of Agriculture - Foreign Agriculture Service, *Major Vegetable oils: World Supply and Distribution*, <http://www.fas.usda.gov>, 2011, accessed 16/04/12

18. U. Biermann, U. Bornscheuer, M. A. R. Meier and J. O. Metzger, *Angew. Chem. Int. Edit.*, 2011, **50**, 3854-3871.
19. N. J. Fox and G. W. Stachowiak, *Tribol. Int.*, 2007, **40**, 1035-1046.
20. B. M. Abdullah and J. Salimon, *Journal of Applied Sciences*, 2010, **10**, 1545-1553.
21. Y. Xia and R. C. Larock, *Green Chem.*, 2010, **12**, 1893-1909.
22. H. Wexler, *Chem. Rev.*, 1964, **64**, 591-611.
23. F. Gregg and C. Goodwin, *SVO: powering your vehicle with straight vegetable oil*, New Society Publishers, Gabriola Island, 2008, p. 32.
24. D. d. S. Martini, B. A. Braga and D. Samios, *Polymer*, 2009, **50**, 2919-2925.
25. A. Köckritz and A. Martin, *Eur. J. Lipid Sci. Tech.*, 2008, **110**, 812-824.
26. J. C. Mol, *Top. Catal.*, 2004, **27**, 97-104.
27. H. L. Ngo and T. A. Foglia, *J. Am. Oil Chem. Soc.*, 2007, **84**, 777-784.
28. J. McMurry, *Organic Chemistry*, 4th edn., Brooks/Cole, Pacific Grove, 1996, pp. 684-685.
29. F. E. Okieimen, O. I. Bakare and C. O. Okieimen, *Ind. Crop. Prod.*, 2002, **15**, 139-144.
30. M. Rüschen Klaas and S. Warwel, *Org. Lett.*, 1999, **1**, 1025-1026.
31. M. Rüschen Klaas and S. Warwel, *Ind. Crop. Prod.*, 1999, **9**, 125-132.
32. S. Sinadinović-Fišer, M. Janković and Z. S. Petrović, *J. Am. Oil Chem. Soc.*, 2001, **78**, 725-731.
33. R. Mungroo, N. Pradhan, V. Goud and A. Dalai, *J. Am. Oil Chem. Soc.*, 2008, **85**, 887-896.
34. V. V. Goud, A. V. Patwardhan, S. Dinda and N. C. Pradhan, *Chem. Eng. Sci.*, 2007, **62**, 4065-4076.
35. I. Hilker, D. Bothe, J. Prüss and H. J. Warnecke, *Chem. Eng. Sci.*, 2001, **56**, 427-432.
36. R. S. Schneider, L. R. S. Lara, T. B. Bitencourt, M. d. G. Nascimento and M. R. d. S. Nunes, *J. Brazil. Chem. Soc.*, 2009, **20**, 1473-1477.
37. S. Warwel and M. Rüschen Klaas, *J. Mol. Catal. B- Enzym*, 1995, **1**, 29-35.
38. A. Campanella, M. A. Baltanas, M. C. Capel-Sanchez, J. M. Campos-Martin and J. L. G. Fierro, *Green Chem.*, 2004, **6**, 330-334.
39. J. M. Sobczak and J. J. Ziółkowski, *Appl. Catal. A-Gen*, 2003, **248**, 261-268.

40. M. T. Benaniba, N. Belhaneche-Bensemra and G. Gelbard, *Eur. J. Lipid Sci. Tech.*, 2007, **109**, 1186-1193.
41. A. E. Gerbase, J. R. Gregório, M. Martinelli, M. C. Brasil and A. N. F. Mendes, *J. Am. Oil Chem. Soc.*, 2002, **79**, 179-181.
42. S. Dinda, A. V. Patwardhan, V. V. Goud and N. C. Pradhan, *Bioresource Technol.*, 2008, **99**, 3737-3744.
43. J. M. Raquez, M. Deléglise, M. F. Lacrampe and P. Krawczak, *Prog. Polym. Sci.*, **35**, 487-509.
44. S. Chakrapani and J. V. Crivello, *J. Macromol. Sci. A* 1998, **35**, 691-710.
45. R. A. Ortiz, D. P. López, M. d. L. G. Cisneros, J. C. R. Valverde and J. V. Crivello, *Polymer*, 2005, **46**, 1535-1541.
46. J. V. Crivello and R. Narayan, *Chem. Mater.*, 1992, **4**, 692-699.
47. S.-J. Park, F.-L. Jin, J.-R. Lee and J.-S. Shin, *Euro. Polym. J.*, 2005, **41**, 231-237.
48. S.-J. Park, F.-L. Jin and J.-R. Lee, *Macromol. Rapid Comm.*, 2004, **25**, 724-727.
49. N. Boquillon and C. Fringant, *Polymer*, 2000, **41**, 8603-8613.
50. A. E. Gerbase, C. L. Petzhold and A. O. Costa, *J. Am. Oil Chem. Soc.*, 2002, **79**, 797-802.
51. S. Tan and W. Chow, *J. Am. Oil Chem. Soc.*, 2011, **88**, 915-923.
52. F.-L. Jin and S.-J. Park, *Mater. Sci. Eng. A-Struct.*, 2008, **478**, 402-405.
53. S.-J. Park, F.-L. Jin and J.-R. Lee, *Macromol. Chem. Physic.*, 2004, **205**, 2048-2054.
54. F.-L. Jin and S.-J. Park, *Polym. Int.*, 2008, **57**, 577-583.
55. G. Lligadas, J. C. Ronda, M. Galià and V. Cádiz, *Biomacromolecules*, 2006, **7**, 3521-3526.
56. H. Uyama, M. Kuwabara, T. Tsujimoto, M. Nakano, A. Usuki and S. Kobayashi, *Chem. Mater.*, 2003, **15**, 2492-2494.
57. J. D. J. van den Berg, N. D. Vermist, L. Carlyle, M. Holčapek and J. J. Boon, *J. Sep. Sci.*, 2004, **27**, 181-199.
58. J. W. Stanley Taft and J. W. Mayer, *The Science of Paintings*, Springer, New York, 2000, p. 36.
59. J. Mallégol, J. Lemaire and J.-L. Gardette, *Prog. Org. Coat.*, 2000, **39**, 107-113.
60. R. T. Holman, *Prog. Chem. Fats other Lipids*, 1954, **2**, 51-98.

61. C. Stenberg, M. Svensson and M. Johansson, *Ind. Crop. Prod.*, 2005, **21**, 263-272.
62. O. Zovi, L. Lecamp, C. Loutelier-Bourhis, C. M. Lange and C. Bunel, *Eur. J. Lipid Sci. Tech.*, **113**, 616-626.
63. S. J. Tuman, D. Chamberlain, K. M. Scholsky and M. D. Soucek, *Prog. Org. Coat.*, 1996, **28**, 251-258.
64. R. van Gorkum and E. Bouwman, *Coordin. Chem. Rev.*, 2005, **249**, 1709-1728.
65. E. R. Mueller, *Ind. Eng. Chem.*, 1954, **46**, 562-569.
66. E. Rudnik, A. Szczucinska, H. Gwardiak, A. Szulc and A. Winiarska, *Thermochim. Acta*, 2001, **370**, 135-140.
67. P. Eyerer, M. Weller and C. Hübner, *Polymers - Opportunities and Risk II: Sustainability, Product Design and Processing*, Springer, Berlin, 2010, p. 122.
68. J. Chen, M. D. Soucek, W. J. Simonsick and R. W. Celikay, *Polymer*, 2002, **43**, 5379-5389.
69. L. J. González-Ortiz, M. Arellano, M. J. Sánchez-Peña, E. Mendizábal and C. F. Jasso-Gastinel, *Polym. Degrad. Stabil.*, 2006, **91**, 2715-2722.
70. J. T. P. Derksen, F. Petrus Cuperus and P. Kolster, *Prog. Org. Coat.*, 1996, **27**, 45-53.
71. J. Powell, *Linoleum*, Gibbs Smith Publisher, Layton, 2003, p. 22.
72. M. N. Belgacem and A. Gandini, *Monomers, Polymers and Composites from Renewable Resources*, Elsevier, Oxford, 2008, p. 321.
73. A. Blennow, M. Hansen, A. Schulz, K. Jorgensen, A. M. Donald and J. Sanderson, *J. Struct. Biol.*, 2003, **143**, 229-241.
74. C. F. Ostertag, in *Cassava Flour and Starch: Progress in Research and Development*, eds. D. Dufour, O. B. G. M. and R. Best, CIAT Publication, Montpellier, 1996, p. 105.
75. International Starch Institute, <http://www.starch.dk/isi/market/index.asp>, 2008, accessed 10/05/12
76. R. P. Ellis, M. P. Cochrane, M. F. B. Dale, C. M. Duffus, A. Lynn, I. M. Morrison, R. D. M. Prentice, J. S. Swanston and S. A. Tiller, *J. Sci. Food. Agr.*, 1998, **77**, 289-311.
77. S. Srichuwong, T. C. Sunarti, T. Mishima, N. Isono and M. Hisamatsu, *Carbohyd. Polym.*, 2005, **60**, 529-538.



78. F. K. Gleason and R. Chollet, *Plant Biochemistry*, Jones & Bartlett Learning, Sudbury, 2012, p. 39.
79. A. Blennow, A. Mette Bay-Smidt and R. Bauer, *Int. J. Biol. Macromol.*, 2001, **28**, 409-420.
80. J. P. Mua and D. S. Jackson, *J. Agr. Food. Chem.*, 1997, **45**, 3840-3847.
81. M. Asaoka, K. Okuno and H. Fuwa, *Agr. Biol. Chem.*, 1985, **49**, 373-379.
82. W. R. Morrison and M. N. Azudin, *J. Cereal. Sci.*, 1987, **5**, 35-44.
83. P. J. Jenkins and A. M. Donald, *Int. J. Biol. Macromol.*, 1995, **17**, 315-321.
84. W. Amass, A. Amass and B. Tighe, *Polym. Int.*, 1998, **47**, 89-144.
85. P. Myllärinen, R. Partanen, J. Seppälä and P. Forssell, *Carbohydr. Polym.*, 2002, **50**, 355-361.
86. N. Singh, J. Singh, L. Kaur, N. Singh Sodhi and B. Singh Gill, *Food Chem.*, 2003, **81**, 219-231.
87. C. Martinez and J. Prodolliet, *Starch - Stärke*, 1996, **48**, 81-85.
88. G. T. Oostergetel and E. F. J. van Bruggen, *Carbohydr. Polym.*, 1993, **21**, 7-12.
89. R. F. Tester, J. Karkalas and X. Qi, *J. Cereal. Sci.*, 2004, **39**, 151-165.
90. D. J. Gallant, B. Bouchet and P. M. Baldwin, *Carbohydr. Polym.*, 1997, **32**, 177-191.
91. J.-L. Putaux, S. Molina-Boisseau, T. Momaur and A. Dufresne, *Biomacromolecules*, 2003, **4**, 1198-1202.
92. T. A. Waigh, P. Perry, C. Riekkel, M. J. Gidley and A. M. Donald, *Macromolecules*, 1998, **31**, 7980-7984.
93. A. C. Bertolini, *Starches: Characterization, Properties and Applications*, CRC Press, Boca Raton, 2010, p. 2.
94. M. Sujka and J. Jamroz, *LWT - Food Sci. Technol.*, 2009, **42**, 1219-1224.
95. M. A. Whittam, T. R. Noel and S. G. Ring, *Int. J. Biol. Macromol.*, 1990, **12**, 359-362.
96. C. Gernat, S. Radosta, G. Damaschun and F. Schierbaum, *Starch - Stärke*, 1990, **42**, 175-178.
97. I. A. M. Appelqvist and M. R. M. Debet, *Food Rev. Int.*, 1997, **13**, 163-224.
98. D. LeCorre, J. Bras and A. Dufresne, *Biomacromolecules*, 2011, **12**, 3039-3046.
99. J. J. M. Swinkels, *Starch - Stärke*, 1985, **37**, 1-5.
100. M. William R, *J. Cereal. Sci.*, 1988, **8**, 1-15.
101. R. F. Tester, X. Qi and J. Karkalas, *Anim. Feed Sci. Tech.*, 2006, **130**, 39-54.

102. A. E. McPherson and J. Jane, *Carbohydr. Polym.*, 1999, **40**, 57-70.
103. S. A. S. Craig, C. D. Maningat, P. A. Seib and R. C. Hosney, *Cereal Chem.*, 1989, **66**, 173-182.
104. C. Simi and T. Emilia Abraham, *Bioproc. Biosyst. Eng.*, 2007, **30**, 173-180.
105. J. N. Bemiller, *Starch - Stärke*, 1997, **49**, 127-131.
106. R. N. Tharanathan, *Crit. Rev. Food Sci.*, 2005, **45**, 371-384.
107. T. Y. Bogracheva, V. J. Morris, S. G. Ring and C. L. Hedley, *Biopolymers*, 1998, **45**, 323-332.
108. A. Vázquez, M. L. Foresti and V. Cyras, in *Biopolymers - New materials for Sustainable Films and Coatings*, ed. D. Plackett, John Wiley and Sons Ltd, Chichester, 2011, pp. 16-19.
109. T. Vasanthan and R. S. Bhatta, *Cereal Chem.*, 1996, **73**, 199-207.
110. A. G. Maaruf, Y. B. Che Man, B. A. Asbi, A. H. Junainah and J. F. Kennedy, *Carbohydr. Polym.*, 2001, **46**, 331-337.
111. R. C. Hosney, K. J. Zeleznak and D. A. Yost, *Starch - Stärke*, 1986, **38**, 407-409.
112. P. J. Jenkins and A. M. Donald, *Carbohydr. Res.*, 1998, **308**, 133-147.
113. D. Cooke and M. J. Gidley, *Carbohydr. Res.*, 1992, **227**, 103-112.
114. R. F. Tester and W. R. Morrison, *Cereal Chem.*, 1990, **67**, 551-557.
115. I. Tan, C. C. Wee, P. A. Sopade and P. J. Halley, *Carbohydr. Polym.*, 2004, **58**, 191-204.
116. J.-I. Jane, in *Chemical and Functional Properties of Food Saccharides*, ed. P. Tomasik, CRC Press, Boca Raton, 2004, pp. 91-92.
117. A.-C. Eliasson and A. Tatham, in *Cereals and Cereal Products: Chemistry and Technology*, eds. David A. V. Dendy and B. J. Dobrzaczyk, Aspen Publishers, Gaithersburg, 2001, p. 74.
118. A. A. Karim, M. H. Norziah and C. C. Seow, *Food Chem.*, 2000, **71**, 9-36.
119. M. J. Miles, V. J. Morris, P. D. Orford and S. G. Ring, *Carbohydr. Res.*, 1985, **135**, 271-281.
120. M. J. Miles, V. J. Morris and S. G. Ring, *Carbohydr. Res.*, 1985, **135**, 257-269.
121. S. G. Ring, P. Colonna, K. J. I'Anson, M. T. Kalichevsky, M. J. Miles, V. J. Morris and P. D. Orford, *Carbohydr. Res.*, 1987, **162**, 277-293.
122. K. J. Zeleznak and R. C. Hosney, *Cereal Chem.*, 1986, **63**, 407-411.
123. M. Gudmundsson, *Thermochim. Acta*, 1994, **246**, 329-341.

124. J. Jane, Y. Y. Chen, L. F. Lee, A. E. McPherson, K. S. Wong, M. Radosavljevic and T. Kasemsuwan, *Cereal Chem.*, 1999, **76**, 629-637.
125. C. V. Leeb and H. P. Schuchmann, in *Product Design and Engineering*, eds. Ulrich Bröckel, Willi Meier and G. Wagner, Wiley-VCH, Weinheim, 2007, vol. 2, p. 404.
126. P. S. Shuttleworth, Switchable adhesives for carpet tiles, Ph.D. Thesis, University of York, 2007.
127. J. W. Mullen and E. Pacsu, *Ind. Eng. Chem.*, 1943, **35**, 381-384.
128. A. Biswas, R. L. Shogren, G. Selling, J. Salch, J. L. Willett and C. M. Buchanan, *Carbohydr. Polym.*, 2008, **74**, 137-141.
129. M. M. Tessler and R. L. Billmers, *J. Polym. Environ.*, 1996, **4**, 85-89.
130. J. M. Fang, P. A. Fowler, J. Tomkinson and C. A. S. Hill, *Carbohydr. Polym.*, 2002, **47**, 245-252.
131. A. D. Betancur, G. L. Chel and H. E. Cañizares, *J. Agr. Food Chem.*, 1997, **45**, 378-382.
132. J. Singh, L. Kaur and N. Singh, *Starch - Stärke*, 2004, **56**, 586-601.
133. R. G. Rohwer and R. E. Klem, in *Starch: Chemistry and Technology*, 2nd edition, eds. J. N. Bemiller and R. L. Whistler, Academic Press, San Diego, 2nd edn., 1984, pp. 529-541.
134. L. Jayakody and R. Hoover, *Food Res. Int.*, 2002, **35**, 665-680.
135. K. Singh Sandhu, N. Singh and S.-T. Lim, *LWT - Food Sci. Technol.*, 2007, **40**, 1527-1536.
136. V. Singh and S. Z. Ali, *Int. J. Food Prop.*, 2008, **11**, 495-507.
137. R. Hoover, *Food Rev. Int.*, 2000, **16**, 369-392.
138. S. Pal, D. Mal and R. P. Singh, *Carbohydr. Polym.*, 2005, **59**, 417-423.
139. Y.-J. Wang and L. Wang, *Carbohydr. Polym.*, 2003, **52**, 207-217.
140. R. E. Wing and J. L. Willett, *Ind. Crop. Prod.*, 1997, **7**, 45-52.
141. R. E. Harmon, S. K. Gupta and J. Johnson, *Starch - Stärke*, 1971, **23**, 197-199.
142. C.-w. Chiu and D. Solarek, in *Starch: Chemistry and technology*, 3rd edition, eds. James N. Bemiller and R. L. Whistler, Academic Press, Burlington, 2009, pp. 629-656.
143. K. Woo and P. A. Seib, *Carbohydr. Polym.*, 1997, **33**, 263-271.
144. A. N. Jyothi, S. N. Moorthy and K. N. Rajasekharan, *Starch - Stärke*, 2006, **58**, 292-299.

145. R. Kavitha and J. N. BeMiller, *Carbohydr. Polym.*, 1998, **37**, 115-121.
146. S.-G. Choi and W. L. Kerr, *LWT - Food Sci. Technol.*, 2003, **36**, 105-112.
147. C. C. Seow and K. Thevamalar, *Starch - Stärke*, 1993, **45**, 85-88.
148. L. Griffin Gerald J, in *Fillers and Reinforcements for Plastics*, eds. Rudolph D. Deanin and N. R. Schott, AMERICAN CHEMICAL SOCIETY, 1974, vol. 134, pp. 159-170.
149. N. St-Pierre, B. D. Favis, B. A. Ramsay, J. A. Ramsay and H. Verhoogt, *Polymer*, 1997, **38**, 647-655.
150. J. L. Willet, in *Starch: Chemistry and technology, 3rd edition*, eds. J. N. Bemiller and R. L. Whistler, Academic Press, Burlington, 2009, pp. 715-745.
151. R. Chandra and R. Rustgi, *Polym. Degrad. Stabil.*, 1997, **56**, 185-202.
152. C.-Y. Huang, M.-L. Roan, M.-C. Kuo and W.-L. Lu, *Polym. Degrad. Stabil.*, 2005, **90**, 95-105.
153. R. L. Evangelista, W. Sung, J. L. Jane, R. J. Gelina and Z. L. Nikolov, *Ind. Eng. Chem. Res.*, 1991, **30**, 1841-1846.
154. C. Nawrath, Y. Poirier and C. Somerville, *Mol. Breeding*, 1995, **1**, 105-122.
155. C. W. Pouton and S. Akhtar, *Adv. Drug Deliver. Rev.*, 1996, **18**, 133-162.
156. S. Godbole, S. Gote, M. Latkar and T. Chakrabarti, *Bioresource Technol.*, 2003, **86**, 33-37.
157. R. Datta, S.-P. Tsai, P. Bonsignore, S.-H. Moon and J. R. Frank, *FEMS Microbiol. Rev.*, 1995, **16**, 221-231.
158. H. Wang, X. Sun and P. Seib, *J. Appl. Polym. Sci.*, 2001, **82**, 1761-1767.
159. J.-F. Zhang and X. Sun, *Biomacromolecules*, 2004, **5**, 1446-1451.
160. L. Averous, L. Moro, P. Dole and C. Fringant, *Polymer*, 2000, **41**, 4157-4167.
161. M. F. Koenig and S. J. Huang, *Polymer*, 1995, **36**, 1877-1882.
162. L. Mao, S. Imam, S. Gordon, P. Cinelli and E. Chiellini, *J. Polym. Environ.*, 2000, **8**, 205-211.
163. Z. Guohua, L. Ya, F. Cuilan, Z. Min, Z. Caiqiong and C. Zongdao, *Polym. Degrad. Stabil.*, 2006, **91**, 703-711.
164. L. Chen, S. Imam, S. Gordon and R. Greene, *J. Polym. Environ.*, 1997, **5**, 111-117.
165. T. Bourtoom and M. S. Chinnan, *LWT - Food Sci. Technol.*, 2008, **41**, 1633-1641.

166. Y. X. Xu, K. M. Kim, M. A. Hanna and D. Nag, *Ind. Crop. Prod.*, 2005, **21**, 185-192.
167. E. Psomiadou, I. Arvanitoyannis and N. Yamamoto, *Carbohydr. Polym.*, 1996, **31**, 193-204.
168. M. L. Fishman, D. R. Coffin, R. P. Konstance and C. I. Onwulata, *Carbohydr. Polym.*, 2000, **41**, 317-325.
169. K. Desai, *AAPS PharmSciTech*, 2005, **6**, E202-E208.
170. R. L. Cunningham, S. H. Gordon, F. C. Felker and K. Eskins, *J. Appl. Polym. Sci.*, 1998, **69**, 957-964.
171. Y. Lu, L. Tighzert, F. Berzin and S. Rondot, *Carbohydr. Polym.*, 2005, **61**, 174-182.
172. *US Pat.*, 5728476, 1998.
173. J. Rösch and R. Mülhaupt, *Polym. Bull.*, 1993, **31**, 679-685.
174. G. Merfeld, C. Molaison, R. Koeniger, A. E. Acar, S. Mordhorst, J. Suriano, P. Irwin, R. S. Warner, K. Gray, M. Smith, K. Kovaleski, G. Garrett, S. Finley, D. Meredith, M. Spicer and T. Naguy, *Prog. Org. Coat.*, 2005, **52**, 98-109.
175. L. Shechter, J. Wynstra and R. P. Kurkijy, *Ind. Eng. Chem.*, 1956, **48**, 86-93.
176. I. N. Zaripov, S. A. Nasybullin, L. M. Lazareva and I. N. Faizullin, *Polym. Sci. U.S.S.R.*, 1980, **22**, 707-715.
177. M. Fedtke, F. Domaratus and A. Pfitzmann, *Polym. Bull.*, 1990, **23**, 381-388.
178. M. Murayama, F. Sanda and T. Endo, *Macromolecules*, 1998, **31**, 919-923.
179. J. H. Clark, *Green Chem.*, 2006, **8**, 17-21.
180. J. H. Clark, *J. Chem. Technol. Biot.*, 2007, **82**, 603-609.
181. T. Werpy and G. Peterson, *Top Value Added Chemicals Form Biomass*, U.S. Department of Energy, 2004.
182. A. R. Mahendran, N. Aust, G. Wuzella and A. Kandelbauer, *Macromol. Symp.*, 2012, **311**, 18-27.
183. Z. Liu and S. Erhan, *J. Am. Oil Chem. Soc.*, 2010, **87**, 437-444.
184. C.-S. Wang, L.-T. Yang, B.-L. Ni and G. Shi, *J. Appl. Polym. Sci.*, 2009, **114**, 125-131.
185. F. I. Altuna, L. H. Espósito, R. A. Ruseckaite and P. M. Stefani, *J. Appl. Polym. Sci.*, 2011, **120**, 789-798.
186. Q. B. Reiznautt, I. T. S. Garcia and D. Samios, *Mater. Sci. Eng., C*, 2009, **29**, 2302-2311.

187. J. Rocks, L. Rintoul, F. Vohwinkel and G. George, *Polymer*, 2004, **45**, 6799-6811.
188. L. Matějka, S. Pokorný and K. Dušek, *Polym. Bull.*, 1982, **7**, 123-128.
189. M. S. Heise and G. C. Martin, *Macromolecules*, 1989, **22**, 99-104.
190. Y.-C. Chen, W.-Y. Chiu and K.-F. Lin, *J. Polym. Sci. Polym. Chem.*, 1999, **37**, 3233-3242.
191. Young Rok Ham, Sun Hee Kim, Young Jae Shin, Dong Ho Lee, Minhee Yang, Ji Hye Min and J. S. Shin, *J. Ind. Eng. Chem.*, 2010, **16**, 556-559.
192. A. Omrani, L. C. Simon, A. A. Rostami and M. Ghaemy, *Thermochim. Acta*, 2008, **468**, 39-48.
193. X. V. Zhang, J. K. Pugh and P. N. Ross, *Electrochem. Solid State Lett.*, 2001, **4**, A82-A84.
194. G. Dalimova and E. Kristallovich, *Chem. Nat. Compd.*, 1999, **35**, 465-468.
195. M. Pire, S. Norvez, I. Iliopoulos, B. Le Rossignol and L. Leibler, *Polymer*, **52**, 5243-5249.
196. W. Galezowski, A. Jarczewski, M. Stanczyk, B. Brzezinski, F. Bartl and G. Zundel, *J. Chem. Soc. Faraday T.*, 1997, **93**, 2515-2518.
197. D. J. Heldebrant, P. G. Jessop, C. A. Thomas, C. A. Eckert and C. L. Liotta, *J. Org. Chem.*, 2005, **70**, 5335-5338.
198. A. Huczynski, M. Ç. Ratajczak-Sitarz, A. Katrusiak and B. Brzezinski, *J. Mol. Struct.*, 2008, **888**, 84-91.
199. I. E. Dell'Erba and R. J. J. Williams, *Polym. Eng. Sci.*, 2006, **46**, 351-359.
200. L. Han, S.-J. Choi, M.-S. Park, S.-M. Lee, Y.-J. Kim, M.-I. Kim, B. Liu and D.-W. Park, *React. Kinet., Mech. Catal.*, 2012, **106**, 25-35.
201. L. Matějka, J. Lövy, S. Pokorný, K. Bouchal and K. Dušek, *J. Polym. Sci.: Polym. Chem. Ed.*, 1983, **21**, 2873-2885.
202. T. A. Osswald and G. Menges, *Materials Science of Polymers for Engineers, 2nd edition*, Hanser Gardner Publications, Inc., Cincinnati, 2003, p. 142.
203. S. Mortimer, A. J. Ryan and J. L. Stanford, *Macromolecules*, 2001, **34**, 2973-2980.
204. M. Wang, Y. Yu, X. Wu and S. Li, *Polymer*, 2004, **45**, 1253-1259.
205. H. H. Winter and F. Chambon, *J. Rheol.*, 1986, **30**, 367-382.
206. United States Department of Agriculture Foreign Agriculture Service, *Field crops - Production*, <http://www.fas.usda.gov>, 2011, accessed 31/08/12

207. R. P. Westhoff, F. H. Otey, C. L. Mehlretter and C. R. Russell, *Ind. Eng. Chem. Prod. Res. Dev.*, 1974, **13**, 123-125.
208. M. A. Kotnis, G. S. O'Brien and J. L. Willett, *J. Polym. Environ.*, 1995, **3**, 97-105.
209. S. Jacobsen and H. G. Fritz, *Polym. Eng. Sci.*, 1996, **36**, 2799-2804.
210. D. Thirathumthavorn and S. Charoenrein, *Starch - Stärke*, 2005, **57**, 217-222.
211. H.-J. Chung, H.-Y. Jeong and S.-T. Lim, *Carbohydr. Polym.*, 2003, **54**, 449-455.
212. Y.-L. Chung and H.-M. Lai, *Carbohydr. Polym.*, 2006, **63**, 527-534.
213. W.-P. Ma and J. F. Robyt, *Carbohydr. Res.*, 1987, **166**, 283-297.
214. J. F. Robyt, J.-y. Choe, J. D. Fox, R. S. Hahn and E. B. Fuchs, *Carbohydr. Res.*, 1996, **283**, 141-150.
215. E. Polaczek, F. Starzyk and P. Tomasik, *Carbohydr. Polym.*, 1999, **39**, 37-42.
216. H. Angellier, J.-L. Putaux, S. Molina-Boisseau, D. Dupeyre and A. Dufresne, *Macromol. Symp.*, 2005, **221**, 95-104.
217. P. J. Heald and B. Kristiansen, *Biotechnol. Bioeng.*, 1985, **27**, 1516-1519.
218. E. Kristo and C. G. Biliaderis, *Carbohydr. Polym.*, 2007, **68**, 146-158.
219. Y.-J. Wang, V.-D. Truong and L. Wang, *Carbohydr. Polym.*, 2003, **52**, 327-333.
220. J.-H. Lin, S.-Y. Lee and Y.-H. Chang, *Carbohydr. Polym.*, 2003, **53**, 475-482.
221. O. S. Lawal, K. O. Adebawale, B. M. Ogunsanwo, L. L. Barba and N. S. Ilo, *Int. J. Biol. Macromol.*, 2005, **35**, 71-79.
222. T. Komiya and S. Nara, *Starch - Stärke*, 1986, **38**, 9-13.
223. Z.-G. Luo, X. Fu, Q.-Y. Gao and S.-J. Yu, *Int. J. Food Sci. Tech.*, 2011, **46**, 429-435.
224. A. A. A. Soliman, N. A. El-Shinnawy and F. Mobarak, *Thermochim. Acta*, 1997, **296**, 149-153.
225. P. Aggarwal and D. Dollimore, *Thermochim. Acta*, 1998, **324**, 1-8.
226. R. Hashaikeh and H. Abushammala, *Carbohydr. Polym.*, 2011, **83**, 1088-1094.
227. C. M. Earnest, in *Compositional Analysis by Thermogravimetry*, ed. C. M. Earnest, American Society for Testing and Materials, Baltimore, 1988, p. 7.
228. Y. Leng, *Materials Characterization - Introduction to Microscopic and Spectroscopic methods*, John Wiley & Sons (Asia), Singapore, 2008, pp. 326-328.
229. P. Jiping, W. Shujun, Y. Jinglin, L. Hongyan, Y. Jiugao and G. Wenyuan, *Food Chem.*, 2007, **105**, 989-995.

- 
230. W. Shujun, Y. Jinglin, Y. Jiugao, C. Haixia and P. Jiping, *Food Hydrocolloids*, 2007, **21**, 1217-1222.
231. D. Schartz and R. L. Whistler, in *Starch: Chemistry and technology, 3rd edition*, eds. J. N. Bemiller and R. L. Whistler, Academic Press, Burlington, 2009, pp. 1-10.
232. Y.-C. Shi, T. Capitani, P. Trzasko and R. Jeffcoat, *J. Cereal. Sci.*, 1998, **27**, 289-299.
233. W. R. Morrison, R. F. Tester, M. J. Gidley and J. Karkalas, *Carbohydr. Res.*, 1993, **245**, 289-302.
234. J. H. Li, T. Vasanthan, B. Rossnagel and R. Hoover, *Food Chem.*, 2001, **74**, 407-415.
235. J. Gao, T. Vasanthan, R. Hoover and J. Li, *Starch - Stärke*, 2012, **64**, 313-325.
236. W. R. Morrison, R. F. Tester, C. E. Snape, R. Law and M. J. Gidley, *Cereal Chem.*, 1993, **70**, 385-391.
237. Y. Song and J. Jane, *Carbohydr. Polym.*, 2000, **41**, 365-377.
238. H. Tang and B. P. Hills, *Biomacromolecules*, 2003, **4**, 1269-1276.
239. R. P. Veregin, C. A. Fyfe, R. H. Marchessault and M. G. Taylor, *Macromolecules*, 1986, **19**, 1030-1034.
240. S. Wang, J. Yu and J. Yu, *Food Chem.*, 2008, **110**, 39-46.
241. P. Le Bail, F. G. Morin and R. H. Marchessault, *Int. J. Biol. Macromol.*, 1999, **26**, 193-200.
242. M. A. Osman, J. r. E. P. Rupp and U. W. Suter, *Polymer*, 2005, **46**, 1653-1660.
243. P. C. LeBaron, Z. Wang and T. J. Pinnavaia, *Appl. Clay Sci.*, 1999, **15**, 11-29.
244. S. Doi, J. H. Clark, D. J. Macquarrie and K. Milkowski, *Chem. Commun.*, 2002, **22**, 2632-2633.
245. R. Hoover, *Food Rev. Int.*, 1995, **11**, 331-346.
246. N. J. Atkin, R. M. Abeysekera, S. L. Cheng and A. W. Robards, *Carbohydr. Polym.*, 1998, **36**, 173-192.
247. A.-M. Hermansson and K. Svegmark, *Trends Food Sci. Tech.*, 1996, **7**, 345-353.
248. K. S. Sandhu, N. Singh and M. Kaur, *J. Food Eng.*, 2004, **64**, 119-127.
249. G. M. Glenn and D. W. Irving, *Cereal Chem.*, 1995, **72**, 155-161.
250. *US Pat.*, 5958589, 1999.



251. J. H. Clark, V. Budarin, F. E. I. Deswarte, J. J. E. Hardy, F. M. Kerton, A. J. Hunt, R. Luque, D. J. Macquarrie, K. Milkowski, A. Rodriguez, O. Samuel, S. J. Tavener, R. J. White and A. J. Wilson, *Green Chem.*, 2006, **8**, 853-860.
252. A. I. Bolivar, R. A. Venditti, J. J. Pawlak and K. El-Tahlawy, *Carbohydr. Polym.*, 2007, **69**, 262-271.
253. S. Doi, Novel starch materials for adsorbents and catalysts, Ph.D. Thesis, Univerisy of York, 2003.
254. M. J. Gronnow, R. Luque, D. J. Macquarrie and J. H. Clark, *Green Chem.*, 2005.
255. V. Budarin, J. H. Clark, F. E. I. Deswarte, J. J. E. Hardy, A. J. Hunt and F. M. Kerton, *Chem. Commun.*, 2005, **23**, 2903-2905.
256. J. W. Park, S. S. Im, S. H. Kim and Y. H. Kim, *Polym. Eng. Sci.*, 2000, **40**, 2539-2550.
257. C.-H. Kim, K. Y. Cho and J.-K. Park, *J. Appl. Polym. Sci.*, 2001, **81**, 1507-1516.
258. M. J. Gidley and P. V. Bulpin, *Carbohydr. Res.*, 1987, **161**, 291-300.
259. A. Shefer, S. Shefer, J. Kost and R. Langer, *Macromolecules*, 1992, **25**, 6756-6760.
260. K. R. Morgan, R. H. Furneaux and R. A. Stanley, *Carbohydr. Res.*, 1992, **235**, 15-22.
261. J. H. Hewitt, M. Linder and S. Pérez, *Carbohydr. Res.*, 1986, **154**, 1-13.
262. C. Rondeau-Mouro, G. Veronese and A. Buleon, *Biomacromolecules*, 2006, **7**, 2455-2460.
263. N. W. H. Cheetham and L. Tao, *Carbohydr. Polym.*, 1998, **36**, 285-292.
264. H. Liu, J. Lelievre and W. Ayoung-Chee, *Carbohydr. Res.*, 1991, **210**, 79-87.
265. J.-O. Kim, W.-S. Kim and M.-S. Shin, *Starch - Stärke*, 1997, **49**, 71-75.
266. C. J. A. M. Keetels, G. T. Oostergetel and T. Van Vliet, *Carbohydr. Polym.*, 1996, **30**, 61-64.
267. X. Zhang, J. Golding and I. Burgar, *Polymer*, 2002, **43**, 5791-5796.
268. R. J. White, V. Budarin, R. Luque, J. H. Clark and D. J. Macquarrie, *Chem. Soc. Rev.*, 2009, **38**, 3401-3418.
269. A. Dufresne, J.-Y. Cavallé and W. Helbert, *Macromolecules*, 1996, **29**, 7624-7626.
270. G. M. Glenn, S. H. Imam and W. J. Orts, *MRS Bull.*, 2011, **36**, 696-702.
271. S. Jeong, S. Yeo and S. Yi, *J. Mater. Sci.*, 2005, **40**, 5407-5411.

272. M. N. Ichazo, C. Albano, J. Gonzalez, R. Perera and M. V. Candal, *Compos. Struct.*, 2001, **54**, 207-214.
273. D. Bikiaris, J. Prinos, K. Koutsopoulos, N. Vouroutzis, E. Pavlidou, N. Frangis and C. Panayiotou, *Polym. Degrad. Stabil.*, 1998, **59**, 287-291.
274. V. B. Gupta, L. T. Drzal, C. Y. C. Lee and M. J. Rich, *Polym. Eng. Sci.*, 1985, **25**, 812-823.
275. L. Hill and S.-B. Lee, *J. Coating. Technol.*, 1999, **71**, 127-133.
276. R. Kumarathanan, A. B. Rajkumar, N. R. Hunter and H. D. Gesser, *Prog. Lipid. Res.*, 1992, **31**, 109-126.
277. M. Tajvidi and G. Ebrahimi, *J. Appl. Polym. Sci.*, 2003, **88**, 941-946.
278. C. Fringant, J. Desbrières and M. Rinaudo, *Polymer*, 1996, **37**, 2663-2673.
279. Y. Li, Y. Fan and J. Ma, *Polym. Degrad. Stabil.*, 2001, **73**, 163-167.
280. X. C. Ge, X. H. Li, Q. Zhu, L. Li and Y. Z. Meng, *Polym. Eng. Sci.*, 2004, **44**, 2134-2140.
281. S. Peng, X. Wang and L. Dong, *Polym. Composite.*, 2005, **26**, 37-41.
282. B. J. Ash, L. S. Schadler and R. W. Siegel, *Mater. Lett.*, 2002, **55**, 83-87.
283. J. Wu and D. D. L. Chung, *Carbon.*, 2004, **42**, 3039\_3042.
284. X. Kornmann, H. Lindberg and L. A. Berglund, *Polymer*, 2001, **42**, 4493-4499.
285. N. Boquillon, *J. Appl. Polym. Sci.*, 2006, **101**, 4037-4043.
286. S. H. Kim, I.-J. Chin and J.-S. Yoon, *Korea Polym. J.*, 1998, **6**, 422-427.
287. E. Guth, *J. Appl. Phys.*, 1945, **16**, 20-25.
288. K. Fagnou and M. Lautens, *Org. Lett.*, 2000, **2**, 2319-2321.
289. A. Berkessel, E. Ashkenazi and M. R. M. Andreae, *Appl. Catal. A-Gen*, 2003, **254**, 27-34.
290. J. Zhang, G. Li, Y. Su, R. Qi, D. Ye, J. Yu and S. Huang, *J. Appl. Polym. Sci.*, 2012, **123**, 2996-3006.
291. N. T. Ahamed, R. S. Singhal, P. R. Kulkarni, D. D. Kale and M. Pal, *Carbohydr. Polym.*, 1996, **31**, 157-160.
292. A. G. Pedroso and D. S. Rosa, *Carbohydr. Polym.*, 2005, **59**, 1-9.
293. Z.-F. Wang, Z. Peng, S.-D. Li, H. Lin, K.-X. Zhang, X.-D. She and X. Fu, *Compos. Sci. Technol.*, 2009, **69**, 1797-1803.
294. R. Santayanan and J. Wootthikanokkhan, *Carbohydr. Polym.*, 2003, **51**, 17-24.
295. Y. Xu, V. Miladinov and M. A. Hanna, *Cereal Chem.*, 2004, **81**, 735-740.

296. S. Saartrat, C. Puttanlek, V. Rungsardthong and D. Uttapap, *Carbohydr. Polym.*, 2005, **61**, 211-221.
297. B. Laignel, C. Bliard, G. Massiot and J. M. Nuzillard, *Carbohydr. Res.*, 1997, **298**, 251-260.
298. R. L. Shogren and A. Biswas, *Carbohydr. Polym.*, 2010, **81**, 149-151.
299. R. L. Shogren, *Carbohydr. Polym.*, 2000, **43**, 309-315.
300. R. Murugan and E. F. V. Scriven, *Aldrichimica Acta*, 2003, **36**, 21-26.
301. A. Corma, S. Iborra and A. Velty, *Chem. Rev.*, 2007, **107**, 2411-2502.
302. J. A. Simms and P. H. Corcoran, *Prog. Org. Coat.*, 1995, **26**, 217-237.
303. A. V. Galanti, B. T. Keen, R. H. Pater and D. A. Scola, *J. Polym. Sci. Polym. Chem. Ed.*, 1981, **19**, 2243-2253.
304. R. Kizil, J. Irudayaraj and K. Seetharaman, *J. Agr. Food Chem.*, 2002, **50**, 3912-3918.
305. J. J. G. van Soest, H. Tournois, D. de Wit and J. F. G. Vliegthart, *Carbohydr. Res.*, 1995, **279**, 201-214.
306. O. Sevenou, S. E. Hill, I. A. Farhat and J. R. Mitchell, *Int. J. Biol. Macromol.*, 2002, **31**, 79-85.
307. Y. Dumoulin, S. Alex, P. Szabo, L. Cartilier and M. A. Mateescu, *Carbohydr. Polym.*, 1998, **37**, 361-370.
308. P. M. Fechner, S. Wartewig, A. Kiesow, A. Heilmann, P. Kleinebudde and R. H. H. Neubert, *Starch - Stärke*, 2005, **57**, 605-615.
309. J. M. Fang, P. A. Fowler, C. Sayers and P. A. Williams, *Carbohydr. Polym.*, 2004, **55**, 283-289.
310. L. A. Bello-Pérez, E. Agama-Acevedo, P. B. Zamudio-Flores, G. Mendez-Montevalvo and S. L. Rodriguez-Ambriz, *LWT - Food Sci. Technol.*, 2010, **43**, 1434-1440.
311. H. Chi, K. Xu, X. Wu, Q. Chen, D. Xue, C. Song, W. Zhang and P. Wang, *Food Chem.*, 2008, **106**, 923-928.
312. S. H. Tay, S. C. Pang and S. F. Chin, *Carbohydr. Polym.*, 2012, **88**, 1195-1200.
313. F. T. G. Dias, R. C. R. Souza and C. T. Andrade, *Macromol. Symp.*, 2011, **299-300**, 139-146.
314. M. Marcazzan, F. Vianello, M. Scarpa and A. Rigo, *J. Biochem. Bioph. Meth.*, 1999, **38**, 191-202.

315. C. F. Liu, R. C. Sun, A. P. Zhang, J. L. Ren, X. A. Wang, M. H. Qin, Z. N. Chao and W. Luo, *Carbohydr. Res.*, 2007, **342**, 919-926.
316. R. Hui, C. Qi-he, F. Ming-liang, X. Qiong and H. Guo-qing, *Food Chem.*, 2009, **114**, 81-86.
317. S. Nagaoka, H. Tobata, Y. Takiguchi, T. Satoh, T. Sakurai, M. Takafuji and H. Ihara, *J. Appl. Polym. Sci.*, 2005, **97**, 149-157.
318. R. Sun and X. F. Sun, *Ind. Crop. Prod.*, 2002, **16**, 225-235.
319. X. F. Sun, R. C. Sun and J. X. Sun, *Bioresource Technol.*, 2004, **95**, 343-350.
320. O. B. Wurzburg, in *Methods in carbohydrates chemistry*, ed. R. L. Whistler, Academic Press, New York, 1964, vol. 4, p. 288.
321. O. S. Lawal, *Carbohydr. Res.*, 2004, **339**, 2673-2682.
322. P. N. Bhandari and R. S. Singhal, *Carbohydr. Polym.*, 2002, **47**, 277-283.
323. L. Zhang, W. Xie, X. Zhao, Y. Liu and W. Gao, *Thermochim. Acta*, 2009, **495**, 57-62.
324. X. F. Sun, R. C. Sun, J. Tomkinson and M. S. Baird, *Carbohydr. Polym.*, 2003, **53**, 483-495.
325. S.-D. Zhang, Y.-R. Zhang, H.-X. Huang, B.-Y. Yan, X. Zhang and Y. Tang, *J. Polym. Res.*, 2010, **17**, 43-51.
326. P. S. Shuttleworth, V. Budarin and J. H. Clark, *J. Mater. Chem.*, 2009, **19**, 8589-8593.
327. R. M. D. Soares, A. M. F. Lima, R. V. B. Oliveira, A. T. N. Pires and V. Soldi, *Polym. Degrad. Stabil.*, 2005, **90**, 449-454.
328. S. Gaan, L. Mauclair, P. Rupper, V. Salimova, T.-T. Tran and M. Heuberger, *J. Anal. Appl. Pyrol.*, 2011, **90**, 33-41.
329. M. Świtła-Żeliazkow, *Polym. Degrad. Stabil.*, 2001, **74**, 579-584.
330. *US Pat.*, 2509873, 1946.
331. *US Pat.*, 3965849, 1975.
332. P. A. M. Steeneken and A. J. J. Woortman, *Carbohydr. Res.*, 2008, **343**, 2278-2284.
333. H. Szymanowski, M. Kaczmarek, M. Gazicki-Lipman, L. Klimek and B. Wozniak, *Surf. Coat. Tech.*, 2005, **200**, 539-543.
334. D. T. Carter, N. Stansfield, R. J. Mantle, C. M. France and P. A. Smith, *Ind. Crop. Prod.*, 2008, **28**, 309-319.

- 
335. Q. Luo, M. Lui, Y. Xu, M. Ionescu and Z. S. Petrovic, *J. Appl. Polym. Sci.*, 2012, DOI: 10.1002/app.37814.
336. A. S. Luyt, J. A. Molefi and H. Krump, *Polym. Degrad. Stabil.*, 2006, **91**, 1629-1636.
337. M. Beltran and A. Marcilla, *Eur. Polym J.*, 1997, **33**, 1135-1142.
338. M. Brebu, C. Vasile, S. Rovana Antonie, M. Chiriac, M. Precup, J. Yang and C. Roy, *Polym. Degrad. Stabil.*, 2000, **67**, 209-221.
339. S. Brunauer, P. H. Emmett and E. Teller, *J. Am. Chem. Soc.*, 1938, **60**, 309-319.
340. S. Thiebaud, J. Aburto, I. Alric, E. Borredon, D. Bikiaris, J. Prinós and C. Panayiotou, *J. Appl. Polym. Sci.*, 1997, **65**, 705-721.
341. A. K. Bledzki and J. Gassan, *Prog. Polym. Sci.*, 1999, **24**, 221-274.
342. A. Bhatnagar and M. Sain, *J. Reinf. Plast. Comp.*, 2005, **24**, 1259-1268.
343. D. K. Setua, M. K. Shukla, V. Nigam, H. Singh and G. N. Mathur, *Polym. Composite.*, 2000, **21**, 988-995.